Report
P-16-17
May 2017

KBS-3H Summary report – Buffer laboratory test

Ola Kristensson
Torbjörn Sandén
Lennart Börgesson

SVENSK KÄRNBRÄNSLEHANTERING AB

SWEDISH NUCLEAR FUEL
AND WASTE MANAGEMENT CO

Box 3091, SE-169 03 Solna
Phone +46 8 459 84 00
skb.se

SVENSK KÄRNBRÄNSLEHANTERING

ISSN 1651-4416
SKB P-16-17
ID 1555191
May 2017

KBS-3H Summary report – Buffer laboratory test

Ola Kristensson, Torbjörn Sandén, Lennart Börgesson
Clay Technology AB

Summary

This report is a compilation of already existing descriptions of laboratory tests performed by Clay Technology which relate to the KBS-3H repository design. The KBS-3H design has been developed jointly by SKB and Posiva since 2002. This report has been prepared within the project phase "KBS-3H – System Design 2011–2016". The tests covered are Big Bertha II–IV and Transition Zone Homogenization.

Big Bertha II, simulating a Supercontainer section, and **Big Bertha III**, simulating a distance block section, are considered providing accurate and important information regarding the initial swelling behavior and swelling pressure development for dry drift conditions with only the water artificially provided at installation, in accordance with DAWE. Swelling pressure, acting on the simulated drift surface, developed despite the dry tests conditions. For Big Bertha II the bentonite which had passed through the Supercontainer shell perforations and occupied the volume outside of the shell was found to have significant variation in density. At positions just outside of perforations, higher density muffin-shaped clay protrusions were formed. This in turn gave rise to variations in the pressure registered between the buffer and simulated drift surface. During the operation of both tests no indications of decreasing swelling pressures were found.

Big Bertha IV, simulating a Supercontainer section, is considered to provide accurate and important information regarding the initial swelling behavior and swelling pressure development when additional water from the rock is available besides the water provided at installation. The test has shown that the Supercontainer-rock gap will be filled with swelling bentonite quite soon after installation. The variation in density of this material was, however, significant (as in the case of Big Bertha II) and the swelling pressure acting on the rock is expected to vary accordingly. The radial pressure, measured in between perforations, showed insignificant pressure build up against the drift surface. At the position of perforations, however, significant swelling pressure buildup is expected. This is indeed the case for Big Bertha V, still in operation when writing this report, which shows significant pressure at these positions.

Transition Zone Homogenization test showed that the transition zone has the expected effect reducing the swelling pressure against the drift plug. Experimental data and the results from using a friction angle between 5° and 10° in an analytical model are in fair agreement.

Sammanfattning

Denna rapport är en sammanslagning av det som rapporterats angående tester genomförda av Clay Technology som berör förvar av KBS-3H design. SKB och Posiva har gemensamt utvecklat KBS-3H alternativet sedan 2002. Denna rapport har framställts inom projektfasen "KBS-3H – System Design 2011–2016". De tester som beskrivs är Big Bertha II–IV och Transition Zone Homogenization.

Big Bertha II, som simulerade en del av en supercontainer, och **Big Bertha III**, som simulerade en del av ett distansblock, anses ge tillförlitlig och viktig information vad gäller initiell svällning och tryckuppbyggnad under torra förhållanden i deponeringstunneln då vatten enbart tillsätts vid installationsfasen enligt DAWE. Testerna visade att det, även under torra förhållanden, byggs upp svälltryck mellan buffert och tunnelvägg. För Big Bertha II fann man att bufferten som trängt ut genom den perforerade delen av supercontainern hade en avsevärd variation i densitet beroende på positionen i förhållande till perforeringsmönstret. Detta i sin tur gav upphov till variationer hos trycket mellan bufferten och den simulerade tunnelväggen. De uppmätta trycken uppvisade ingen minskade trend för något av de bägge testerna.

Big Bertha IV, som simularade en del av en supercontainer, anses ge tillförlitlig och viktig information vad gäller initiell svällning och tryckuppbyggnad då vatten finns tillgängligt vid tunnelväggen även efter installationsfasen. För dessa förhållanden fylldes den initiellt tomma spalten mellan supercontainer och den simulerade tunnelväggen relativt snabbt med bentonit som svällde/pressades ut genom perforeringarna. Precis som för Big Bertha II erhölls en varierande densitet hos bufferten utanför supercontainern. Variationen var beroende av positionen i förhållande till perforeringsmönstret. Mellan perforeringarna var det uppmätta trycket mot tunnelväggen mycket begränsat. Big Bertha V, som fortfarande är i drift när detta skrivs, visar å andra sidan signifikanta tryck mitt för perforeringarna vilket är att vänta med tanke på densitetsvariationen.

Transition Zone Homogenization testet visade att funktionen hos detta system var som önskat och förväntat. Trycket minskade avsevärt vid positionen för pluggen jämfört med det fullt utvecklade svälltrycket som genererades vid distansblocket. Analytiska lösningar som erhölls för friktionsvinklarna 5° och 10° överensstämde relativt väl med experimentell data.

Contents

1 Introduction

This report comprise descriptions regarding *Big Bertha* (BB) II–IV, and *Transition Zone Homogenization* (TZH) carried out by Clay Technology. All tests relate to the KBS-3H design alternative. The purpose for compiling this report is to provide a reference for the included tests. The basis for this report are internal PMs describing the tests.

In this introductory section, in order to set the tests into their proper context and introduce related nomenclature, a brief description of the relevant parts of the KBS-3H design alternative is first given. Then follows a short introduction of the tests where the purpose and their main characterizing features are outlined. For completeness two related tests, BB I and BB V, are also included.

After this follows more detailed descriptions of the four addressed tests. Individual chapters have been assigned to each of the tests. In each of the individual chapters the test setup, operation, and dismantling are described, and thereafter results and analysis are given.

The last chapter is a summary of comments given, conclusions drawn and comparisons made between related tests.

In order to try to enhance readability, some information originally given in the main text of the internal PMs has been repositioned into appendices.

1.1 KBS-3H design

Here follows a brief overview of the KBS-3H design focusing on the parts relevant for the tests described. A detailed description can be found in Autio et al. (2008) and SKB (2012).

KBS-3H denotes a *horizontal* design alternative within the KBS-3 method. The KBS-3H design has been developed jointly by SKB and Posiva since 2002. This report has been prepared within the project phase "KBS-3H – System Design 2011–2016". Canisters containing spent nuclear fuel are sequentially emplaced horizontally in approximately horizontal deposition drifts as shown in the close-up in Figure 1-1. The repository, situated at about 400–500 m depth in the bedrock, consists of parallel deposition drifts bored from a niche in the central tunnel as shown in Figure 1-1.

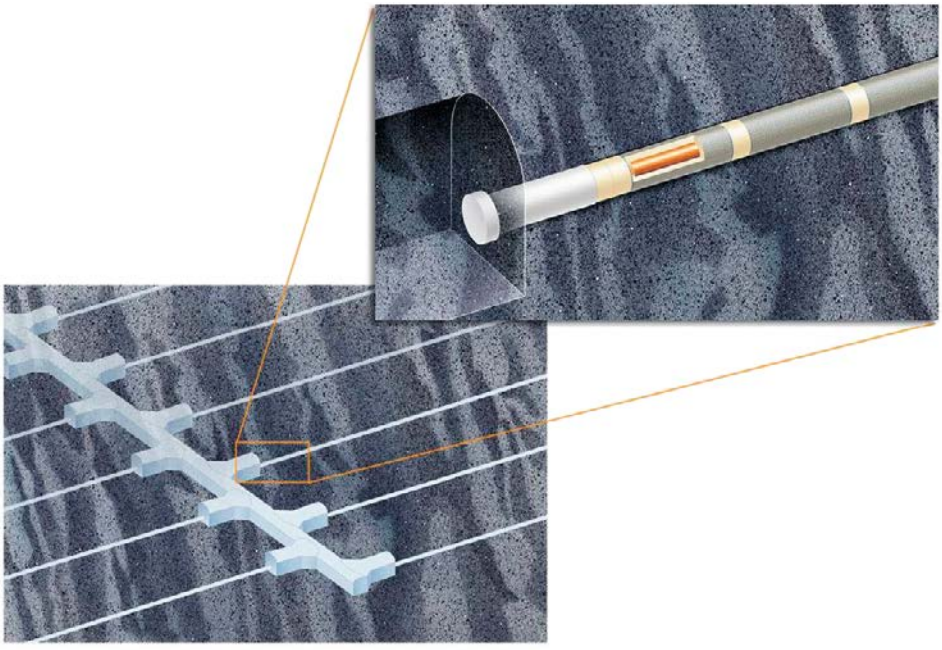

Figure 1-1. *Illustration of a central tunnel with deposition drifts in KBS-3H.*

Figure 1-2 contain a schematic drawing of a deposition drift where the internal components are shown. The components of relevance for the present report are the *Supercontainer* (SC), *Distance block* (DB), Pellet filling, and Transition block.

The SC consists of a canister surrounded by buffer blocks which are confined by a partially perforated metal shell, see Figure 1-3. The use of SC-units assembled prior to the installation enhances the possibility to control the buffer properties closest to the canister and simplifies the installation.

The SCs are separated by cylindrical DBs in order to restrict the temperature and seal off each canister-position from the next, and thereby prevent water and bentonite transport along the drift.

The combined pellet filling and transition block on the left side of the compartment plug and drift plug in Figure 1-2 are called *Transition Zones* (TZs), see Figure 1-4. The main purpose of the TZ is to decrease the pressure acting on the plugs.

The reference KBS-3H design alternative is based on the *Drainage, Artificial Watering and air Evacuation* (DAWE) installation concept. An important part of the DAWE concept is the artificial water filling of the open outer slot between the SC/DBs and drift wall at the end of the installation sequence after that the drifts have been sealed with the compartment/drift plugs.

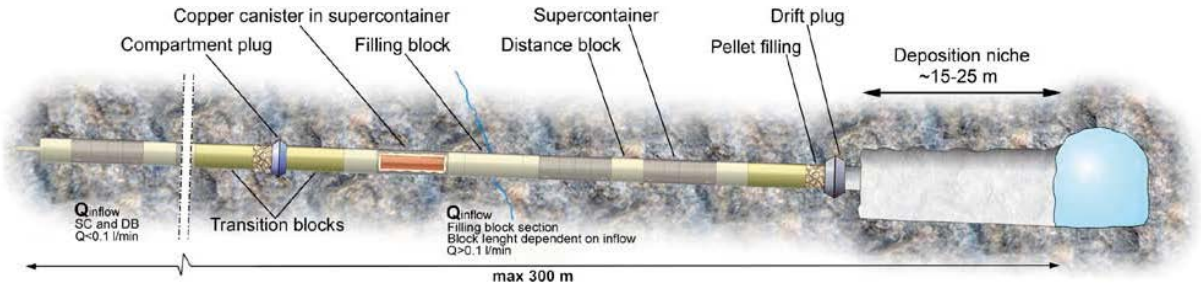

Figure 1-2. *Schematic drawing of a vertical cut through the central tunnel, deposition niche, and an equipped deposition drift in KBS-3H.*

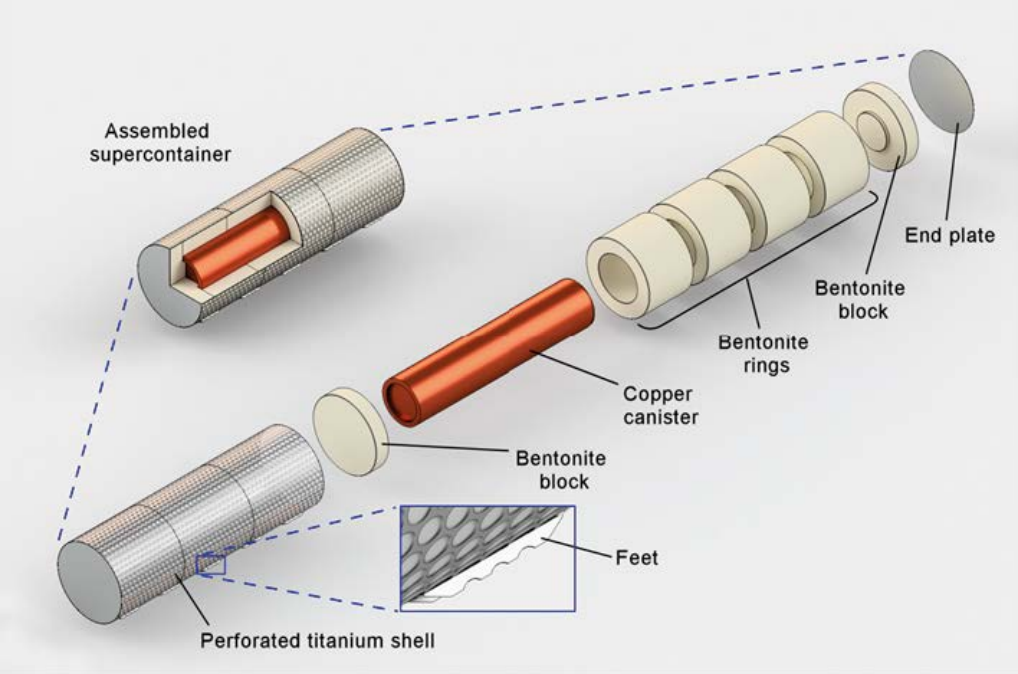

Figure 1-3. *The canister and buffer (ring-shaped and cylinder-shaped bentonite blocks) are contained within a partially perforated metal shell (denoted 'titanium shell' in the drawing). All components form the so called Supercontainer in the KBS-3H design.*

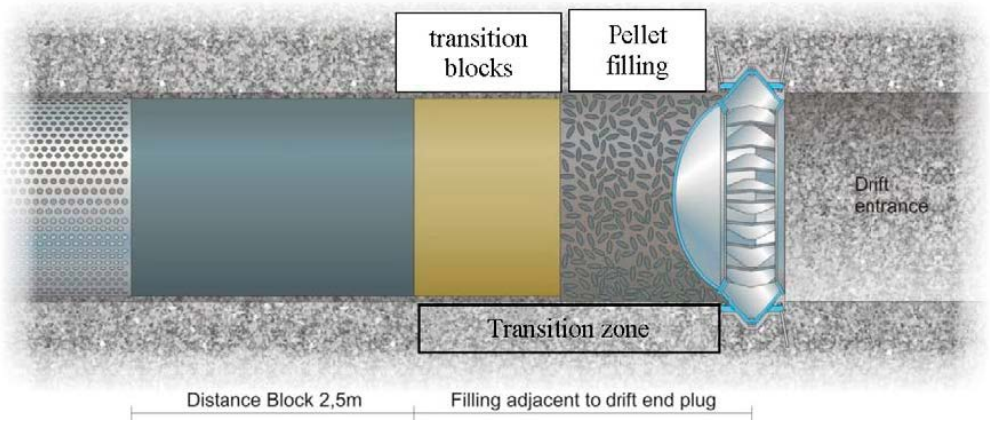

Figure 1-4. *The transition zone, consisting of transition blocks and pellet filling, situated between the drift plug and last distance block.*

1.2 KBS-3H related laboratory tests carried out by Clay Technology

In order to facilitate detailed studies of the behavior of buffer components included in the KBS-3H design, laboratory tests have been carried out by Clay Technology. Different tests were designed as to simulate different parts of a KBS-3H repository under different conditions. In Table 1-1 the KBS-3H laboratory tests performed at Clay Technology which are addressed in this report are identified. Some abbreviations used in the forthcoming are, BB for Big Bertha, the name of the test equipment used and TZH for Transition Zone Homogenization.

Table 1-1. Identification of the KBS-3H laboratory tests performed at Clay Technology.

Name	Simulated system
BB I[1]	DB section, final state, dry conditions
BB II	SC section, initial state, dry conditions
BB III	DB section, initial state, dry conditions
BB IV	SC section, initial state, wet conditions
BB V[1]	SC section, final state, wet conditions
TZH	TZ section

(1) Not described in detail in this report.

In this report BB II, BB III, BB IV and TZH are fully described. BB I has been reported in SKB (2012, pp 150–156) and BB V is still in operation at the time writing this report. A full description of these two tests is therefore not included in this summary report. For completeness, however, all tests in Table 1-1 will briefly be addressed when outlining the KBS-3H laboratory tests performed at Clay Technology below.

All mentioned tests have common traits. They were all isothermal; thus, no heat generating component has been included as to simulate the presence of the spent nuclear fuel. The tests only simulate parts of, or smaller scale of, the actual KBS-3H design to get manageable tests both with respect to handling and runtime. In all tests stresses were recorded during operation and after dismantling the buffer was sampled and analyzed with regard to water content and dry density.

As mentioned above, the Big Bertha denotation of five of the tests comes from the use of parts from the test equipment bearing this name. The BB test equipment used in the tests was manufactured in 2003 in order to perform large scale tests within the KBS-3H design. The original plan was to perform a long term homogenization test where the bentonite after installation and water filling should have access to additional water from filters placed on the “rock” wall, see the white areas in the principle drawing provided in Figure 1-5. The equipment consists of two separate enclosure sections, one with a length of 1 050 mm and the other with a length of 350 mm. The sections can be mounted together to a unit and lids be mounted at the ends. The longer section was intended for a SC unit and the shorter for a DB.

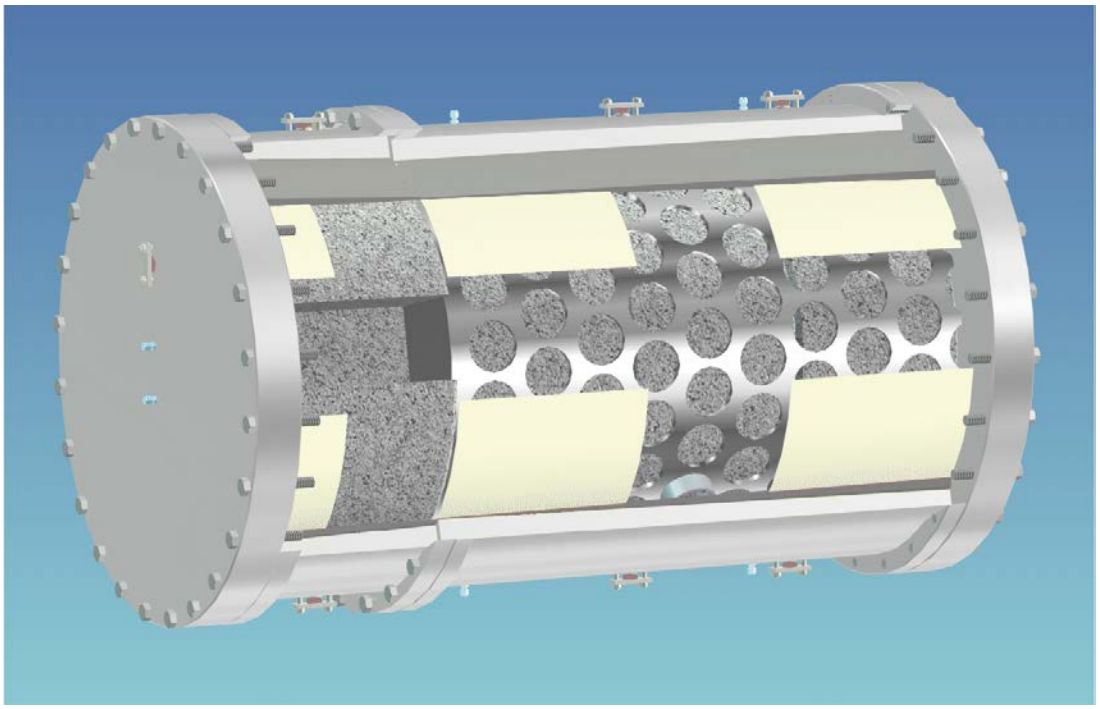

Figure 1-5. *Schematic drawing of the "Big Bertha" test equipment.*

In the tests described in this report, however, the two units have been used separately, the shorter for the BB I, BB III and BB IV tests and the longer unit for the BB II and BB V tests. Since at times two of the tests were operated in parallel, it was necessary to complete the equipment shown in Figure 1-5 with two additional steel lids.

Below follows a brief description of all the tests relevant for this summary report. A compilation of characterizing design/layout data for the KBS-3H laboratory tests is given in Table 1-2.

BB I was used for studying the capability of the buffer to prevent rock debris from the drift wall to fall out into the initially open slot. The changed stress conditions after excavation together with the heating may result in so called spalling of the drift rock wall. The pressure generated by the swelling buffer could, however, prevent this to have an effect on the repository performance. BB I simulated a DB section subjected to dry conditions, i.e. no water was added after the initial artificial wetting when water filled up the outer slot. No buffer block was manufactured for this test, an unused buffer block was available from earlier unrelated tests. It had a water content of 10 % and dry density of 1 989 kg/m^3. It should be noted that this is not in accordance with the KBS-3H design.

BB II and **BB III** mainly aimed at providing more knowledge about the issue regarding spalling as described above for BB I. With hindsight, the tests have also been beneficial for understanding the initial water uptake and swelling process of the buffer at dry conditions and also when developing numerical models of the THM processes in the system. BB II and BB III again simulated dry conditions, this time for a SC and a DB section, respectively. Buffer blocks were manufactured according to the specifications of the KBS-3H design. Three blocks, with water contents 10.5–10.7 % and dry densities 1 904–1 937 kg/m^3, were manufactured for BB II and one block, with water content 21.4 % and dry density 1 718 kg/m^3, was manufactured for BB III. BB II was equipped with a perforated steel shell with dimensions corresponding to that of the perforated copper shell which was part of an earlier design.

BB IV mainly aimed at providing a possibility for studying the initial water uptake and swelling process of the buffer in a SC section when water is supplied at the drift rock wall. The test also provides information about the initial evolution of the buffer which can be used for testing models simulating the KBS-3H system. The buffer block had a water content of 10.4 % and a dry density of 1 906 kg/m^3. The test was equipped with a perforated steel shell with dimensions corresponding to that of the perforated titanium shell present in the later KBS-3H design.

BB V mainly aims at providing a possibility to study the final state of the buffer within a SC section when supplied with water at the drift rock wall. The final state is here defined as when the test has come to equilibrium; water does not flow into the test cell and the monitored pressures are constant. The test will provide information about the final state of the buffer which can be used for testing models simulating the KBS-3H system. The buffer blocks had water contents of 10.4–10.9 % and dry densities of 1 892–1 937 kg/m^3 at installation. The test is equipped with a perforated steel shell with dimensions corresponding to that of the titanium shell.

TZH was intended for investigating the evolution and final state regarding water uptake, deformation and pressure in a TZ section. The test provides information for the plug design and the design of the TZ itself. Solutions obtained from an analytical model could also be evaluated and compared against the obtained test data. 18 cylindrical blocks with a water content of 20.9 % and dry densities in the range of 1 694–1 710 kg/m^3 were used in the test. The individual pellets had a water content of about 14.1 % and a dry density of 1 841 kg/m^3. The dry density of the pellet filled volume was about 1 000 kg/m^3.

Table 1-2. Compilation of characterizing design/layout data for the KBS-3H laboratory tests performed at Clay Technology. Abbreviations: DB = Distance block, SC = Supercontainer, TZ = Transition zone.

Name	Section	State	Water at installation	Additional water	Duration [days]	Length [mm]	Main focus of study
BB I	DB	Final	Salt[1] content 1.2 %	No	490	350	Spalling prevention
BB II	SC (Cu[2])	Initial	Tap water	No	230	1 080	Spalling prevention
BB III	DB	Initial	Tap water	No	218	350	Spalling prevention
BB IV	SC (Ti[3])	Initial	Tap water	Salt[1] content 1.0 %	180	350	Water uptake & deformation
BB V	SC (Ti[3])	Final	Tap water	Salt[1] content 1.0 %	>2 years (ongoing)	1 080	Water uptake & deformation
TZH	TZ	All	Tap water	Salt[1] content 1.0 %	273	1 000	Deformation & pressure

(1) Na 50 % and Ca 50 %.

(2) Cu = A steel representation of a copper shell with 10 mm thickness was used. (Earlier design).

(3) Ti = A steel representation of a titanium shell with 6 mm thickness was used. (Later design).

2 BB II

The main focus of this study was the capability of the SC buffer to prevent thermally induced spalling at the drift rock wall. Extremely dry conditions were simulated. No water was allowed to enter the system except that, in accordance with DAWE, artificially provided at installation. The buffer blocks were prepared as to simulate the initial state of the system.

2.1 BB II: Test setup

The test equipment in BB II, see Figure 2-1, only included the longer section of the complete BB equipment, see Figure 1-5. Thereby an extra steel lid was needed to close the enclosure. The main dimensions of the enclosure are shown in Figure 2-1. The enclosure tube section had a length of 1 080 mm, an inner diameter of 800 mm in the 300 mm long indicated midsection, and an inner diameter of 804 mm in the outer sections of 380 mm and 390 mm length, respectively. The larger diameter at the two outer sections were prepared as to install filters for simulating water bearing fractures.

After the emplacement of the SC there was a remaining empty volume between the SC gable and enclosure steel lid of 10 mm. In this volume a special manufactured PVC disc (D=798 mm and t=10 mm) was fitted, see Figure 2-1.

The total pressure (or normal total stress component) acting on the enclosure was determined at five positions by use of force transducers. Pistons with a diameter of 20 mm, fitted in cylindrical openings in the enclosure, transferred the force acting on the inside of the enclosure (on the inner piston end surface) to the load cells positioned on the outside of the enclosure. Radial total pressures were measured at positions C1, C2, D1, and D2, and axial total pressure were measured at the open end of the SC, see Figure 2-1.

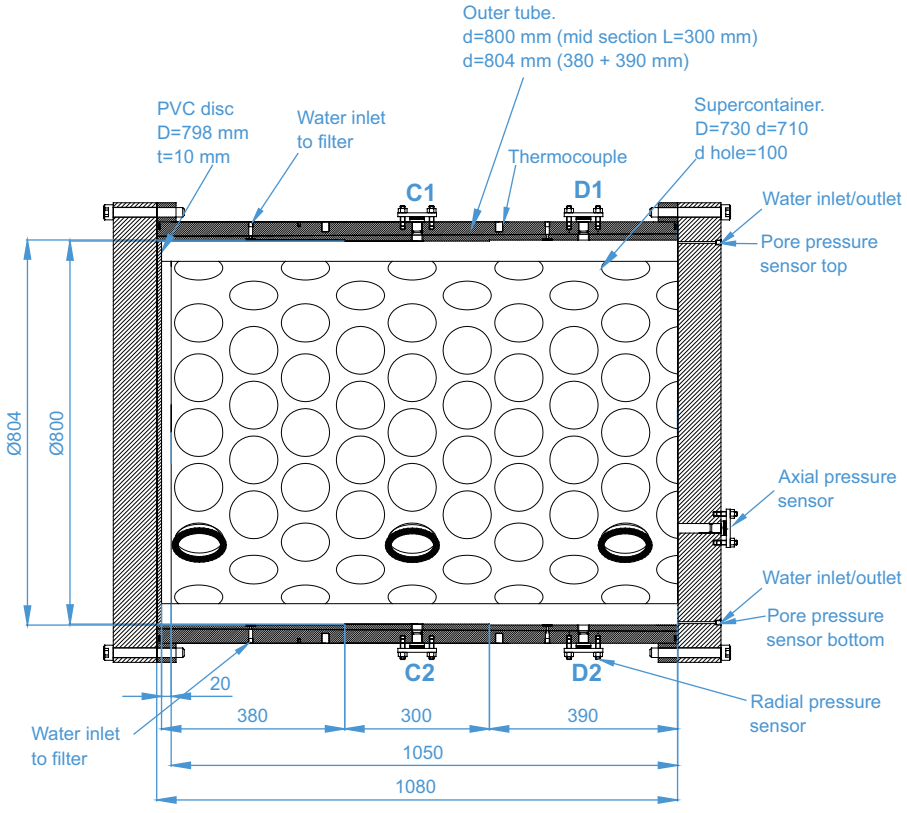

Figure 2-1. *BB II. Schematic drawing showing the BB II test equipment.*

The lid at the SC open end was equipped with valves in order to facilitate the artificial water filling; one for water inlet at the bottom most position and one for de-airing at the top most position. After having finished the water filling, pressure sensors were fitted at the inlets in order to measure the water pressure.

The temperature of the test cell was logged and the temperature and relative humidity of the room was registered in order to monitor the surrounding climate.

More information about the sensors can be found in Appendix B1.

2.1.1 BB II: SC shell representation

The used equipment included a SC shell representation made out of steel. At the time performing this test the KBS-3H design included a SC shell made out of copper with somewhat different dimensions as compared to the current design where the SC shell is made out of titanium.

The dimensions were adapted to the BB scale (Figure 2-2). The total length was 1 070 mm, where 1 050 mm consists of the perforated cylinder and 20 mm of the disc-shaped gable. The inner and outer diameter were 710 and 730 mm, respectively, which means that the radial slot between the SC and the "drift wall" (the BB enclosure) was 35 mm when perfectly centered. The perforation of the SC shell consisted of circular holes with a diameter of 100 mm, positioned according to the drawing provided in Figure 2-2. The degree of perforation was close to 60 %. In addition, the SC design also included six feet made out of 35 mm lengths of 100 mm pipe that were welded to the cylindrical surface in accordance with what is shown in Figure 2-2.

2.1.2 BB II: Buffer

The bentonite blocks were manufactured using a special mold with an inner diameter of 1 000 mm. The bentonite used was MX-80 Wyoming from a batch delivered to SKB during 2012. The blocks were machined to a diameter of 700 mm after compaction.

The blocks were compacted using a pressure of 56 MPa with the as-delivered material which had a water content of between 10.5 to 10.7 %. In conjunction with the manufacturing, the block dimensions and achieved density after compaction were determined. During the assembling of the test, block weights and block heights were measured again and based on these data the bulk density of the blocks could be calculated. It was noticed that the blocks had expanded somewhat and therefore the calculated densities were somewhat lower as compared to what had been determined earlier. A compilation of all block data is provided in Table 2-1.

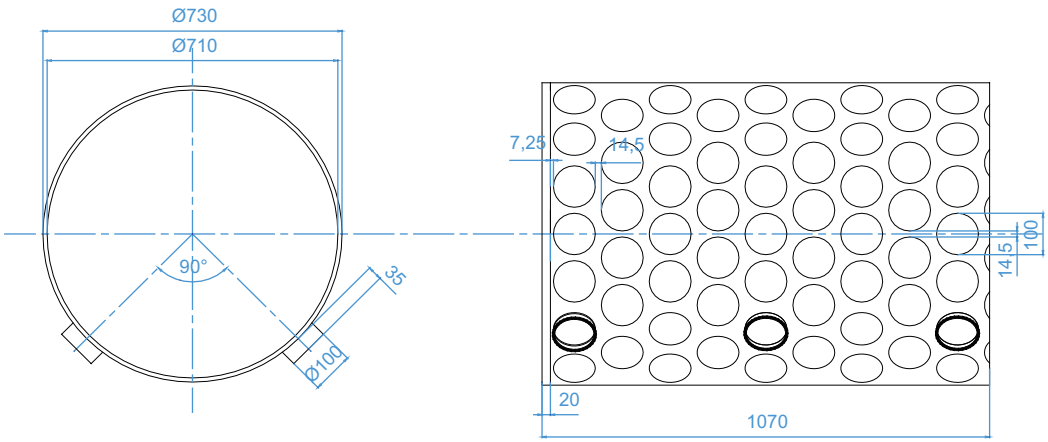

Figure 2-2. *BB II. Technical drawing of the SC shell representation adapted for the BB test equipment.*

Table 2-1. BB II. Compilation of block data.

Block parameters determined in conjunction with manufacturing and machining			
Block no.	***BB II012A2***	***BB II012A3***	***BB II012A14***
Water content [%]	10.5	10.7	10.6
Bulk density [kg/m^3]	2 140	2 109	2 106
Dry density [kg/m^3]	1 937	1 906	1 904
Diameter [mm]	700±1	700±1	700±1
Height [mm]	344.4	353.3	348.8
Block parameters determined in conjunction with test assembly			
Weight [kg]	276	280	278
Height [mm]	346.1	353.5	350
Bulk density* [kg/m^3]	2 072	2 058	2 064
Dry density* [kg/m^3]	1 875	1 859	1 866
Degree of saturation [%]	60.5	60.0	60.2

* These densities were calculated from the weight and dimensions determined during the test assembly.

2.2 BB II: Operation

The operational phase started with the artificial water filling, injecting water through a 6 mm tube at a pressure of 5 meters water head at the same time as air was escaped through the dedicated outlet valve. 120.9 liters of water was injected during 4 hours.

Below follows a description of the pressure evolution during the operational phase. Some additional information regarding the measurements is given in Appendix B2. A description of early pressure responses is given in Appendix B3 and sensor data regarding room climate is given in Appendix B4.

In Figure 2-3 it can be seen that the total pressure was similar in the top and bottom within cross sections. There was, however, a significant difference between the two cross sections C and D. The difference was found to be an effect from different sensor positions in relation to the perforation pattern of the SC, see Section 2.4.3. Buffer sampled adjacent to the sensors showed that there was a significant difference in dry density. The registered total radial pressure also showed some small daily variations that are believed to be related to the variations in temperature.

Figure 2-3 also shows that the pore pressure increases fast at the test start up (see Appendix B3 for higher resolution during the first hours) and reaches a maximum value of 60–65 kPa after four days before the pressure started to decrease. After about 80 days the pore pressure reached zero. This indicates that all water was absorbed by the bentonite and no more water was available to generate pore pressure.

The laptop used for storing sensor data was stolen during the operational phase, see Appendix B2. The hatched lines in Figure 2-3 indicate the period, day 197 to day 230, where no data is available due to this.

The axial total pressure and test cell temperature are shown in Figure 2-4. At test start a pressure of 169 kPa was registered by the load cell, which corresponds to a pre-stress load of 53 N. After about 60 days the axial total pressure started to increase slowly and after day 107 it begun to increase more rapidly. At the time for termination, the registered axial total pressure was more than 2 MPa. Analysis of material samples at this position showed that the bentonite have had significant water uptake also at some distance from the block´s outer surface.

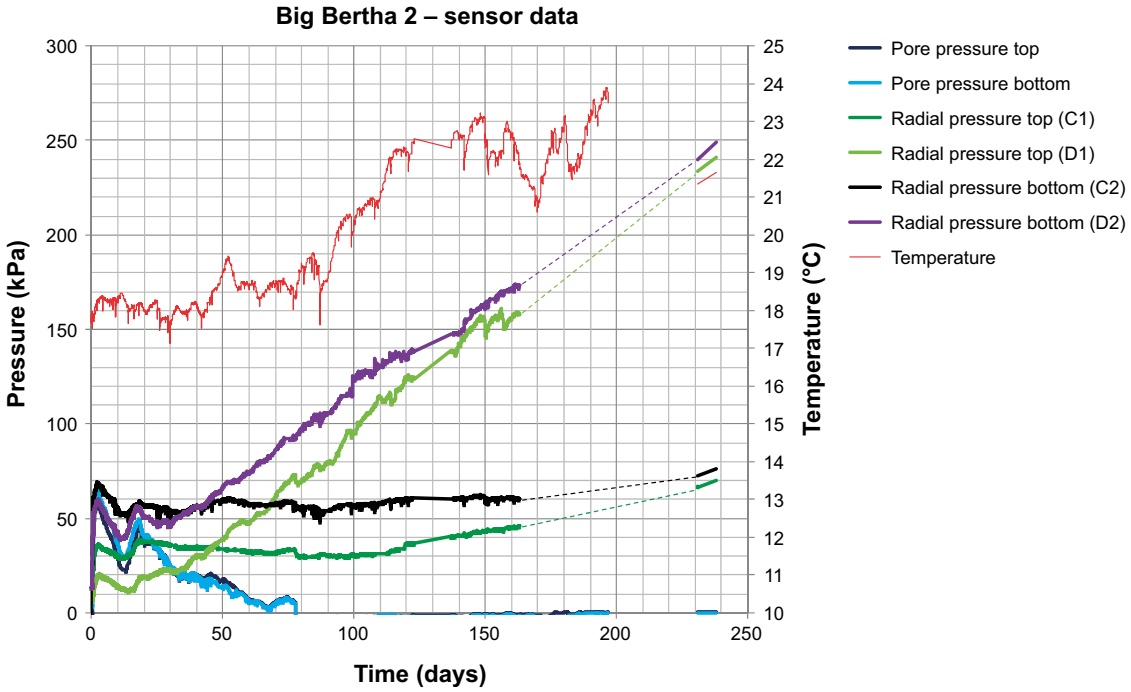

Figure 2-3. *BB II. Evolutions of radial total pressure, pore pressure and test cell temperature in BB II.*

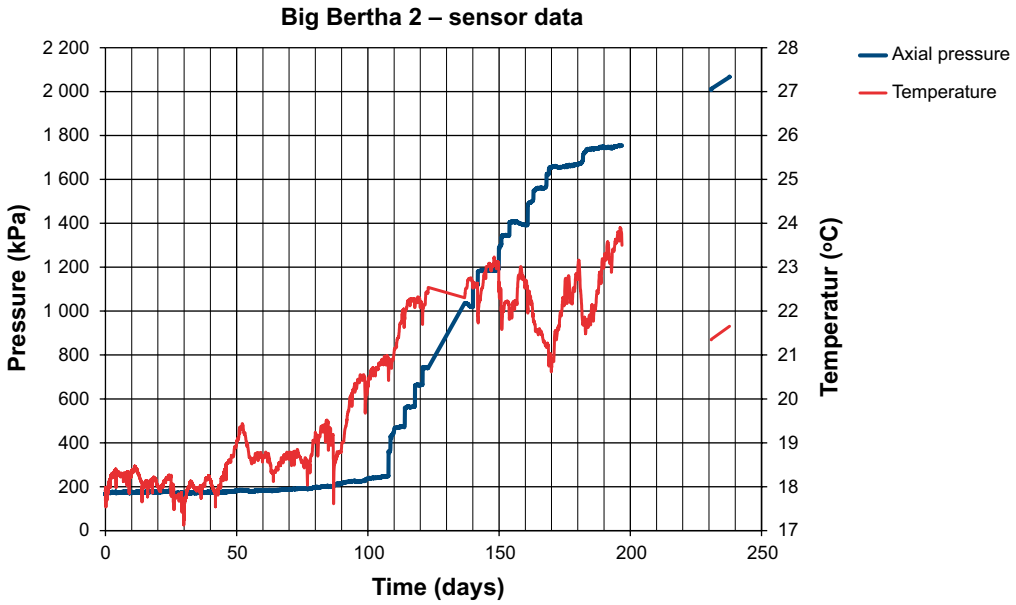

Figure 2-4. *BB II. Evolutions of axial total pressure and test cell temperature in BB II.*

2.3 BB II: Dismantling and sampling

An extensive sampling of the bentonite was performed at test dismantling. Due to the amounts of material and relatively large and heavy equipment components, a sampling plan with an adaptable strategy and a well-defined coordinate system was worked out in advance. During the dismantling much effort was devoted to prevent drying of the bentonite. At pauses all exposed bentonite surfaces were covered with plastic sheets.

The coordinate system used for the sampling is shown in Figure 2-5. The chosen cross sections and directions are marked in the figure. A coding system was made up based on the position of every single sample. E.g. sample B_135_75 was taken in cross Section B in direction 135° at a radial distance of 75 mm from the test cell wall.

An example of the sampling plan for one direction of a cross section is shown in Figure 2-6. In all eight directions there were three samples (approx. 12 mm width) taken in the SC-rock gap, one sample in the perforation of the SC shell (approx. 10 mm width) and three samples with a diameter of 20 mm just inside the SC shell. In direction 0°, 90°, 180° and 270° there were nine additional samples with a diameter of 30 mm taken towards the center. Finally one sample was drilled out at the center position. The bentonite inside the SC was not possible to be sampled in cross section A due to the SC gable which is welded against the perforated shell.

The SC-rock gap width was determined in conjunction with the test assembly and directly when the lids were opened at test dismantling, Appendix B5 contains the results from the pre and post operational phase measurements.

The first sampling that was carried out concerned the material just inside of the total pressure sensors. Thereafter, the lids were removed and sampling of the buffer in the different cross sections was performed.

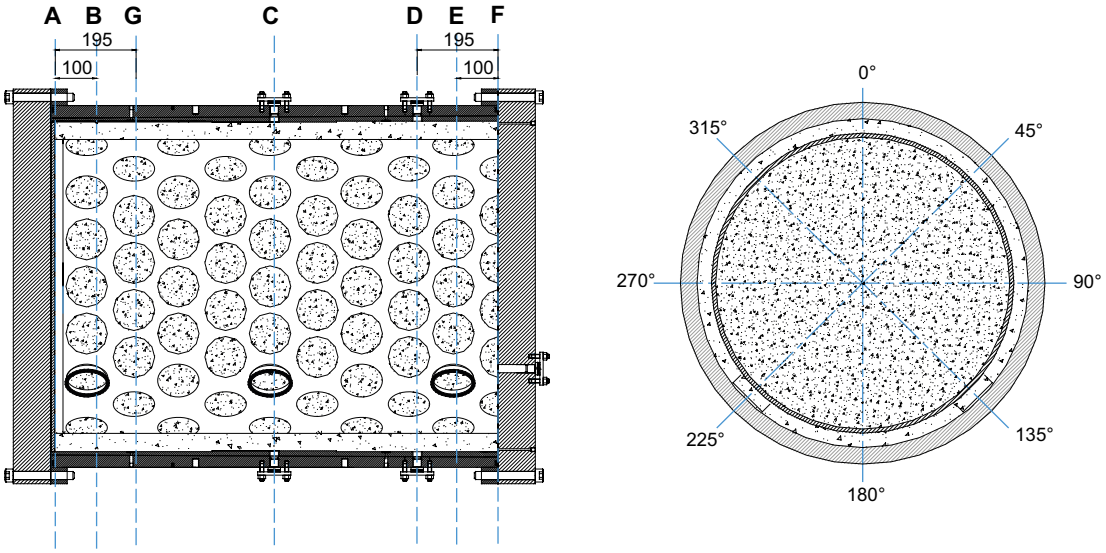

Figure 2-5. *BB II. LEFT: definition of the cross sections chosen for sampling. RIGHT: definition of the angular coordinate chosen for sampling when looking from A towards F.*

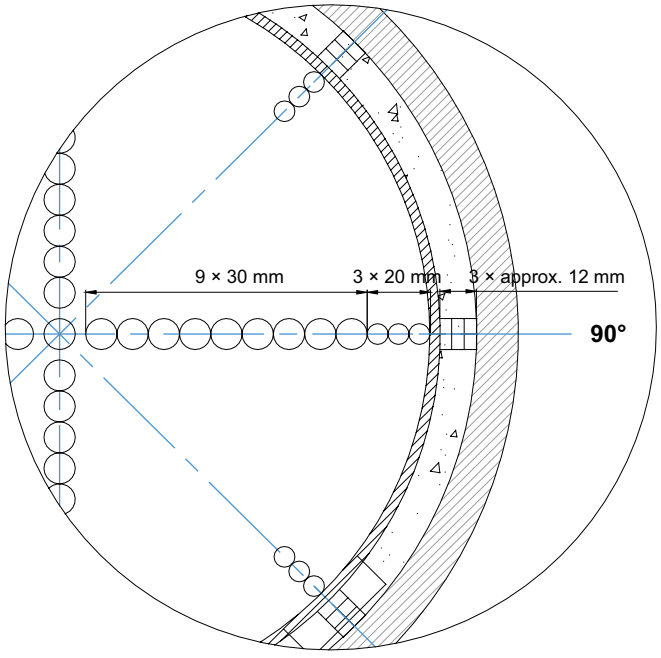

Figure 2-6. *BB II. Close-up of a cross section profile showing the sampling plan.*

Samples were also taken in all six feet of the SC. These samples were taken continuously as the SC was removed from the test cell. Samples were also taken continuously in the perforation holes of the SC shell in each of the cross sections.

In some of the cross sections (mainly B) the sampling accuracy was possibly affected by cracks and layers in the blocks, but despite this only a few samples from the original plan were missed. The sampling only failed on seven samples; one sample in the SC-rock gap of cross section A and six samples inside the SC in cross section B (due to the block breaking, see Section 2.3.7, it was very difficult to determine exact coordinates in this cross section).

Below follows a selection of photographs taken and observations made during the dismantling and sampling of the test.

2.3.1 BB II: Cross section A

Figure 2-7 shows the view directly after removal of the lid. At this point it was observed that the SC shell had moved about 10 mm outwards. This could come from an immediate axial elastic expansion.

To the right in Figure 2-7 the "muffin"-shaped appearance of the outer part of the buffer after expanding through the perforated SC shell is clearly seen. The muffins were more articulated in the upper part of the SC-rock gap. In the lower part of the SC-rock gap the bentonite appeared to be significantly more homogenous.

2.3.2 BB II: Cross section F

The SC-rock gap was significantly more homogenized in this section as compared to section A. Still, however, some air filled volumes were observed between the perforations, especially so in the upper part. Figure 2-8 shows an overview of cross section F and an example showing the sampling of the SC-rock gap.

Figure 2-9 shows the process marking out the planned sample pattern of cross section F before sampling and an overview of cross section F after sampling.

2.3.3 BB II: Cross section E

The work procedure with uncovering and sampling of cross section E inside the SC shell is shown in (1)–(4) in Figure 2-10. In (1) the muffin-shaped clay protrusions are clearly seen. Even so, the material within the SC-rock gap appeared to be more homogenized as compared to cross section A and B. The white arrows in (1) and (2) indicate signs of relative motion between SC shell and buffer.

2.3.4 BB II: Cross section D

The remaining hole after the sampling at the position of the radial total pressure measurement can be seen to the left in Figure 2-11. The position of the perforation pattern of the SC shell in relation to the sample taken at 45° is clearly visible in the right photo of Figure 2-11. It was noticed that holes used for lifting the blocks were placed very close to nearby samples which could have an influence on the results, Figure 2-12.

2.3.5 BB II: Cross section C

The muffin-like protrusions of the bentonite in the SC-rock gap was more apparent here as compared to sections D, E and F and more empty volumes were also observed in between the muffins, see (1) in Figure 2-13. This was also evident when studying a cut along the C cross section which is shown in (2) of Figure 2-13. The muffins had connected during homogenization and held together with such strength that large parts could be removed as can be seen in (3) of Figure 2-13. After removing the outer part of the SC shell the protruding block fell off in one piece which can be seen in (4) of Figure 2-13. As can be seen, the piece of block fell apart to some extent when hitting the floor. A number of layers could clearly be seen in the block and this observed structure may have an influence of the dry density determinations of these parts.

Figure 2-7. *BB II, cross section A. LEFT: cross section directly after the lid was removed. RIGHT: close up of the "muffins".*

Figure 2-8. *BB II, cross section F. LEFT: cross section directly after the lid was removed. RIGHT: sampling of the SC-rock gap.*

Figure 2-9. *BB II, cross section F. LEFT: marking out the sample pattern inside the SC. RIGHT: overview of cross section F after the sampling.*

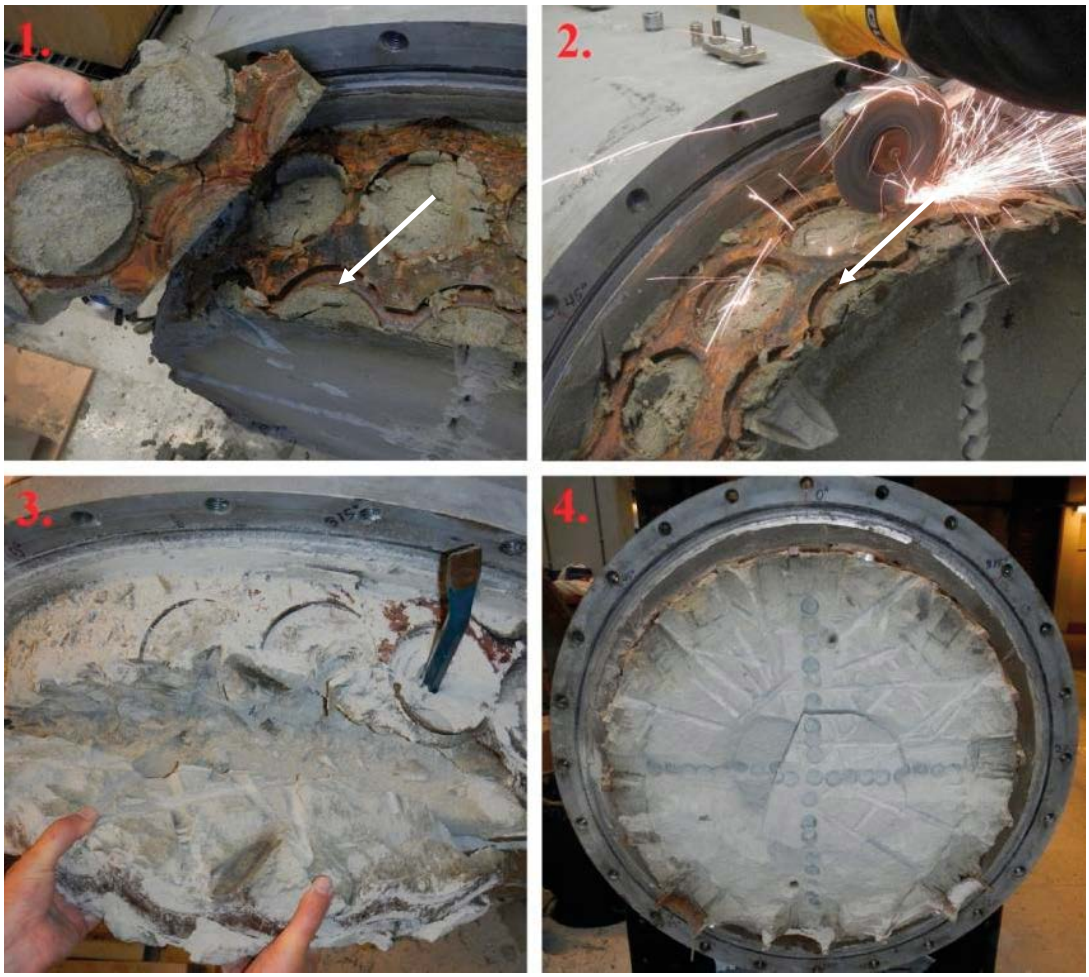

Figure 2-10. *BB II, cross section E. (1) The bentonite in the SC-rock gap is removed. (2) An angle grinder is used to cut the shell. (3) The block is stitch-drilled in radial direction and protruding part breached off using chisels. (4) Cross section E after sampling.*

Figure 2-11. *BB II, cross section D. LEFT: the hole from the sampling in the radial total pressure measurement position. RIGHT: the relative position between the sample taken at 45° and the perforation pattern is clearly seen.*

Figure 2-12. *BB II, cross section D. LEFT: cross section D after complete sampling. RIGHT: one of the holes used for lifting the blocks was located nearby the sampling profile.*

Figure 2-13. *BB II, cross section C. (1) Muffin-shaped protrusions with empty volumes between some of the muffins. (2) Cut through the material within the SC-rock gap. (3) The bentonite within the SC-rock gap still held together when removed from the SC surface. (4) During the dismantling/sampling a protruding block part fell off in one piece.*

2.3.6 BB II: Cross section G

Whole muffin samples were obtained from cross section G to make a more detailed analysis of the density and water content distribution within a muffin, see Figure 2-14.

2.3.7 BB II: Cross section B

The SC shell was cut at cross section B and in an attempt to remove the steel shell it fell apart as shown in Figure 2-15. The block fell apart in such a way that parts of cross section B ended up in both pieces. Eventually, the sampling turned out successful and only one or two samples were lost in each of the four directions (totally six lost samples).

Figure 2-14. *BB II, cross section G. LEFT: A muffin sample viewed from the bottom. RIGHT: A muffin sample viewed from the top.*

Figure 2-15. *BB II, cross section B. The block fell apart and the inner samples had to be taken from the left piece while the outermost samples had to be taken from the right piece.*

2.4 BB II: Results and analysis

The sampling described above was considered successful. A total of 582 samples were taken and analyzed for water content and density as described in Appendix A. Some of the results are shown and discussed below. All data obtained from analyzing the samples are shown graphically in Appendix B6.

2.4.1 BB II: Results – radial total pressure measurement positions

The radial total pressures were quite different in the two cross sections chosen for measurements and therefore information regarding the bentonite condition in these positions was considered interesting. Figure 2-16 shows how the water content varies in the SC-rock gap in all four positions. In the outermost parts of the SC-rock gap, cross section C has the clearly highest water content. There was much less difference in water content closer to the SC shell.

The dry densities in all four sampling positions are shown in Figure 2-17. The dry density close to the cell wall is significantly higher in cross section D. Just as in the case of the water content, the differences in dry density is much smaller closer to the SC shell.

Table 2-2 shows a compilation of all data from the samples in Figure 2-16 and Figure 2-17 including degree of saturation. Data from the sample taken in the axial total pressure measurement position (Cross section F in Table 2-2) is also included in the table. At dismantling the pore pressure was zero and therefore the total pressure is considered entirely as being generated by the swelling clay, this part of the pressure is called *swelling pressure* in the following. The swelling pressure obtained at each position at test termination is added to the table for comparison. An obvious correlation is seen between dry density closest to the cell wall and swelling pressure. The sample from the axial total pressure measurement has a degree of saturation of 75.9 %. Fully saturated MX-80 of this dry density is expected to generate swelling pressures about 12 MPa, see for instance Karnland et al. (2006).

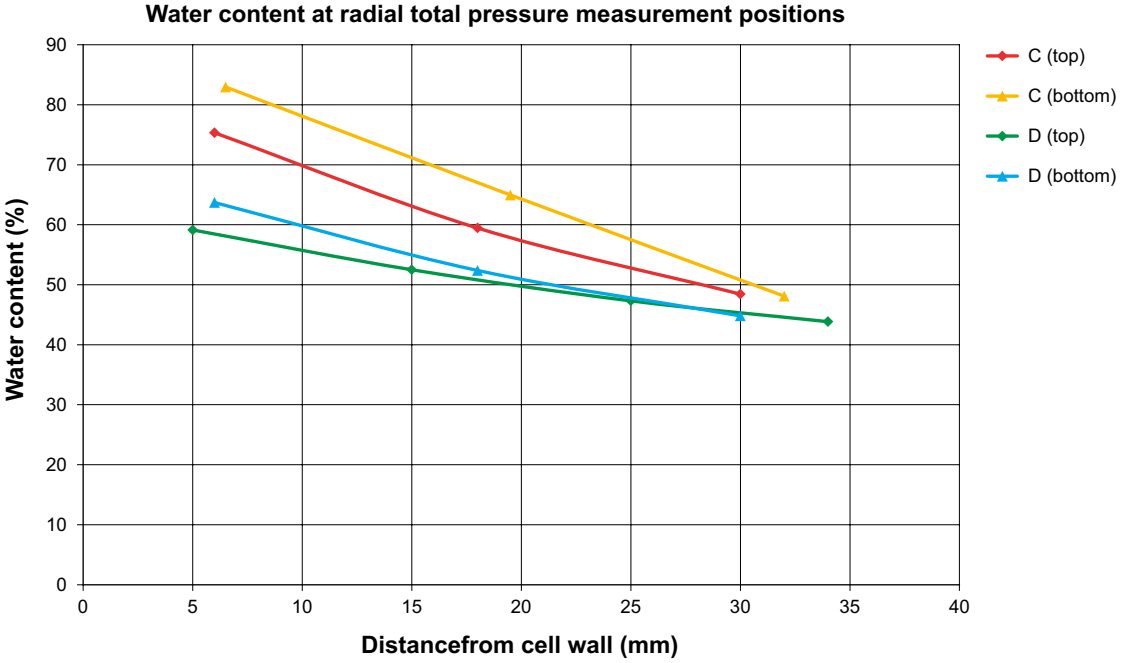

Figure 2-16. *BB II. Water content in the samples taken at radial total pressure measurement positions. Cross section C has clearly higher water content closer to the cell wall.*

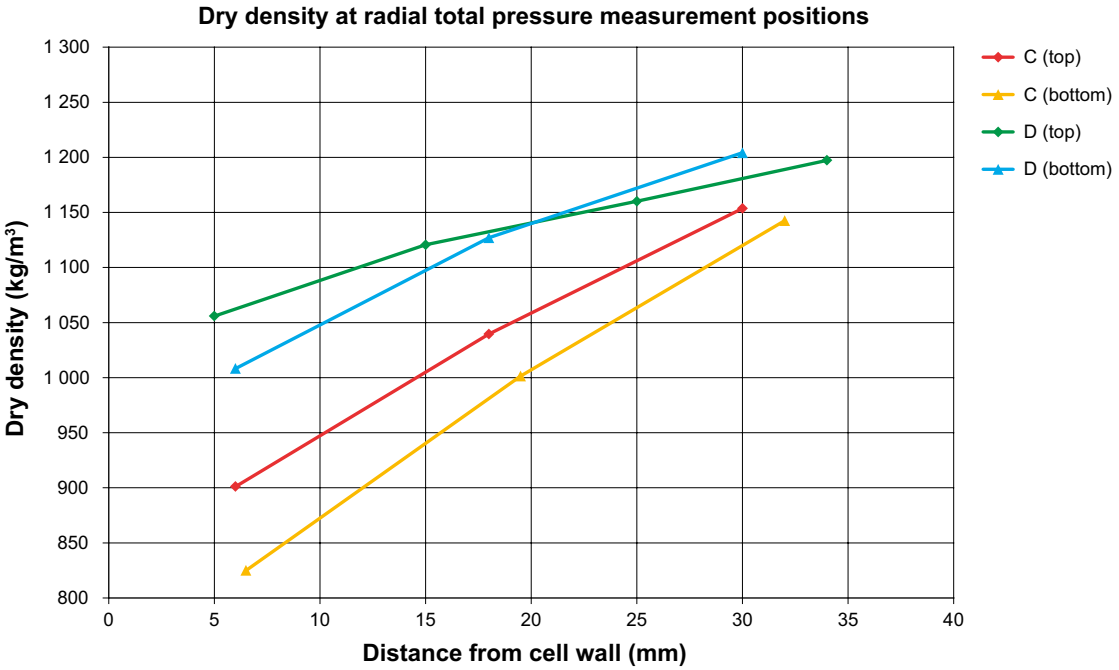

Figure 2-17. *BB II. Dry density in the samples taken at radial total pressure measurement positions. Cross section D has clearly higher dry density closer to the cell wall.*

Table 2-2. BB II. All data from the analysis of the samples taken at the radial and axial total pressure measurement positions. Swelling pressures at test dismantling are added to the table.

Cross section	Direction [°]	Radial distance from cell [mm]	Water content [%]	Dry density [kg/m³]	Degree of saturation [%]	Swelling pressure at test dismantling [kPa]
C	0	6	75.3	901	100.4	70
C	0	18	59.5	1040	98.7	–
C	0	30	48.4	1154	95.5	–
C	180	6.5	83.0	825	97.3	76
C	180	19.5	65.0	1001	101.7	–
C	180	32	48.1	1143	93.3	–
D	0	5	59.1	1056	100.7	241
D	0	15	52.5	1121	98.6	–
D	0	25	47.3	1160	94.2	–
D	0	34	43.8	1197	92.2	–
D	180	6	63.7	1008	100.8	249
D	180	18	52.4	1127	99.3	–
D	180	30	44.8	1204	95.2	–
F	135	200	18.1	1671	75.9	2067

The results from these measurements are further discussed in Section 2.4.3 were also explanations for the large differences in swelling pressure are provided.

2.4.2 BB II: Results – cross sections

Much effort was put in providing a good overview of the water content and dry density distribution over the cross sections selected for analysis. Profiles were plotted with water content, dry density and degree of saturation as a function of the radial distance from the test cell wall. As an example the plotted profiles from cross section D are shown and commented below. The complete data from all cross sections are provided in Appendix B6.

Figure 2-18 shows the water content profiles in cross section D. There is some spreading of the water content close to the cell wall and it does not seem to be related to the directions. Closest to the cell wall the highest water contents are found in 45° and 225°, which are opposite directions, and the lowest water contents are found in 0° and 180° which are also opposite directions. The spread of the water content decreases with the distance from the cell wall and the distribution is very symmetric from 100 mm towards the center.

The dry density profiles from cross section D are shown in Figure 2-19. A similar trend as in the water content distribution is seen; more spread values close to the cell wall and very little spread further in against the center. A variation from 880 kg/m^3 to 1 050 kg/m^3 was determined at the outermost parts, which is very similar to the differences observed just inside the radial total pressure measurement positions (see Section 2.4.1). This is most likely an effect from the sample position relative to the SC perforation hole positions in the SC shell.

Some variations in the dry density are also observed from about 100 mm to 200 mm from the test cell wall. This is probably connected to the structure inside the blocks. In Figure 2-20 a large part of a block that fell to the floor during sampling of cross section C is shown. A number of somewhat tapered layers are visible in the block. This layered structural integrity indicate layered density, probably resulting from the block manufacturing process. This is observed also in cross section D and E. When cross section B was to be sampled the block fell apart and a few samples were lost in each direction. Also here the layers could be clearly seen.

Degree of saturation profiles are shown in Figure 2-21. In the SC-rock gap the bentonite seems to be fully saturated in most samples. As expected, the degree of saturation decreases with the distance from the cell wall. The degree of saturation varies quite widely at the radial distances were the spread in dry density was observed. Further in towards the center of the blocks there is very little spread in the values.

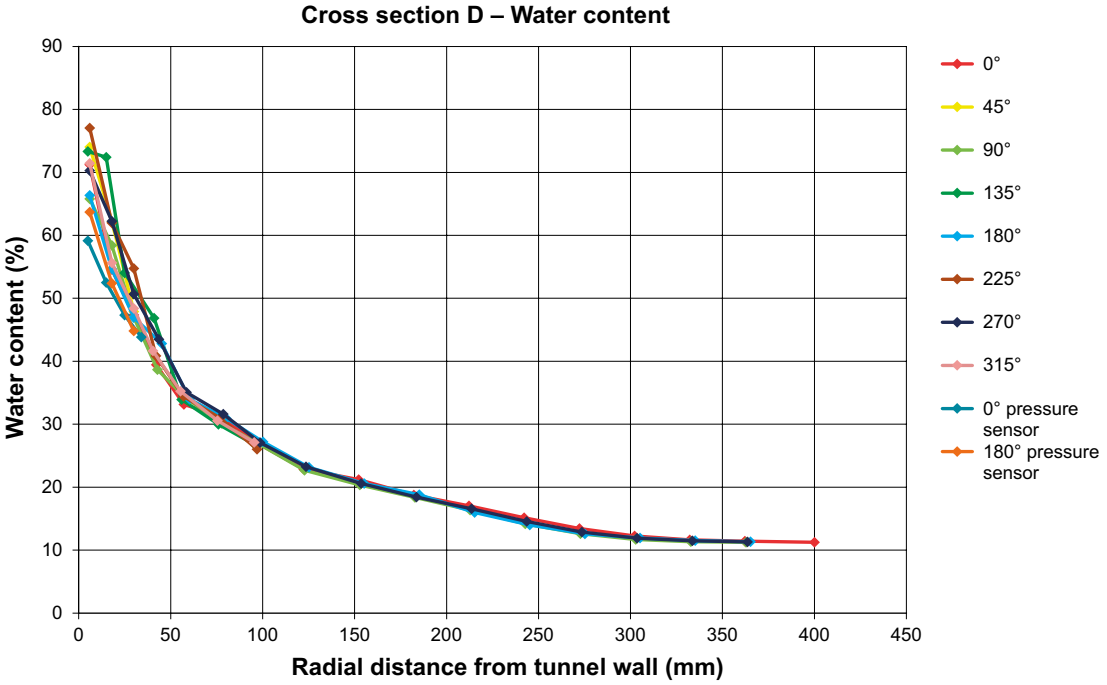

Figure 2-18. *BB II, cross section D. Radial profile of water content.*

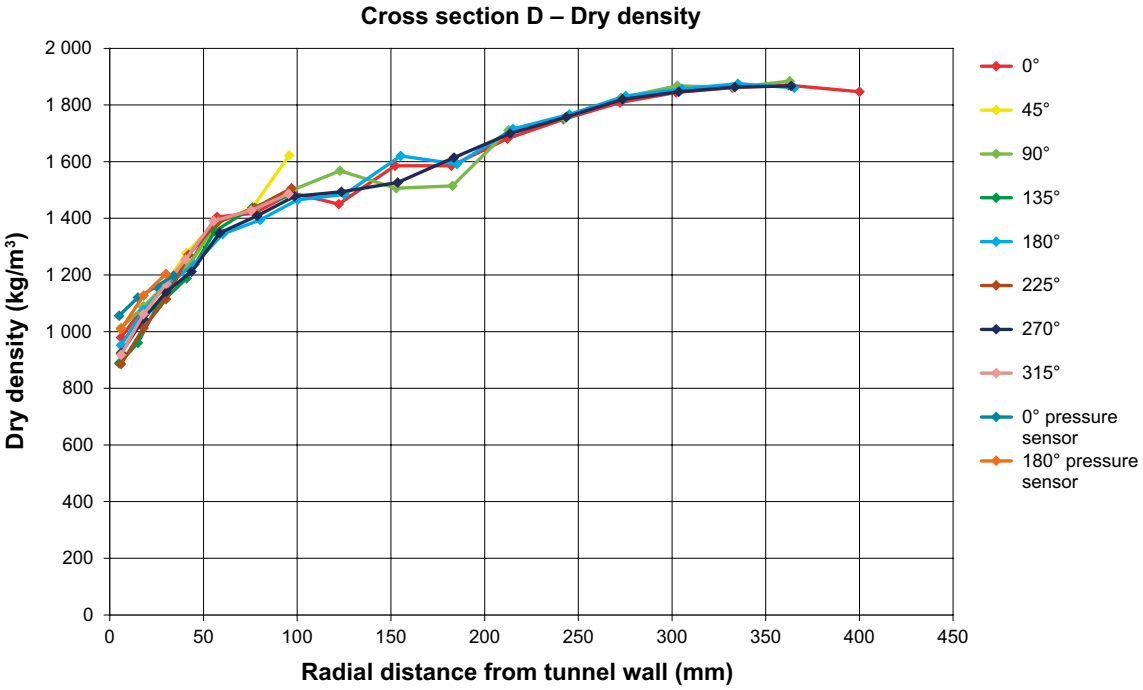

Figure 2-19. *BB II, cross section D. Radial profile of dry density*

Figure 2-20. *BB II, cross section C. A layered structure was revealed when a large block part fell to the floor.*

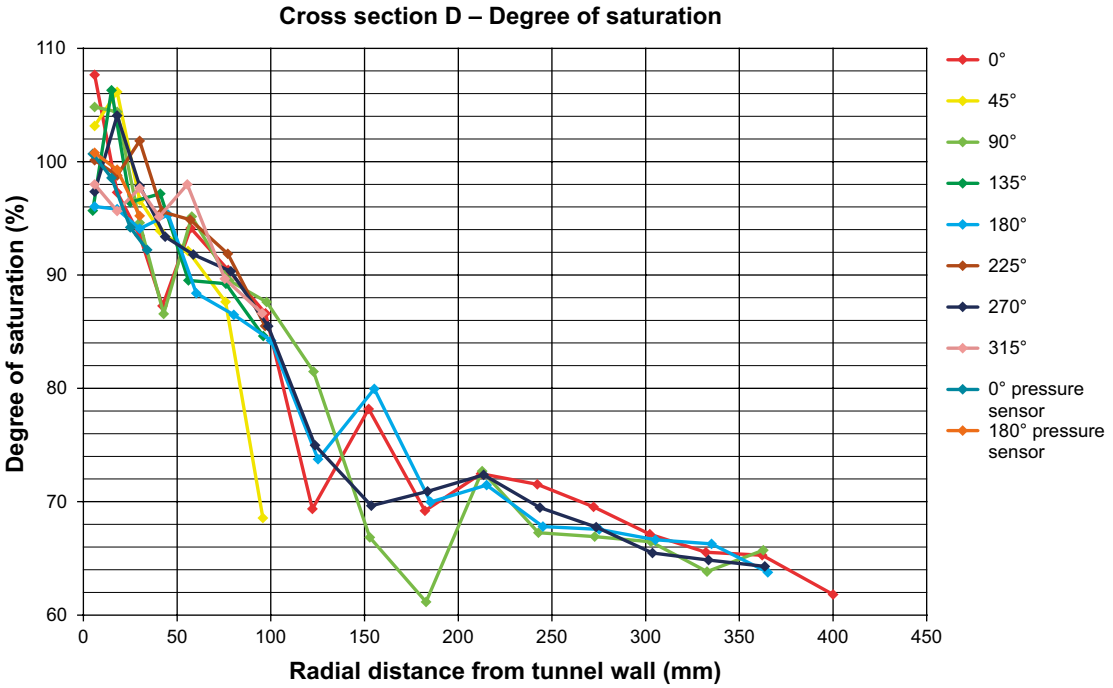

Figure 2-21. *BB II, cross section D. Radial profiles of degree of saturation.*

2.4.3 BB II: Results – SC – rock gap

The muffin-shaped structures originate from the bentonite swelling and being extruded out through the perforations in the SC shell. When the bentonite protrusions reached the enclosure wall the continued clay flow was directed along the enclosure wall and eventually clay coming from neighboring perforations merged. This motion resulted in the, often merged, muffin-shaped structures observed at dismantling. This process seemed to have gone somewhat further closer to the open end (cross section F) as compared to the closed end (cross section A) of the SC shell. Empty volumes between the muffins were most common at the top at cross section A.

At cross section G, four muffins were sampled (in directions 0°, 90°, 180°, 270°) for analysis. Each of the sampled muffins was then divided in 17 samples according to Figure 2-22. Material on each side of the base of the perforation from which the muffin material had come was taken as two samples (X1 and X2). The material on top of the perforation was divided in five sections (1–5) in the plane of the SC shell and three (A, B, C) in the perpendicular direction.

The results from the muffin sample at 0° in cross section G are presented here and the results from the remaining three samples are presented in Appendix B6. Figure 2-23 shows the water content in the 0° sample. It is clearly seen that the water content is increasing closer to the test cell wall and further out from the sample (perforation) center.

The dry density of the 0° sample in cross section G is shown in Figure 2-24. The dry density is significantly lower close to the test cell wall (Level A) and between muffins. Figure 2-25 shows the degree of saturation in the 0° sample in cross section G. The sample is completely saturated in Level A and between the muffins.

The formation of muffins explains the large differences in measured radial swelling pressure between cross sections C and D. A schematic drawing showing the positions of the pressure sensors relative the perforated holes of the SC shell is provided in Figure 2-26. The radial pressure sensors in section D were positioned over the central parts of a muffin where the highest densities were found and, as a consequence, the highest swelling pressures are anticipated, see Figure 2-26. The sensors in cross section C were, on the other hand, positioned at the edge of a muffin, where densities were found to be considerably lower (as compared to the D position densities) and pressures thereby anticipated to be lower as well.

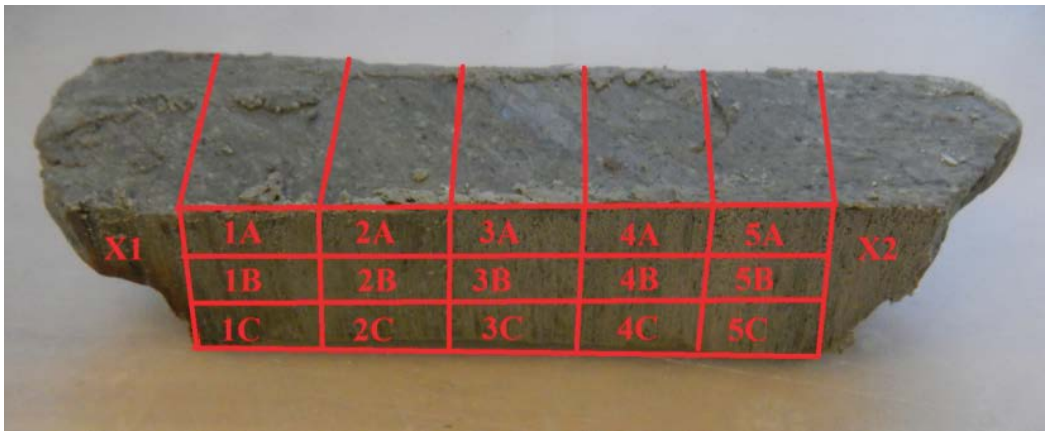

Figure 2-22. *BB II, cross section G. Sample distribution within one of the muffin specimens. Sample X1 and X2 represents the bentonite between the muffins.*

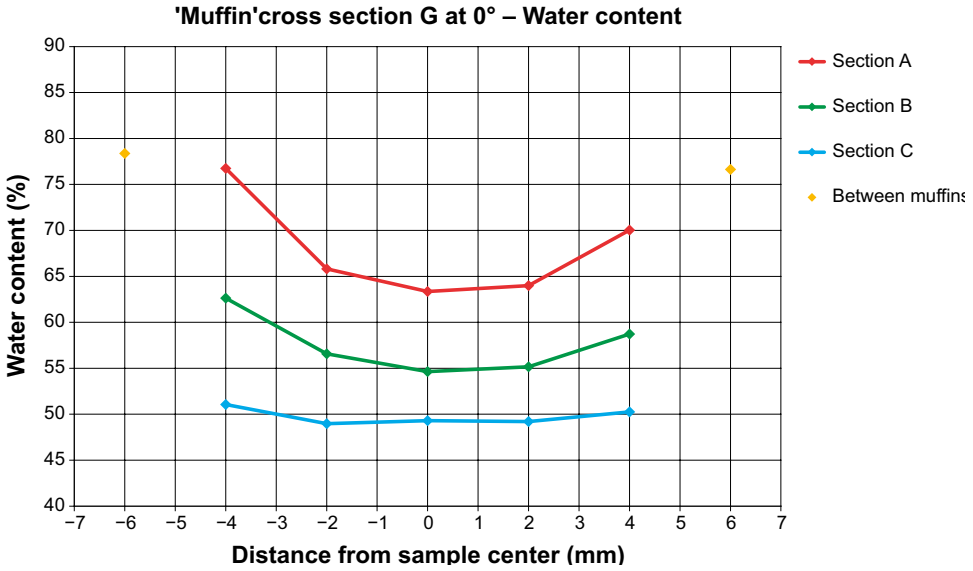

Figure 2-23. *BB II, cross section G. Water content of muffin sampled at 0° in cross section G.*

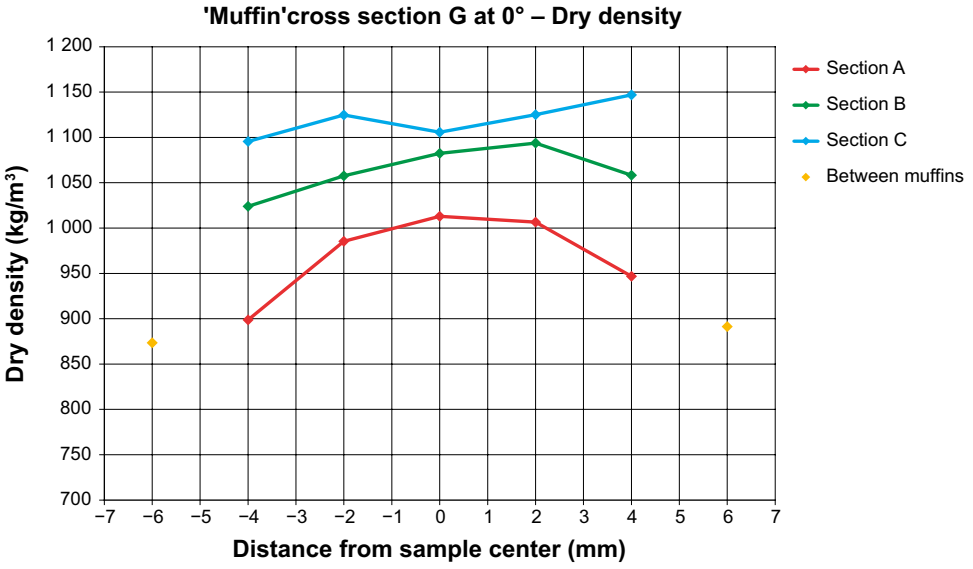

Figure 2-24. *BB II, cross section G. Dry density in muffin sampled at 0° in cross section G.*

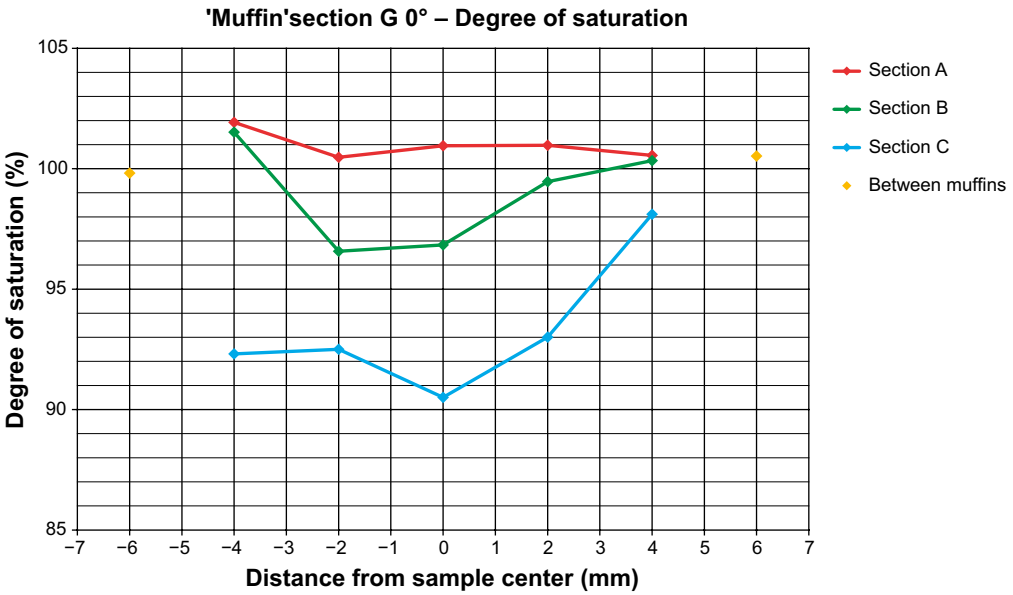

Figure 2-25. *BB II, cross section G. Degree of saturation in muffin sampled at 0° in cross section G.*

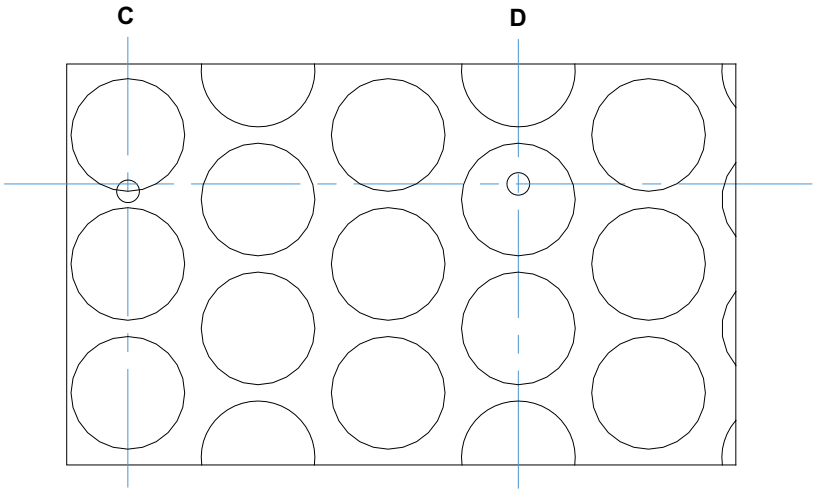

Figure 2-26. *BB II. Radial pressure sensor positions relative to the SC perforation at the top. The positions are almost the same at the bottom.*

2.5 BB II: Comments regarding radial swelling pressure development

In spite of some issues occurring during the operational phase of the BB II test, which affected the data recording process, see Appendix B2, the data produced by BB II test have been a significant part of its success.

The registered data shows that almost instantly at test start, radial total pressure started to build up at the four positions where it was measured. Total pressure may consist of water pressure and "swelling pressure", produced by the clay adsorbing water. For BB II the registered total pressure was in the beginning equal to the water pressure, where the water in the gap transferred the bentonite swelling pressure to the "rock". After some time however, the swelling bentonite reached the "rock" surface and started to pressurize the rock directly.

A positive water pressure was registered during the first 80 days. The water pressure increased up to 65 kPa after approximately 2 days but after 80 days it had decreased to zero. The exact duration for which a pore pressure were registered (80 days) should perhaps be taken with a grain of salt.

Since the pore pressure sensors were positioned on the outside of the lid there could be a situation where the bentonite pressurized water occupying the channels through the lid but there was no water volume between the bentonite and the enclosure wall. No water volume is therefore judged to have been present in the outer gap after 80 days and the registered radial pressure was thereafter a pure swelling pressure from the bentonite.

At termination of the test, after 238 days, the radial pressure varied between 70 to 250 kPa. The higher values were detected in cross section D (195 mm from the end) and the lower in cross section C (in the center of the 1 050 mm long assembly). The large variation in radial pressure has been suggested to depend on the position relative to the perforation pattern.

A description of the kinetic process in the outer part of the SC-system could be as follows. Initially, the swelling bentonite flows through the perforations across the open outer slot and gets in contact with the "rock" surface. Then, "muffin-shaped" clay protrusions are formed when the clay flows along the rock surface and subsequently, muffins are merged together to various degree, dependent on the local conditions.

In the experiment, the homogenization seemed more developed in the lower half of the test. When comparing the positions of the radial pressure sensors relative to the position of the perforation pattern, it was clear that the higher swelling pressures where registered at the central parts of a muffin (with higher density) and the lower swelling pressures where registered in positions between the muffins (with lower density).

2.6 BB II: Comments regarding density distribution

The blocks inside the SC had an initial dry density between 1 859 and 1 875 kg/m^3 and a water content of 10.6 % which yields a degree of saturation of 60 %. The sample analysis showed that there was a strong radial density gradient from the "rock" surface to the block center for all cross sections.

The radial density profile could be described using the character within three radial sections (the radial coordinate given below is directed from the test cell wall and inwards):

1. 0–50 mm: The density closest to the test cell wall varied between 800 and 1 000 kg/m^3 with the highest values in the lower half of the test setup. Just inside the SC shell, at 50 mm, the density had increased to between 1 200 and 1 400 kg/m^3.
2. 50–100 mm: The density varied between 1 200 and 1 400 kg/m^3 just inside the shell up to approximately 1 500 kg /m^3 at 100 mm.
3. 100–400 mm: The density was very similar in all directions at this part. The innermost part, at 300–400 mm, had a density very close to the initial density (1 859 to 1 875 kg/m^3) i.e. this part had not swollen.

It should be noted that the samples from the SC-rock gap were taken from the "muffins". Between the muffins, close to the SC however, there were open voids. Thus, the average density of the buffer in the SC-rock gap was lower than what is given above.

3 BB III

The main focus of this study was the capability of the DB buffer to prevent thermally induced spalling at the drift rock wall. Extremely dry conditions were simulated. No water was allowed to enter the system except that, in accordance with DAWE, artificially provided at installation. The buffer blocks were prepared as to simulate the initial state of the system.

3.1 BB III: Test setup

The test equipment consists of the shorter section of the BB equipment (see Figure 1-5). An extra steel lid was manufactured and used to close the test cell on the side where the longer section originally should be connected. The main dimensions and features of the test equipment are shown in Figure 3-1. The inner diameter of the test cell varies between 800 and 804 mm. The larger diameter is at one section originally made in order to install a filter for simulating a water bearing fracture, Figure 3-1. The length of the test cell is 350 mm.

The test cell and the lids are equipped with outlets (the same type as described for BB II) that make it possible to measure the radial and axial total pressure. Each measuring point consists of a piston with a diameter of 20 mm that transfers the swelling pressure from the bentonite to a load cell placed on the outside. The radial and axial pressure measurements are marked in Figure 3-1.

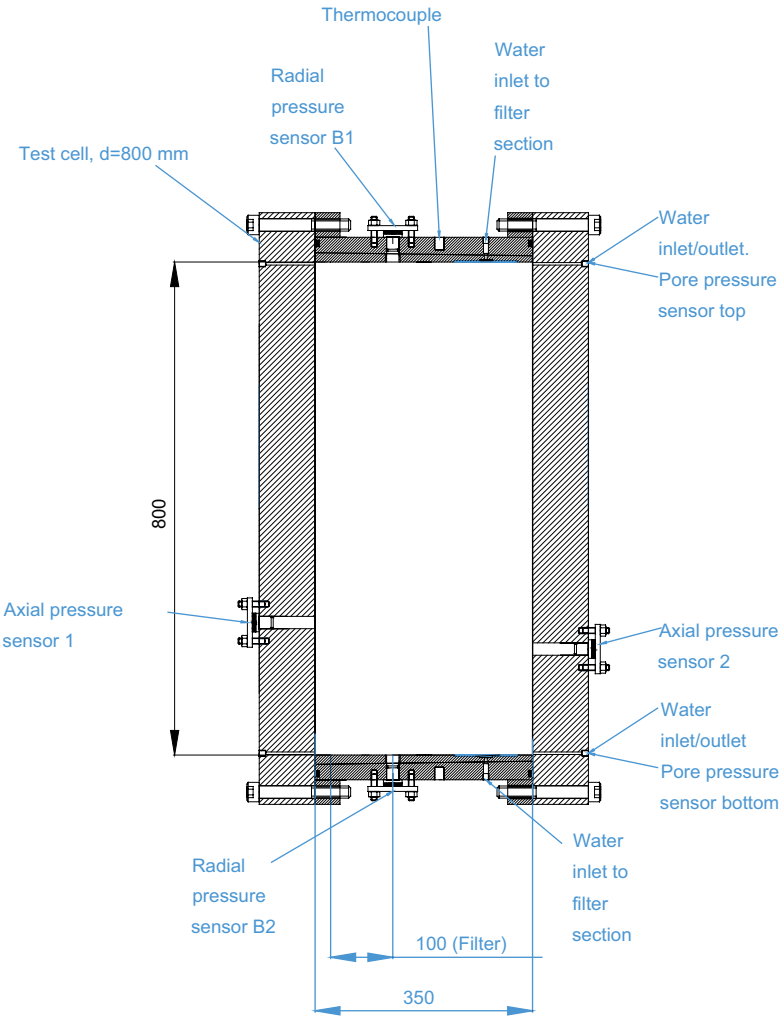

Figure 3-1. *BB III. Schematic drawing showing the BB III test equipment.*

Two valves used for de-airing and water filling were connected on one of the lids to the block-rock gap. One was placed as low as possible (water filling) and one as high as possible (de-airing).

One of the most important objectives of the tests was to determine the radial swelling pressures. In the test two radial pressure sensors were included. In addition, two load cells were used to register the axial total pressure, one at each end of the test cell. Two pore pressure sensors were also connected, one at the water inlet valve and one at the de-airing valve. The temperature of the test cell was registered together with the temperature and relative humidity of the room in order to monitor the surrounding climate.

More information about the sensors can be found in Appendix C1.

3.1.1 BB III: Buffer

The bentonite block was manufactured in an almost identical way and with the same MX-80 bentonite as the blocks used in BB II (see Section 2.1.2), but there were some different features. The distance blocks are designed to have a lower dry density and higher water content. The raw material was therefore mixed to a water content of 21.4 % and compacted using the compaction pressure 36 MPa. The bulk density of the distance block is similar to the bentonite blocks inside the SC, but since the water content is higher the dry density is lower.

After compaction the block was transported to Finland where it was milled to a diameter of 715 mm. Finally it was transported back to Clay Technology in Lund, Sweden. During transports and between manufacturing and processing the blocks were wrapped in double plastic covers in order to prevent them from drying.

During the assembly of the test, block weight and dimensions were again determined and based on these figures the bulk density of the block was calculated. Compared to the buffer blocks in BB II the distance block hade expanded very little, which is logical since the water content is much higher, and the calculated density was almost the same as the one determined earlier. Table 3-1 shows a compilation of data from the distance block. The water content determined in conjunction with the block manufacturing was used also when calculating the dry density at the assembly.

Four bolts, screwed into pre-drilled holes in the block, acted as “feet” centralizing the block in the test equipment at installation.

Table 3-1. BB III. Compilation of block data.

Block parameters determined in conjunction with manufacturing and machining	
Block no.	***BB II012B1***
Water content [%]	21.4
Bulk density [kg/m^3]	2086
Dry density [kg/m^3]	1718
Diameter [mm]	715±1
Height [mm]	354.1
Block parameters determined in conjunction with test assembly	
Weight [kg]	292
Height [mm]	350 (adjusted)
Bulk density* [kg/m^3]	2078
Dry density* [kg/m^3]	1712
Degree of saturation [%]	95.3

* These densities were calculated from the weight and dimensions determined during the test assembly and a water content of 21.4 %.

3.2 BB III: Operation

The operational phase started with the artificial water filling, injecting water through a tube at about 3 meters of water head at the same time as air was escaped through the dedicated outlet valve. 36.3 liters of water was injected during 1.5 hours.

Just like in the BB II test low radial swelling pressures was expected, mainly depending on the large initial gap and the fact that there should not be access to additional water after the first artificial water filling of the gaps, and therefore efforts were made to have load cells with a suitable range. However, one of the 445 N load-cells (measuring radial pressure at the top) turned out to not give reliable values and was therefore exchanged to a load-cell with 2 225 N capacity after approx. 24 hours test duration. The calibration and the validation showed that this load cell had a good accuracy within the desired range so this was not considered to influence the registered data. Below follows a description of the pressure evolution during the operational phase. Some additional information regarding the sensors is given in Appendix C1. A description of early pressure responses is given in Appendix C2 and sensor data regarding room climate is given in Appendix C3.

Registered sensor data from the entire test is shown in Figure 3-2. It can be seen how the radial total pressure follows the pore pressure quite closely for the first 30 days. The highest observed pore pressure was observed at the bottom sensor; 46 kPa on day 29. On day 59 the pore pressure had decreased to zero and the radial total pressure could now be completely considered as a swelling pressure. The radial swelling pressure continued to increase throughout the test and by test termination on day 218 it was 99 kPa at the top and 136 kPa at the bottom. The temperature variations have had a small influence on the pressure measurements on the daily basis but they are not assessed to have influenced the trends in the pressure measurements.

The registered axial total pressure from both sides was negative throughout almost the entire test, except for the first 25 days, see Figure 3-3. A load cell cannot register tensile stress and therefore the registered data was not assessed to be a reasonable outcome. The results from the sampling just inside the axial sensor positions, see Section 3.4.1, show that there have been a small increase of water content and at the same time a small decrease of density compared to the initial. The degree of saturation was close to the initial at termination. It is uncertain if a swelling pressure should occur under these circumstances. The validation of the sensors showed, however, an error of 1.25 % and 1.75 % at maximum load on the load cell. This confirms that the calibration was valid also after the test and that the negative pressure registered must be due to some other problem, probably earth fault at the electrical connection between sensor and data logger.

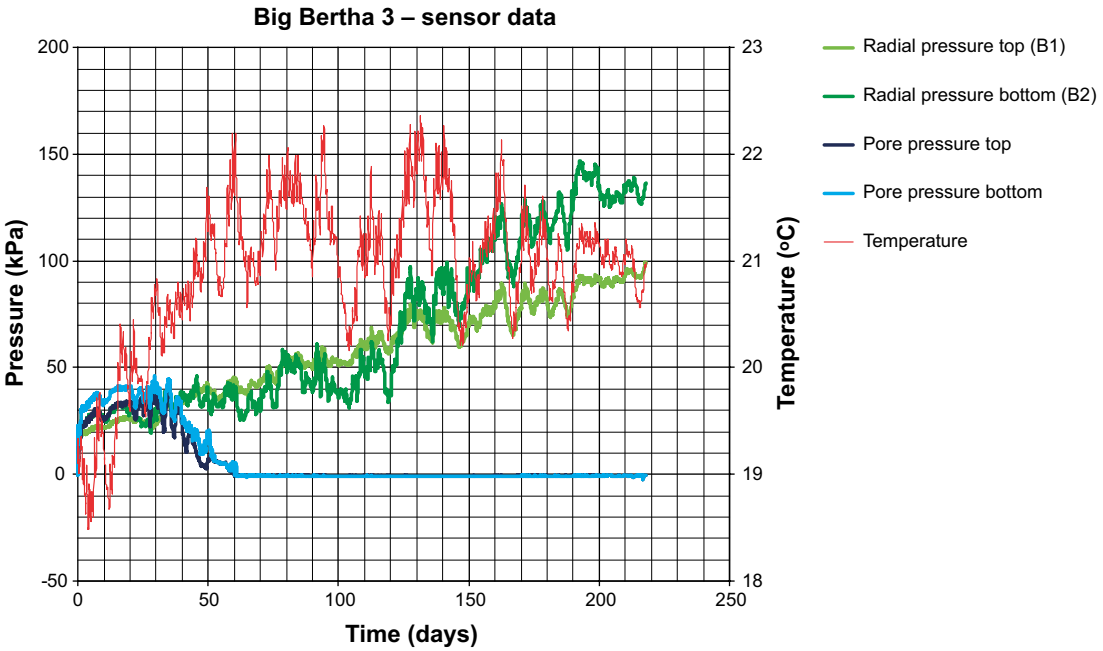

Figure 3-2. *BB III. Evolutions of radial total pressure, pore pressure and temperature in BB III.*

3.3 BB III: Dismantling and sampling

A coordinate system similar to the one used in BB II was defined, see Figure 3-4. The chosen cross sections and the directions are marked out to the left in the figure. The position of cross section B was chosen since it was logical to sample the cross section in which the radial total pressure was measured. Cross section C was chosen to make the analysis symmetric. The same naming system was used as in the BB II test. Every sample was named after cross section, direction and radial distance from the test cell wall. E.g. A_90_60 was taken in cross section A in direction 90° at a radial distance of 60 mm from the test cell wall.

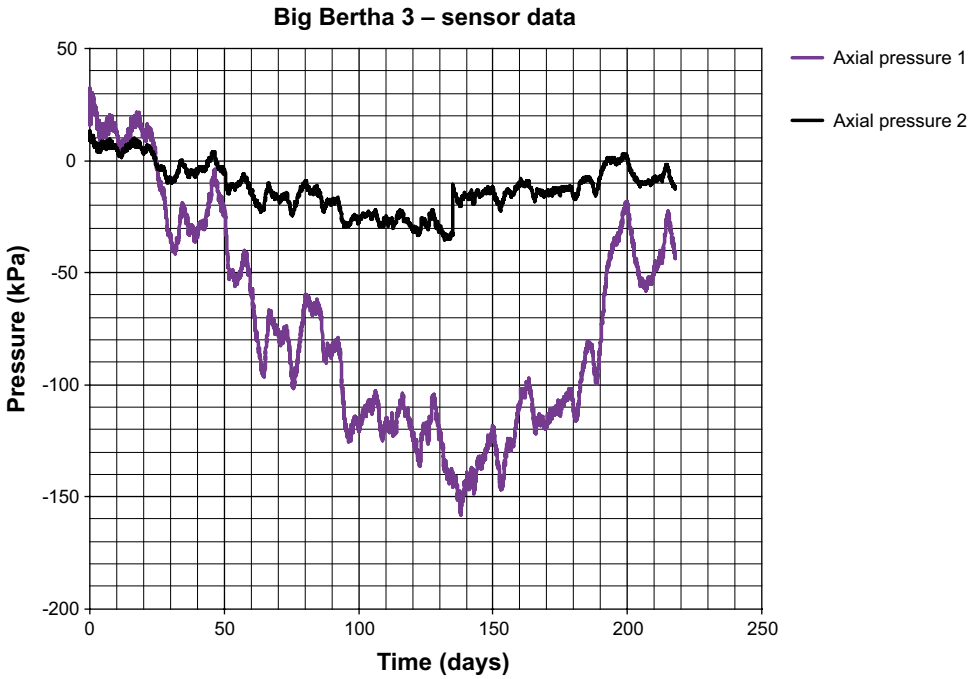

Figure 3-3. *BB III. Evolutions of axial total pressure in BB III.*

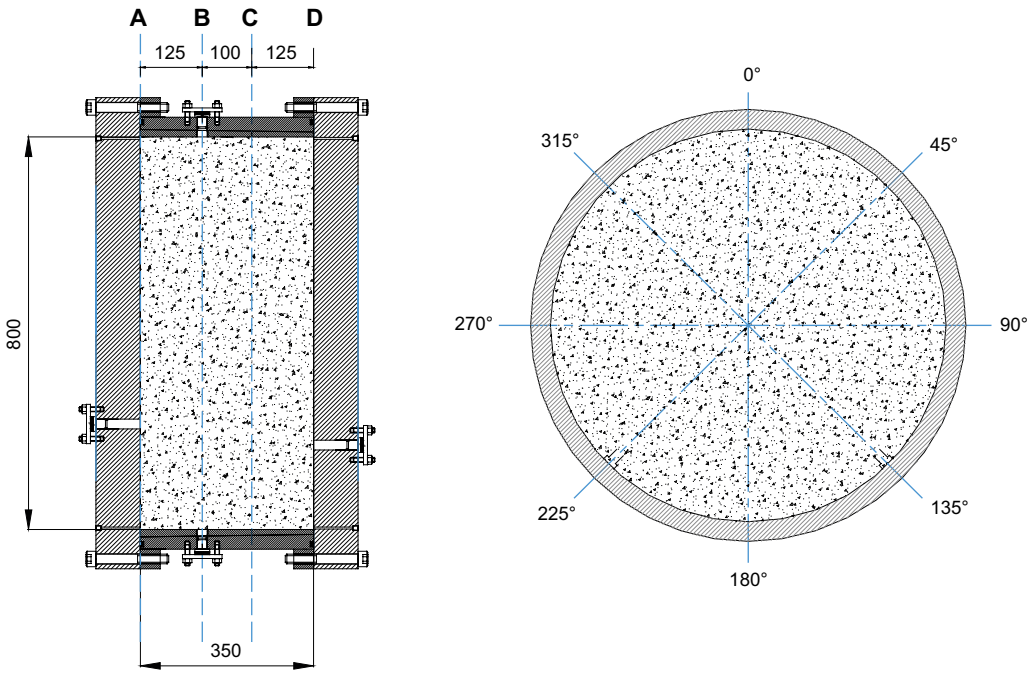

Figure 3-4. *BB III. LEFT: definition of the cross sections chosen for sampling. RIGHT: definition of the angular coordinate chosen for sampling when looking from A towards D.*

The samples planned to be taken in a fully sampled cross section profile are shown in Figure 3-5. In all eight directions three 15 mm samples were taken in the outermost part against the test cell wall and also two additional 30 mm samples. In four directions (0°, 90°, 180° and 270°) there were additional 9 adjacent 30 mm samples taken all the way into the center. A final sample was taken in the center position. Samples were also taken at the radial and axial total pressure measurement positions.

Below follows a selection of photographs taken and observations made during the dismantling and sampling of the test.

3.3.1 BB III: Cross section A

Also in this cross section two different types of sampling took place; the bentonite at the axial total pressure sensor was sampled (225°, 200 mm from the test cells wall) and the cross section was sampled according to plan. Figure 3-6 shows sampling of cross section A with the knife-technique (1), sampling with the hand-drill and hole-saw technique (2) and the fully sampled cross section (3).

3.3.2 BB III: Cross section D

Sampling of cross section D was performed in an identical way as for cross section A. The position of the axial total pressure measurement was in line with the 180° profile and therefore two originally planned samples were discarded to make it possible to take the sample at the axial total pressure measurement position (200 mm from the test cell wall). Figure 3-7 shows cross section D after sampling.

3.3.3 BB III: Cross section B

Two types of sampling took place in cross section B. Sampling of the buffer close to the positions of the radial total pressure measurements and sampling according to the cross section sampling plan as given in Figure 3-5. In Figure 3-8 the cross section at uncovering and finalized sampling are shown to the left and right, respectively.

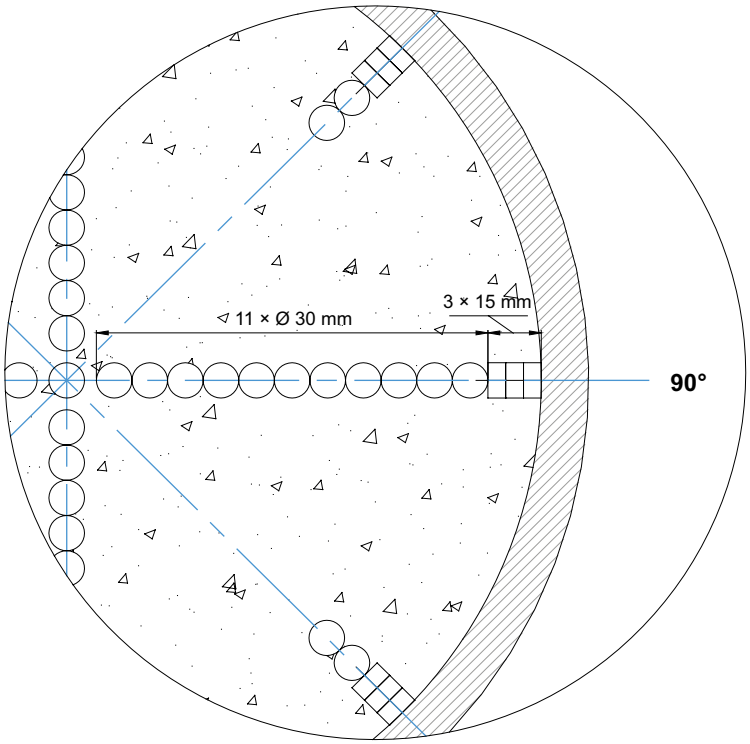

Figure 3-5. *BB III. Close-up of a cross section profile showing the planned sampling of each cross section.*

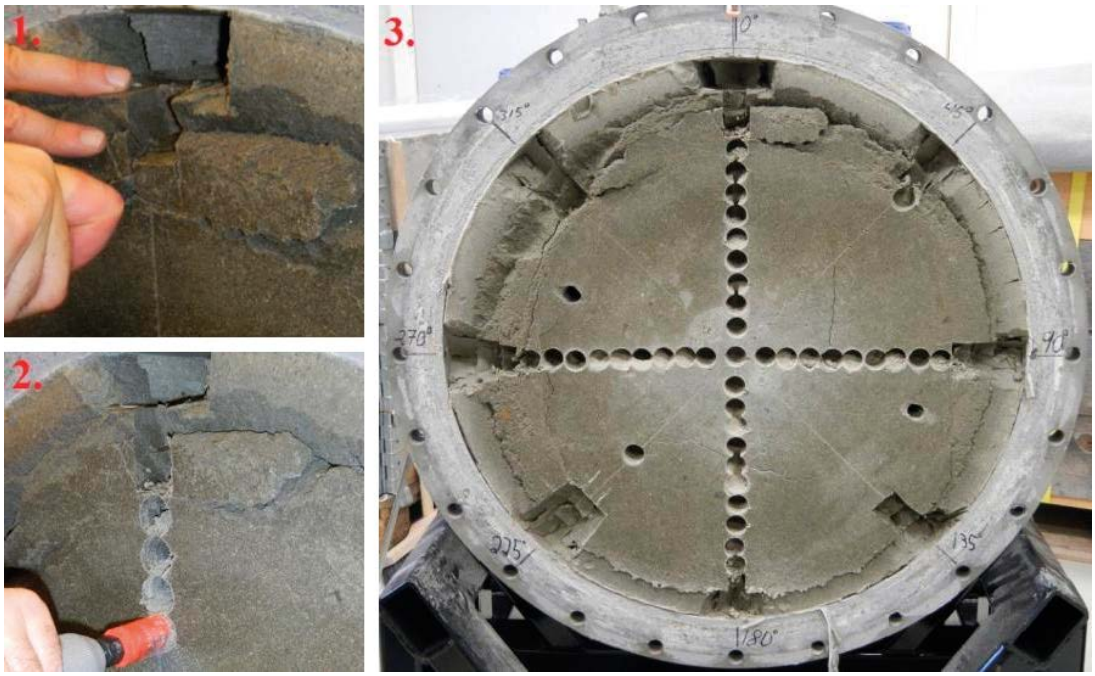

Figure 3-6. *BB III, cross section A. (1) Sampling with knife technique. (2) Sampling with the core drill technique. (3) The cross section after complete sampling.*

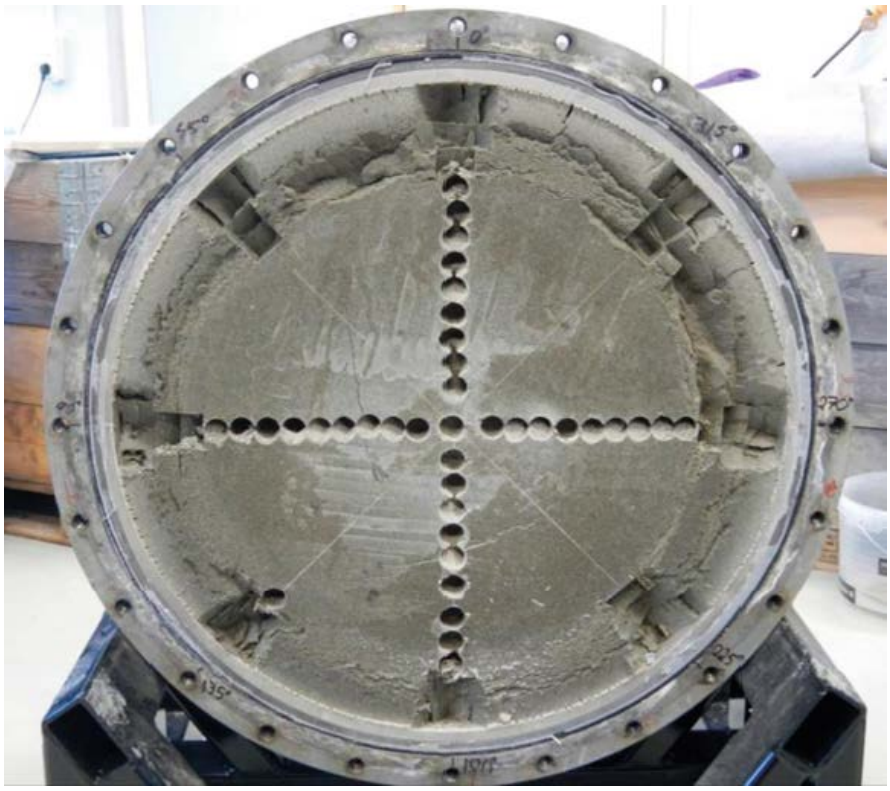

Figure 3-7. *BB III, cross section D. Cross section after complete sampling.*

3.3.4 BB III: Cross section C

Figure 3-9 shows cross section C after the complete sampling. As seen in the photo a large block part (against the cell wall from 270°–0°) fell off and had to be sampled separately. Therefore two samples in 315° and one sample in 0° were lost.

Figure 3-8. *BB III, cross section B. LEFT: Uncovering of cross section B. RIGHT: Cross section B after complete sampling.*

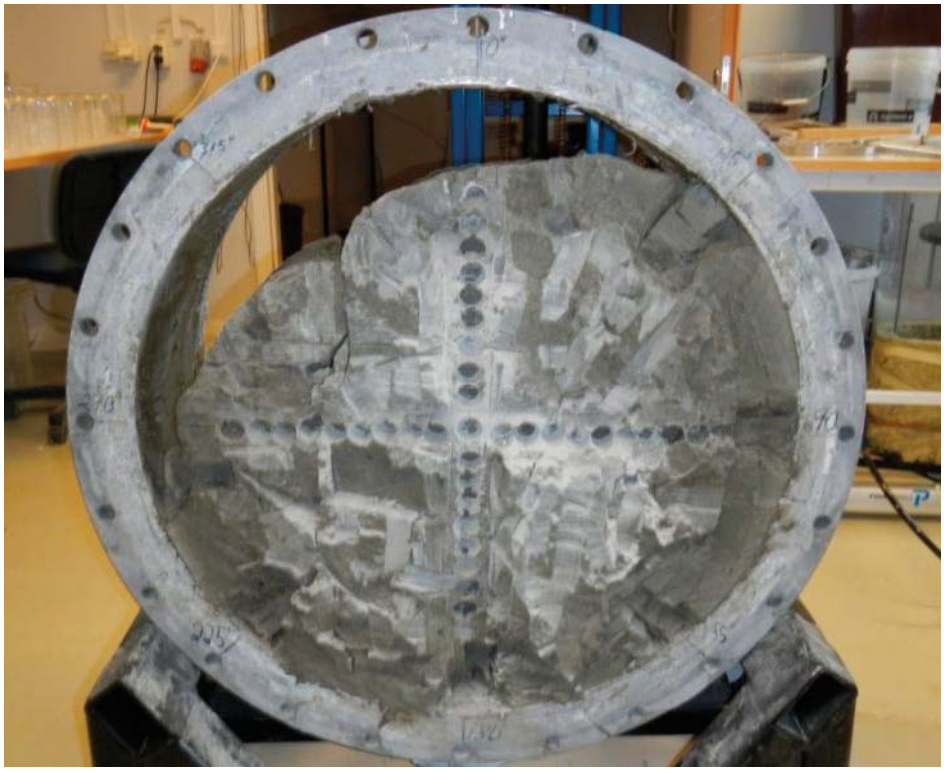

Figure 3-9. *BB III, cross section C. Cross section after complete sampling. A large block part fell off and had to be sampled separately. Therefore a total of three samples were lost.*

3.4 BB III: Results and analysis

The sampling was successful and only 5 samples were lost. Out of 315 planned samples 310 were successfully taken and analyzed for water content and density. Some of the results are shown and discussed below. All data obtained from analyzing the samples are shown graphically in Appendix C4.

3.4.1 BB III: Results – total pressure measurement positions

The pore pressure was zero at dismantling so the total pressure can therefore be considered entirely as being generated by clay expansion, what is called swelling pressure in the following. The radial swelling pressures were quite similar at test dismantling, but the registered swelling pressure in the bottom was slightly higher. Figure 3-10 shows the water content and Figure 3-11 shows the dry density of the samples taken at the radial total pressure measurement positions. The dry density was somewhat higher in the bottom sample, which was expected since the swelling pressure was slightly higher in this position.

Table 3-2 shows the complete data from all total pressure measurement positions, including axial directions (A and D). The radial swelling pressures are also shown in the table.

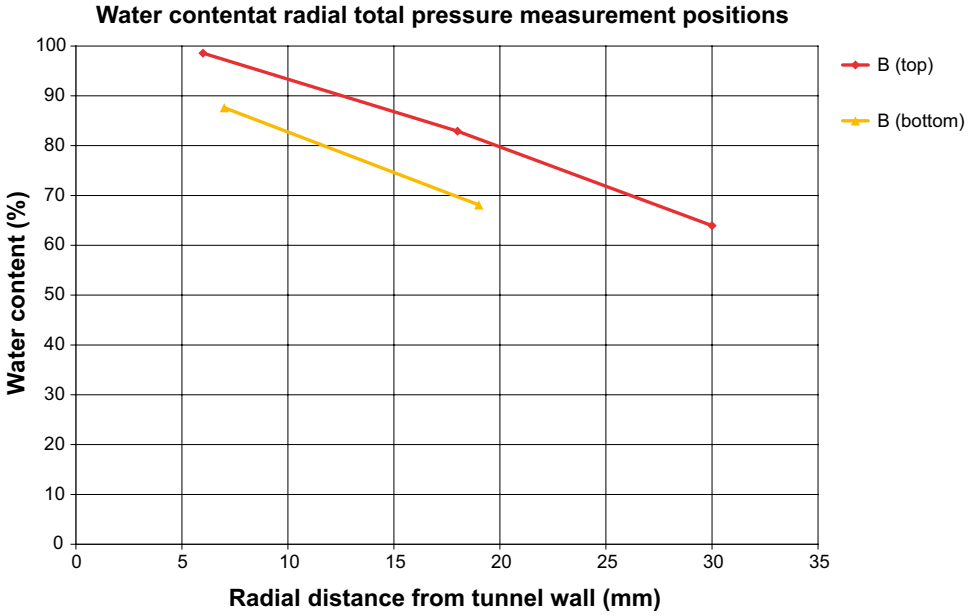

Figure 3-10. *BB III. Water content for the samples taken at the radial total pressure measurement positions plotted versus the radial distance from the test cell wall.*

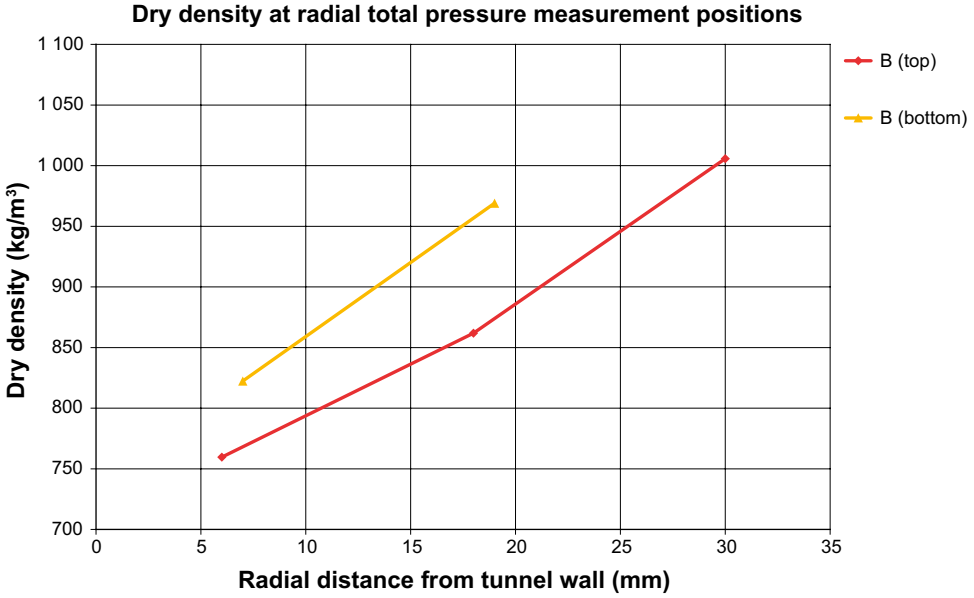

Figure 3-11. *BB III. Dry density for the samples taken at the radial total pressure measurement positions plotted versus the radial distance from the test cell wall.*

Table 3-2. BB III. Data from samples taken just inside the pressure measurement positions.

Cross section	Direction [°]	Radial distance from cell [mm]	Water content [%]	Dry density [kg/m^3]	Degree of saturation [%]	Swelling pressure [kPa]
B	0	6	98.6	760	103.0	99.1
B	0	18	82.9	862	103.5	
B	0	30	64.0	1006	100.8	
B	180	7	87.6	822	102.3	136.3
B	180	19	68.1	969	101.3	
A	225	200	24.3	1641	97.3	–
D	180	200	24.3	1629	95.5	–

3.4.2 BB III: Results – cross sections

Much effort was put into making a good overview of the water content and dry density distribution over the cross sections selected for analysis. Profiles have been plotted showing water content, dry density and degree of saturation as a function of the radial distance from the test cell wall. The plotted profiles from cross section B are shown as an example in Figure 3-12. The complete data from all cross sections are found in Appendix C4.

Figure 3-12 shows the water content profiles in cross section B. Initially the block had a water content of 21.4 %. The water content has no or very little change from about 300 mm distance from the test cell wall and inwards to the block center. Note that the water content in the samples taken at the positions of radial total pressure measurement matches the other eight profiles well.

Figure 3-13 shows the dry density profiles in cross section B. Also in this plot there is no observed difference from the samples taken at the positions of radial total pressure measurement and the other profiles. The innermost sample for the 270° direction has a slightly lower value than the surrounding samples. This is likely the effect of a disturbed density determination.

The degree of saturation profiles are shown in Figure 3-14. In the block-rock gap the bentonite seems fully saturated in most samples. The degree of saturation was high in the distance block at installation and is therefore expected to be unchanged throughout the test from about 300 mm from the enclosure wall and inwards (i.e. the region where no or very little water uptake has occurred, Figure 3-12). The inner most sample in the 270° profile shows a somewhat low value. This origins from what is suspected to be a disturbed density determination mentioned above when discussing the dry density profiles in Figure 3-13.

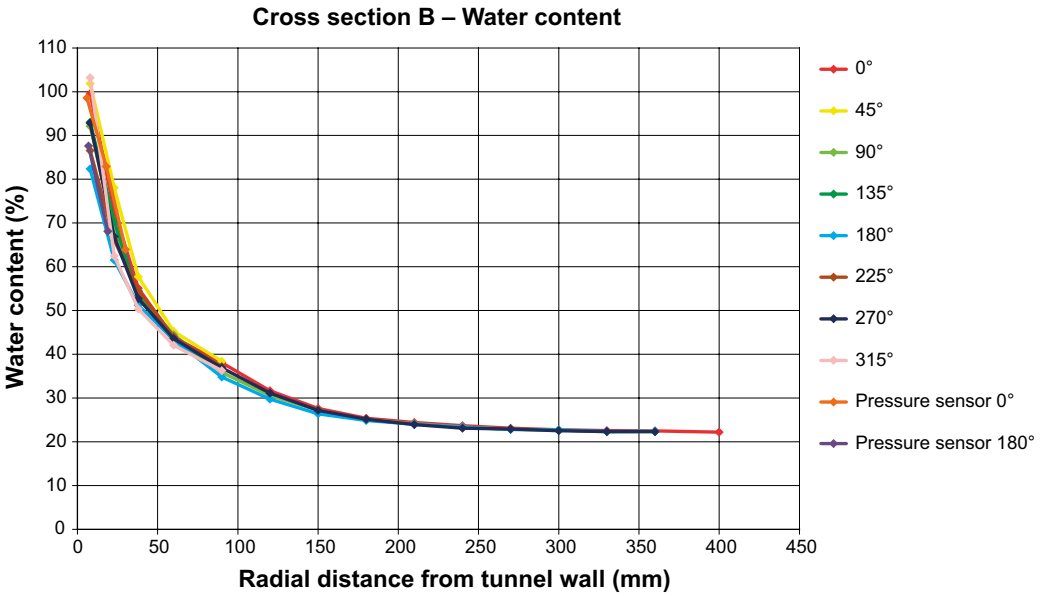

Figure 3-12. BB III. Radial profile of the water content in cross section B plotted versus the radial distance from the drift wall.

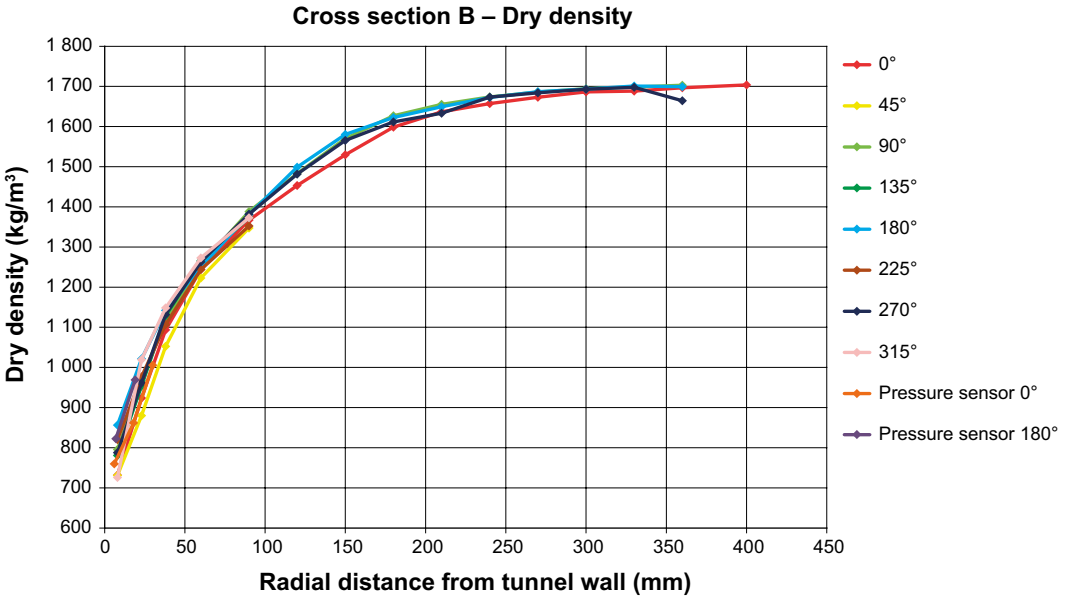

Figure 3-13. *BB III. Radial profiles of dry density in cross section B plotted versus the radial distance from the test cell wall.*

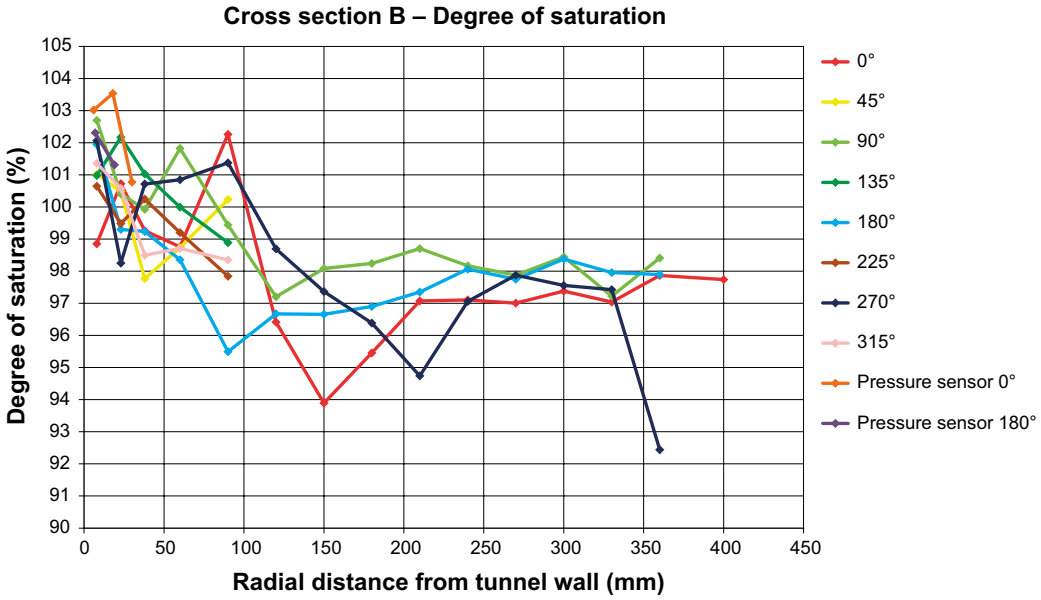

Figure 3-14. *BB III. Radial profiles of the degree of saturation in cross section B plotted versus the radial distance from the test cell wall.*

3.5 BB III: Comments regarding radial swelling pressure development

The pressure behavior of the BB III test was similar to BB II. Immediately after the gaps being water filled and the valves being closed, the water pressure started to increase. The maximum water pressure, approximately 45 kPa, was reached after 30 days. After that the water pressure started to decrease to become zero after 60 days. The radial pressure was at this time approximately 40 kPa. After 218 days the radial swelling pressure was 100 kPa at the top and 140 kPa at the bottom. The difference between top and bottom measurements probably depend either on:

- Sedimentation of bentonite in the free water during the beginning of the test, which increased the density at the bottom, or
- An eccentric installation of the blocks.

Analyzing the samples of cross section A, B, C and D showed that there were small differences in densities at the top and at the bottom (see Appendix C4).

3.6 BB III: Comments regarding density distribution

The distance block had an initial dry density of 1 712 kg/m^3 and an initial water content of 21.4 % which yielded a degree of saturation of 95 %. The sampling after the test showed there was a strong radial density gradient from the “rock” surface into the block center for all cross sections.

The radial density gradient could be described by using three radial sections (the radial coordinate starts at the test cell wall):

1. 0–50 mm: The density closest to the test cell wall (0 mm) varied between 650 and 850 kg/m^3. The outer sections, A and D, showed the lowest densities; probably dependent on friction acting on the interface between the swelling bentonite and the steel lids. At 50 mm the density had increased to between 1 150 and 1 250 kg/m^3.
2. 50–100 mm: The density varied between 1 150 and 1 250 kg/m^3 at 50 mm up to and above 1 400 kg/m^3 at a distance of 100 mm.
3. 100–400 mm: The densities were similar in all directions for this section. The innermost sub-section between 300–400 mm had a density close to the initial density. Thus, these parts had not been swelling.

4 BB IV

This test mainly aimed at studying the initial water uptake and swelling process of the buffer in a SC section when water is supplied at the drift rock wall. The test also provides information about the early evolution of the buffer which can be used for testing models simulating the KBS-3H system. The buffer blocks were prepared as to simulate the initial state of the system.

4.1 BB IV: Test setup

The test layout is shown in Figure 4-1. The test equipment was the same as was used in BB III, but completed with a steel SC shell representation with dimensions according to the latest KBS-3H design including a titanium SC shell.

A filter mat with a width of 100 mm was positioned in the recess that goes all around the test cell periphery. The filter mat simulated a water bearing fracture zone, feeding the bentonite with additional water during the test duration. The amount of water consumed by the bentonite was measured continuously during the operational phase.

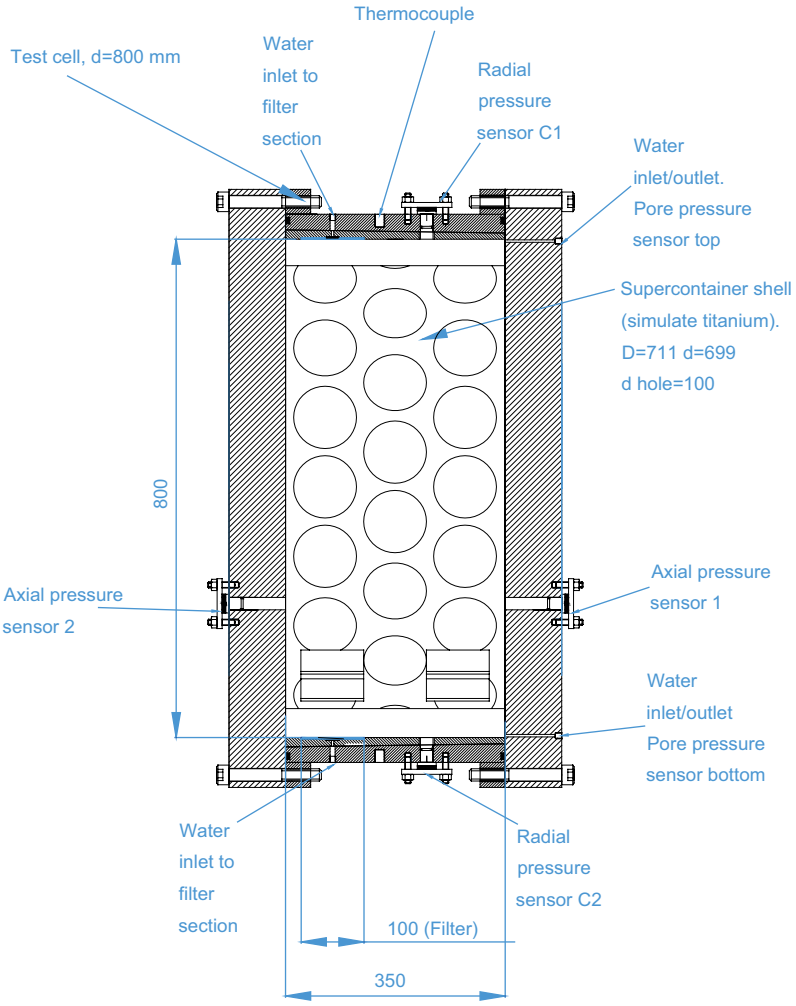

Figure 4-1. *BB IV. Schematic drawing showing the BB IV test layout.*

Load cells were installed at four positions. Two measuring radial total pressure at the same cross section, positioned 125 mm from one of the end lids, (C1 and C2), and two measuring the axial total pressure installed in the lids (A1 and A2). Both axial total pressure sensors were positioned 200 mm from the enclosure wall. A1 was positioned in the 135° direction at the side supplied with water and A2 in the 225° direction on the opposite side. Two pore pressure sensors were also installed, one at the lower water inlet valve and one at the upper de-airing valve. The temperature of the test cell was registered and also the temperature and relative humidity of the room in order to monitor the surrounding climate.

4.1.1 BB IV: SC shell representation

The SC shell representation was made out of steel and had the appearance shown in Figure 4-2. The dimensions were adapted to the then new SC shell design in titanium, i.e. the outer diameter and the wall thickness were decreased as compared to the SC shell made of copper. In accordance with the full scale design, the SC shell was equipped with feet as to be centered in the enclosure.

4.1.2 BB IV: Buffer

The bentonite block was manufactured in the beginning of 2012 in Ystad, Sweden. There was a small deviation regarding the bentonite block diameter when adapted to the BB-scale. The block diameter, 687 mm, was 3 mm smaller than ideal, resulting in a larger gap width between block and SC. Despite this deviation in dimension the buffer block was used in the test since it was the only block available at the time of installation with the otherwise correct properties.

The block data is provided in Table 4-1. The upper part of the table provides data determined in conjunction with the manufacturing of the block while the lower part provides data determined in conjunction with the test assembly. The bulk density and dry density provided in the lower part of the table was calculated using the latest determined weight, dimensions and water content.

As shown in Table 4-1 the buffer block had a dry density of 1 915 kg/m^3 and a water content of 10.8 %. These figures should be compared with the figures set for the reference design (dry density = thus somewhat high (10 kg/m^3 higher than the design maximum) while the water content was well within the set range.

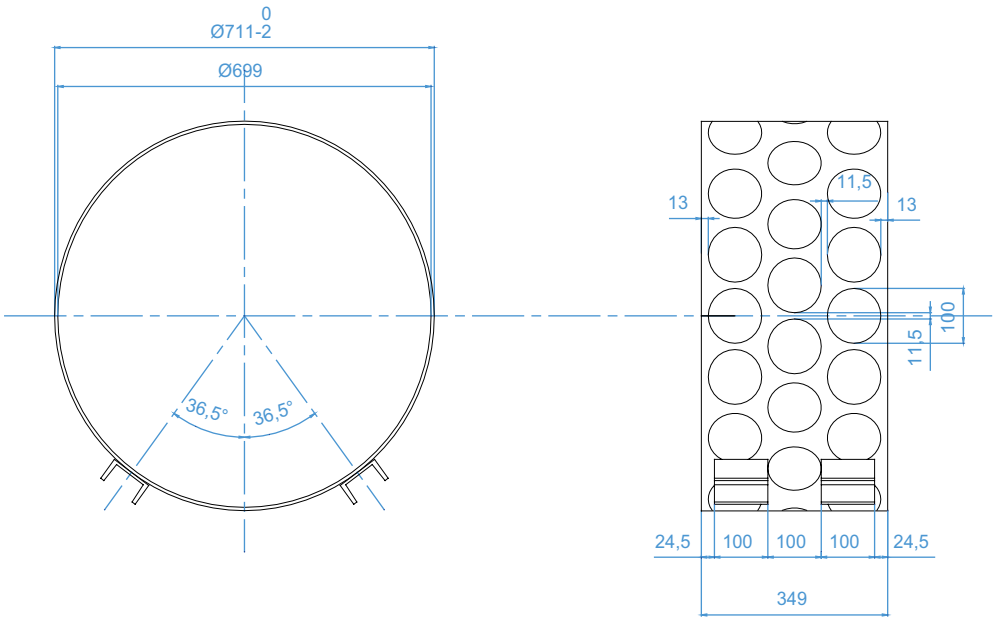

Figure 4-2. *BB IV. Technical drawing of the SC shell that was used in the BB IV test.*

Table 4-1. BB IV. Compilation of block data for BB IV.

Block parameters determined in conjunction with manufacturing and machining	
Block no.	***BB II012A6***
Water content [%]	10.4
Bulk density [kg/m^3]	2 104
Dry density [kg/m^3]	1 906
Diameter [mm]	687 (measured after machining)
Height [mm]	349.9
Block parameters determined in conjunction with test assembly	
Weight [kg]	276.1
Height [mm]	350
Diameter [mm]	688
Water content [%]	10.8
Bulk density* [kg/m^3]	2 122
Dry density* [kg/m^3]	1 915
Degree of saturation [%]	66

* The bulk density and the dry density were calculated using the weight, dimensions and water content determined in conjunction with test assembly.

It should also be mentioned that parts of the block broke off during the installation work at three positions due to preexisting cracks. One piece broke off from the cylinder edge (see Figure 4-3), and was then utilized for determination of the water content, and two other pieces broke off from parts adjacent to two of the lifting holes, see Figure 4-4. The volume of all parts broken off from the block was estimated to approximately 356 cm^3.

Figure 4-3. *BB IV. The SC is installed and adjusted in the test cell. A part of the bentonite block has fallen off at the left side.*

Figure 4-4. *BB IV. Parts have fallen off the block in conjunction to the lifting holes.*

4.2 BB IV: Operation

The operational phase started with the artificial water filling according to DAWE, injecting tap water through a tube, with an inner diameter of 4 mm, connected to the lower inlet point. Water was injected at about 2.5 meters of water head (25 kPa) at the same time as air was allowed to escape through the dedicated outlet valve. The water filling continued until water emerged at the valve coming from the top connection to the filter. Both the inlet valve and the outlet valve were closed when water emerged.

The total time for the artificial water filling was 1 hour and 7 minutes. During this time 43.4 liters of water was injected i.e. an average of 0.65 liters/min. The available volume of the SC-rock gap was calculated to 44.3 liters. The difference between the injected volume and the calculated available volume was thus 0.9 liters.

The ion strength of the used tap water was measured to below 2 mmol/L, which is far below the ion strength set by dissolved accessory minerals in the MX-80 clay. The solubility of e.g. gypsum, which is present in the MX-80 clay (Karnland et al. 2006), is approximately 15 mmol/L at room temperature.

After the artificial filling of the void space, a tube coming from a vessel, Figure 4-5, containing water with a salinity of 1 % (50/50 NaCl/$CaCl_2$) was connected to both inlets to the filter (at top and bottom). The bentonite in the test cell had after that free access to water with a pressure of approx. 2 meter water head (20 kPa).

Below a description of the evolution of the system throughout the operational phase is given. Some additional information regarding the sensors can be found in Appendix D1. A description of early pressure responses is given in Appendix D2 and sensor data regarding room climate is given in Appendix D3.

During the first three days in operation, approximately 1.6 liters of water were pressed out from the test cell. In the earlier BB tests (BB I, BB II and BB III) the inlet and outlet valves were closed after the water filling (there was no access to additional water) and an increasing water pressure was registered. In this test (BB IV) the pore water system was connected to a vessel with water, which means that instead of building up a water pressure in a locked volume, water was instead ejected.

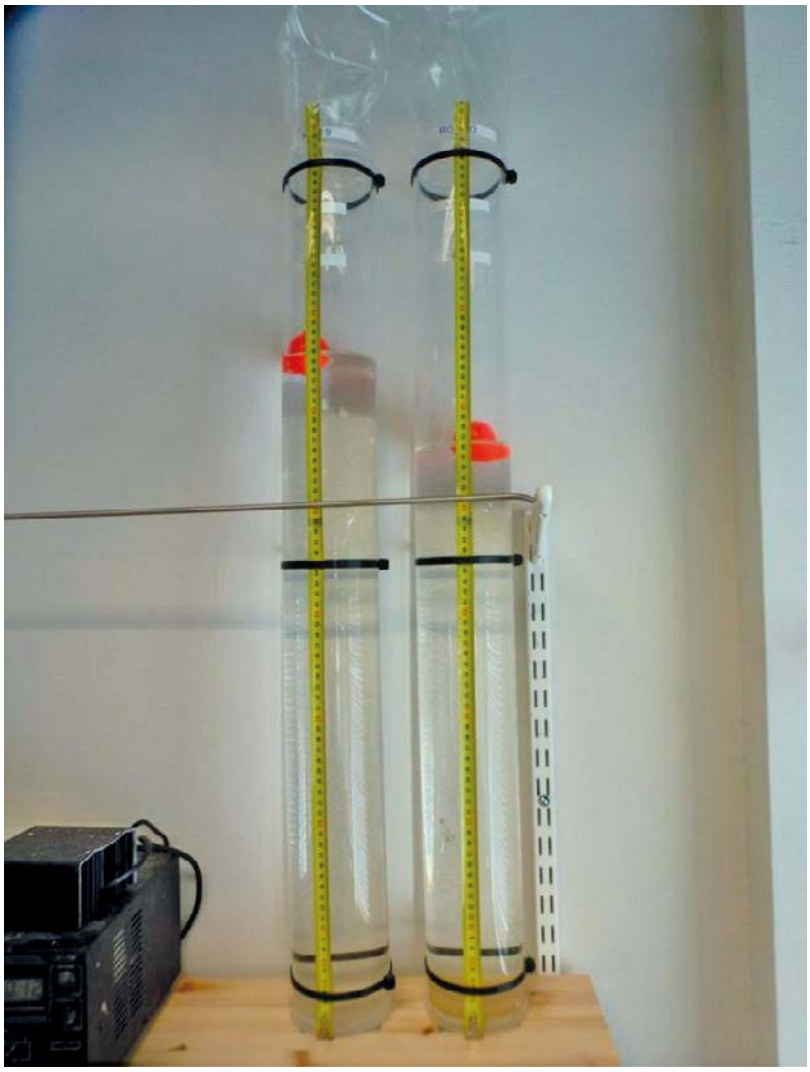

Figure 4-5. *BB IV. Photo showing the vessels used for measuring the early water consumption. The vessels contain water with a salinity of 1 %. The left vessel was connected to the equipment.*

The consumed water during the operational phase is shown in Figure 4-6. Following notes describe actions taken and overall trends related to the water consumption during operation:

- During day 3 to day 10, the water uptake was very close to zero, but then the water consumption started to increase somewhat.
- In order to ensure that the water saturation continued without any problems with air trapped in the filters, new vessels that could be pressurized were installed, Figure 4-7. Day 45, the water pressure was increased to 200 kPa and day 48 it was increased to 400 kPa (black lines in the graph provided in Figure 4-6).
- Approximately once a week, the valve at the top (connected to the filter mat) of the test cell, was carefully opened and some pressurized air released. The air originates from the compacted blocks and is released from the bentonite as the water saturation proceeds.
- The water uptake has continued with a rather constant rate until the test termination, but would be expected to decrease with time the nearer full saturation the block reaches. The total amount of water needed for full saturation is calculated to 59.2 liters.
- Twenty-four hours before test termination the back-pressure was decreased from 400 kPa to zero.
- Just before starting the removal of the first lid, the tubes feeding water to the filter mats were removed and remaining water in the filter was let out.

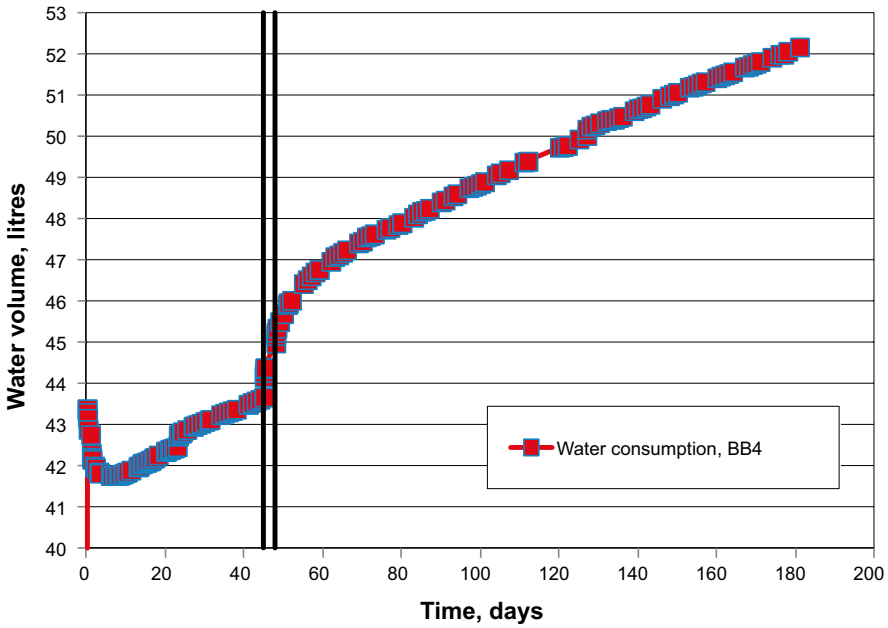

Figure 4-6. *BB IV. The water consumption plotted versus time. The first artificial filling was made with 43.4 liters during 1h and 7 minutes. The two vertical black lines shows the time for the water pressure increase (200 and 400 kPa, respectively).*

Figure 4-7. *BB IV. Cells used to apply pressurized water to the filters in the test.*

The graph in Figure 4-8 shows the axial total pressures, the radial total pressures, the pore pressures and the test cell temperature registered during the test. In order to show the complete pressure development for the axial pressure sensor A1, another graph is provided in Figure 4-9 where the range in pressure on the y-axis has been extended.

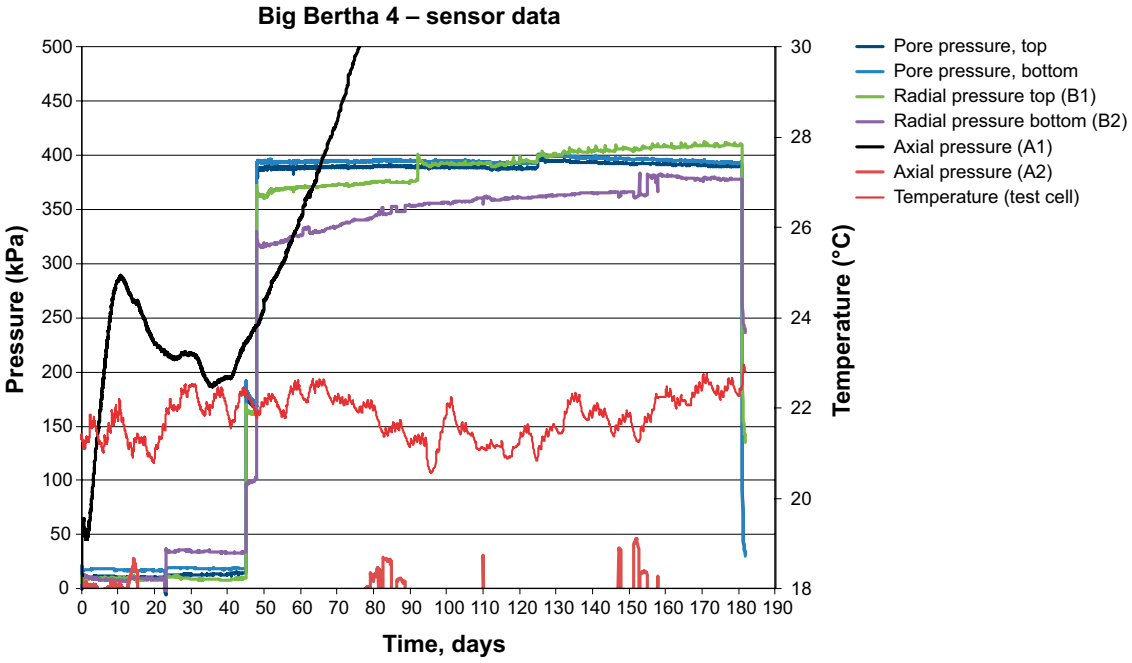

Figure 4-8. *BB IV. Radial total pressure and pore pressure data plotted versus time. The temperature of the test cell is also included in the figure.*

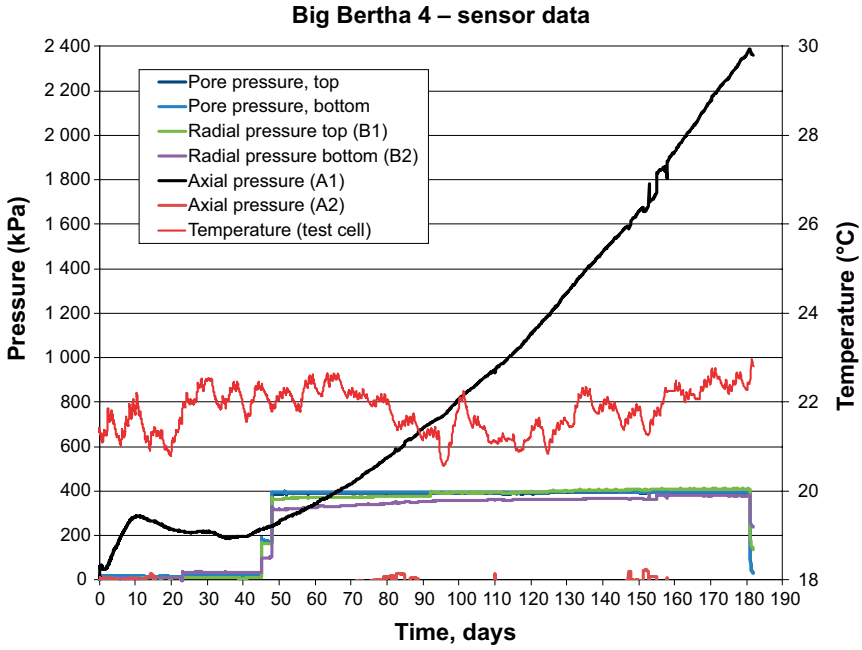

Figure 4-9. *BB IV. Radial total pressure and pore pressure data plotted versus time. The temperature of the test cell is also included in the figure.*

All registered total pressures are very low in the beginning of the test except for the axial pressure in position A1. This sensor registers a pressure of 275 kPa after 13 days (Figure 4-8). The axial pressure in this position has continued to increase during the test period and at the time for termination the pressure had reached almost 2 400 kPa. The axial pressure sensor in position A2 has only registered some minor scattered peaks (maximum 50 kPa) during the operation. The large difference in pressure between the two sensors is difficult to explain.

The data from the sample analysis showed that the bentonite density at the position of sensor A1 is somewhat higher than corresponding position of sensor A2, but this cannot fully explain the difference.

In order to measure a relevant pressure, full contact between the piston, transferring the pressure to the load cell, and the bentonite block is important. Photos provided in Section 4.3 show the contact points against the bentonite block for the two axial sensors A1 and A2. There is a visual difference between the clay contact surfaces. The contact surface for sensor A2 is somewhat darker as compared to that for A1, which may indicate that swelling has occurred at this point, i.e. the piston may not have been in direct contact with the bentonite from the beginning. If such swelling, prior to contact, has only occurred at one sensor position, it may be another reason for the difference between A1 and A2 responses.

The registered pore pressure has been very close to the applied water pressure (4 bars) which is expected since the sensors are positioned at the water inlets. The registered radial pressure has been in the same range as the applied pore pressure which indicates that the swelling pressures (pressures originating from clay swelling) against the test cell wall in these positions were very low.

The most probable explanation for the low pressure is that the radial sensor positions in this test were positioned between two of the perforated rows of holes. This was later confirmed during the dismantling, see Section 4.3. In an earlier performed test including a SC shell, BB III, there was an obvious difference in density of the material outside of the SC shell (in the SC-rock gap), dependent on the position relative to the perforation holes. In the BB III test, however, there was no access to additional water after the artificial wetting. In BB IV the homogenization of the bentonite was expected to increase in the SC-rock gap with time and a pressure build up was expected to take place also in these positions after further wetting.

The temperature was rather constant during test time, Figure 4-8. Small daily variations can, however, be seen on the temperature curve and these can also be seen on the pressure curves as a small noise. The effect of the temperature variations on the test results was, however, assessed to be very small, e.g. see investigations made by Birgersson et al. (2010).

4.3 BB IV: Dismantling and sampling

To facilitate the management of the sampling a coordinate system similar to the one used in BB II and BB III was defined, see Figure 4-10.

The cross sections were sampled according to the following:

- Cross-section A and D, positioned directly inside the steel lids, were sampled immediately after removal of the lids. The samples were assumed to be undisturbed i.e. the SC was not to be moved before sampling.
- Cross-section B and C were positioned 125 mm from section A and D, respectively. The samples close to the radial pressure sensors, positioned in line with section C were considered interesting in order to understand the monitored pressures. The material filling the initially empty gap between the SC and enclosure wall were sampled without moving the SC for both sections. The sampling of the bentonite inside the SC was made after having moved the SC forward, cutting the SC shell and then removing the protruding bentonite to expose the cross section of interest.

The position of cross section B was chosen since it was logical to sample the cross section in which the radial total pressure was measured. Cross section C was chosen to make the analysis symmetric. The same naming system was used as in the BB II test. Every sample was named after cross section, direction and radial distance from the test cell wall. E.g. A_90_60 was taken in cross section A in direction 90° at a radial distance of 60 mm from the test cell wall.

An example of the sampling plan for one direction of a cross section is shown in Figure 4-11. In all eight directions there were four samples (approx. 11 to 12 mm width) taken in the SC-rock gap and three samples with a diameter of 20 mm just inside the SC shell. In direction 0°, 90°, 180° and 270° there were nine additional samples with a diameter of 30 mm taken towards the center. Finally one sample was drilled out at the center position.

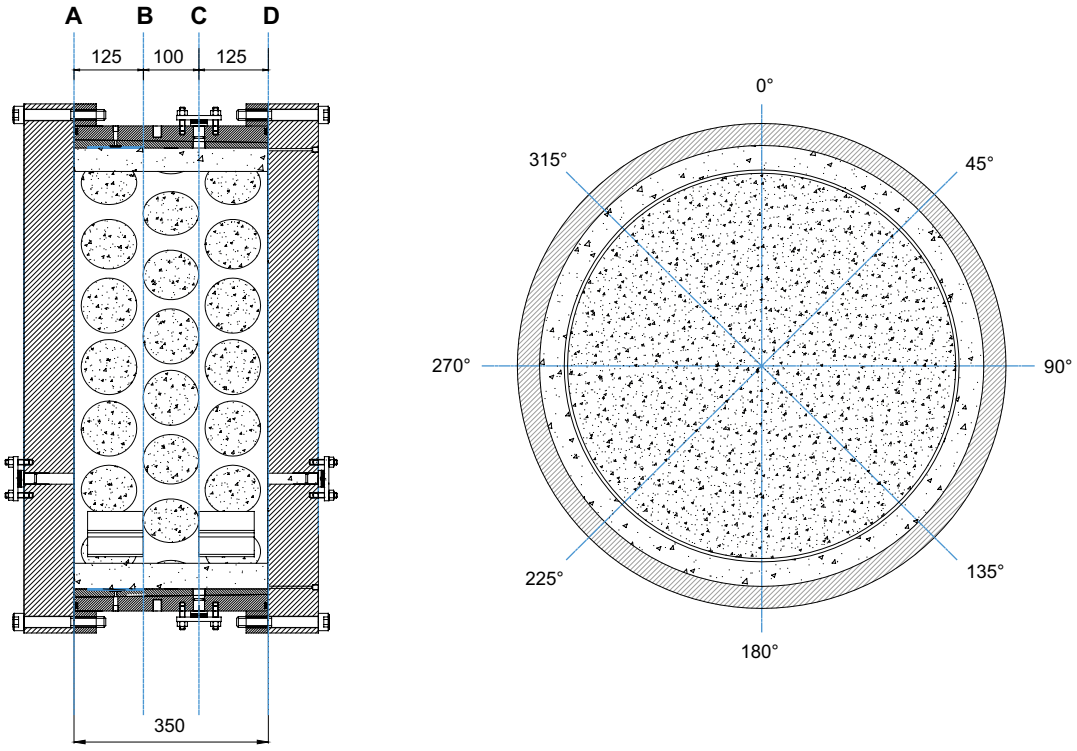

Figure 4-10. *BB IV. LEFT: Cross sections chosen for sampling. RIGHT: The eight directions in each cross section chosen for sampling (seen from section A).*

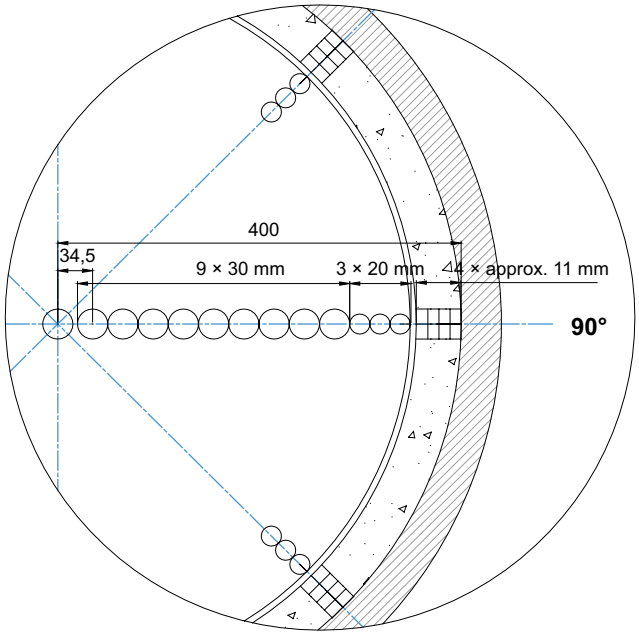

Figure 4-11. *BB IV. Close-up of a cross section profile showing the sampling plan.*

Below follows a selection of photographs taken and observations made during the dismantling and sampling of the test.

4.3.1 BB IV: Cross section A

A small elastic expansion of the bentonite in relation to the SC shell was noticed when the steel lid covering cross-section A was removed. The bentonite in the SC-rock gap expanded approximately 1.5 mm in relation to the SC and the buffer block inside the SC expanded approximately 4.5 mm in relation to the SC.

An overview of the exposed surface of cross-section A is provided to the left in Figure 4-12. The photo shows that the outer parts of the block inside the SC shell were darker and seem to have been more saturated as compared to the innermost parts. As can be seen in both Figure 4-12 and Figure 4-13, the SC-rock gap was completely filled with swollen bentonite. A close-up of the lower part, provided to the right in Figure 4-12, shows that the volumes surrounding the feet (positioned at 143.5° and 216.5°) have been completely clay-filled as well. To the right in Figure 4-13 the footprint of the axial pressure piston on the buffer surface is visible (A2, direction 225°). This sensor was not registering any pressure during the operation. A sample was taken at this position.

When sampling the cross section the bentonite close to the SC shell was found to have relatively low density and also seemed to be highly saturated. The sampling of the inner parts of the block was made using a handheld core drill (D=30 mm). Due to the friction generated the water content of the samples may have been affected somewhat.

The photo to the left in Figure 4-14 shows the technique for measuring the distance between SC and the inner wall of the test cell. The result is provided in Appendix D4. The right photo in Figure 4-14 shows an overview of cross-section A after having finished the sampling.

Figure 4-12. *BB IV, cross section A. LEFT: The bentonite surface just inside the steel lid in cross section A. RIGHT: Close up showing the bentonite filled SC-rock gap. The space inside the feet has also been filled up with bentonite gel.*

Figure 4-13. *BB IV, cross section A. LEFT: Close up showing the bentonite filled SC-rock gap. RIGHT: Close up showing the position of where the piston of the axial pressure measurement A2 has been in contact with the bentonite block surface. A sample was taken at this position.*

4.3.2 BB IV: Cross section D

When uncovering cross-section D, see Figure 4-15, the bentonite surface in this cross-section was found to be similar to that of cross-section A. The SC-rock gap was completely filled with lower density buffer. The outermost part of the buffer inside the SC shell had a darker appearance, indicating highly saturated conditions, and the innermost parts of the buffer had a lighter color, indicating dryer conditions, see Figure 4-15.

Figure 4-16 shows a close-up of cross-section D in direction 135°, and an arrow indicate the position where the piston in the axial pressure measurement A1 had been in contact with the bentonite. This sensor had registered a swelling pressure of almost 2 400 kPa at the time for dismantling, see graph provided in Figure 4-9. The contact area, however, has a light color, indicating dry conditions, and a good explanation for the high swelling pressure measured is not obvious. All sensors were checked after termination of the test and the function of this sensor was controlled and found to work properly.

Figure 4-17 shows a photo of the central parts of the block in cross-section D. A clear fracture, separating the inner and outer part of the buffer can be seen. The buffer separated along this fracture when sampling cross-section B and C.

Figure 4-14. *BB IV, cross section A. LEFT: Measuring the distance between SC and the inner test cell wall. RIGHT: Overview of cross-section A after having finished the sampling.*

Figure 4-15. *BB IV, cross section D. LEFT: The bentonite surface just inside the steel lid in section D is uncovered. RIGHT: Close up showing the bentonite filled SC-rock gap. The gap seems to have been filled up completely by the swelling bentonite.*

Figure 4-16. *BB IV, cross section D. Close-up of cross-section D showing the position where the piston measuring the axial pressure (A1, 135 °) has been in contact with the bentonite.*

Figure 4-17. *BB IV, cross section D. Close up showing the central parts of cross section D. There is a very clear fracture separating the innermost part from the rest of the block. The fracture was found to be present through the whole block.*

The photo in Figure 4-18 shows a close-up of cross-section D, in direction 135° and 180°, after having finished the sampling. A sample was drilled out at the position of the contact surface between the buffer and the piston transferring the force to the axial pressure sensor A1.

Figure 4-18. *BB IV, cross section D. Close-up of cross section D, directions 135° to 180° after having finished the sampling.*

4.3.3 BB IV: Cross section B

Before sampling related to cross section B the buffer and SC were separated from the enclosure as can be seen in Figure 4-19. The buffer in the SC-rock gap in cross-section B was sampled while the package was hanging in the lifting straps; also additional material was here sampled for later analyses, Figure 4-20.

The next action was to uncover the bentonite inside the SC in cross-section B by cutting off the SC shell, Figure 4-21. The exposed buffer surface just below the SC shell that had been in direct contact with the steel was discolored by the corroding steel, see Figure 4-22. To investigate density and water content heterogeneity; extra buffer samples were taken directly below a perforation and in between three perforations, directly below the steel, see Figure 4-23.

In order to uncover cross-section B, the block was seam drilled in the radial direction, Figure 4-24. After having drilled all the way around the block a special saw was used to cut off the remaining bentonite, see photo provided in Figure 4-32.

The photo in Figure 4-25 shows a part of the bentonite that fell off during the seam-drilling. Besides the fracture present in the central parts of the block, see Figure 4-17, there was also a weakness at this side of the block edge, with a direction of approximately 45° from the block´s flat surface. This weakness could, however, only be seen during the working with the block.

After having uncovered cross-section B the sampling of the surface started. Figure 4-26 shows the sampling technique that included a hand held machine for drilling out cores with a diameter of 30 mm.

4.3.4 BB IV: Cross section C

Three types of sampling took place in cross section C. Sampling of the buffer close to the positions of the radial total pressure measurements, sampling of the buffer in the SC-rock gap, and sampling according to the cross section sampling plan as given in Figure 4-11

When sampling the buffer close to the two radial pistons in cross-section C, the buffer surface was found to be wet, see photo in Figure 4-27. The photo to the right shows an actual clay sample which also looked very wet and had a gel-like consistency.

Figure 4-19. *BB IV, cross section B. After having finished the sampling of the SC-rock gap in cross section C, the rest of the SC including the swollen bentonite was lifted out from the test cell.*

Figure 4-20. *BB IV, cross section B. Close up showing a bentonite piece in section A–B. (Specimen S2, see Section 10.4.2).*

Figure 4-21. *BB IV, cross section B. In order to uncover the bentonite in cross section B parts of the SC shell was cut off.*

Figure 4-22. *BB IV, cross section B. Photo showing the uncovered bentonite block surface after removal of a SC shell part*

Figure 4-23. *BB IV, cross section B. Close up showing some extra sampling performed. One sample was drilled out from the middle of a perforated hole and one from the area between three holes (Specimen S8, see Section 10.4.2)*

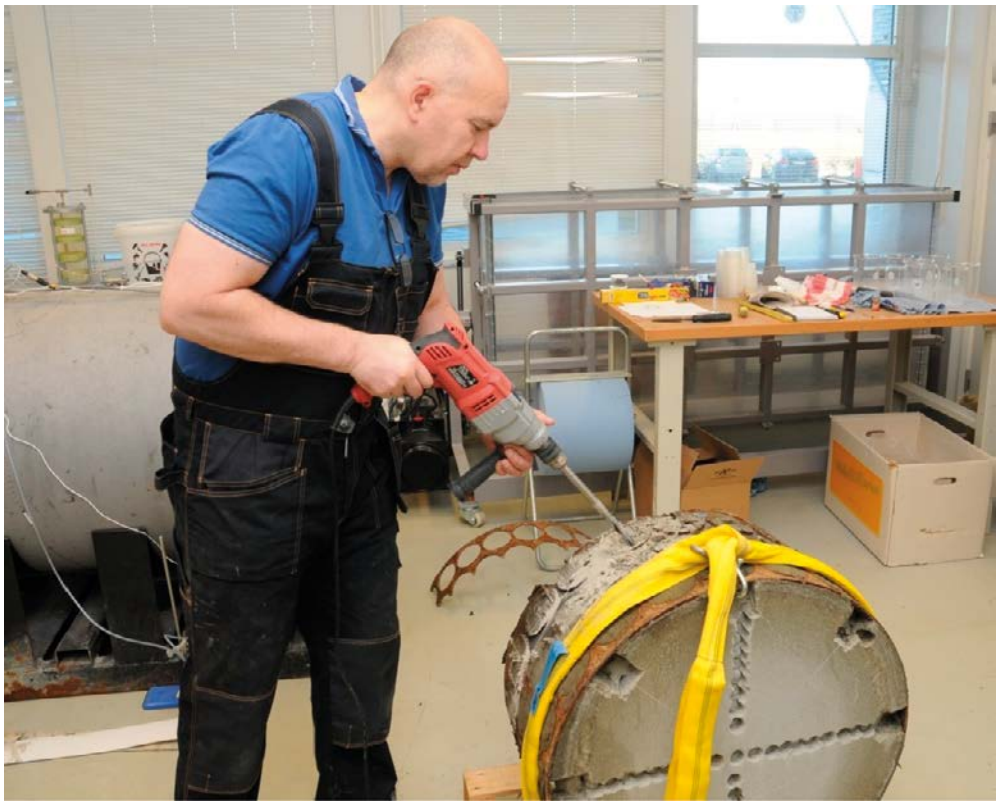

Figure 4-24. *BB IV, cross section B. In order to uncover cross section B inside the SC the bentonite was removed by using a combination of seam drilling and sawing.*

Figure 4-25. *BB IV, cross section B. A part of cross section B has been uncovered.*

Figure 4-26. *BB IV, cross section B. After having uncovered cross section B completely the sampling of the bentonite started. The sampling was made by use of a small core drill.*

Larger pieces of bentonite from the gap could be removed from the SC shell and were saved for later analyses, see photos provided in Figure 4-28 and Figure 4-29. No empty voids were present in the initially empty gap outside the SC (Figure 4-28) and the bentonite had completely swollen into the feet structures (Figure 4-29). A close-up photo of one SC foot is provided in Figure 4-30. During the sampling, however, large differences in density and water content, dependent on the position relative to the perforations, could be noticed.

Figure 4-27. *BB IV, cross section C. LEFT: Photo showing the uncovered bentonite surface inside the piston of radial pressure measurement C1 before sampling. RIGHT: the sample taken from just inside the piston of the radial pressure measurement C1.*

Figure 4-28. *BB IV, cross section C. A bentonite piece has come loose from the SC surface. As shown in the photo there are no empty voids present in the SC-rock gap. The gap is completely filled with bentonite.*

Figure 4-29. *BB IV, cross section C. Photo showing a bentonite piece sampled from the SC-rock gap. The protrusion which can be seen on the surface facing right is material which has swelled into one of the feet.*

Figure 4-30. *BB IV, cross section C. Close-up showing a SC foot.*

The uncovering of cross section C inside the SC was quite laborious. It included cutting the SC shell, seam drilling, and finally sawing the remaining connected parts of the buffer. Photos taken during this process are shown below in Figure 4-31 to Figure 4-34. An internal fracture of the block left an excessive central part of the block remaining (see Figure 4-33) which had to be machined away. After having marked up the sampling directions the cross-section was sampled according to the plan and the cross section after sampling is shown in Figure 4-35.

Figure 4-31. *BB IV, cross section C. Seam drilling to uncover cross section C.*

Figure 4-32. *BB IV, cross section C. Sawing off the material left between the drilled boreholes.*

Figure 4-33. *BB IV, cross section C. Uncovering cross-section C. Note that there is an obvious fracturing separating the outer parts and the central part.*

Figure 4-34. *BB IV, cross section C. Photo showing the block part that was removed in order to uncover cross-section C.*

Figure 4-35. *BB IV, cross section C. Photo showing cross-section C after sampling.*

4.4 BB IV: Results and analysis

In total 372 samples were taken from the four cross-sections. In addition, 214 samples were taken from the SC-rock gap in order to in more detail study the swelling behavior through the perforated SC steel shell. This means that in total, 586 samples taken for analysis regarding water content and in most cases also dry density. Some of the results are shown and discussed below. All data obtained from analyzing the samples are shown graphically in Appendix D5.

4.4.1 BB IV: Results – conditions at total pressure measurement positions

The registered radial total pressure was close to zero in the two points, C1 and C2, where it was measured. Information regarding the conditions at these positions was therefore interesting. The water content and density was determined for the buffer material sampled just inside of the sensors. Figure 4-36 shows how the water content varies in the SC-rock gap. The water content was almost twice as high inside C1 (240–280 %) as compared to C2 (125–160 %).

Dry densities are shown in Figure 4-37. The dry density is higher inside C2 compared to C1, but the densities are still too low to result in a detectable swelling pressure.

Table 4-2 shows a compilation of the data in Figure 4-36 and Figure 4-37 together with the corresponding degree of saturation. Data from analyzing the samples taken inside of the two axial total pressure measurements, A1 and A2, is included in the table as well as the measured total pressure (swelling pressure + pore pressure) at test termination. The low radial swelling pressure at C1 and C2 could be explained by their positions in relation to the perforations of the SC shell, in between the perforated holes, see Figure 4-41.

When analyzing the material sampled at the axial pressure sensor A1, the bentonite was found only to have taken up a small amount of water and was far from saturated. Thus, the high total pressure registered by A1 was not a result from significant swelling of the bentonite nearby the sensor. The difficulty experienced disassembling the experiment when removing the bolts attaching the steel lid and the observed expansion of the buffer, however, both indicate that the buffer indeed was subjected to significant axial stress.

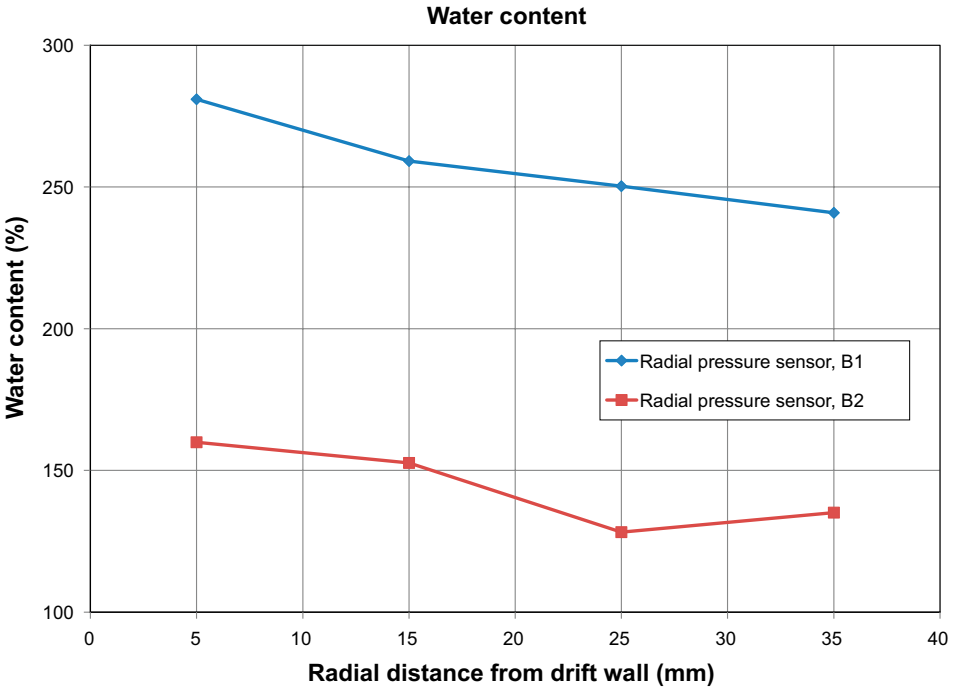

Figure 4-36. *BB IV. Water content in the samples taken just inside the radial total pressure measurement positions.*

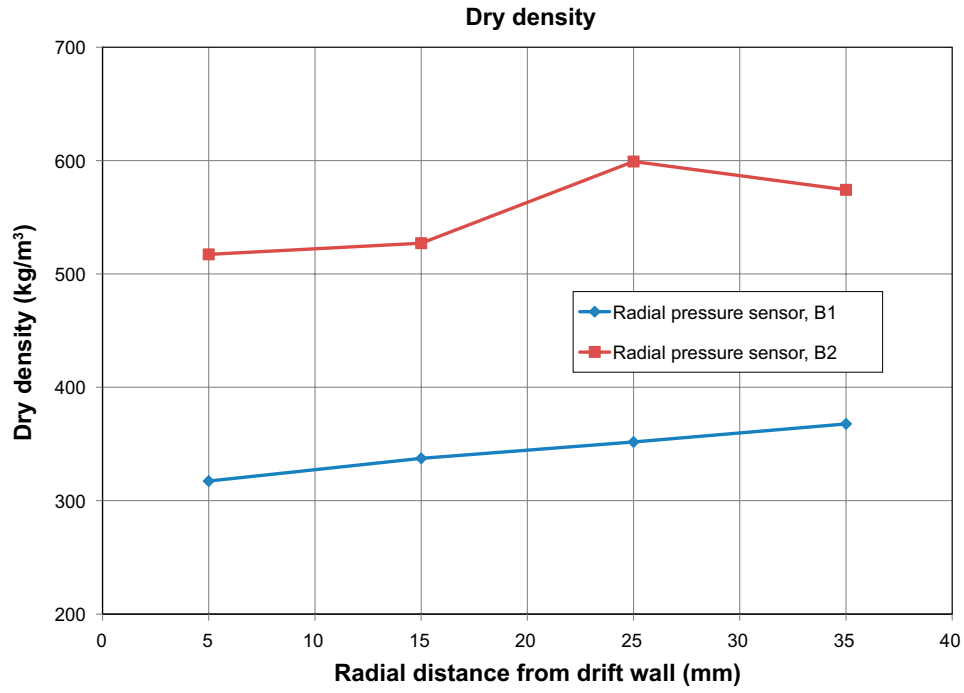

Figure 4-37. *BB IV. Dry density in the samples taken just inside the radial total pressure measurement positions.*

One possible explanation for the high axial total pressure measured at A1 could come from a situation where a localized pressure acted on the piston. This would amplify pressure generated by swelling in the outer parts. Such a localized pressure condition could be the case if the block have had a local geometric “high” point at the position of the sensor.

Table 4-2. BB IV. Data from the analysis of samples taken just inside the radial and axial total pressure measurement positions. Swelling pressures at test dismantling are added to the table.

Description	Cross section	Direction [°]	Radial distance from cell [mm]	Water content [%]	Dry density [kg/m^3]	Degree of saturation [%]	Total pressure [kPa]
Radial, C1	C	0	5	280.9	317	101	410
Radial, C1	C	0	15	259.1	337	99	
Radial, C1	C	0	25	250.3	352	101	
Radial, C1	C	0	35	240.9	368	102	
Radial , C2	C	180	5	159.9	517	102	378
Radial , C2	C	180	15	152.6	527	99	
Radial , C2	C	180	25	128.2	599	98	
Radial , C2	C	180	35	135.1	574	98	
Axial, A2	A	225	200	16.6	1 734	76	0
Axial, A1	D	135	200	15.1	1 782	75	2 380

4.4.2 BB IV: Results – cross sections

Cross section data has been visualized using contour plots in order to facilitate an overview of the distribution of water content, dry density and degree of saturation over the different cross-sections, see Figure 4-38, Figure 4-39 and Figure 4-40. The data is also given in terms of radial profiles in Appendix D5.

The radial water content distribution was similar in all cross-sections. The variation in water content was large in the SC-rock gap, mainly between 50 to 200 % with some exceptions. The large variation depends on the perforation pattern of the SC shell which has resulted in a heterogeneous swelling of the bentonite. Outside a perforation the water content of the bentonite is lower and the density higher while the situation is the opposite in between the perforated holes. The sampling of the SC-rock gap was performed according to the described sampling plan, which was not dependent on the perforation pattern. The variation in results is, however, assessed to represent the actual situation in the gap.

The radial gradient in density could be described using three sections depending on the radial distance to the enclosure wall:

1. 0–50 mm: Close to the wall the density varied between 300 and 800 kg/m^3 with few exceptions. Close to the SC shell, both on the outside and inside, the density had markedly increased, and the variation was high from 800 to 1 400 kg/m^3.
2. 50–300 mm: The bentonite had underwent a significant water uptake and swelling. This resulted in a strong density gradient, 1 300–1 500 kg/m^3 close to the SC and up to 1 900 kg/m^3 at 300 mm from the enclosure wall.
3. 300–400 mm: The innermost parts of the buffer had a dry density of about 1 850 to 1 920 kg/m^3, i.e. close to the installation density.

The evaluated degree of saturation was close to 100 % at the outermost parts, 0–80 mm from the enclosure wall. The variation was rather high, 80–120 %, reflecting the large variation in density and water content in this part. Thus, also the individual samples may be heterogeneous. Since each sample was divided in two pieces, one for determination of the water content and one for determination of the density, the evaluated degree of saturation might therefore be somewhat unrepresentative if the properties of the two sample pieces were different.

At the distance between 80–200 mm from the enclosure wall, the degree of saturation can be seen to decrease down to about 68–72 % which is the magnitude remaining to the block center.

There is a tendency for somewhat higher average density in the SC-rock gap (0–50 mm) at the lower part of the buffer, at least in the two inner cross sections B and C, see e.g. the graphs provided in Appendix D5, where the density profiles in direction 135°, 180° and 225° are higher as compared to the other directions. This might depend on sedimentation of bentonite particles during the early swelling into the water filled gap.

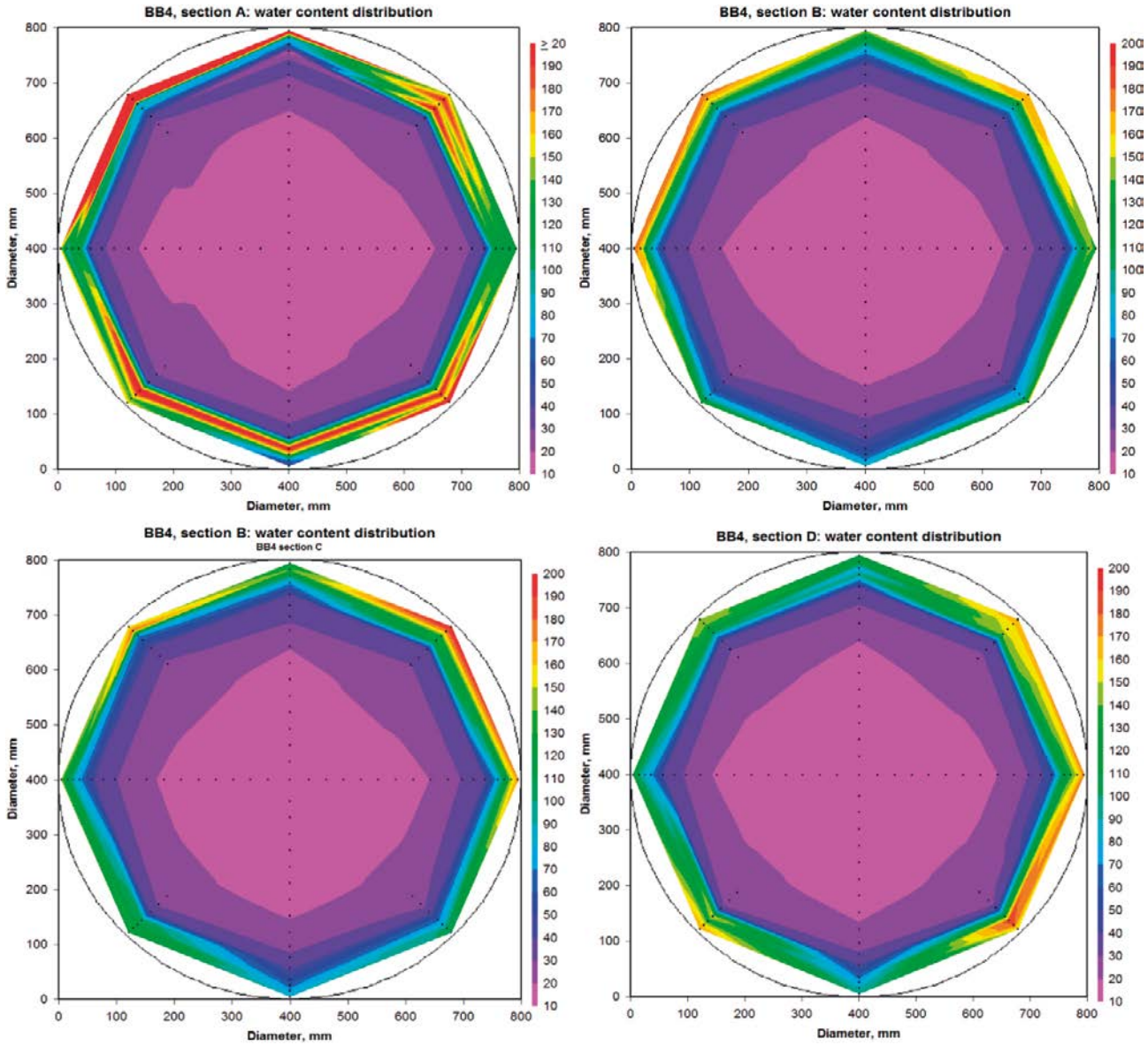

Figure 4-38. *BB IV. Contour plots showing the water content distribution in the four cross sections investigated.*

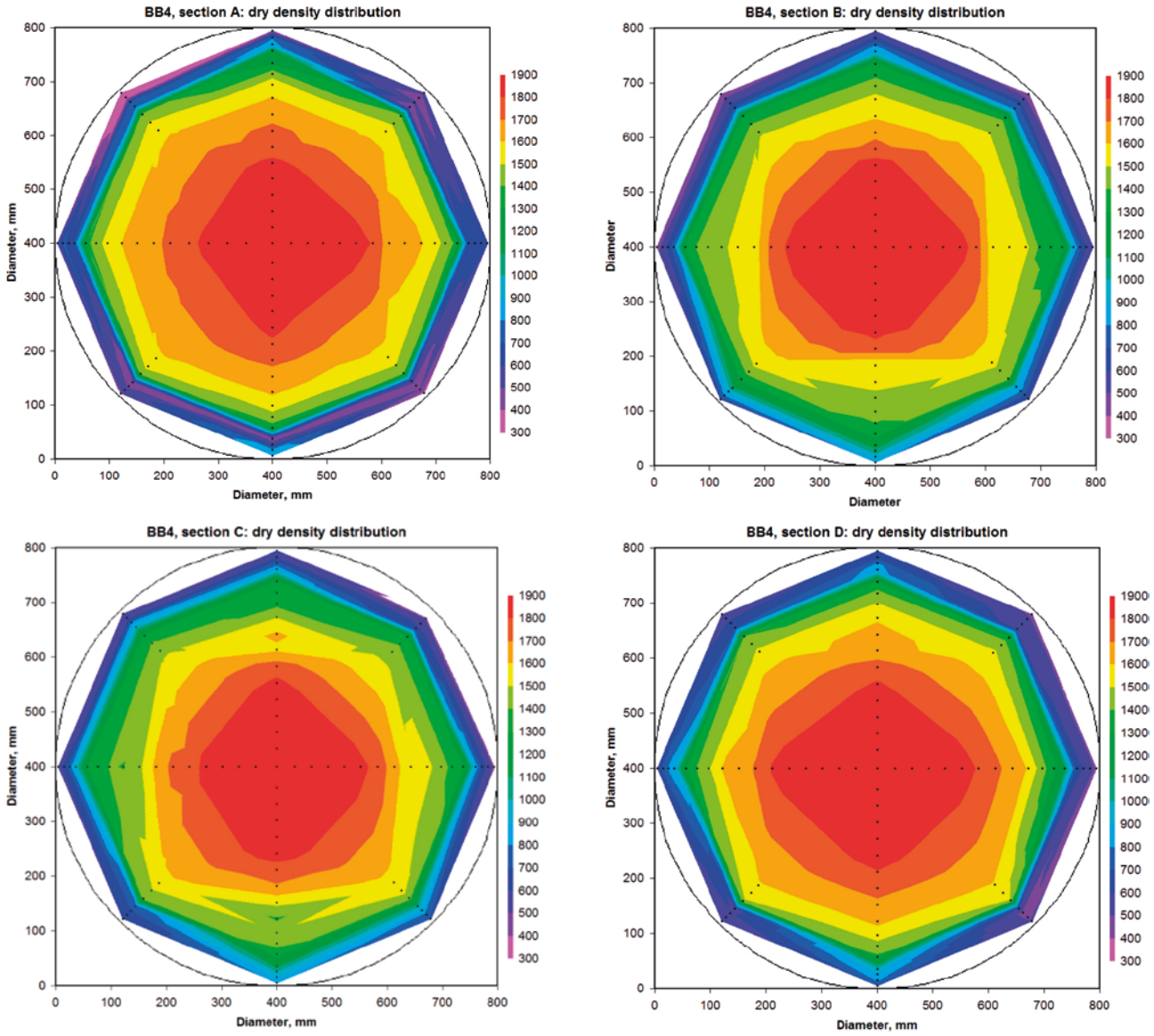

Figure 4-39. *BB IV. Contour plots showing the dry density distribution in the four cross sections investigated.*

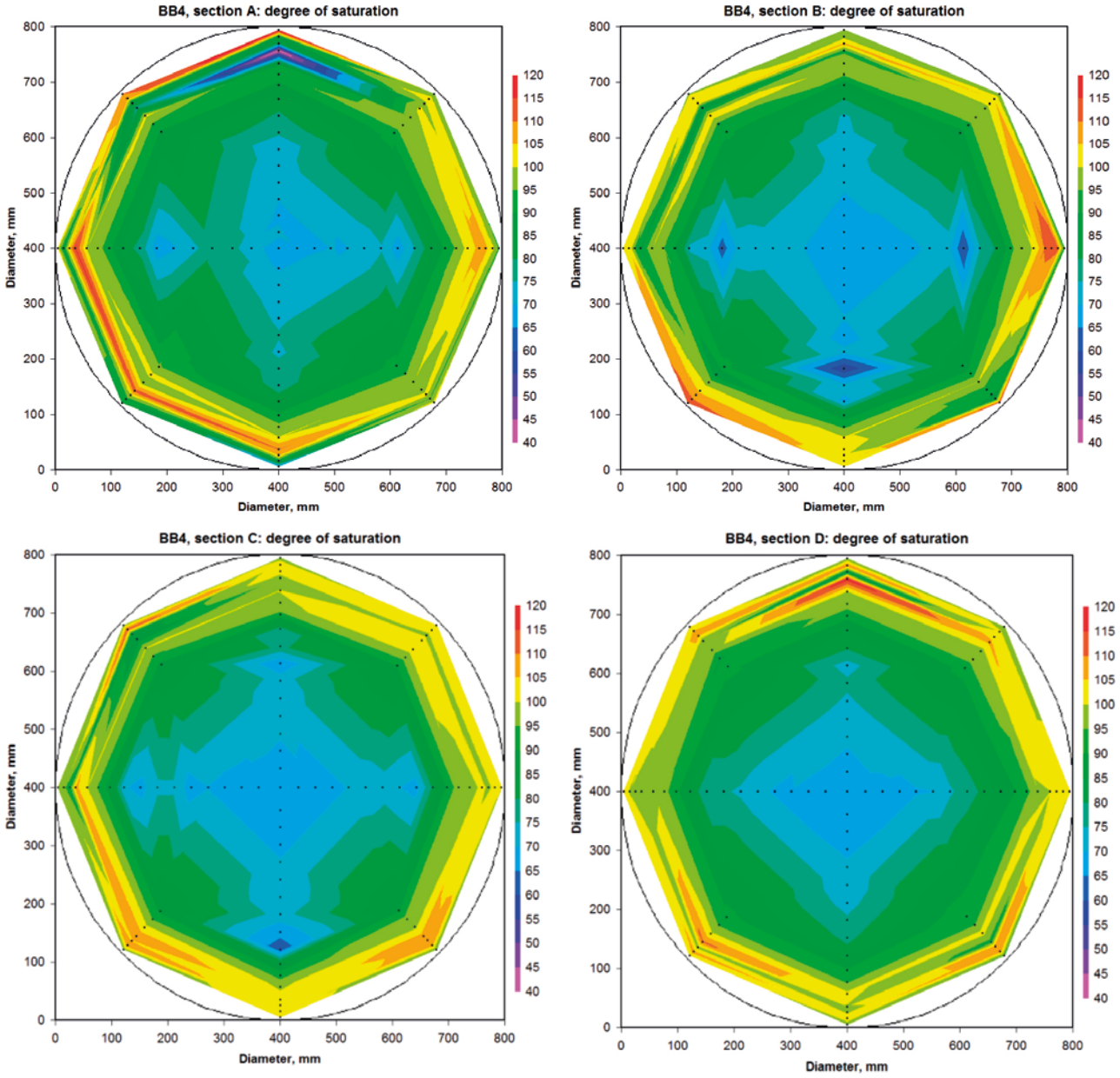

Figure 4-40. *BB IV. Contour plots showing the degree of saturation distribution in the four cross sections investigated.*

4.4.3 BB IV: Results – SC-rock gap

Eight specimens were taken from the SC-rock gap in order to determine the water content and dry density distribution. The gap was completely filled with swollen bentonite but it was obvious that it was very heterogeneous regarding water content and density.

A schematic drawing in Figure 4-41 shows the eight specimen positions in relation to the SC shell. The drawing also shows the position of the two radial pressure sensors and the feet in relation to the SC perforation.

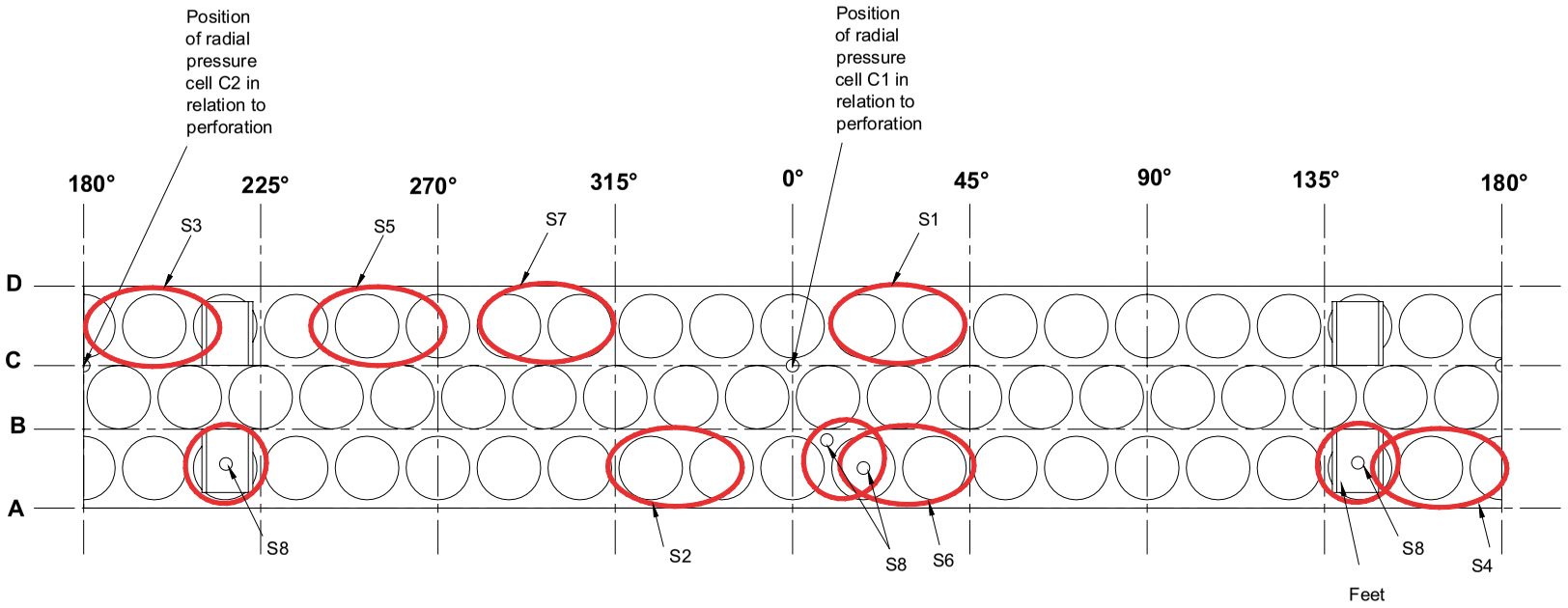

Figure 4-41. *BB IV. Schematic showing the unfolded SC. The red rings shows were specimens have been cut out from the SC-rock gap. In addition the positions of feet and the positions of the radial pressure sensors in relation to the perforation are also marked.*

The analysis can be divided in following three sets of specimens:

1. The samples cut out from specimen S1, S2 and S5 were analyzed both regarding water content and density. The number of samples was limited. Samples were taken from above the perforation and in between the perforations, and at three levels; close to the test cell wall, in the middle and close to the SC.
2. The samples cut out from specimen S3, S4, S6 and S7 were analyzed only regarding the water content. Specimens S3 and S6 were divided in pieces at every cm across the specimen length and at three levels.
3. Specimen S8 included drilling out cores (D=20 mm) from the bentonite in the middle of a perforated hole just beneath the SC shell level, from just beneath the SC steel in between the perforations and from two positions beneath the position of two of the feet.

Below, the results and analysis for S2, S6 and S8 are given as typical examples. In Appendix D5 results and analysis for all specimens are given.

BB IV: Results – SC-rock gap: Specimen S2

This specimen was taken from the area between cross-section A and B, in direction between 315° and 0° (see photo provided in Figure 4-20). Four samples were cut out above the perforated holes and three in between the perforated holes, Figure 4-42. Each sample was divided at three levels at different distances from the drift wall (inner test cell wall). In total 21 samples were analyzed regarding water content and density.

The results from the tests are shown in Figure 4-43. All samples are assessed to be water saturated. The variation in density and water content between the different positions and between the three levels is, however, strong. The samples taken above the perforated hole have a dry density between 800 and 1 130 kg/m^3, with the lowest densities close to the test cell wall. The dry density between the perforated holes is lower, between 420 and 950 kg/m^3. It is also obvious that the four samples taken above the perforation have a very similar radial density profile while the variation in density is much higher depending on level for three samples taken from the area between the perforated holes.

BB IV: Results – SC-rock gap: Specimen S6

This specimen was taken from the area between cross-sections A and B, in direction between 0° and 45°. Samples were cut at every cm along the length of the specimen at three levels positioned at different distances from the drift wall (inner test cell wall), Figure 4-44. In total 60 samples were analyzed regarding water content.

The results from the tests are shown in Figure 4-45. The variation in water content between the different positions and between the three levels is strong. The samples taken above the perforated hole (approximately 2–12 cm distance of the specimen length) has a water content of 75–80 % close to the SC shell (Level C), between 95–120 % at Level B (in the middle of the SC-rock gap) and between 120–170 % at Level A (close to the test cell wall). The water content increases markedly, the closer to the edge of the perforated hole and the highest water contents are found in between two perforated holes e.g. at a distance of 1 and 13 cm along the specimen length where the water content is close to 200 % at the outermost parts (Level A).

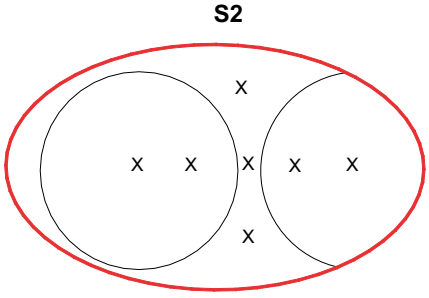

Figure 4-42. *BB IV. Schematic drawing showing the approximate positions of the samples taken from specimen S2, see also overview provided in Figure 4-41.*

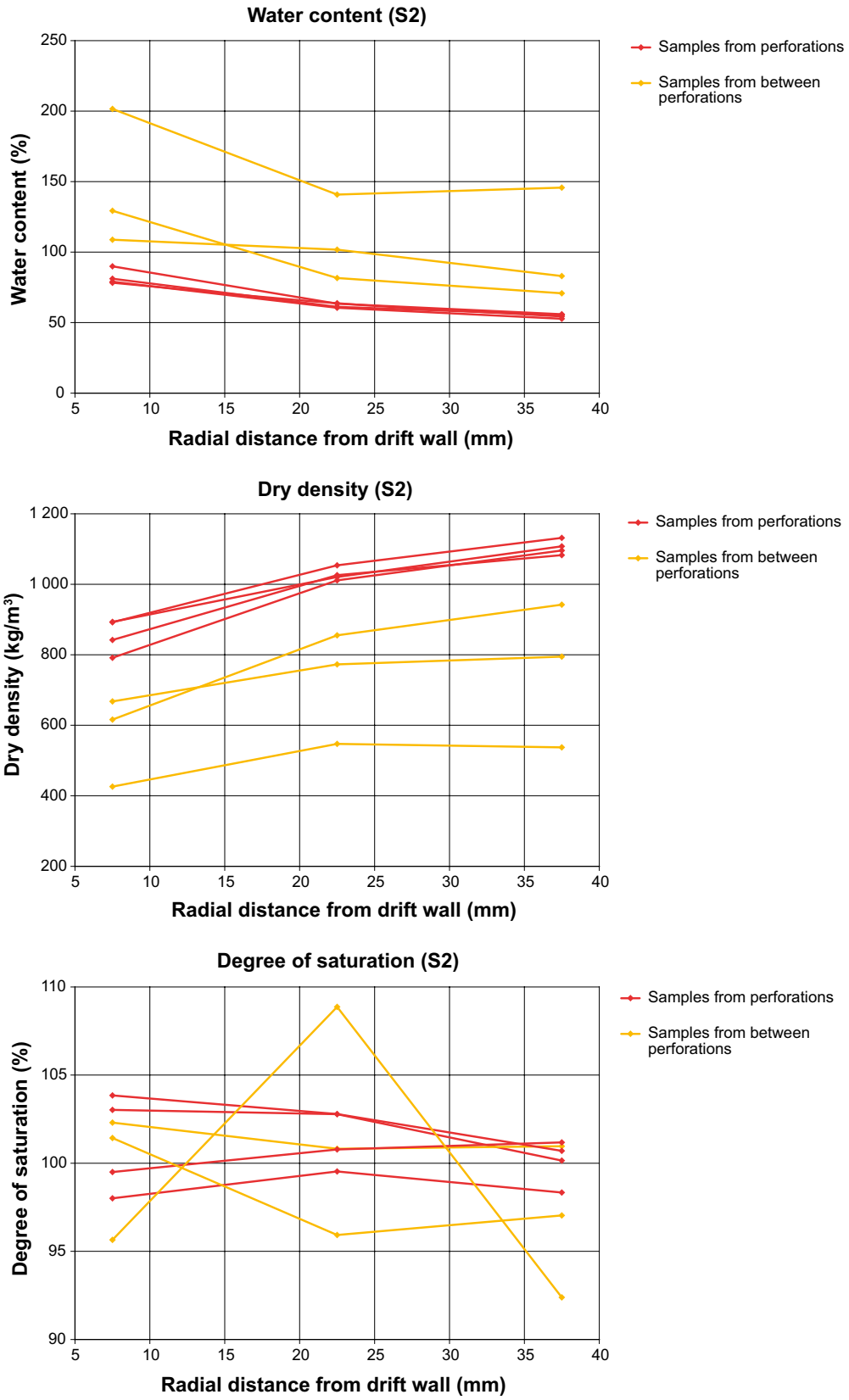

Figure 4-43. *BB IV. Upper: Water content distribution plotted versus the distance from the inner test cell wall (drift wall). Middle: Dry density plotted versus the distance from the inner test cell wall (drift wall). Lower: Degree of saturation plotted versus the distance from the inner test cell wall (drift wall).*

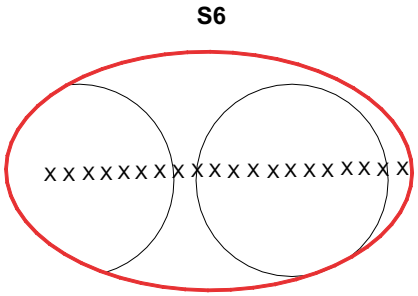

Figure 4-44. *BB IV. Schematic drawing showing the approximate positions of the samples taken from specimen S6, see also overview provided in Figure 4-41.*

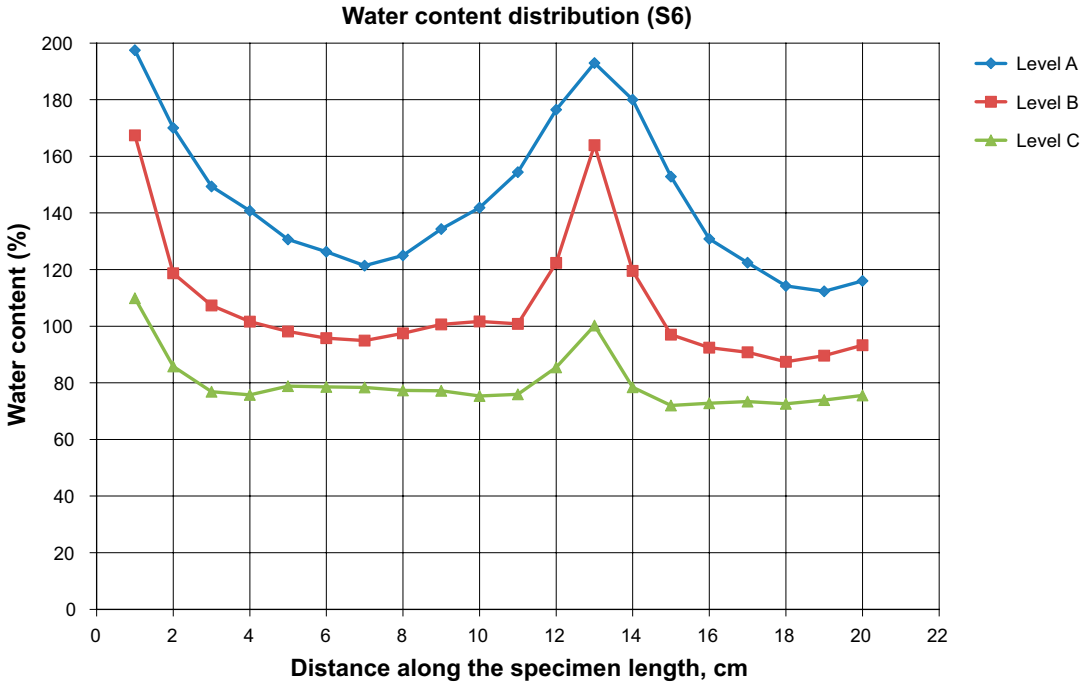

Figure 4-45. *BB IV. Water content distribution plotted versus the distance along the specimen length.*

The rather dense sampling of specimens S3 and S6 illustrates well the heterogeneous bentonite in the SC-rock gap. There are obvious differences in water content (and density) both depending on the position in relation to the perforation and also depending on the radial distance from the test cell wall.

BB IV: Results – SC-rock gap: Specimens S8

These specimens include four core-drilled samples drilled out from the area between cross-sections A and B. Two of the core-drilled samples were drilled out in direction between 10° and 25°, at the level for the inside of the SC shell; one sample was drilled out at the middle of a perforated hole and one at the midpoint between the perforations, see photo provided in Figure 4-23. The other two core-drilled samples were drilled out from the area inside the SC shell at the two feet positioned in section A-B. In addition samples were taken from the inside of the feet positioned in direction 216.5° i.e. inside the U-shape of the feet. In total 8 samples were analyzed regarding water content and density.

The results from the tests are shown in Table 4-3. From the results the following can be concluded:

1. The two samples drilled out from inside the SC shell and from the middle of a perforated hole respectively (sample 1 and 2) show that there is a very clear difference in density between these two positions. The bentonite inside the SC shell has not swelled as much as the bentonite in the middle of a perforated hole which has resulted in a clear difference in density.
2. The sampling of the bentonite inside the SC shell at the position of the feet (samples 3 and 4) shows that the feet have restricted the swelling of the bentonite locally at these positions.
3. The inside of the feet was completely filled with bentonite gel. The density was, however, rather low, between 300 and 400 kg/m^3.

Table 4-3. BB IV. Table providing data from the analysis of bentonite samples taken just below the SC shell and inside the feet.

Sample	Description	Cross section	Direction [°]	Water content [%]	Dry density [kg/m^3]	Degree of saturation [%]
1	Between perforation	A,B	10	35.5	1 384	98
2	In the middle of perforation	A,B	20	41.9	1 280	99
3	Inside SC shell at foot position	A,B	143.5	31.8	1 464	98
4	Inside SC shell at foot position	A,B	216.5	31.3	1 488	100
5	Inside foot 1	C,D	216.5	221.8	396	102
6	Inside foot 2	C,D	216.5	241.8	368	103
7	Inside foot 3	C,D	216.5	207.5	413	101
8	Inside foot 4	A,B	216.5	301.2	295	99

4.5 BB IV: Comments regarding radial swelling pressure development

The test design included two radial pressure measurements. Both sensors have reacted distinctly on changes in the applied water pressure, which indicate proper performance. However, none of them have registered any swelling pressure (difference between measured total pressure and applied pore pressure). The explanation for this is that both sensors have been positioned between perforations. Although the SC-rock gap has been completely filled with saturated bentonite, the density in the volumes just outside of sections of solid SC shell has been too low, between 300 and 600 kg/m^3, to register any swelling pressure. The investigations of material from the SC-rock gap have shown that the variation in water content and density is high and completely dependent on the position in relation to the SC perforation pattern.

4.6 BB IV: Comments regarding water content and density distribution

The block inside the SC had an initial water content of 10.8 % and a dry density of 1 915 kg/m^3 which yields a degree of saturation of 66 %. The sampling of the bentonite after test termination has shown that there are strong radial density and water content gradients present after six months´ test period.

The SC-rock gap was completely filled with bentonite gel. The analysis has shown that the gel is completely water saturated. The variation in water content and density is, however, highly depending on the radial distance and the position in relation to the SC perforation pattern. The highest densities are found right above the perforations while the lowest densities are found between the holes i.e. above the SC shell.

The radial density gradient can be divided into three parts depending on the radial distance to the test cell wall:

1. 0–50 mm: The density closest to the test cell wall varies between 300 and 800 kg/m^3 with a few exceptions. Close to the SC shell, outside and inside, the density has markedly increased but the variation is still high, 800–1 400 kg/m^3.
2. 50–300 mm: The bentonite is clearly influenced of water uptake and has swelled, resulting in a strong density gradient, 1 300–1 500 kg/m^3 close to the SC and up to approximately 1 900 kg/m^3 at 300 mm from the test cell wall.
3. 300–400 mm. The innermost parts of the block has a dry density of approximately 1 850 to 1 920 kg/m^3 i.e. close to the installed block density.

5 Transition Zone Homogenization (TZH)

This test mainly aimed at investigating the evolution and final state regarding water uptake, deformation and pressure in a Transition Zone (TZ) section. The test provides information important for the plug design and the design of the TZ itself.

5.1 TZH: Test setup

The setup used for the TZH test differed from the previously described test setups which used the BB equipment. A drawing of the test setup is provided in Figure 5-1. The scale of the test setup as compared to the real design was about 1:10.8.

Two connected steel tubes, each 550 mm long and with an inner diameter of 175 mm, ensured mechanically stiff conditions to accurately representing the drift. A 2 mm thick filter mat (HDPE) was installed inside the steel tubes, which decreased the drift diameter to 171 mm, in order to provide water to the buffer. There were four inlets/outlets to the filter which made it possible to completely fill up and de-air the test volume with water.

The effective test length was 1 000 mm whereof 121 mm contained pellet filling, on the inside of the plug-side, and the remaining part was filled with bentonite blocks. The inner half, only containing blocks, was denoted the *distance block section* and the outer half, containing both blocks and pellets, the *transition zone section*.

Pistons installed at both ends made it possible to measure the axial pressure in both directions, i.e. both on the block side (Axial pressure 1) and on the pellet side (Axial pressure 2), see Figure 5-1. Radial pressure was measured at six points:

- Four sensors (1:A, 1:B, 2:A, 2:B) positioned at different distances from the pellet filled part. Two of the sensors were measuring the pressure upwards and the other two were measuring the pressure downwards. The positions of the sensors are indicated in Figure 5-1.
- Two sensors (3:A, 3:B) were positioned in the pellet filled part of the test cell; one sensor (3B) at a distance of 30 mm from the plug and the other (3A) at a distance of 100 mm from the plug. The positions of the sensors are indicated in Figure 5-1.

Water consumption was also registered during the operational phase. The amount of water required at installation was determined by weighing and the continued amount of water absorbed by the bentonite together with the applied water pressure were registered by use of special equipment, a GDS (an advanced pressure/volume controller).

Room climate, temperature and relative humidity, was also registered during the operational phase.

5.1.1 TZH: Bentonite blocks

The bentonite blocks needed for the tests were manufactured with the same quality as required for the full scale. The MX-80 Wyoming bentonite had a water content of 20.9 % (21 % ± 1 % is required) and after compaction the blocks had an average dry density of 1 699 kg/m^3 (1 712 ± 20 kg/m^3 is required), see compilation of block data provided in Table 5-1.

Manufacturing was performed at Clay Technology AB using a special mold. The blocks had a diameter of 175 mm after compaction and were then machined down to a diameter of 163.1 mm. The blocks were stored in plastic bags until just before installation in the test cell.

Before installation, the blocks were equipped with feet in order to centralize them in the tube, Figure 5-2. A foot consisted of a M6 bolt screwed into a threaded hole in the block. The target gap size between bentonite blocks and “rock” was 3.95 mm.

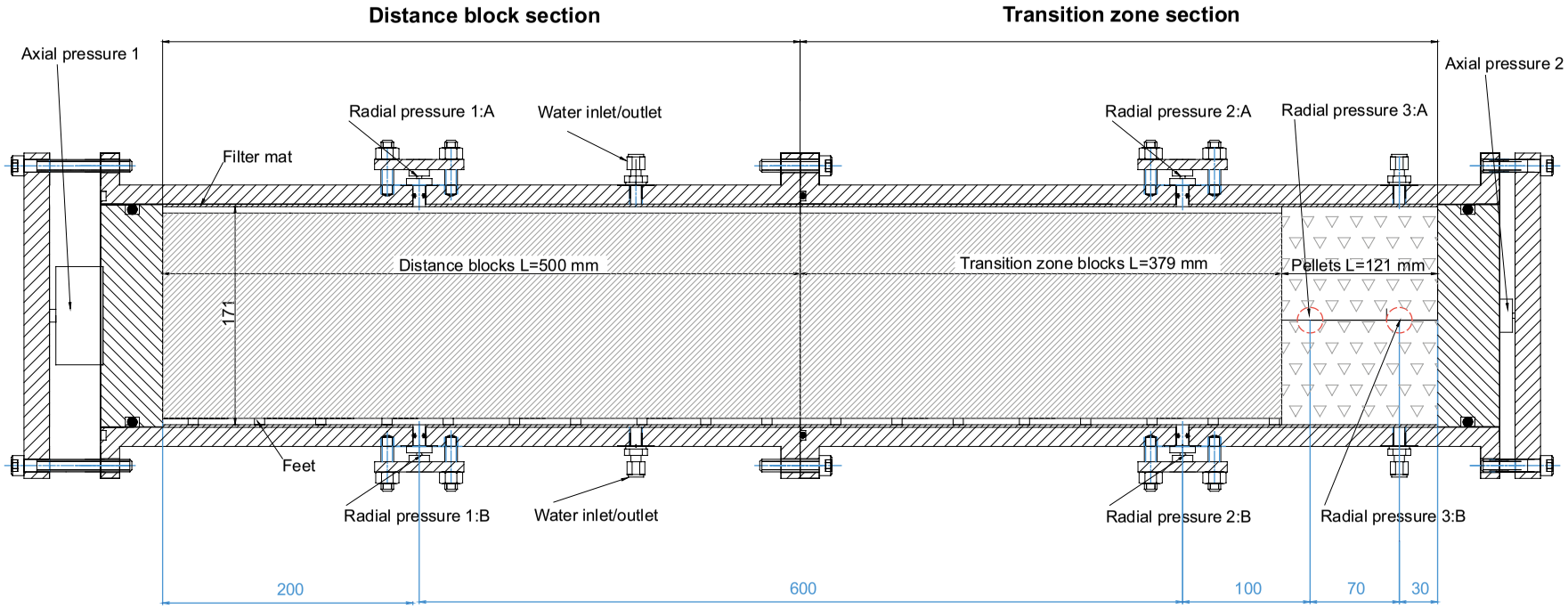

Figure 5-1. *TZH. Schematic drawing of the test layout. The inner half (left 500 mm) is called the "distance block section" and the outer half (right 500 mm) is called the "transition zone section".*

Figure 5-2. *TZH. Photo of a bentonite block. The screws used to simulate the feet can be seen at the mid-height of the block periphery.*

Table 5-1. TZH. Compilation of block data. The blocks are numbered from the inner end (left in Figure 5-1).

Block no.	Diameter mm	Height mm	Mass g	Water content %	Bulk density kg/m^3	Dry density kg/m^3	Remark
1	163.1	50.65	2168.9	20.9	2053	1698	
2	163.1	50.80	2169.4	20.9	2047	1694	
3	163.1	50.03	2156.8	20.9	2067	1710	
4	163.1	50.62	2174.2	20.9	2059	1703	
5	163.1	50.52	2162.3	20.9	2052	1697	
6	163.1	50.45	2155.3	20.9	2048	1694	
7	163.1	50.75	2168.9	20.9	2049	1695	
8	163.1	50.30	2163.8	20.9	2063	1706	
9	163.1	50.10	2153.0	20.9	2060	1704	
10	163.1	43.00	1849.8	20.9	2063	1706	Block height adjusted
11	163.1	50.25	2145.9	20.9	2047	1694	
12	163.1	50.15	2148.5	20.9	2056	1701	
13	163.1	50.40	2150.5	20.9	2048	1694	
14	163.1	50.05	2135.6	20.9	2048	1694	
15	163.1	50.55	2160.5	20.9	2051	1697	
16	163.1	50.20	2152.5	20.9	2058	1702	
17	163.1	50.95	2179.2	20.9	2053	1698	
18	163.1	26.10	1113.2	20.9	2052	1697	Block height adjusted
Average					**2054**	**1699**	

As indicated in Table 5-1 two of the blocks (no. 10 and no. 18) were reshaped in order to fit all blocks within 879 mm. The sum of all individual block heights, however, is 875.9 mm, 3.1 mm less as compared to the installed total block length.

The mismatch between totally installed and summed individual block lengths comes from imperfections at the block interfaces. This will of course also occur in a real, full scale, repository. The difference in lengths (0.354 %) makes the installed average block density ρ_d=1 693 kg/m^3 slightly lower than the average calculated in Table 5-1 ρ_d=1 699 kg/m^3.

5.1.2 TZH: Bentonite pellets

The MX-80 Wyoming bentonite pellets used in the test were manufactured using the roller compaction method which resulted in pillow-shaped pellets with a dry density of 1 841 kg/m^3 and a water content of 14.1 %.

The dry density of the pellet filling, also including voids between pellets, is specified to 1 000 kg/m^3 in the reference design. Tests showed that the available pellets yielded a bulk dry density of 981 kg/m^3 without compaction, so in order to reach the right density, the pellet filling was slightly compacted at installation by manual stacking of some pellets. 3.171 kg of pellets were installed.

5.2 TZH: Operation

After installation of blocks and pellets, the voids in the test setup were filled up artificially with tap water according to the DAWE design. Instead of letting the tubes go through the plug, however, the water inlets at top and bottom of the test cell were used for de-airing and filling, respectively. The ion strength of the tap water was measured to below 2 mmol/L, which is far below the ion strength set by dissolved accessory minerals in the MX-80 clay. The volume of injected water during the artificial water filling was 3.425 liters, very close to the calculated volume of 3.426 liters.

During the remaining of the operational phase the bentonite had access to additional water (simulated formation water) from the filter mats installed at the tube wall. The filters were connected to a GDS which controlled the water pressure to 20 kPa. The additional water was given a salinity of 1 % (50/50 $NaCl/CaCl_2$) which is expected to be similar to the field conditions at Olkiluoto and Forsmark during installation. About once a week the filter was de-aired by flushing water through it.

Immediately after the artificial water filling the bentonite started to take up additional water. The graph provided in Figure 5-3 shows the water uptake plotted versus time together with the measured room temperature.

The total volume of water taken up by the bentonite at the time for test termination was 4.11 liters (4.158 liters was calculated to be needed in order to reach full saturation). The maximum water uptake, 4.29 liters, was registered after approximately 2 months but at this time water started to flow out from the test cell.

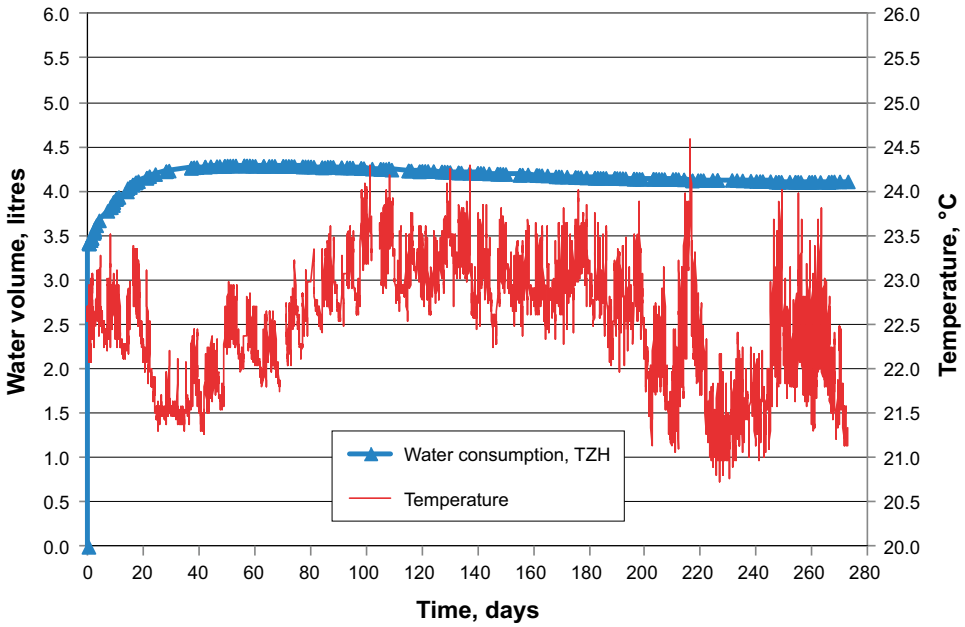

Figure 5-3. *TZH. Water consumption as function of time. The room temperature is also provided in the graph.*

One explanation for this behavior may be that compressed air was trapped in the blocks during compaction. During the water saturation process, the trapped and compressed air was released from the bentonite and ended up in the filters in an expanded state.

In order to ensure that the bentonite has had full access to water and that no air was trapped in the filter, water was circulated through the filter approximately once a week. During this circulation it was observed that air bubbles did leave the system. It is, however, probable that there were parts of the filter where air could still be trapped and the amount of trapped air in the filter increased with time which could cause the apparent reduction in water volume.

The registered swelling pressure as function of time is provided in Figure 5-4. In order to facilitate the reading the maximum values at time for termination are also provided in Figure 5-5 (boxes beside the sensor positions).

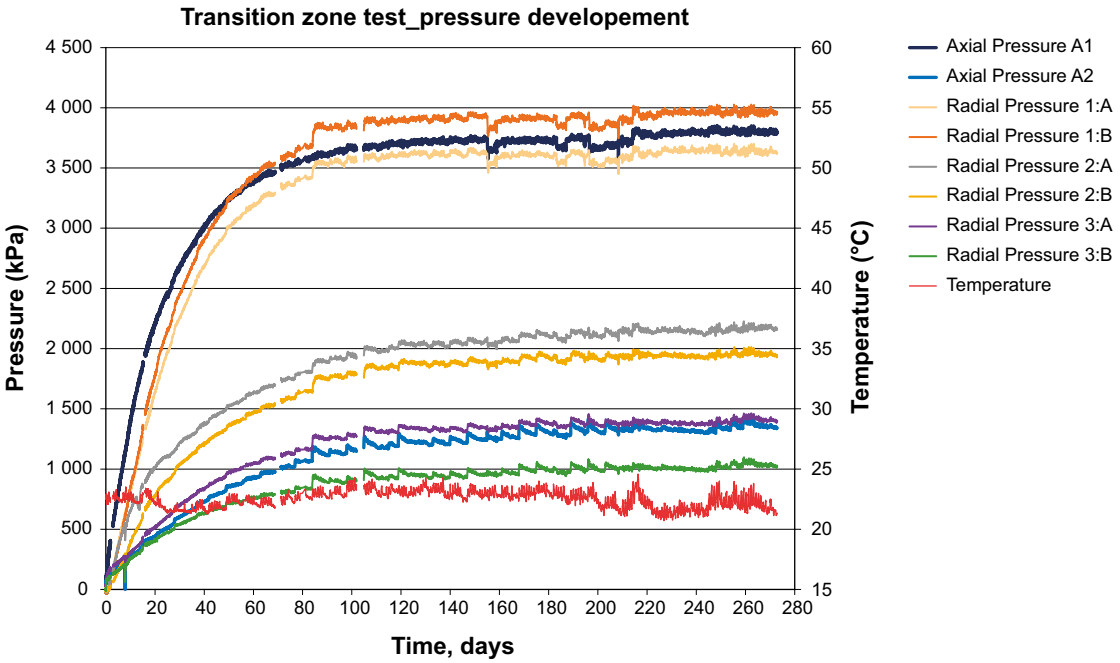

Figure 5-4. *TZH. Swelling pressure plotted versus time. The room temperature is also provided in the graph.*

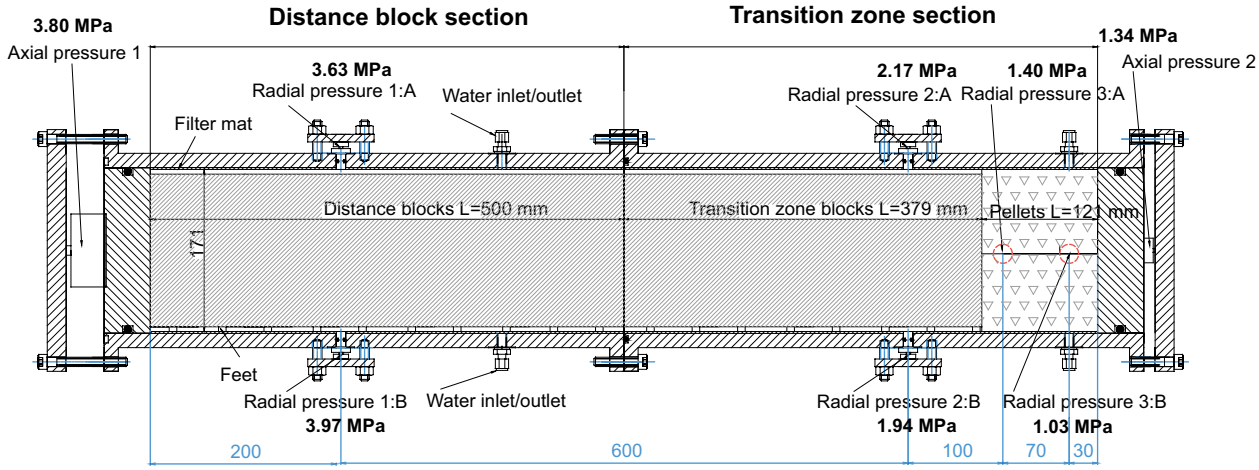

Figure 5-5. *TZH. Schematic drawing showing the positions of the pressure measurements. The registered swelling pressure data after 273 days test duration (2015-08-31) is provided in the boxes.*

The registered swelling pressures are all very logical. The graph shows that the swelling pressure increased fast in the distance block section up to between 3 600–4 000 kPa (axial pressure sensor A1 and radial pressure sensor 1:A and 1:B) after about 4 months. The swelling pressure on the pellet side was at the same time between 1 000 and 1 400 kPa (axial pressure sensor A2 and radial pressure sensor 3:A and 3:B) while the radial sensors placed approximately 80 mm from the pellet filling (2:A and 2:B) registered swelling pressures close to 2 000 kPa.

The graph also shows that the maximum pressures were reached after approximately 4 months. After this time only minor changes in pressure development can be seen.

The influence of temperature variations in the room had been small. The small steps that can be seen on the pressure curves, approximately every seven days, correspond to water circulation in the filter mats.

5.3 TZH: Dismantling and sampling

When dismantling the experiment the two steel tubes were first separated, see Figure 5-6. A hydraulic jack was thereafter mounted between a counter hold and the axial piston made of PVC (A1), Figure 5-7. The bentonite was then pushed out of the steel tube, marked so that the directions could be identified and wrapped in plastic until the sampling could start, see Figure 5-8.

When dismantling the transition zone section, the hydraulic jack was applied on the block side to avoid deformation of the low density clay at the pellet filling side. As Figure 5-9 shows, the bentonite moved somewhat in relation to the plastic filter during the dismantling. The complete specimen, however, was removed from the test cell in one piece without any problems. Also this part was wrapped in plastic until it was time for sampling.

When performing the sampling, one cm thick axial slices were sawed out from the bentonite columns. Two different sample patterns, a coarser, shown in Figure 5-10, and a finer, shown in Figure 5-11, were used. A repeated sequence of four courser followed by one finer was used along the column length.

Figure 5-12 and Figure 5-13 show the uncovered distance block section before sampling when viewing from the 1:B and the 1:A side, respectively. Figure 5-14 shows the uncovered transition zone section before sampling.

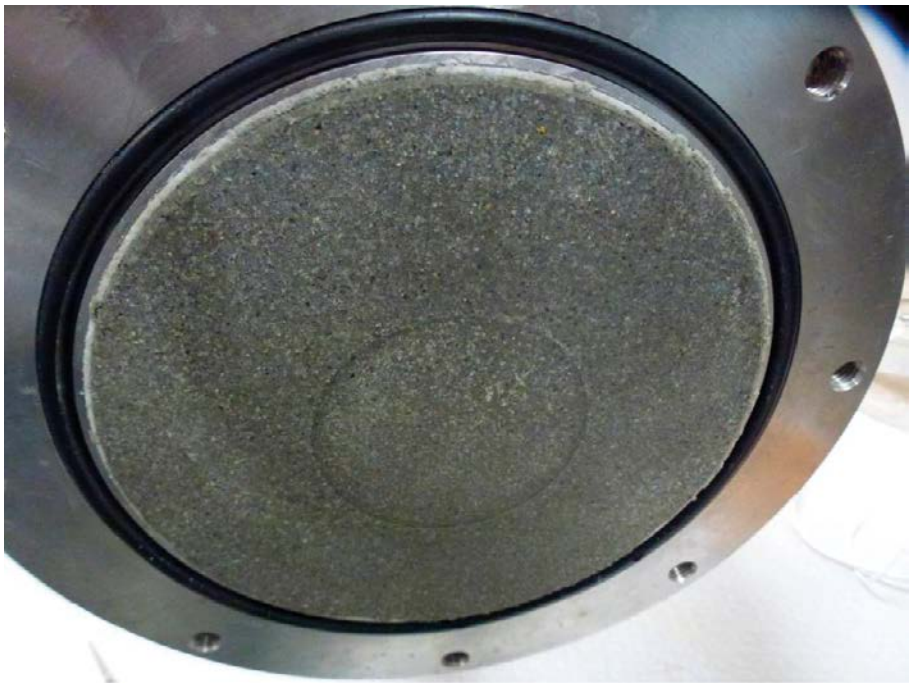

Figure 5-6. *TZH. Photo showing the exposed bentonite after having divided the test cell at the midpoint. The central ring mark comes from the compaction.*

Figure 5-7. *TZH. The bentonite in each of the test cell halves was pushed out using a hydraulic piston.*

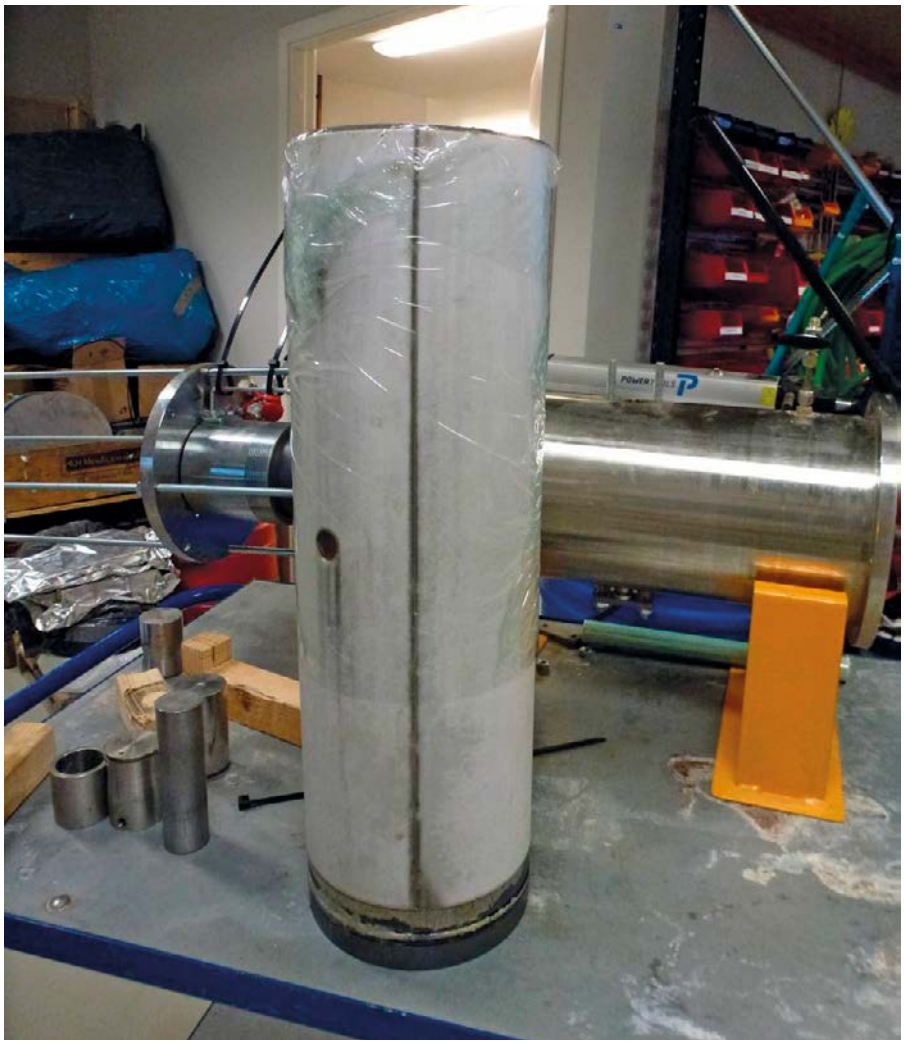

Figure 5-8. *TZH. The distance block section (block side) has been removed. The bentonite is still covered with the plastic filter and a protective layer of thin plastic has been wrapped around to prevent drying.*

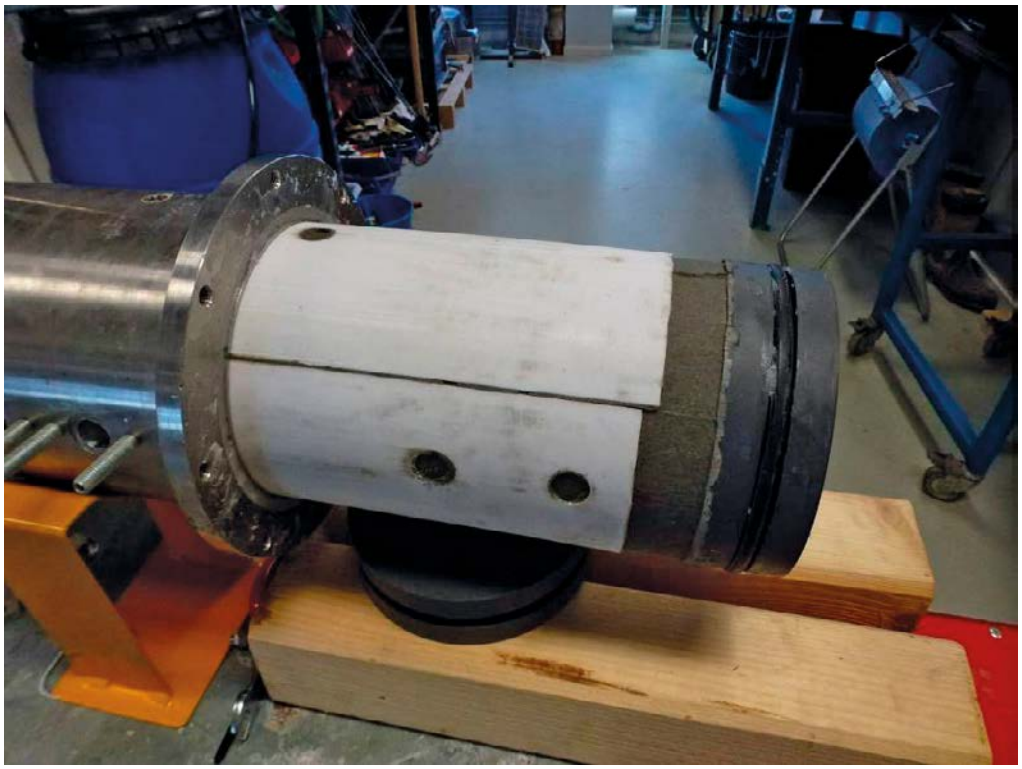

Figure 5-9. *TZH. Photo showing the extraction of the transition zone section including the pellet filling. The holes in the plastic filter show the positions of the radial pressure measurements. Note that the bentonite specimen has moved somewhat in relation to the plastic filter.*

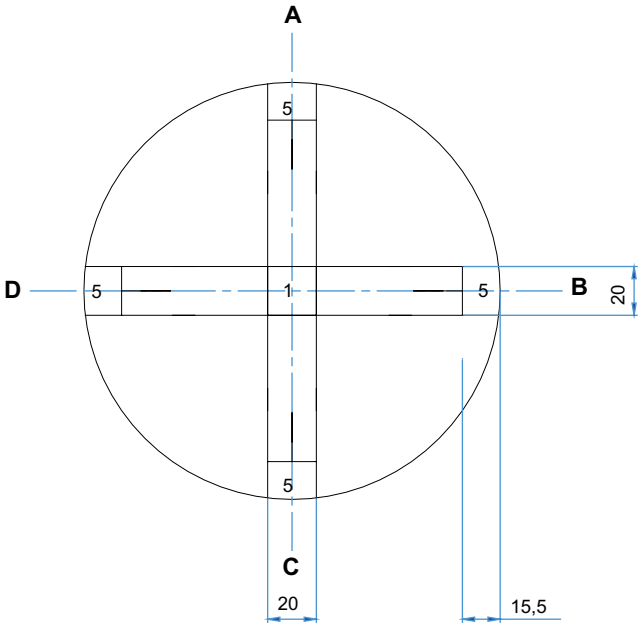

Figure 5-10. *TZH. Cross section showing the sample locations when sampling every cm in axial direction*

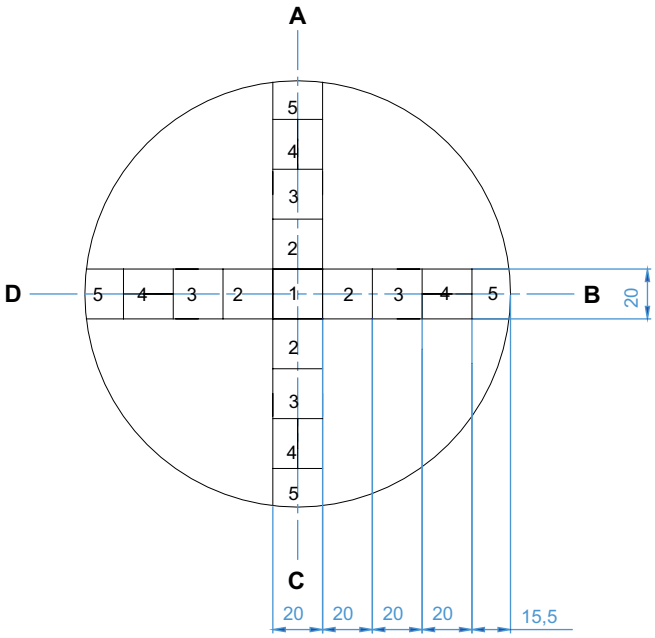

Figure 5-11. *TZH. Cross section showing sample locations when sampling every fifth cm in axial direction*

Figure 5-12. *TZH. The plastic filter has been removed. Note the two rows of feet used to centralize the blocks. The circular point at the middle marked red is where the piston from the radial pressure measurement 1:B was located.*

Figure 5-13. *TZH. View of the top side and the position of pressure measurement 1:A. Note the cracks from the earlier block boundaries.*

Figure 5-14. *TZH. The transition zone section containing both pellets and blocks is ready for sampling (former pellet section is to the right and outside is the PVC piston with a central O-ring mounted). No evident block boundaries could be seen before the sampling started on this half, but some appeared at the left part i.e. at the block side, after start cutting.*

5.4 TZH: Results and analysis

All data are given in Appendix E4, in the present section however only a subset is commented and discussed.

5.4.1 TZH: Full scale versus laboratory scale

The laboratory test was performed in the scale 1:10.8. All dimensions were adapted to the scale; gap widths, the required length of the pellet filled section (assuming a friction angle of 10°), and the total length of the transition zone according to the performed modelling (Appendix E5 and Appendix E6). The initial density of the blocks and pellets used in the test aimed to be within the accepted variation of the reference design for a KBS-3H repository (SKB 2012). The different dimensions of the components in both the full scale reference design and in the laboratory test together with the required block and pellet quality are provided in Table 5-2. The calculated density after saturation in a block section is also presented.

As shown in the table, the densities of the blocks that have been used in the test were slightly lower than intended but still within the accepted variation. Consequently the saturated density after homogenization was also slightly too low. The expected average dry density in a block section that has only swelled in radial direction was calculated to be 1 546 kg/m^3 when using the average density of the individual blocks.

Table 5-2. TZH. Comparison between data of the full scale reference design and the performed laboratory test regarding dimensions, block and pellet quality and the calculated density after homogenization.

Property	Full scale	Accepted variation	Laboratory test
Dimensions			
D rock, mm	1 850		171
D transition block, mm	1 765		163.1
Gap block-rock, mm	42.5		3.95
Block quality			
Bulk density, kg/m^3	2 072		2 054
Dry density, kg/m^3	1 712	±20	1 699
Water content, %	21	±1	20.9
Pellet quality			
Bulk density, kg/m^3	1 141		1 141
Dry density, kg/m^3	1 000		1 000
Water content, %	21		14.1
After homogenization (Distance block section)			
Saturated density, kg/m^3	2 000	±50	1 992
Dry density, kg/m^3	1 559		1 546

5.4.2 TZH: Block heights

The height of all blocks were individually measured at the time for installation. During sampling it was possible to detect the former joints between the blocks that had been located furthest from the pellet filled section and also to perform new measurements of their heights. All measurements were made with a digital caliper. The measurements of the block height at installation were easy to perform while the measurements at termination were more difficult (not perfectly even surfaces etc.).

The results from the measurements of block heights are provided in Table 5-3. The change in block height is rather similar for all measured blocks; between 0.7 and 1.5 mm. The results from this measurement show that there is a fairly similar swelling for all these blocks. If the first 10 blocks, starting at the inner end of the distance block section, are considered, the initial total height of these blocks is 497.3 mm and the final total height is 508.9 mm, yielding an average homogeneous axial swelling of 2.3 %.

Table 5-3. TZH. Comparison of block heights determined at the time for installation and after test termination. Note that it was not possible to detect all block interfaces during test termination.

Block no.	Block height at installation [mm]	Block height at termination [mm]	Change in height [mm]
1	50.7	52.0	1.4
2	50.8	51.7	0.9
3	50.0	51.5	1.5
4	50.6	51.5	0.9
5	50.5	51.2	0.7
6	50.5	51.6	1.2
7	50.8	51.8	1.0
8	50.3	51.7	1.4
9	50.1	51.5	1.4
10	43.0	44.4	1.3
11	50.3	51.0	0.8
12	50.2	51.0	0.9
13	50.4	na	na
14	50.1	na	na
15	50.6	na	na
16	50.2	na	na
17	51.0	na	na
18	26.1	na	na

5.4.3 TZH: Sample analyses

Figure 5-15 shows a contour plot of the water content distribution over the complete specimen length, the upper graph showing a cross section including direction. A and C, and the lower graph showing a cross section including direction. B and D (see description in Figure 5-10 and Figure 5-11). Corresponding contour plots with the dry density distribution and the degree of saturation are provided in Figure 5-16 and Figure 5-17.

Some comments to the contour plots:

- The contour plots verify that there is no or very small influence of direction (A, B, C and D) i.e. there is an almost perfect axisymmetric distribution regarding water content and dry density along the specimen length.
- The blocks in the distance block section (between 0 and approximately 500 mm) have an almost similar radial density distribution. The central parts have a density varying between 1 515 to 1 560 kg/m^3 while the outermost parts, close to the test cell wall, have a density between 1 400 to 1 500 kg/m^3.
- The lower density seen in parts of the section close to the inner end (0 mm) is mainly caused by lower density in the outermost samples as also seen in Figure E-3 to Figure E-10 in Appendix E4. The apparent lower density for the inner samples is not seen in those diagrams and is judged to be caused by interpolations of the plot program. However, the lower density at the periphery close to the bottom is probably caused by friction against the bottom that somewhat hinders the swelling.
- The pellet filling had a dry density of 1 000 kg/m^3 after installation. The lowest density in the former pellet filling at time for termination was close to 1 300 kg/m^3 (approximately 50 mm of the former pellet has this density). From this density, 1 300 kg/m^3, there is a clear density gradient up to approximately 1 550 kg/m^3 (between 500 and 950 mm).

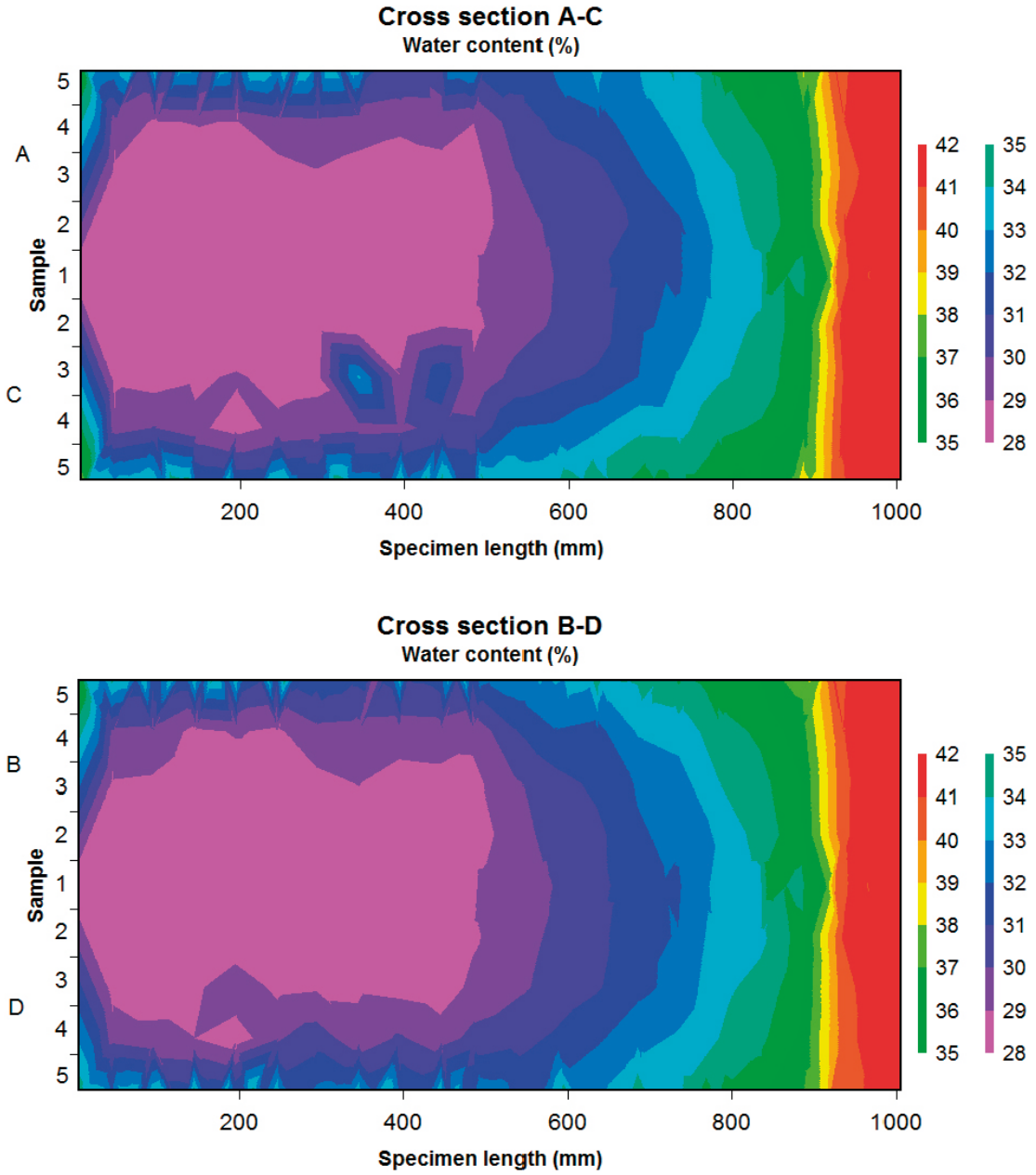

Figure 5-15. *TZH. Contour plots showing the water content distribution in cross section A-C (upper) and B-D (lower).*

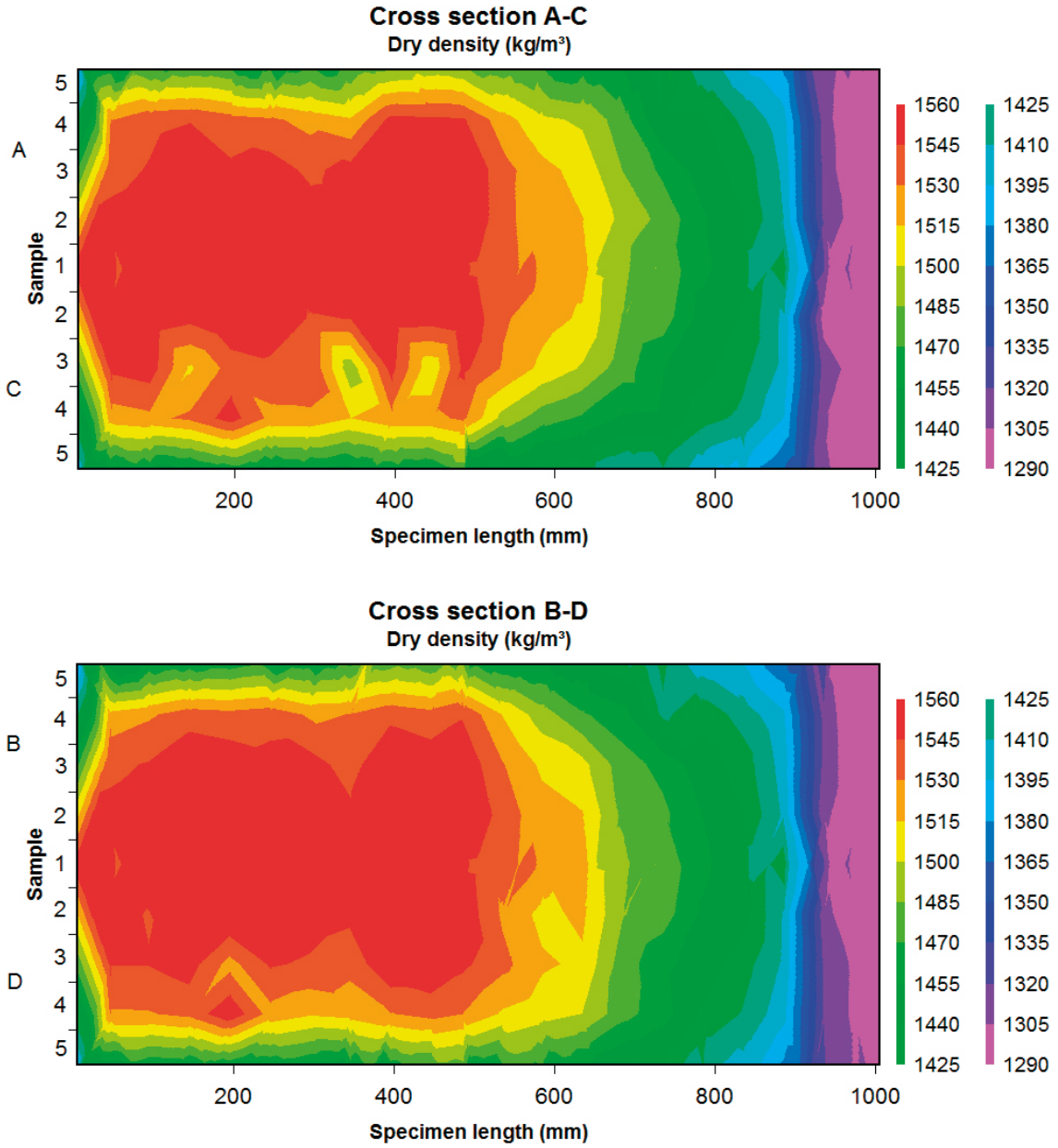

Figure 5-16. *TZH. Contour plots showing the dry density distribution in cross section A-C (upper) and B-D (lower).*

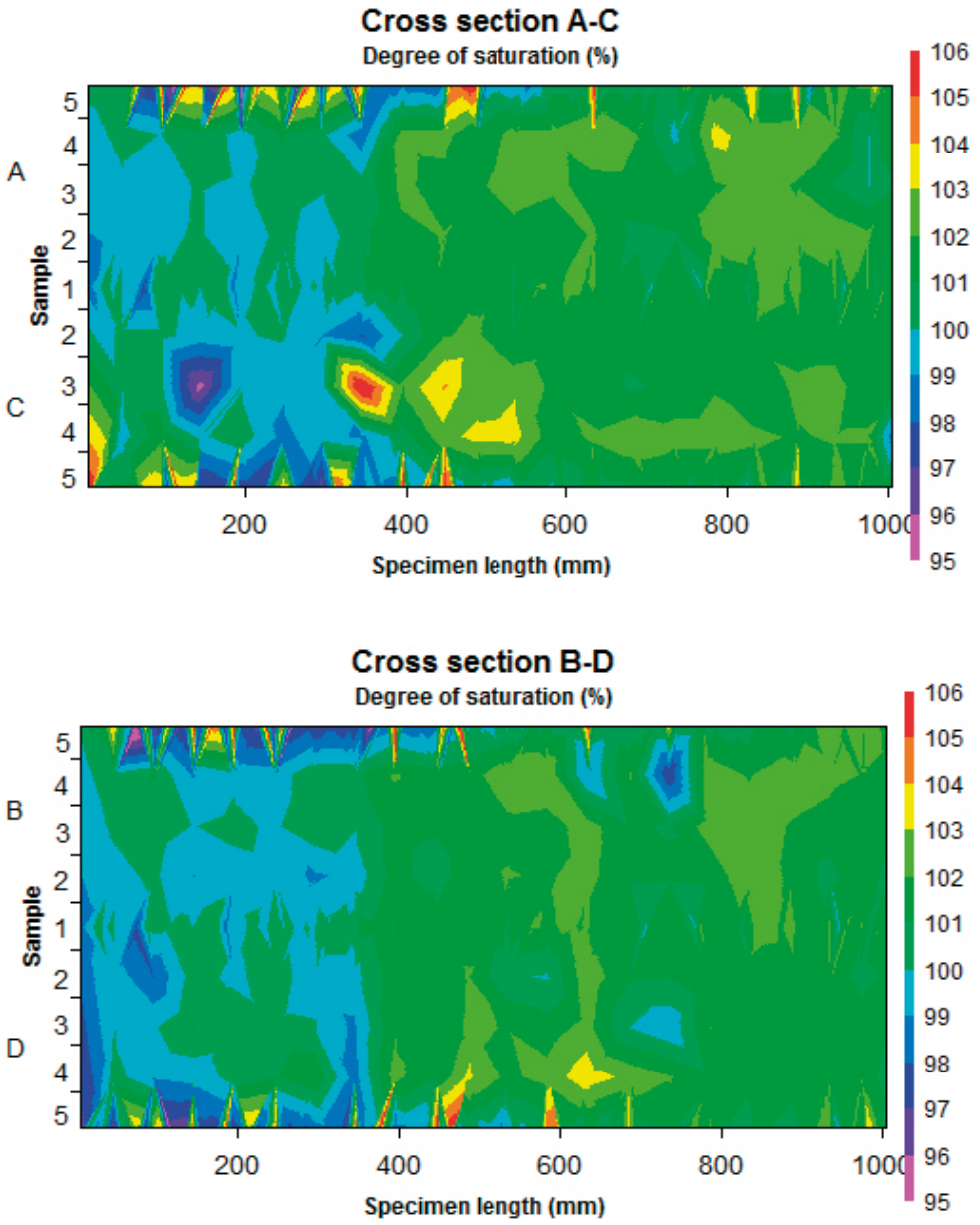

Figure 5-17. *TZH. Contour plots showing the degree of saturation distribution in cross section A-C (upper) and B-D (lower).*

5.4.4 TZH: Comparison between experimental data and analytical model solutions

Analytical methods have been used to estimate the swelling pressure against the drift plug as a function of the length of the transition zone to the position where the density is unchanged in a KBS-3H repository, Appendix E5. The results from these estimations have later also been adapted to the performed scale test, Appendix E6. The calculations made for the full scale refer only to stresses and strains after equilibrium and the results can therefore be directly scaled down to the dimensions of the scale test as done in Appendix E6. The results are, however, very dependent on the applied friction angle (shear resistance between bentonite and rock) which varies depending on the swelling pressure.

The performed laboratory test was dimensioned for a friction angle of 5 degrees, which according to the calculations would result in a swelling pressure on the plug of approximately 1 400 kPa and a needed length of the transition block zone (influenced by the swelling) of 587 mm i.e. the total test length including the pellet filled section would for this friction angle be 708 mm (121 + 587), as also shown in Table 5-4. In order to have some margins and include a potential distance block section it was decided to have a total test length of 1 000 mm.

The results from the test showed that the swelling pressure against the plug was approximately 1 340 kPa i.e. very close to the calculated result (1 400 kPa) for the friction angle 5°. The length of the transition block zone that was influenced by the swelling bentonite was estimated to approximately 500 mm in the test, which is shorter than the calculated 708 mm and more in agreement with the results for the friction angle 10°. As mentioned earlier, the calculated results are very depending on the applied friction angle, which also varies depending on the swelling pressure i.e. the friction angle will vary along the test length. By using the test results the friction angle could be estimated to be somewhere between 5 and 10 degrees, but the evaluation is complicated by the inhomogeneous density distribution in radial direction.

Table 5-4. TZH. Required length of the transition blocks and the required total length of the equipment (from PM provided in Appendix 2).

Friction angle ϕ	Total length L_T [mm]	Length of transition block L [mm]	Swelling pressure on the plug [mm]
5°	708	587	1413 kPa
10°	527	406	771 kPa
20°	348	227	315 kPa
30°	277	156	146 kPa

In order to further analyze the results and the comparison with the modelling results averaging of the results in radial direction has been done. In doing so the measured densities must be weighted in relation to the square section area that corresponds to the sample location. Figure 5-18 shows the sampling scheme from Figure 5-11 and the corresponding areas to be weighted.

Table 5-5 shows the area corresponding to the different sample locations and the derivation of the weight.

The weights shown in Table 5-5 have been used to calculate the average dry density of each 5 cm section in each direction A-D according to the density plots in Figure E-3, Figure E-5, Figure E-7, and Figure E-9. The results are summarized in Figure 5-19. Since the relations are very similar and the test thus regarded as axis-symmetric the average of these curves can be calculated and plotted as shown in Figure 5-20.

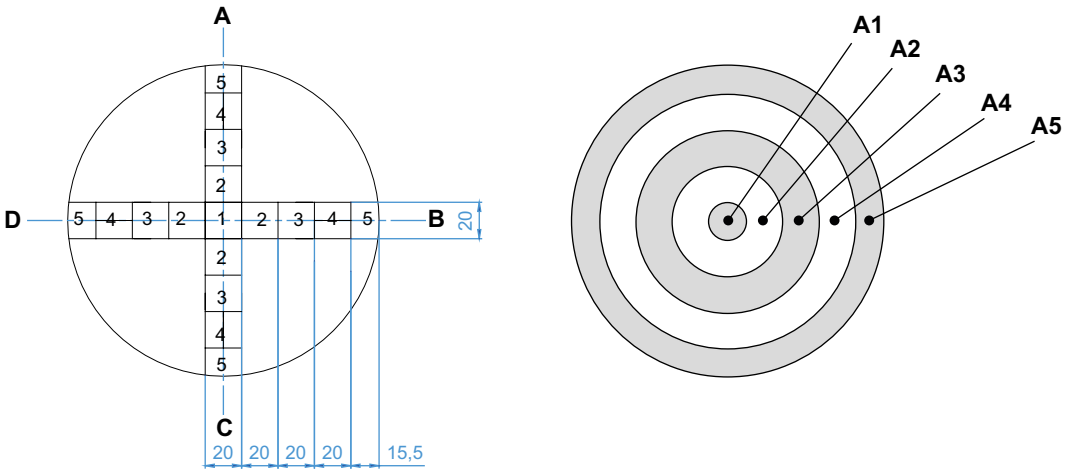

Figure 5-18. *TZH. Sampling scheme and corresponding area used for weighting.*

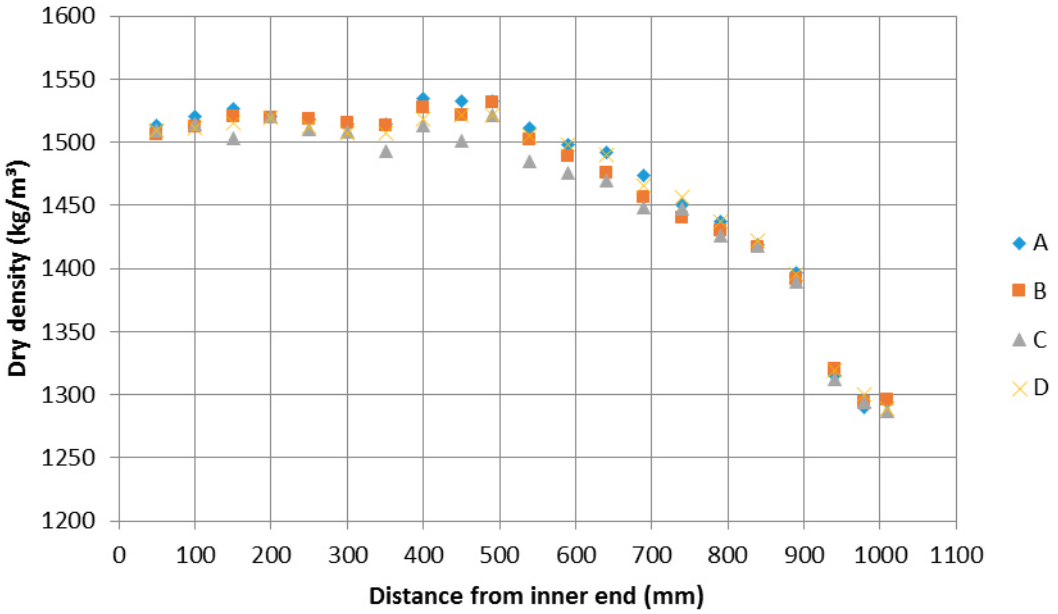

Figure 5-19. *TZH. Calculated average dry density in each 5 cm section weighted according to Table 9-4 plotted versus the distance from the inner end of the distance block section.*

Table 5-5. TZH. Weighting of the sample location.

Sample location	Inner radius [mm]	Outer radius [mm]	Area/π [mm²]	Weight [–]
1	0	10	100	0.0137
2	10	30	800	0.1094
3	30	50	1600	0.2189
4	50	70	2400	0.3283
5	70	85.5	2410.25	0.3297
Total	**0**	**85.5**	**7310.25**	**1.0**

The relation in Figure 5-20 is interesting. A number of observations can be done:

- There is a slight reduction in density close to the inner end, which probably can be explained by some initial displacements at the contact in the beginning of the test.
- There is a small increase in density at 400–500 mm from the end. This is more difficult to explain but it is analyzed below.
- The density is approximately constant for the distance block section (first 500 mm) at the dry density about ρ_d=1 515 kg/m^3.
- Between 500 mm and 890 mm, corresponding to the block part of the transition zone, the density decreases almost linearly to ρ_d=1 390 kg/m^3.
- Then at the pellet part of the transition zone there is a fast drop to ρ_d=1 300 kg/m^3 between 890 mm and 940 mm.
- Finally the density is fairly constant at ρ_d=1 300 kg/m^3 for the last 60 mm.

This observations can be used to make a simplified model of the results. Figure 5-21 shows the "model" and the measured average values. The initial average dry density distribution and the two predicted distributions using the friction angle 5 and 10 degrees between the bentonite and the surrounding steel cylinder are also shown.

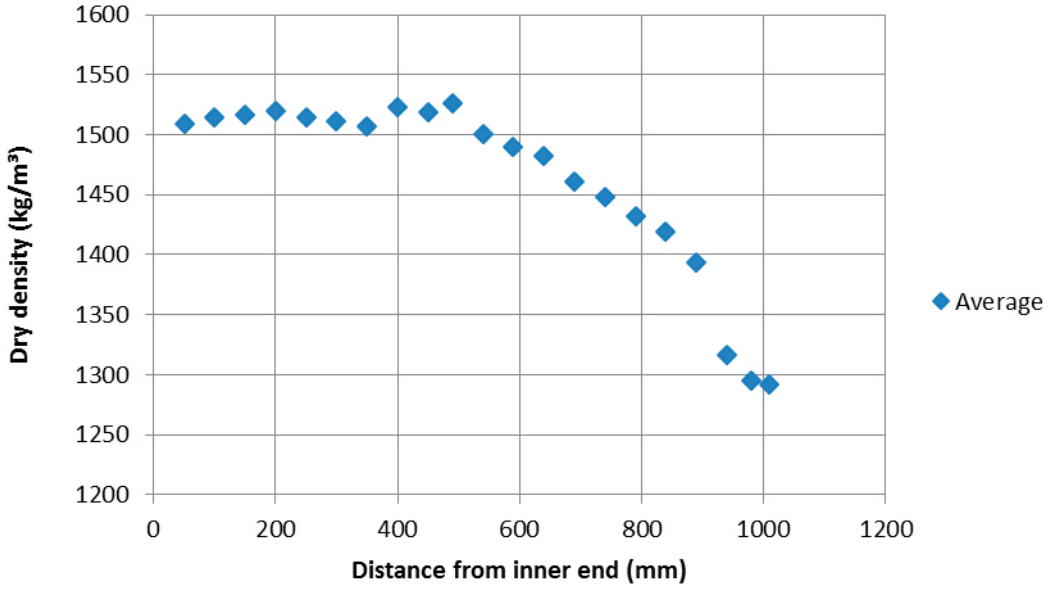

Figure 5-20. *TZH. Calculated average dry density of the relations shown in Figure 9-13 plotted versus the distance from the inner end of the distance block section.*

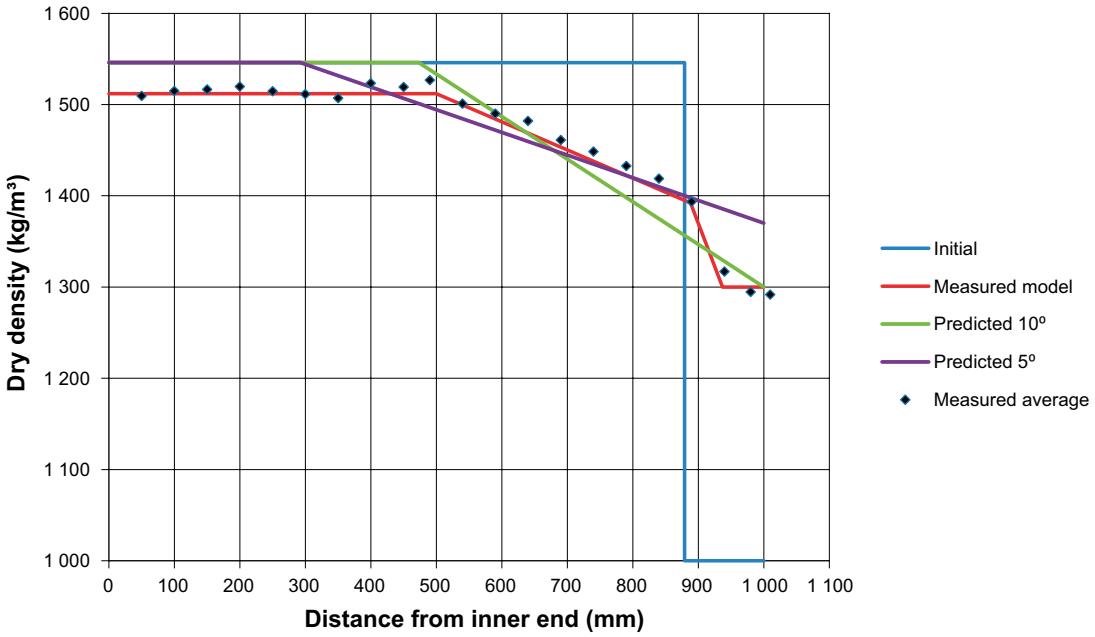

Figure 5-21. *TZH. Measured average dry density (according to Figure 5-20) plotted versus the distance from the inner end of the distance block section together with the initial and the simplified measured model as well as the two results of the predictions using ϕ=5° and 10° friction angle.*

The average density at the distance block section the first 500 mm ρ_d=1 515 kg/m^3 is clearly lower than the average density at installation ρ_d=1 546 kg/m^3. This indicates a homogeneous swelling of 2.1 %, which can be compared to the swelling of each installed block in the distance block section measured at excavation. According to Section 5.4.2 this swelling is 2.3 %, which thus agrees well with the average density measurements.

The reason for this even swelling is not clear. It is though possible that the swelling took place early in the test due to water penetrating between the blocks before the radial swelling had created any friction against the periphery. A reason could be an early cracking of the blocks, which was observed in other tests for KBS-3V where this phenomenon caused an early upwards swelling. The small elevation of the density between 400 mm and 500 mm could be explained by slightly less swelling for those blocks.

There is a similar constant dry density distribution at the pellet part close to the outer end and a strong density decrease between 890 and 940 mm. The final pellet part has though increased its dry density from ρ_d=1 000 kg/m^3 to ρ_d=1 300 kg/m^3, which shows that there is probably a similar compression before the friction against the periphery has full effect that can explain some of that density increase (but not all since the dry density is rather high).

It is difficult to compare the measured results with the predicted since the analytical calculation does not take neither the initial compression/expansion into account nor the radial inhomogeneity. The measured change in density gradient between the block part and the pellet part, which is judged to be caused by the different behavior during swelling and compression, is not captured by the simplified analytical method. However, the length of the zone from the outer end to where the reduction in density begins indicates a friction angle of 10° rather than 5°.

It is also interesting to compare the measured and modelled swelling pressure against the end lids. Table 5-6 shows some comparisons.

Table 5-6. TZH. Comparison between measured and calculated stresses on the end faces

Identification	Axial stress at inner end [kPa]		Axial stress at outer end [kPa]	
	Measured	Calc. from ρ_d	Measured	Calc. from ρ_d
Test	3770	4270	1310	835
Pred. ϕ=5°		5410		1413
Pred. ϕ=10°		5410		771

Table 5-6 shows a rather complicated situation. At the inner end the measured stress is lower than the "predicted" (which corresponds to the initial condition), mainly because the prediction does not take the homogeneous density decrease into account, but it is also a little lower than calculated from the measured dry density (according to Equations E-1 and E-2 in Appendix E5). At the outer end the measured stress 1 310 kPa is in rather good agreement with the prediction at ϕ=5° (1 413 kPa), but clearly higher than both the stress calculated from the measured dry density (835 kPa) and the predicted at ϕ=10° (771 kPa). So the measured stress on the simulated plug agrees with the predicted at ϕ=5° but the measured dry density agrees with the predicted at ϕ=10°. However, the friction angle is a function of the swelling pressure and thus varies along the steel tube. The change in dry density profile between the block part and the pellet part of the transition zone section also indicates this.

Figure 5-22 shows a comparison between modelled and measured stress distribution along the steel tube.

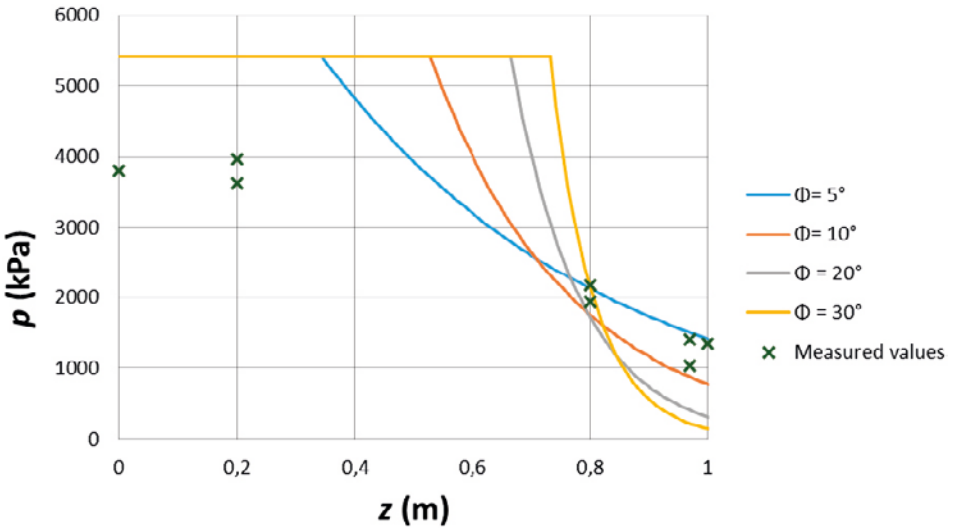

Figure 5-22. *TZH. Modelled swelling pressure distribution at different friction angles and measured by the transducers on the steel tube and the end lids.*

The comparison in Figure 5-22 shows that the measured swelling pressure in the distance block section is rather constant as predicted but lower. This is in agreement with that the density is lower than predicted. In the transition zone section the measured values are in good agreement with the prediction for friction angle between 5 and 10 degrees. Also the pressure gradient agrees well.

It is thus difficult to evaluate a certain friction angle but it seems to be between 5° and 10°. This is also in agreement with the expectations since the friction angle of the bentonite itself varies in the measured stress range between 9° and 13° (Börgesson et al. 1995) and should be about half for the contact bentonite steel i.e. between 4.5° and 6.5° (Dueck et al. 2014). In order to have a more relevant evaluation a finite element modelling of the test should also be done.

The friction between a rock surface and bentonite depends very much on the surface roughness of the rock, i.e. the results of the boring of the drift. If the surface is very rough the failure has to go through the bentonite itself and the friction angle should thus for that case be the higher value. If the surface is very smooth the failure goes between the bentonite and the rock and the friction angle should for that case be close to that of a smooth steel surface. A large part of the test had a filter as surface and since the filter is rather rough it is possible that the test corresponds to a rock with a rough surface. See also Börgesson et al. (1995).

6 Discussion and conclusions

Below follows a compilation of comments and conclusions given in the PMs describing the tests. BB II and BB III were reported in a merged fashion and the comments and conclusions chapter are here kept in this format. BB IV and TZH are given individual subchapters. Finally, comparative subchapters with comments and conclusions regarding comparisons between BB II / BB III and BB IV / BB II are given.

6.1 Comments and conclusions regarding BB II and BB III

The following comments and conclusions were made when analyzing the results from BB II and BB III:

- The tests are regarded as to represent the short term swelling behavior at these extremely dry conditions well. The gap widths and initial densities of the blocks are in close agreement to what is used at the full scale MPT test.
- The results from the radial pressure measurements in both tests show that, also at these extremely dry conditions, there will be a pressure build up against the rock wall. The pressure will after 7–8 months, according to the test results, be between 70 and 250 kPa around a SC and between 100 and 140 kPa around a distance block.
- The degree of saturation was close to 100 % for all samples taken from the material within the initially empty gaps and was found to decrease with increasing distance from the outer surface. The radial gradient in degree of saturation was larger for BB II as compared to BB III. This originated from the difference in initial start value, about 60 % for BB II and about 95 % for BB III. At excavation the degree of saturation for the innermost part of the buffer was evaluated to approximately 65 % for BB II and about 96–98 % for BB III.
- There were no indications of decreasing swelling pressure during the tests. The pressure continued to increase throughout the entire test duration.
- The daily temperature variations in the test laboratories could be seen as small variations in the registered pressure. An increase in temperature gave an increase in pressure. The pressure development over time was, however, not affected.
- The gaps were “artificially” water filled according to the DAWE reference design at installation. In BB II 120.9 liters were used at installation, 1.37 liters more than the calculated initial gap volume of 119.5 liters. In BB III 36.3 liters were used at installation, 0.47 liters more than the calculated initial gap volume of 35.83 liters. The main reason for the additional volumes is believed to stem from water uptake of the bentonite during water filling. The duration of the setup of the BB II test was three times that of the BB III test, which could explain the larger volume of water uptake in the former.
- The BB II test shows that the radial pressure against the rock around the SC will vary depending on the position in relation to the perforation pattern of the SC. Directly on the outside of the perforations higher pressures develop as compared to positions in between perforations. This comes from the density variations due to the character of the flow (swelling/extrusion) of the bentonite through the perforations, where higher density “muffins” develop on the outside of the perforations. Between the muffins empty voids were present close to the SC shell but bentonite covered almost all of the simulated rock surface.
- In BB II the SC was standing on feet (steel tubes welded to the SC shell just over a perforated hole). At sampling all feet were found to be filled with bentonite and the analyzed samples showed that the density was slightly higher inside a foot than outside. This depends on the fact that the bentonite had flowed into a closed volume with no possibility to expand in radial direction.

- For both tests the sample analysis showed that there are strong gradients both in water content and dry density from the simulated outer rock surface to the block center. The main parts of the blocks have been involved in the redistribution of material, only the innermost parts, 0–100 mm from block center, seem to be unaffected and have the same density and water content as at installation.
- At dismantling, the two tests had been running for 230 (BB II) and 218 (BB III) days, respectively. The registered radial pressures were slowly increasing at all measured points. This shows that the homogenization process was still slowly ongoing. The tests simulate extremely dry conditions where there is no access to water from the rock and it is difficult to predict how the swelling pressure would develop under other conditions. In a real repository also drifts considered dry will most probably provide some water and this will of course enhance the conditions for homogenization.

The two tests are considered to give important information regarding the swelling behavior and swelling pressure development when installing SCs and distance blocks according to the KBS-3H design in dry deposition drifts. The tests have shown that there will be a pressure build up against the rock walls also at these dry conditions which is considered to be favorable in order to prevent thermal spalling of the rock wall. It is, however, not known if the achieved pressures are high enough in order to prevent spalling from occurring. The APSE experiment, described in Andersson (2007), indicated that a confinment pressure about 100–200 kPa could be sufficient to prevent spalling.

It should be noted that the geometry and the temperature in a real repository differ from those for the tests. The difference in geometry is not expected to affect the results significantly due to the short test period. Increase in temperature and development of a radial temperature gradient is however expected to increase the water content and density gradients. It may also cause cracking of the bentonite blocks, which may influence the wetting evolution significantly.

6.2 Comments and conclusions regarding BB IV

The following comments and conclusions came from studying the results of the BB IV test:

- During the artificial water filling at installation, 43.4 liters were injected. The available volume was calculated to 44.3 liters. The difference between the injected volume and the calculated volume was −0.9 liters.
- During the first three days approximately 1.6 liters of water were pushed out from the test cell. This was the result of the early swelling of the bentonite in the open system configuration. In this sense the test design deviates from the real case, where high backpressure is expected in the rock which prevents water outflow from the drift. In a closed system a pore pressure build up is expected (see e.g. results from the BB II test).
- A water pressure of 400 kPa was applied after 45 days. The water uptake was rather constant between day 60 and day 182, when the test where terminated. There was, however, a small decreasing tendency by time.
- The test is believed to provide an accurate representation of the SC-system short term behavior for actual conditions; the width of the initial empty SC-rock gap and initial densities of the buffer blocks were close to what is planned to be used in the full scale.
- The radial pressure measurements showed insignificant pressure build up against the rock wall in areas located between the perforated holes. On the outside of a perforation, however, significant swelling pressure buildup is expected, which is the indication from the still running BB V test. The expected radial pressure on the rock after about 6 months is therefore between 0 and 200–400 kPa, based on results from BB IV and BB V (not yet reported). The magnitude is expected to depend on the position in relation to the SC shell perforation pattern.
- The degree of saturation was assessed to be 100 % for all samples taken from the SC-rock gap even if there was a variation in the results (see explanation given in Section 6.5). The degree of saturation was found to decrease almost linearly from fully saturated at 50 mm (from the test cell wall) down to the installation state value at 200 mm (from the test cell wall). The innermost part from 300 to 400 mm (from the test cell wall) was almost unaffected.

The BB IV test is considered to have given important information regarding the swelling behavior and swelling pressure development around a SC when additional water from the rock is available. The test has shown that the SC-rock gap will be filled with swelling bentonite quite soon after installation. The variation in density of this material will, however, be large and consequently also the swelling pressure acting on the rock.

A similar test still running, BB V, is planned to be terminated after being fully saturated. The results from both tests, BB IV and BB V, will give important information regarding the water uptake, swelling and homogenization of the bentonite in a SC-system in a KBS-3H repository.

It should be noted that the geometry and the temperature of the BB IV test setup differ from those expected in a real repository. The difference in geometry is not expected to give a significant difference due to the short test period. The heat generated by the canister in the real repository will, however induce a temperature gradient which dries the inner part of the bentonite blocks. This increases the radial water content gradient and may also cause fractures to develop in the bentonite blocks, which may significantly influence the wetting evolution.

6.3 Comments and conclusions regarding TZH

The following comments and conclusions resulted from studying the TZH test:

- The bentonite blocks underwent an initial homogeneous axial swelling of 2–3 %. This was probably caused by water flowing along block joints during the initial wetting when the friction between the blocks and surrounding tube still was insignificant.
- After the initial axial swelling of a few percent, half of the buffer did not show any additional swelling during the test. The length of this “unaffected zone” corresponds to what the analytical model gives using a friction angle of 10° between the bentonite and the surrounding filter.
- The decrease in density between the unaffected zone and the simulated drift plug, governed by the swelling of the blocks, compression of the pellet filling and friction against the wall, agreed well with the analytical model when using a friction angle of 10°.
- The swelling pressure acting on the “drift plug” was however higher than that obtained when using 10° in the analytical model and in better agreement when using 5°.

The main conclusion of the test is that the transition zone has the expected effect reducing the swelling pressure against the drift plug. Experimental data and analytical calculations using a friction angle between the bentonite and the rock between 5° and 10° are in fair agreement. The conditions and stress evolution are however more complicated than represented by the analytical model. It is therefore proposed to perform a numerical simulation of the system in order to better understand the processes and results.

6.4 Comparison between BB II and BB III

When comparing BB II, simulating a SC section, and BB III, simulating a distance block section, the significant differences in the test setups have to be remembered. The most obvious difference is the existence of the SC shell in BB II, but the differences in initial properties of the bentonite blocks (water content and dry density) are also significant.

The mentioned differences influence the rate at which the swelling bentonite can fill up the outer gap and start to build up swelling pressure. The perforated SC shell reduces the effect from bentonite swelling by decreasing the “effective” bentonite surface and introducing additional friction for the bentonite flowing through the perforations. The driving forces for water uptake and swelling are, however, larger for the drier bentonite blocks inside the SC than for the distance blocks that have higher initial water content.

It should also be mentioned that there was a difference in test duration between the two tests; 238 days for BB II and 218 days for BB III; this is, however, assessed to have an insignificant influence on the results.

Comparisons of the state of the buffer at dismantling in terms of water content and dry density can be performed by using the information in Figure 6-1 and Figure 6-2.

Figure 6-1 shows data from cross section F in the BB II test and cross section A in the BB III test, i.e. cross sections positioned at the buffer ends just inside of the steel lids. The differences between the tests are not very significant for these cross sections. The density gradient is, however, somewhat smaller for the BB III test and the bentonite seem to be more evenly distributed in the gap.

Figure 6-2 shows data from cross section D in the BB II test and cross section B in the BB III test, i.e. cross sections positioned centrally in the tests. The figure shows that there are significant differences in water content at the outermost parts close to the rock wall; approximately 60–80 % for BB II and 80 to 100 % for BB III. The densities close to the rock wall are lower for BB III (750–850 kg/m^3) as compared to BB II (900–1 050 kg/m^3). It should be noted that for BB II the given range in "average density" has been calculated without consideration to the empty voids between the clay muffins and therefore is higher than the anticipated homogenized value.

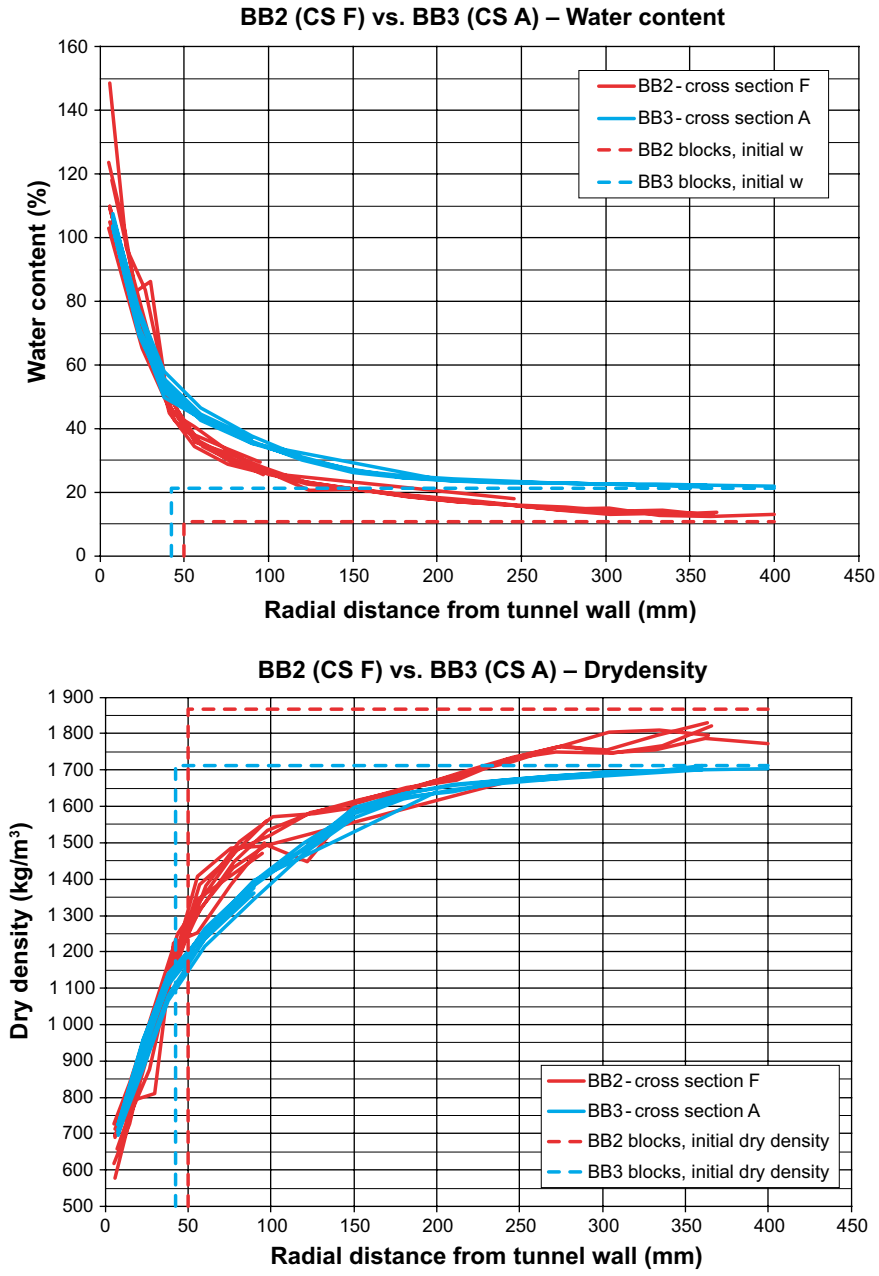

Figure 6-1. *Comparison between cross sections positioned just inside the steel lids for the two BB tests. Upper: Water content for all samples plotted versus the radial distance from the test cell wall. Lower: Dry density for all samples plotted versus the radial distance from the test cell wall.*

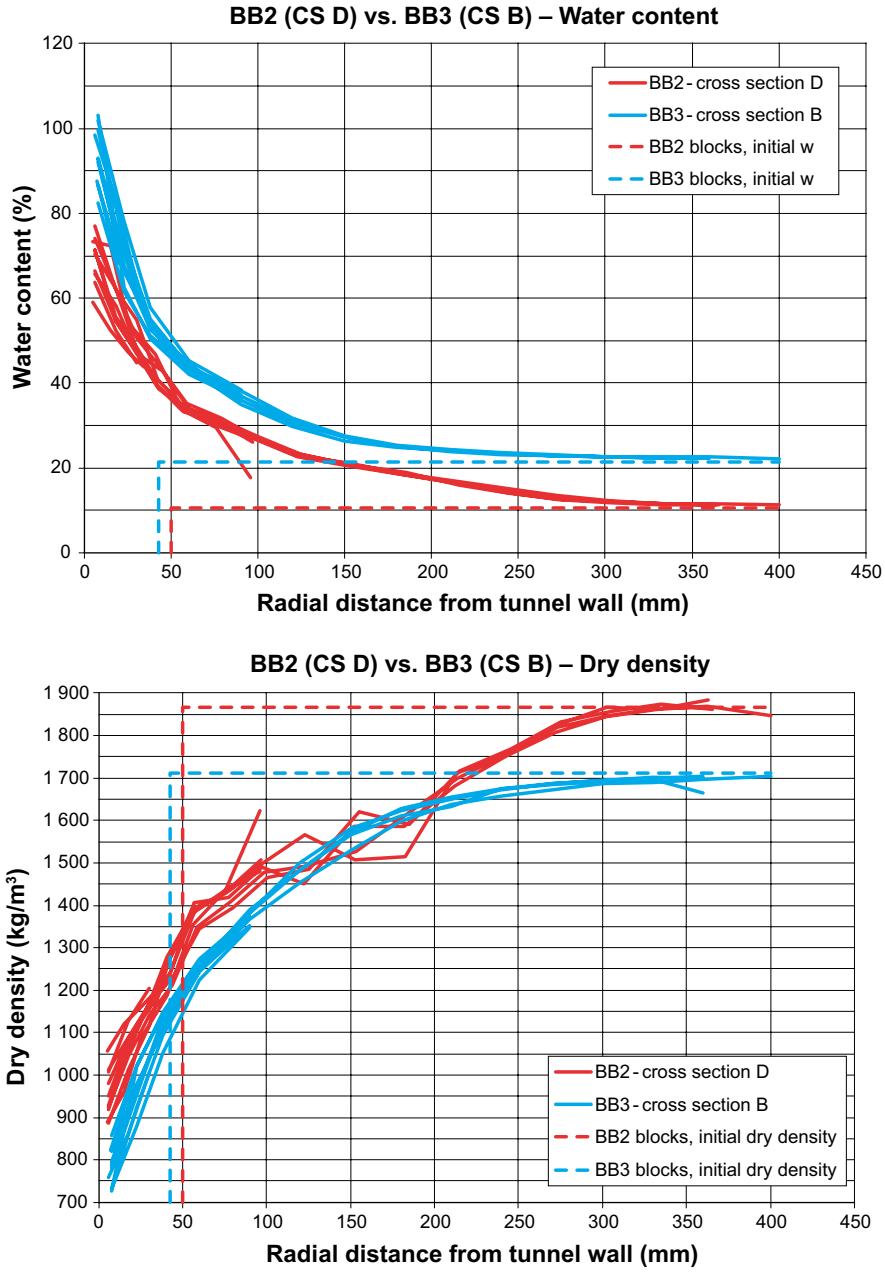

Figure 6-2. *Comparison between cross sections positioned in the mid parts of the two BB tests. Upper: Water content for all samples plotted versus the radial distance from the test cell wall. Lower: Dry density for all samples plotted versus the radial distance from the test cell wall.'*

6.5 Comparison between BB IV and BB II

BB II and BB IV both included a SC with buffer blocks. The main difference between the BB II test and the more recent BB IV test was that the former had no access to additional water after the artificial water filling given by the DAWE reference design. In the latter, the bentonite had access to additional saline water (simulating ground water) via filter mats installed at the test cell periphery. The water supplied to the filters was pressurized to 400 kPa. Besides this main difference there are a number of minor differences:

- The BB II test had a length of 1 050 mm i.e. it was three times longer than the BB IV test.
- The SC dimensions were slightly different. In BB II the SC had an outer diameter of 730 mm and an inner diameter of 710 mm. Corresponding figures for the SC used in the BB IV test is 711 mm and 699 mm. The differences depend on the fact that the SC design has changed during the project from being made out of copper to being made out of titanium.

- Due to the more recent SC design, the block dimensions were altered. In the BB II test the blocks had an outer diameter of 700 mm and in the BB IV test the block diameter was 688 mm (which should have been 690 mm in order to achieve the same nominal gap between block and SC as in the full scale).
- There were also minor differences regarding the initial block dry density and water content in both tests:
  - BB II: water content=10.5–10.7 % and dry density=1 867 kg/m^3
  - BB IV: water content=10.8 % and dry density=1 915 kg/m^3
- BB II was running for 238 days and BB IV for 182 days.

In spite of the differences listed above, a comparison of the two tests would give important information regarding the importance of access to additional water and how it influences the homogenization process.

Figure 6-3 shows the obtained profiles of water content, dry density and degree of liquid saturation distribution for the two tests at cross sections that are located in the middle or close to the middle of the tests, cross section D for BB II and cross section B for BB IV.

When comparing the profiles belonging to the two tests following comments can be made:

- The most obvious difference between the two tests is the variation in water content and dry density in the SC-rock gap (0–50 mm). In this region, the water contents are higher and the densities lower in the BB IV test. This depends on the fact that in the BB II test the bentonite swelled through the SC perforation like "muffins", leaving empty space between them. The individual "muffins" had rather high density and since the sampling was made in them, the graph only shows an apparent high density which does not reflect the reality (the average density in the gap is obviously much lower). This behavior of course depends on the lack of water.
- The variation in density and water content is high in the SC-rock gap in the BB IV test. This was found to depend on the sample position in relation to the perforation of the SC shell. Above a perforated hole, the density was higher (water content lower) and in between the perforated holes, i.e. over the steel shell, the density was lower (water content higher).
- The region inside the SC, at 50 to 300 mm radial distance from the test cell wall, is rather similar in both tests. There is a larger variation in dry density within each of the tests as compared to the variation in water content, which results in smoother water content profiles.
- The innermost part of the block, at 300–400 mm, almost has initial conditions for both tests.
- The bentonite in the initial empty SC-rock gap, at 0–50 mm, is assessed to be completely water saturated for both tests. The maximum degree of saturation is of course 100 % and the variation shown in Figure 6-3, about 90–110 %, depends on the procedure used when calculating. The degree of saturation is calculated according to:

$$S_r = \frac{w \cdot \rho \cdot \rho_s}{\rho_w [\rho_s \cdot (1 + w) - \rho]},$$

using the determined water content and density for a certain sample. The determination of density and water content for a sample is, however, performed on different parts of that sample. Since the variation in density and water content is relatively large at a relatively small length scale, determined by the scale of the perforation pattern, it may so be that the determined water content for one part of the sample is too high as compared to the determined density for the other part of the sample. This in turn results in a calculated degree of saturation higher than 100 %.

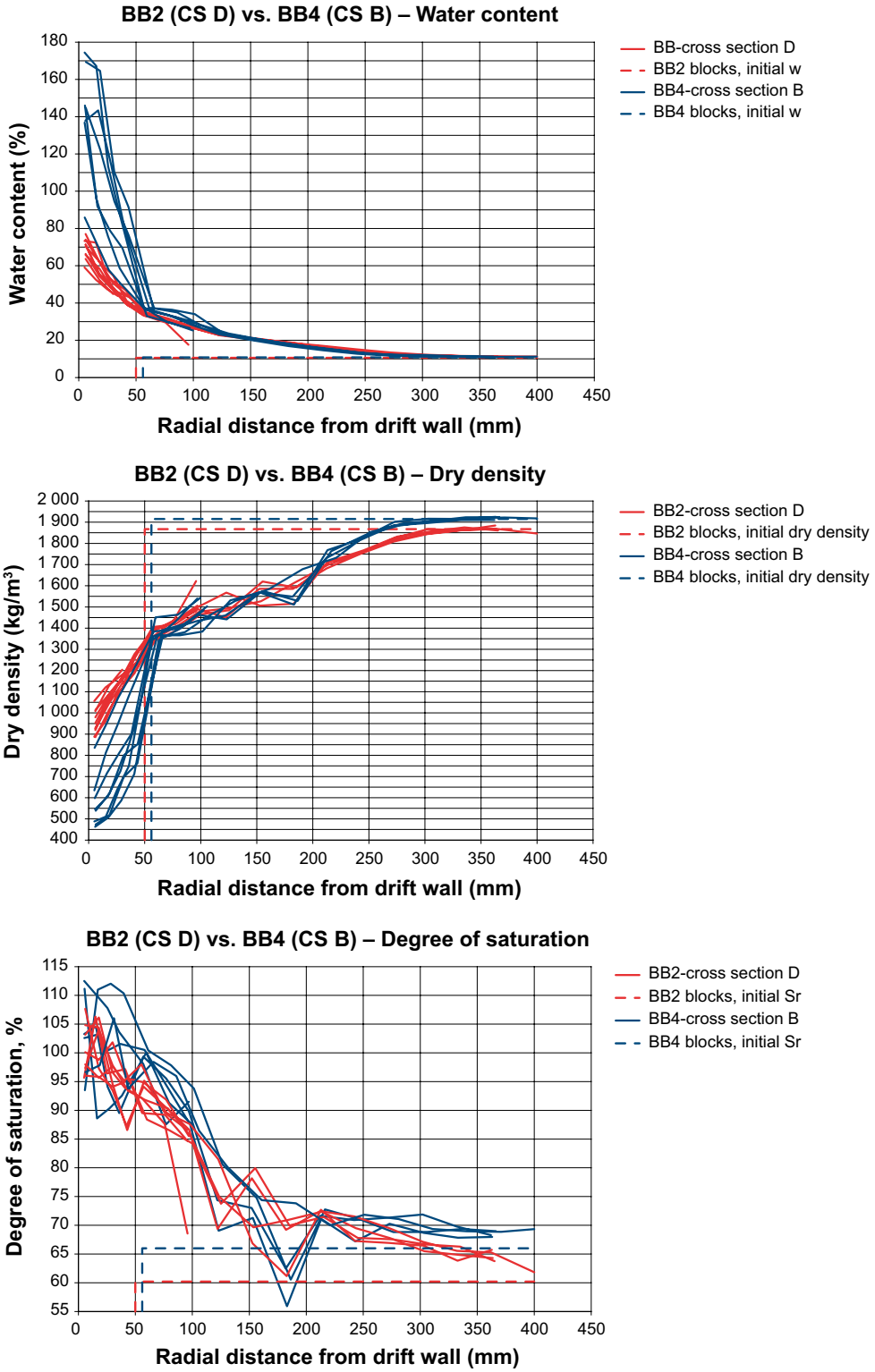

Figure 6-3. *Comparison of results obtained from BB II and BB IV. Upper: Water content distribution plotted versus the distance from test cell wall. Middle: Dry density plotted versus the distance from test cell wall. Lower: Degree of saturation plotted versus the distance from test cell wall.*

References

SKB's (Svensk Kärnbränslehantering AB) publications can be found at www.skb.com/publications.

Andersson C J, 2007. Äspö Hard Rock Laboratory. Äspö Pillar Stability Experiment, Final report. Rock mass response to coupled mechanical thermal loading. SKB TR-07-01, Svensk Kärnbränslehantering AB.

Autio J, Johansson E, Hagros A, Anttila P, Rönnqvist P, Börgesson L, Eriksson M, Halvarsson B, Berghäll J, Kotola R, Parkkinen I, 2008. KBS-3H Design description 2007. SKB R-08-44, Svensk Kärnbränslehantering AB.

Birgersson M, Karnland O, Nilsson U, 2010. Freezing of bentonite. Experimental studies and theoretical considerations. SKB TR-10-40, Svensk Kärnbränslehantering AB.

Börgesson L, Johannesson L-E, Sandén T, Hernelind J, 1995. Modelling of the physical behaviour of water saturated clay barriers. Laboratory tests, material models and finite element application. SKB TR 95-20, Svensk Kärnbränslehantering AB.

Dueck A, Goudarzi R, Börgesson L, 2014. Buffer homogenisation, status report 2. SKB TR-14-25, Svensk Kärnbränslehantering AB.

Karnland O, Olsson S, Nilsson U, 2006. Mineralogy and sealing properties of various bentonites and smectite-rich clay materials. SKB TR-06-30, Svensk Kärnbränslehantering AB.

SKB, 2012. KBS-3H complementary studies, 2008–2010. SKB TR-12-01, Svensk Kärnbränslehantering AB.

Åkesson M, Kristensson O, Börgesson L, Dueck A, Hernelind J, 2010. THM modelling of buffer, backfill and other system components. Critical processes and scenarios. SKB TR-10-11, Svensk Kärnbränslehantering AB.

Appendix A

Determination of water content and density

Determination of water content and dry density have been performed at Clay Technology in Lund. The analysis were to the major part performed at the same day as the sampling took place. For some BB IV samples, however, the analysis had to be postponed a few days during which the samples were stored wrapped in plastic in order to prevent drying.

Every sample was divided in two parts; one used for determining water content and one for determining bulk density. The sample division were made by a cut in the radial direction to make sure that the two pieces represented the same average radial position.

Below follows a description of how the water content and densities were determined.

A1 Water content

One sample-half was placed in an aluminum tin and the bulk mass (m_b) was determined by use of a laboratory balance. After 24 hours of drying at 105 °C the dry mass (m_s) was determined immediately after take out. From these measurements the water mass (m_w) was obtained as,

$$m_w = m_b - m_s \ ,$$

and the water content (w) could be calculated according to,

$$w = \frac{m_w}{m_s} .$$

A2 Bulk density, dry density and degree of saturation

In order to estimate the bulk density of the other sample-half, the apparent weight in air ($m_b g$) and when submerged in paraffin oil ($m_{bp} g$) were determined. An expression for the volume,

$$V == \frac{(m_b - m_{bp})}{\rho_p},$$

where ρ_p denotes the paraffin oil density, can be derived by combining the force balance equations "in air" and "in paraffin oil". The bulk density was then calculated according to,

$$\rho_b = \frac{m_b}{V}$$

When the water content and the bulk density had been obtained for a sample (one property from each half) it was possible to estimate the dry density (ρ_d according to,

$$\rho_d = \frac{\rho_b}{1+w} .$$

Since the density of the particles (ρ_s) and the density of the water (ρ_w) are known, the degree of saturation (S_r) can also be calculated,

$$S_r = \frac{w \cdot \rho \cdot \rho_s}{\rho_w [\rho_s \cdot (1+w) - \rho]} .$$

In the calculations, a particle density of 2 780 kg/m^3 and water density of 1 000 kg/m^3 were used.

Appendix B

Additional BB II information

B1 BB II: Sensor information

Table B-1 shows a compilation of all the sensors used in the test. The load cells used for radial total pressure had a capacity of 445 N and the one used for axial total pressure a capacity of 4 450 N. The swelling pressure was transferred to the load cells by pistons with a diameter of 20 mm, corresponding to a maximum swelling pressure of 1 400 kPa for the radial sensors and 14 MPa for the axial sensor. This was considered sufficient for the potential total pressure in both directions. The pore pressure sensors had a working range between 0–1 000 kPa. This was expected to cover the potential pore pressure with wide margin.

Table B-1. BB II. Compilation of all sensors used in the test.

Sensor type	Number	Supplier	Model	Remark	Signal
Load cell	4	Honeywell	53	Radial 0–445 N	V
Load cell	1	Honeywell	53	Axial: 0–4 450 N	V
Pore pressure	2	Druck Amtele	PTX610	0–1 000 kPa	mA
Temperature	1	UK	PT100	Test cell	mA
Temperature and RH	1	Vaisala	HMP230	Room climate	mA

B2 BB II: Information regarding the measurements

Since it was expected that the radial swelling pressures in this test should be rather low, mainly depending on the large initial gap and the fact that there should not be access to additional water after the first artificial water filling of the gaps, a lot of efforts were made in order to have measurements with high accuracy, e.g. load cells with suitable range, careful calibration of the sensors etc. Despite these preparatory efforts, problems occurred during the test time regarding these measurements:

- Calibration. The pre-calibration of the sensors was made with too low resolution of the logger. The number of value figures was only four instead of five. This problem was, however, discovered in conjunction with the subsequent control of the sensors. A new calibration was made and after a re-calculation it was possible to recover figures with higher accuracy.
- Movement of the test. After 163 days of test duration it was necessary to move the test assembly due to ongoing construction work at the Department of Structural Engineering. The equipment was moved about 5 meters with a hand pallet truck. It was possible to perform this movement without disconnecting any sensors and with a continuous logging of data. However, this procedure turned out to influence the four 100 lbs load cells registering radial total pressure. After day 163 it was no longer possible to read the signal of the four 100 lbs load cells and no more data was registered. These sensors had a separate power supply (5V) which was likely a part of the issue. Despite a comprehensive trouble shooting it was not possible to solve this problem.
- Stolen computer. In late August it was discovered that the laptop used for logging of the test was stolen. It took several weeks before this was discovered due to the summer holidays. The backup log file and the software were installed to a new laptop in the beginning of September and it was possible to receive data again. Data from all sensors was lost from day 197 (July 30) to day 230 (September 2). When the new logging session was in operation, data from all sensors could be registered again including the four radial load cells which were functioning again.

Despite the problems it is believed that the presented data is reliable although there is no data at all available from a period of 33 days and no radial total pressure data for a period of 68 days. The trends regarding the pressure development to day 163 continue also after 230 days.

B3 BB II: Early pressure evolution

Figure B-1 shows the total pressure and pore pressure evolution during the first hours of the test. Before the test starts, a radial total pressure of 7–27 kPa was registered by the load cells. This depends, however, on a certain pre-stress of the load cells in order to keep them in place. Calculated from the 20 mm pistons used to transfer the stress this corresponds to a load of 2.2–8.5 N on the load cells.

After closing the inlet and de-airing valves the pore pressure increased directly. The corresponding pressure increase could also be seen on the two radial pressure measurements positioned at the bottom while the reaction on the two sensors at the top was much more limited. The difference in registered pressure between top and bottom is difficult to explain. There is of course theoretically an initial higher pressure at the bottom depending on the water head (0.8 m=8 kPa). However, after closing the valves the pressure build-up at an early stage was expected to be the same in all positions since they are all in connection with the SC-rock gap.

B4 BB II: Room climate

The registered relative humidity of the room, temperature of the room and temperature of the test cell are shown in Figure B-2. The test was started in mid-January and was terminated in the beginning of September. During the test period, there have been rather large variations of the temperature. In the beginning of the test the temperature was below 18 °C and in the end it was close to 23 °C. Besides the variations during the year there have also been daily variations in climate. The full range of registered temperature varies from 9.5–22.8 °C in the room. The large dips in the room temperature are explained by the ports of the room being opened occasionally on an almost daily basis. The temperature of the test cell is more slowly changed than the air temperature in the room, which is clearly seen in the figure. The relative humidity was rather low during the cold winter months but increased in the end to between 60 and 70 %.

The pore pressure build up indicates that the system is closed and successfully sealed. Therefore the variations in the relative humidity of the room are not expected to have influenced the test results at all. The temperature variations have had a small influence on the pressure measurements due to heat expansion in the bentonite and water inside the test cell.

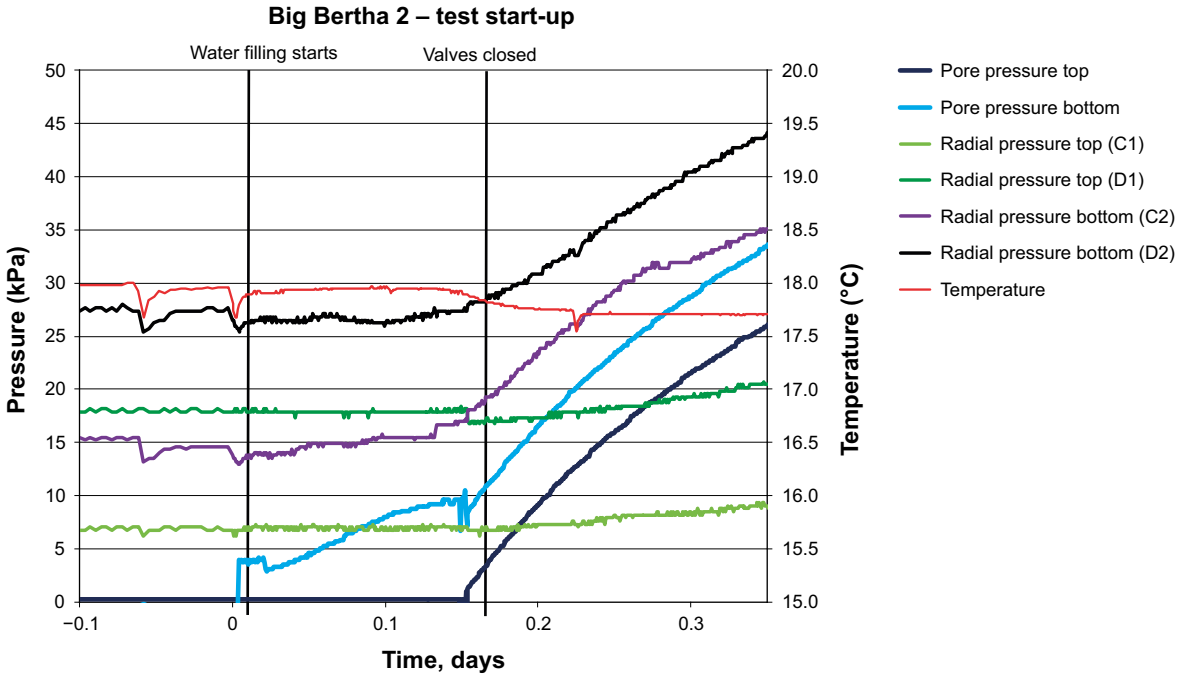

Figure B-1. *BB II. Pore pressure, radial total pressure and temperature plotted versus time during the first hours of the test.*

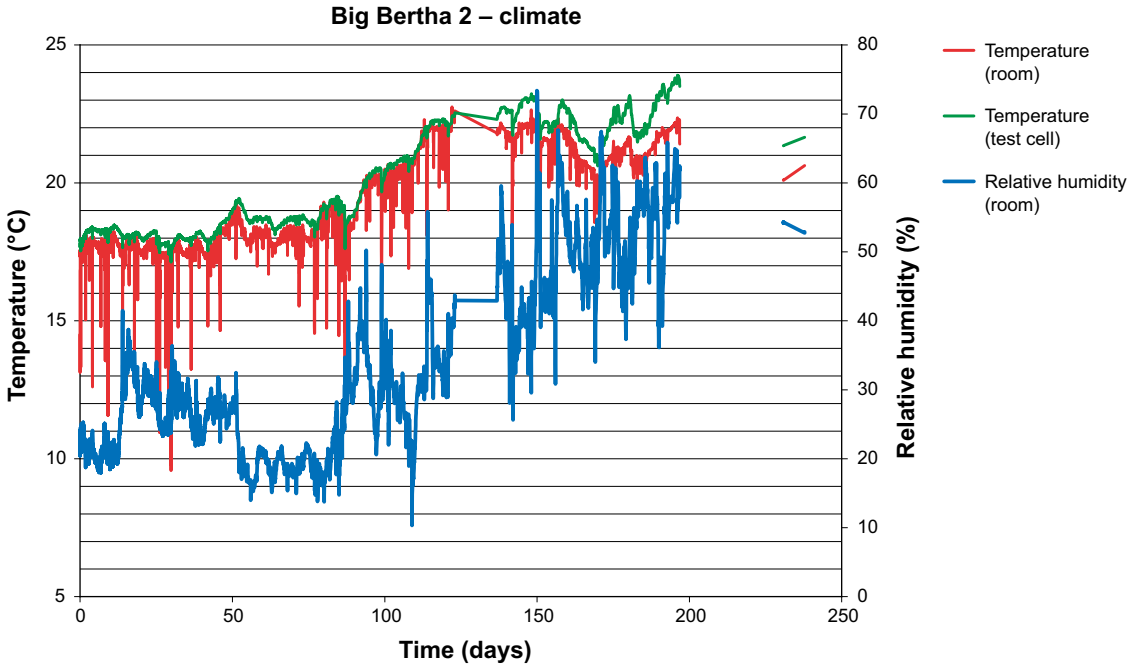

Figure B-2. *BB II. Registered relative humidity of the room, temperature of the room and temperature of the test cell.*

B5 BB II: Measurements of the SC-rock gap

In the SC-rock gap the radial distance from the cell wall was easily determined with a ruler. However, the samples inside the SC were taken after the SC had been removed (except for cross-section F) from the test cell. Thereby the radial distance from the cell wall to the sample had to be determined by measuring the distance to the SC periphery and then adding the width of the SC-rock gap.

There are some small differences observed in the SC-rock gap width before and after the test as can be seen in Table B-2. It is probable that the swelling pressure from the bentonite blocks has moved the whole SC in relation to the test cell. The swelling pressure locally has affected the shape of the not perfectly round SC. Thereby the SC-rock gap width could have been changed slightly.

Table B-2. BB II. The SC-rock gap width was determined at test assembly and at test dismantling. There are some small differences observed in the SC-rock gap width before and after the test. In the table "drift wall" = "inner surface of the test cell"

Cross section	Direction [°]	Distance tunnel wall-supercontainer [mm]	
		Before	After
A (blind end plate)	0	37.0	38
A (blind end plate)	45	34.5	35
A (blind end plate)	90	37.5/38.0	37
A (blind end plate)	135	37.5	36
A (blind end plate)	180	37.0	37
A (blind end plate)	225	36.5	37
A (blind end plate)	270	33/35.0	37
A (blind end plate)	315	36.0	37
F (open end)	0	34.2	37
F (open end)	45	32.2	36
F (open end)	90	40.4	38
F (open end)	135	40.2	36
F (open end)	180	39.4	41
F (open end)	225	37.6	37
F (open end)	270	38.9	39
F (open end)	315	38.0	35

B6 BB II: Analysis data

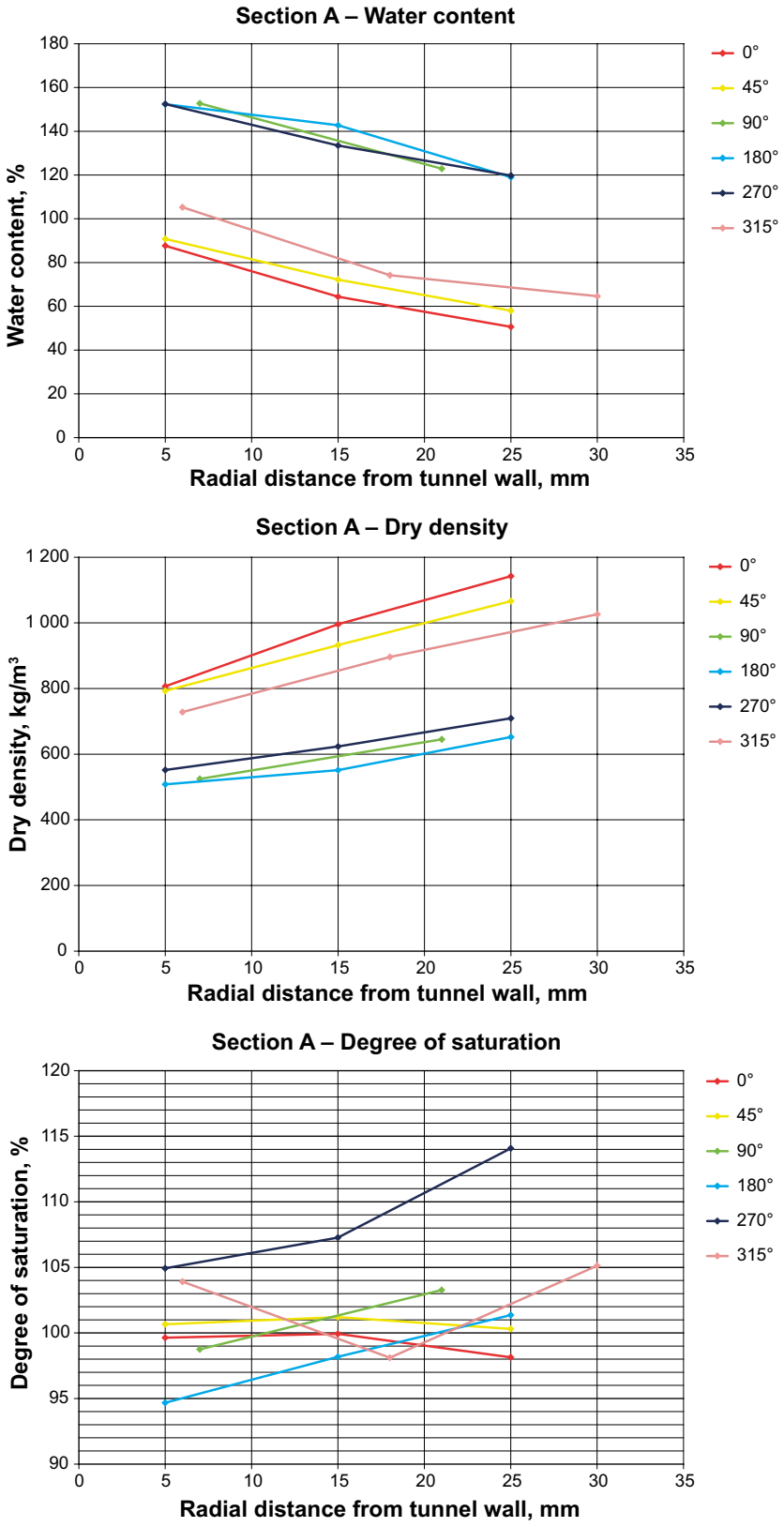

Figure B-3. *BB II. Section A data.*

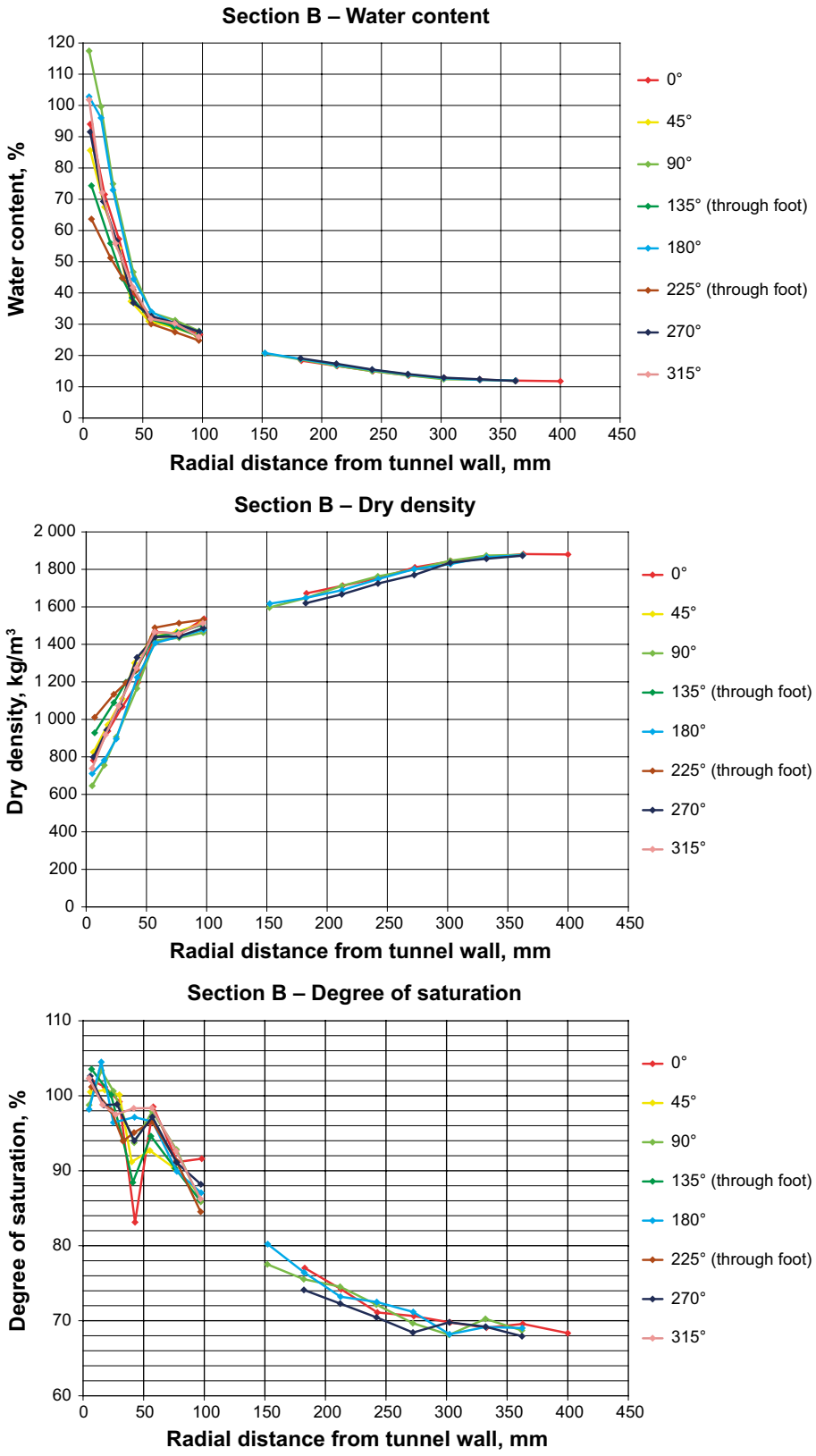

Figure B-4. *BB II. Section B data.*

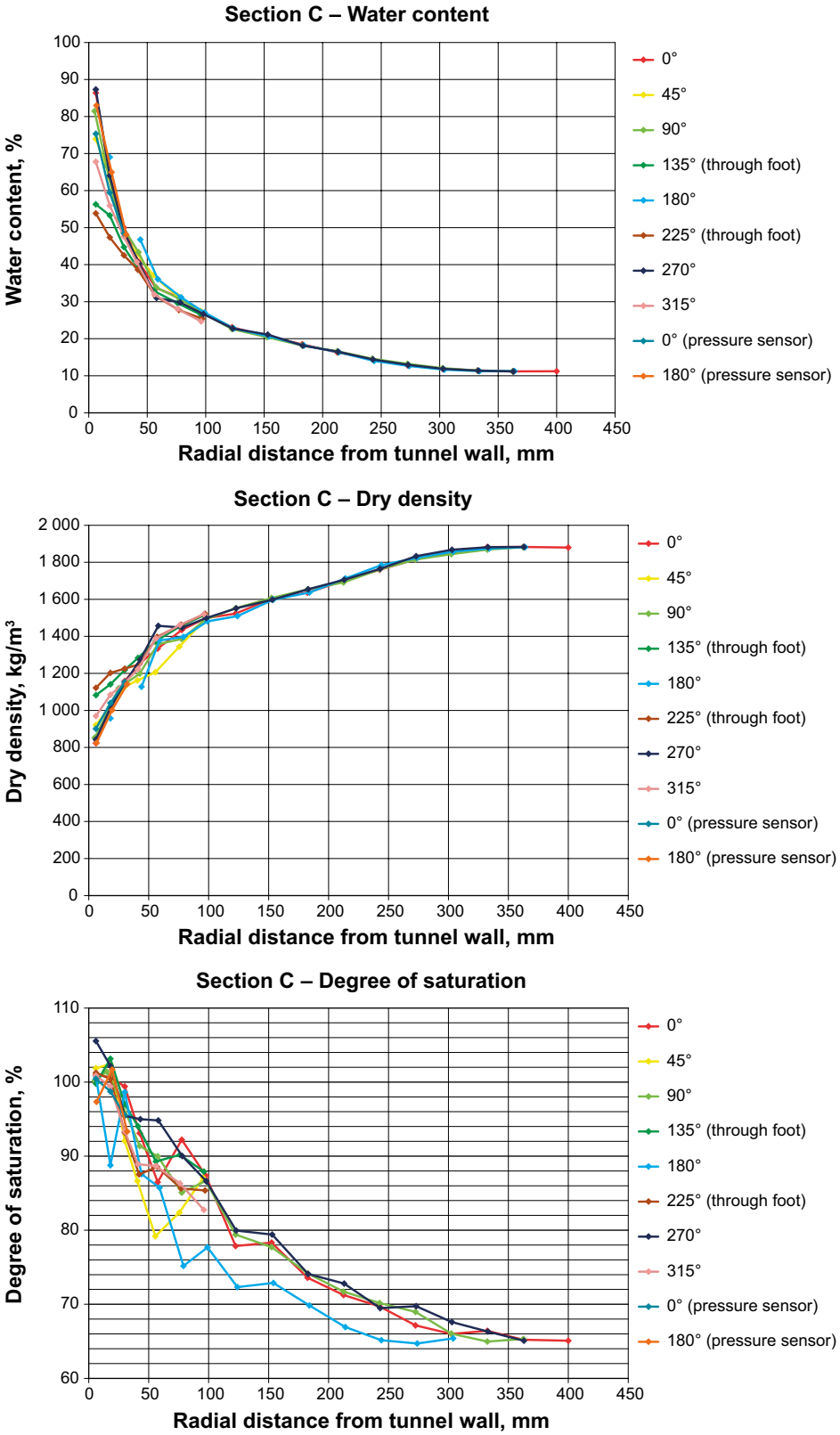

Figure B-5. *BB II. Section C data.*

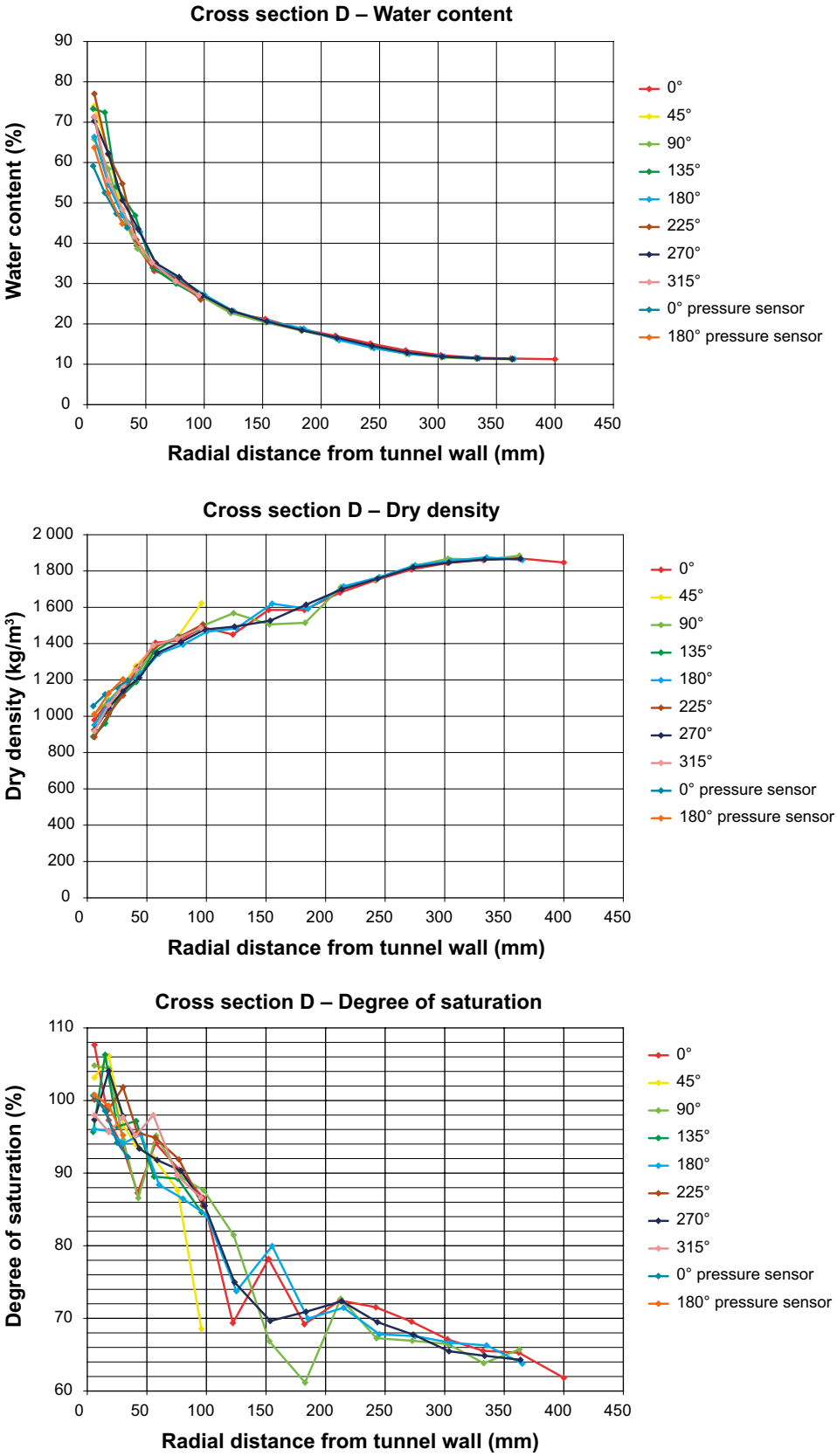

Figure B-6. *BB II. Section D data.*

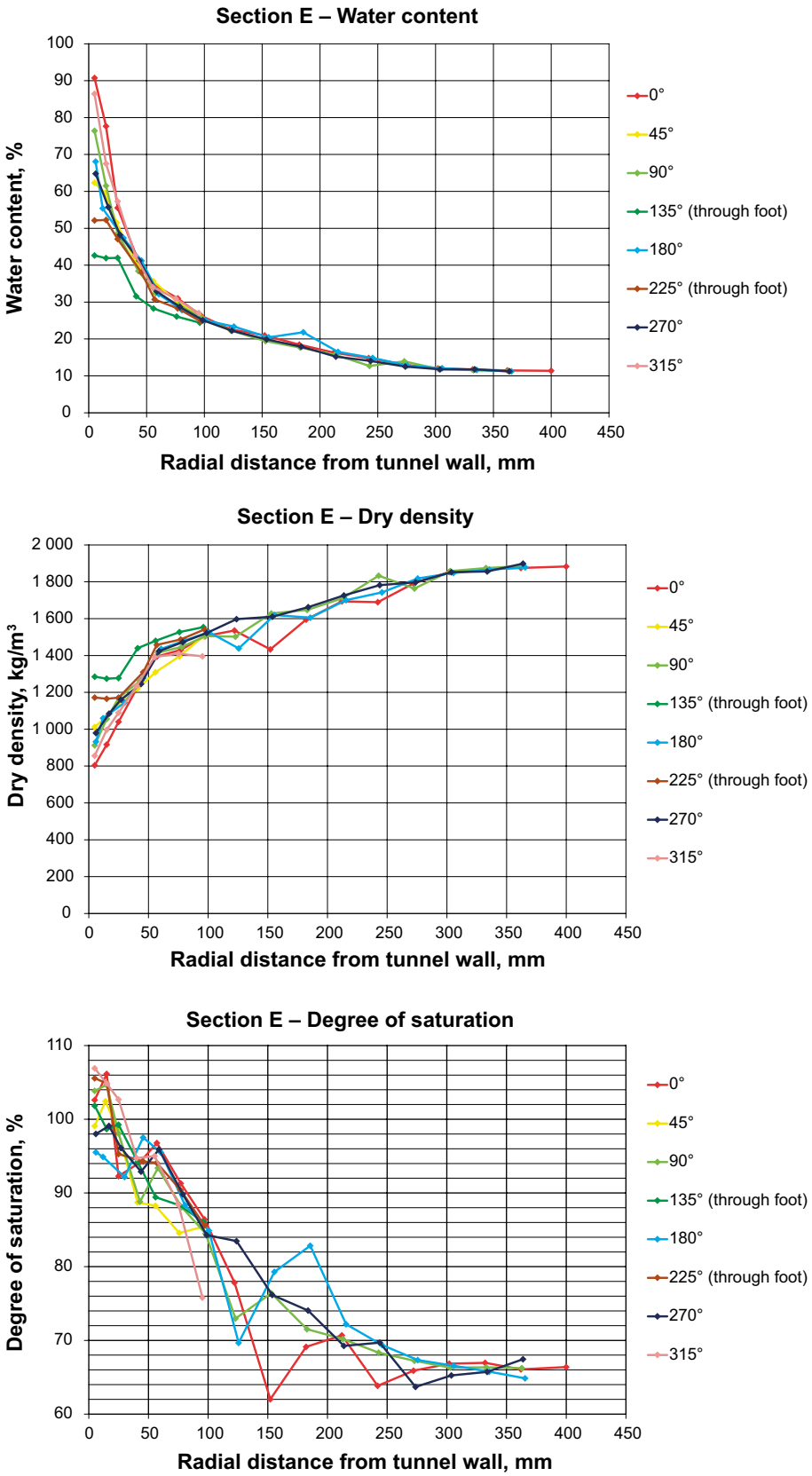

Figure B-7. *BB II. Section E data.*

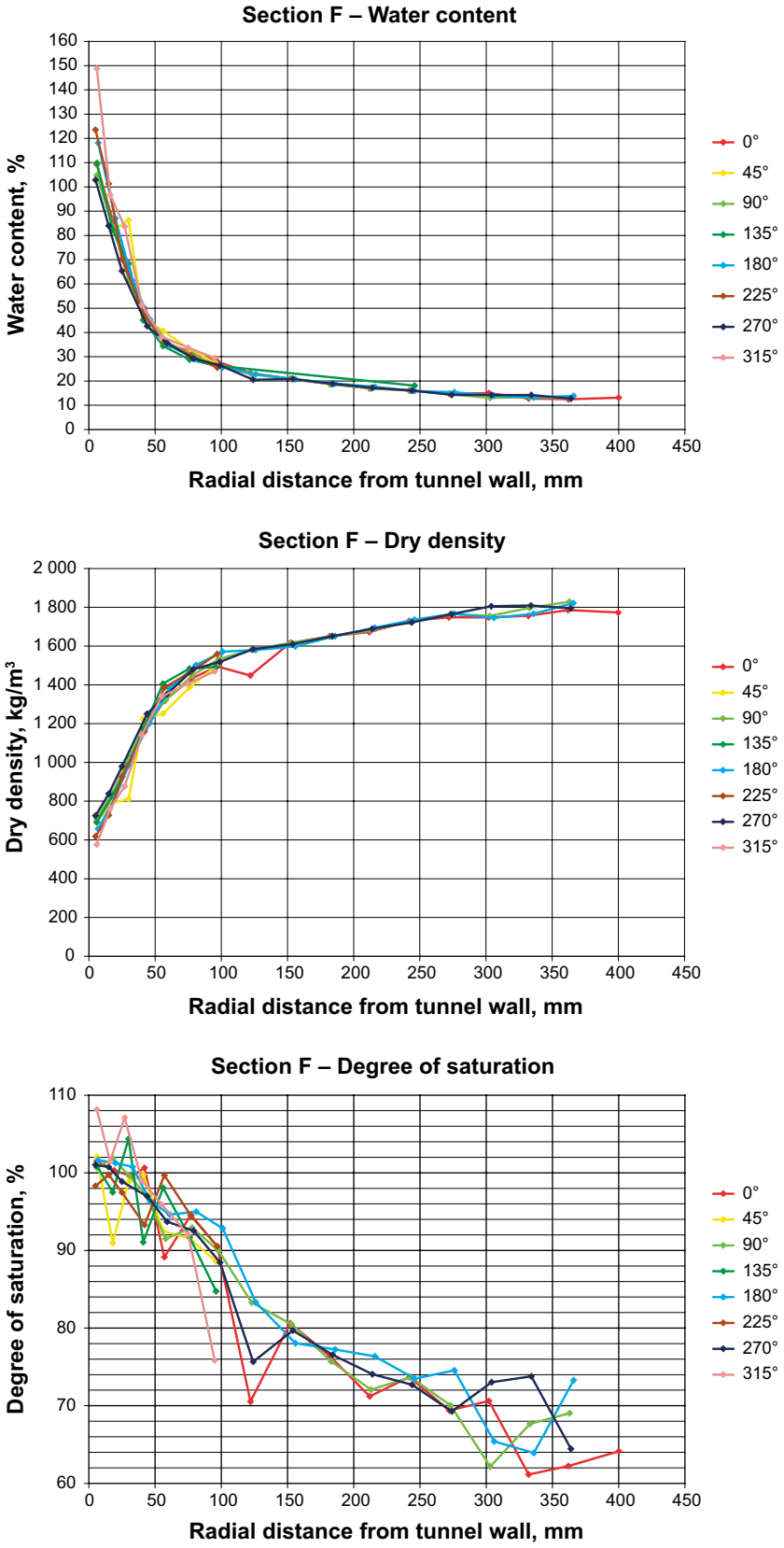

Figure B-8. *BB II. Section F data.*

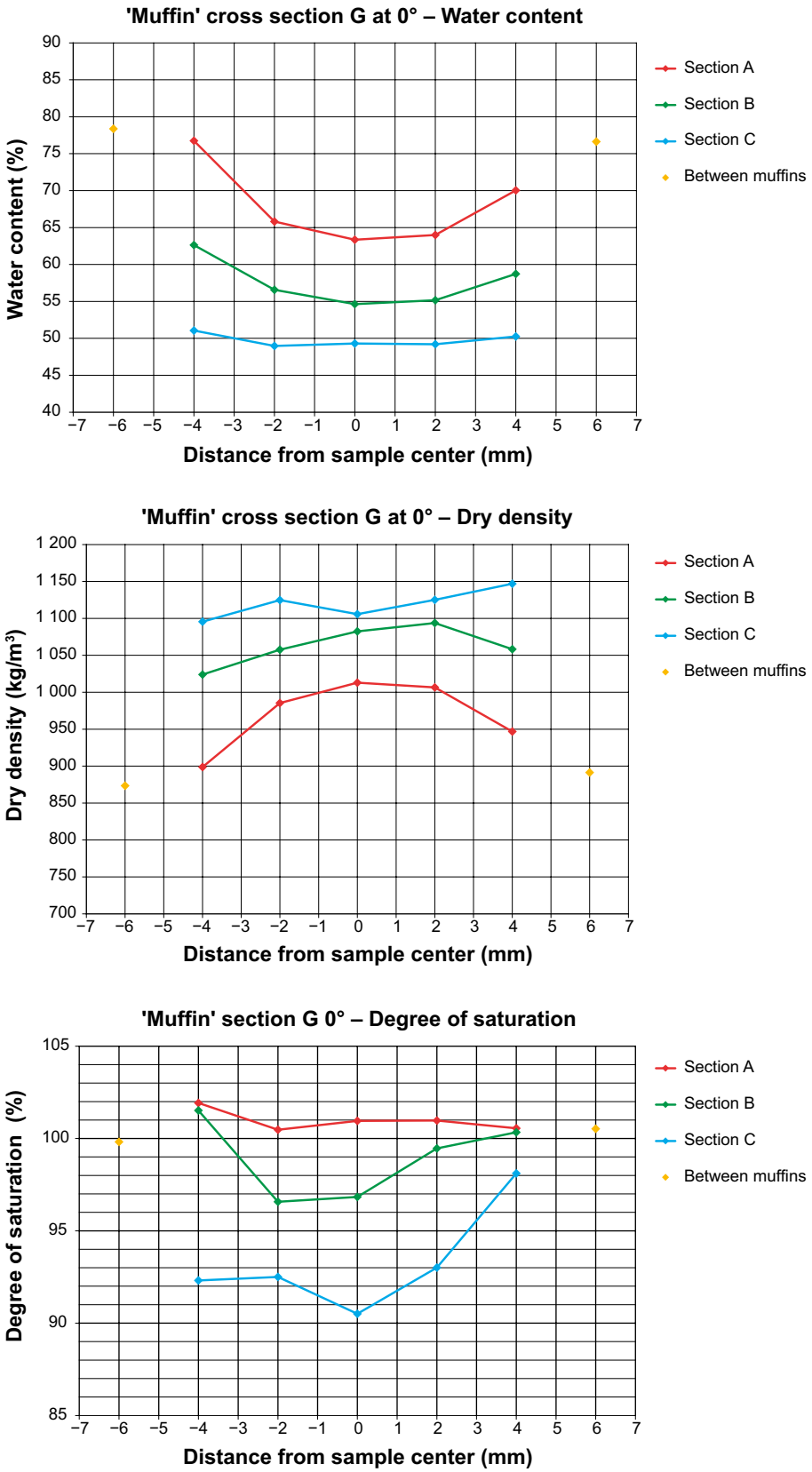

Figure B-9. *BB II. Muffin data section G 0°.*

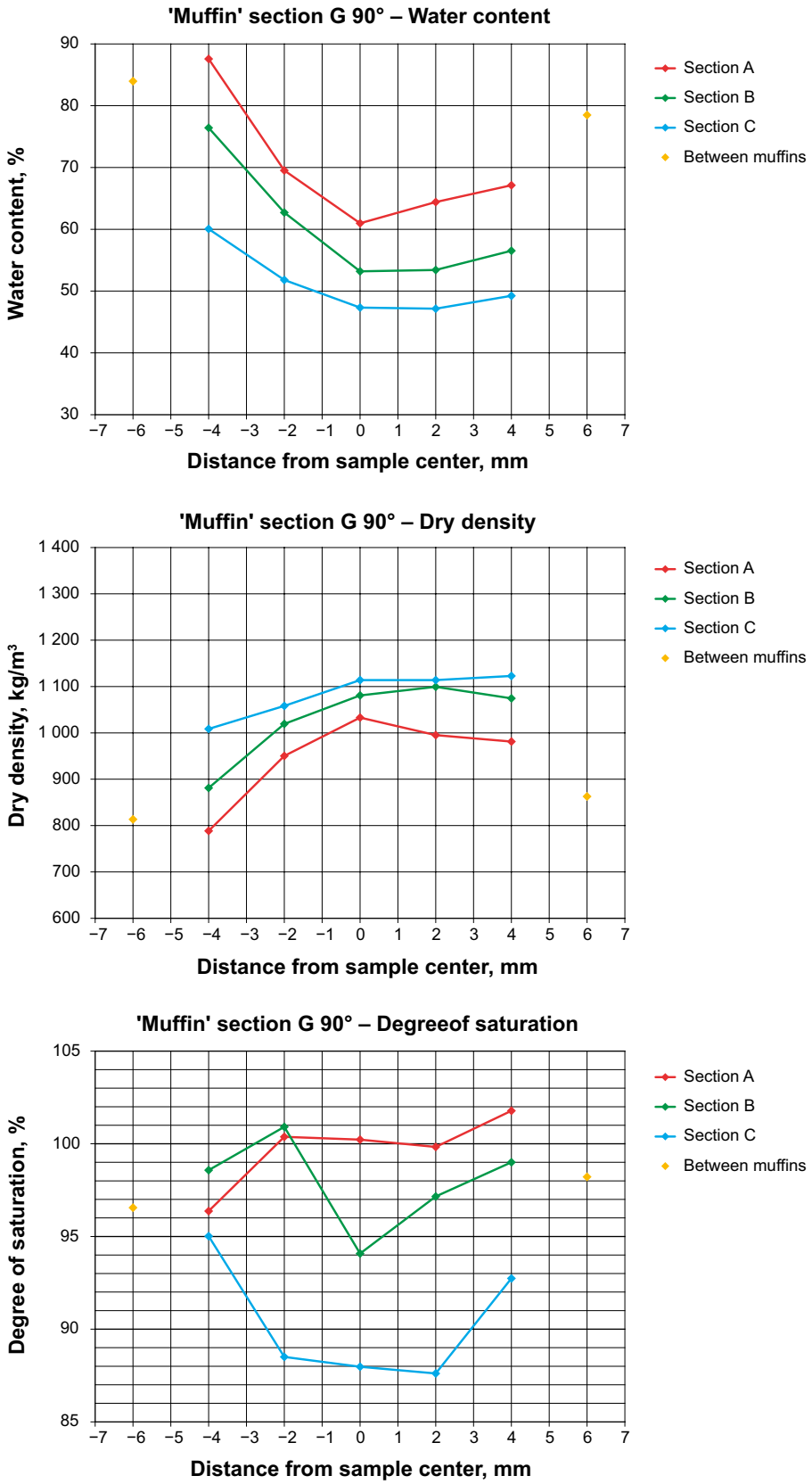

Figure B-10. *BB II. Muffin data section G 90°.*

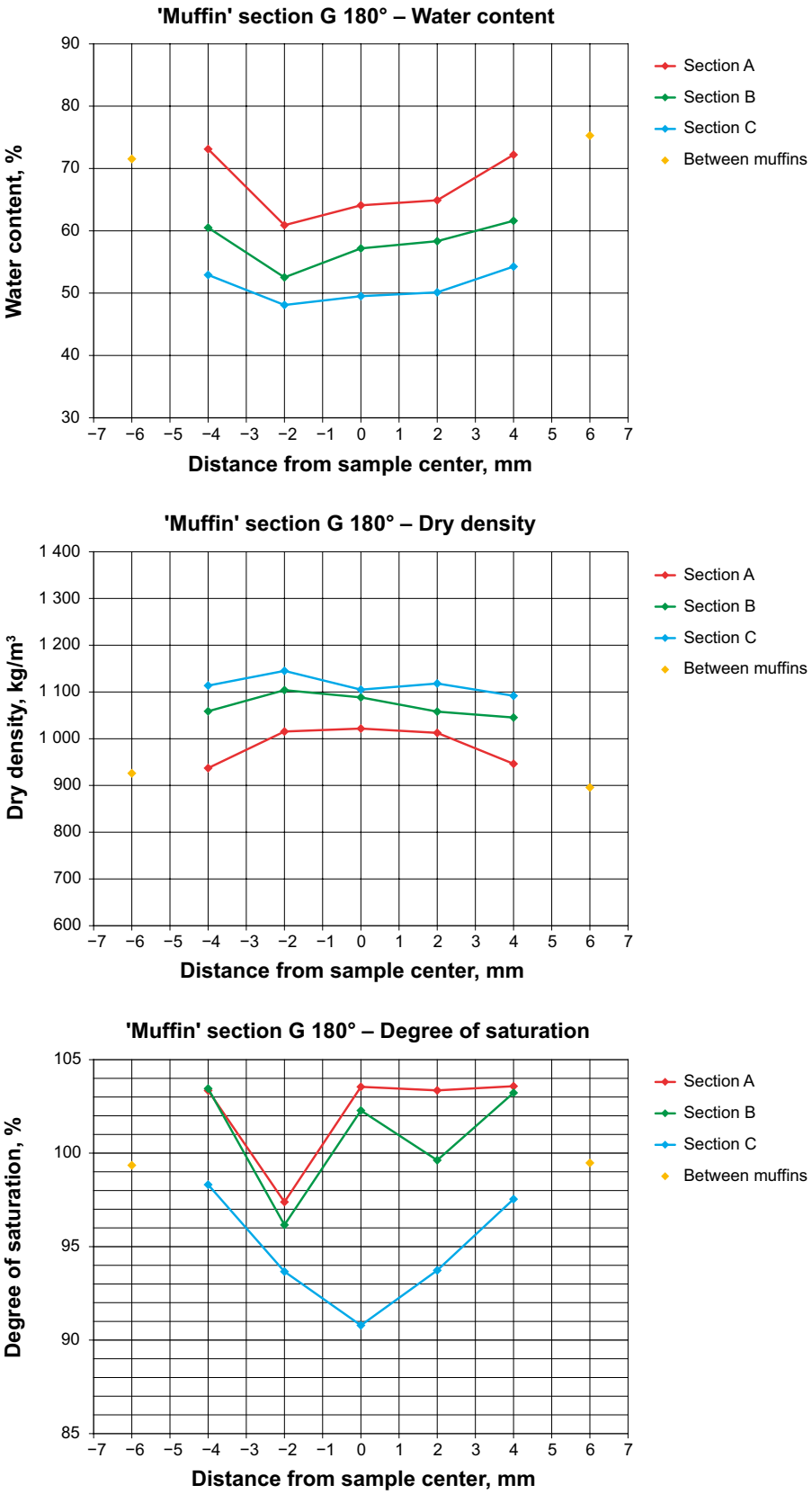

Figure B-11. *BB II. Muffin data section G 180°.*

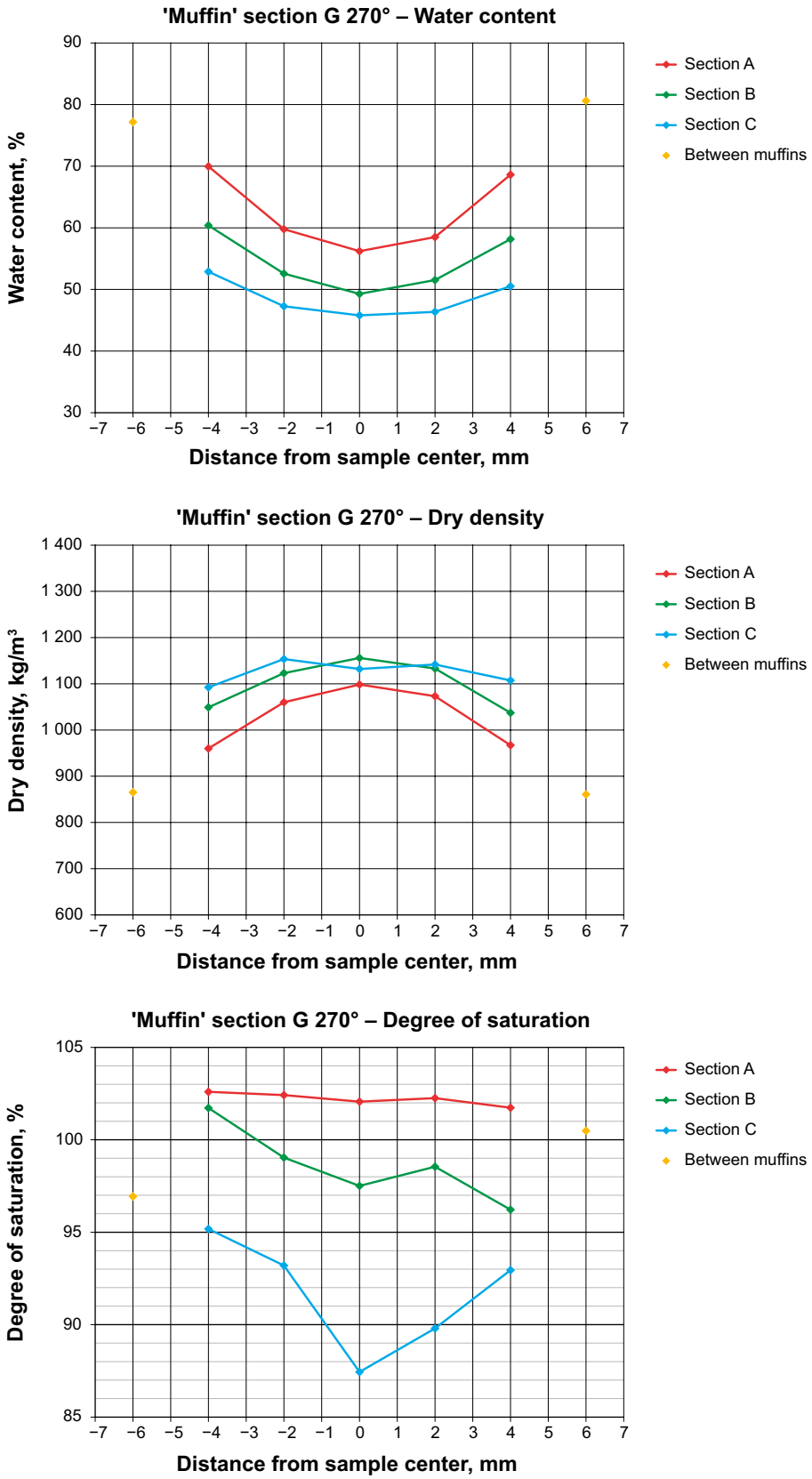

Figure B-12. *BB II. Muffin data section G 270°.*

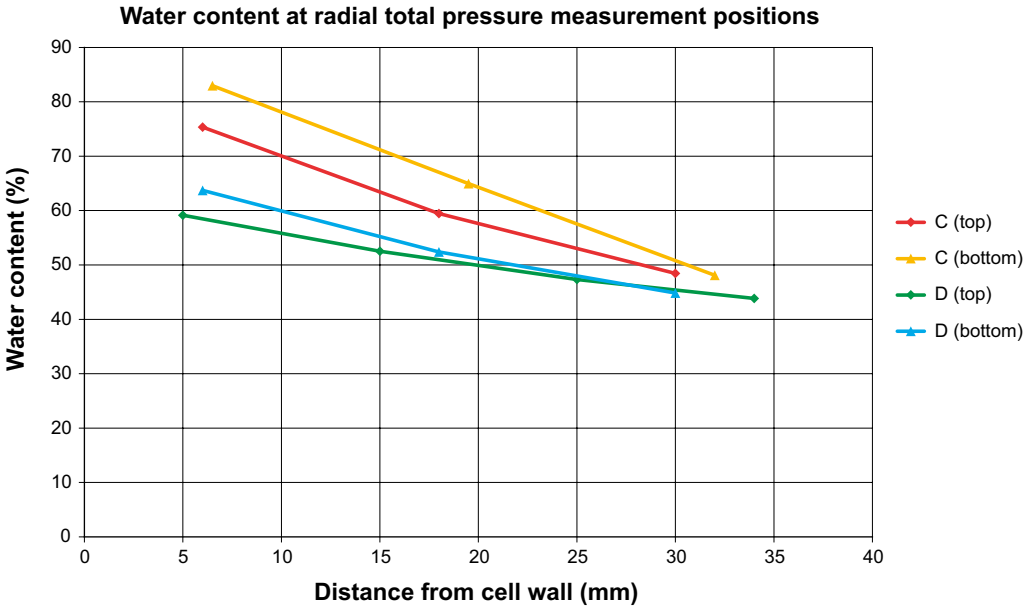

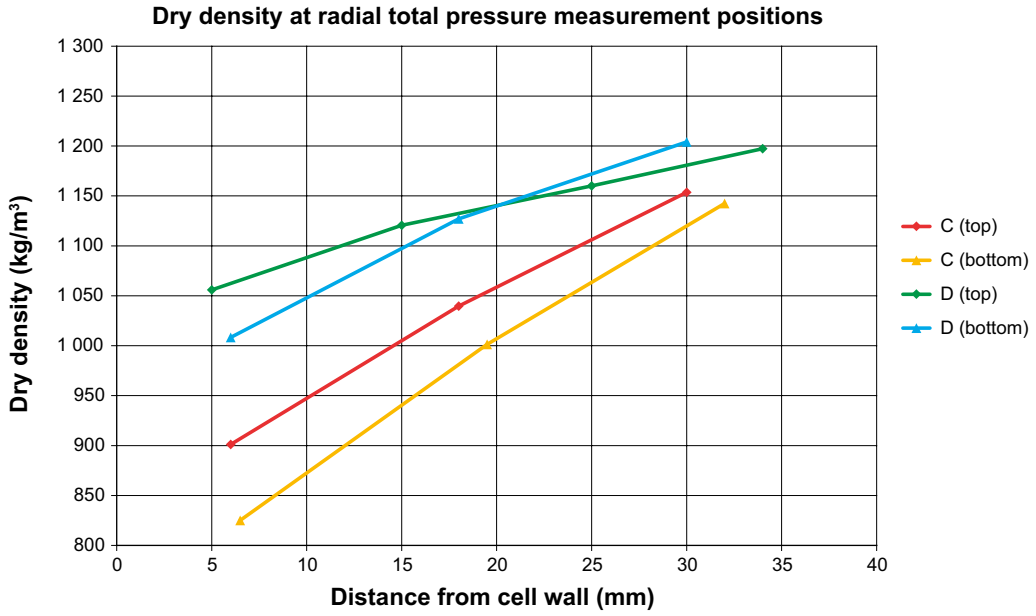

Figure B-13. *BB II. Radial total pressure measurement position data.*

Appendix C

Additional BB III information

C1 BB III: Sensor information

Table C-1 shows a compilation of all sensors used in the test. Two load cells were used for radial total pressure measurements. They had a capacity of 445 N and 2 225 N respectively. Both load cells used in axial direction had a capacity of 4 450 N. The load was for all sensors transferred via a piston (diameter of 20 mm) to the load cells. The sensors measuring the radial pressure had a maximum range of 0–1 400 kPa and 7 000 kPa, respectively. The load cells measuring axial total pressure could measure up to 14 MPa within the specified range. This was considered to cover the potential total pressure in both directions. The pore pressure sensors had a pressure range of 0–1 000 kPa. This was expected to cover the potential pore pressure with wide margin.

Table C-1. Compilation of instruments used in the BB III test.

Sensor type	Number	Supplier	Model	Remark	Signal
Load cell	1	Honeywell	53	Radial: 0–445 N	V
Load cell	1	Honeywell	53	Radial: 0–2 225 N	V
Load cell	2	Honeywell	53	Axial: 0–1 000 4 450 N	V
Pore pressure	2	Druck Amtele	PTX610	0–1 000 kPa	mA
Temperature	1	UK	PT100	Test cell	mA
Temperature and RH	1	Vaisala	HMP230	Room climate	mA

C2 BB III: Early pressure evolution

Figure C-1 shows the pore pressure and the total pressure evolution during the first hours of the test. In the period of water filling the response in the bottom pore pressure sensor could clearly be seen. The pressure increased in the same rate as the increase of the water level inside the test cell. The top pore pressure sensor did not respond until the water level had reached the top and the valves were closed. It was also possible to see some response in the bottom radial total pressure. However, the signal from the load cell first indicates a decrease in load. This may be a temperature effect from the inflowing water that obviously will cool the bottom parts of the test cell first. The temperature is registered in the top of the test cell and it is clearly seen that the cooling effect from the inflowing water is not seen in the PT100 sensor until the test cell is entirely filled and the valves are closed. However, the radial load cell in the bottom was cooled already during the first minutes.

During the first 25 hours the signal from the load cell registering radial total pressure in the top was not stable (the sensor was later exchanged) and therefore no data was available from that sensor for this period.

C3 BB III: Room climate

The registered relative humidity of the room, temperature of the room and temperature of the test cell are shown in Figure C-2. The test was started in mid-March and the equipment was placed in a quite stable environment compared to the BB II test. The temperature ranged from 20.7–23.7 °C during the test which is a much smaller range than the BB II test. The relative humidity of the room was very similar to the BB II test and ranged from 10–20 % at the start to about 70 % by the test termination.

The pore pressure build-up observed in the test start indicates that the system is closed and successfully sealed. Therefore the variations in the relative humidity of the room are not expected to have an influence on the test results. The temperature variations have had a small influence on the pressure measurements.

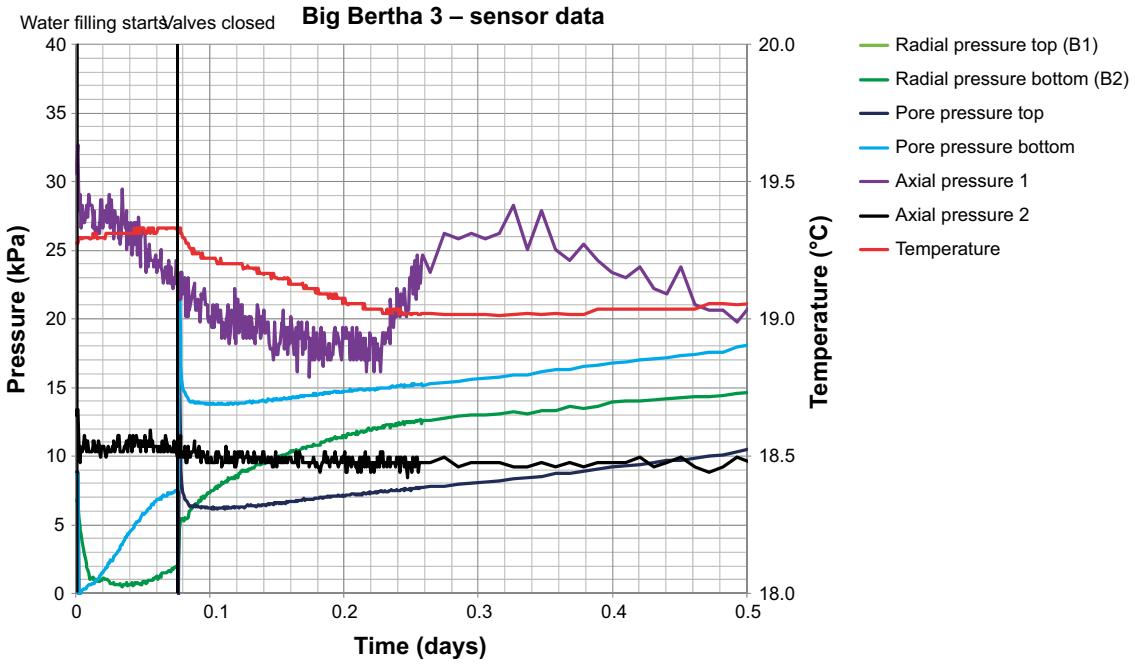

Figure C-1. *BB III. Pore pressure, radial total pressure and test cell temperature during the first hours of the test.*

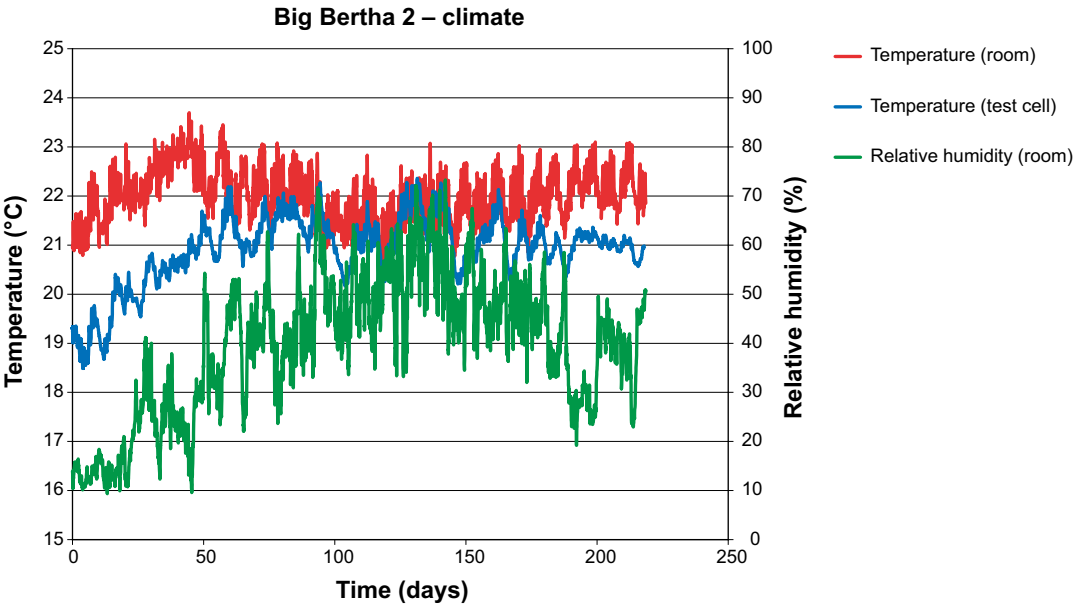

Figure C-2. *BB III. Registered relative humidity of the room, temperature of the room and temperature of the test cell plotted versus time.*

C4 BB III: Analysis data

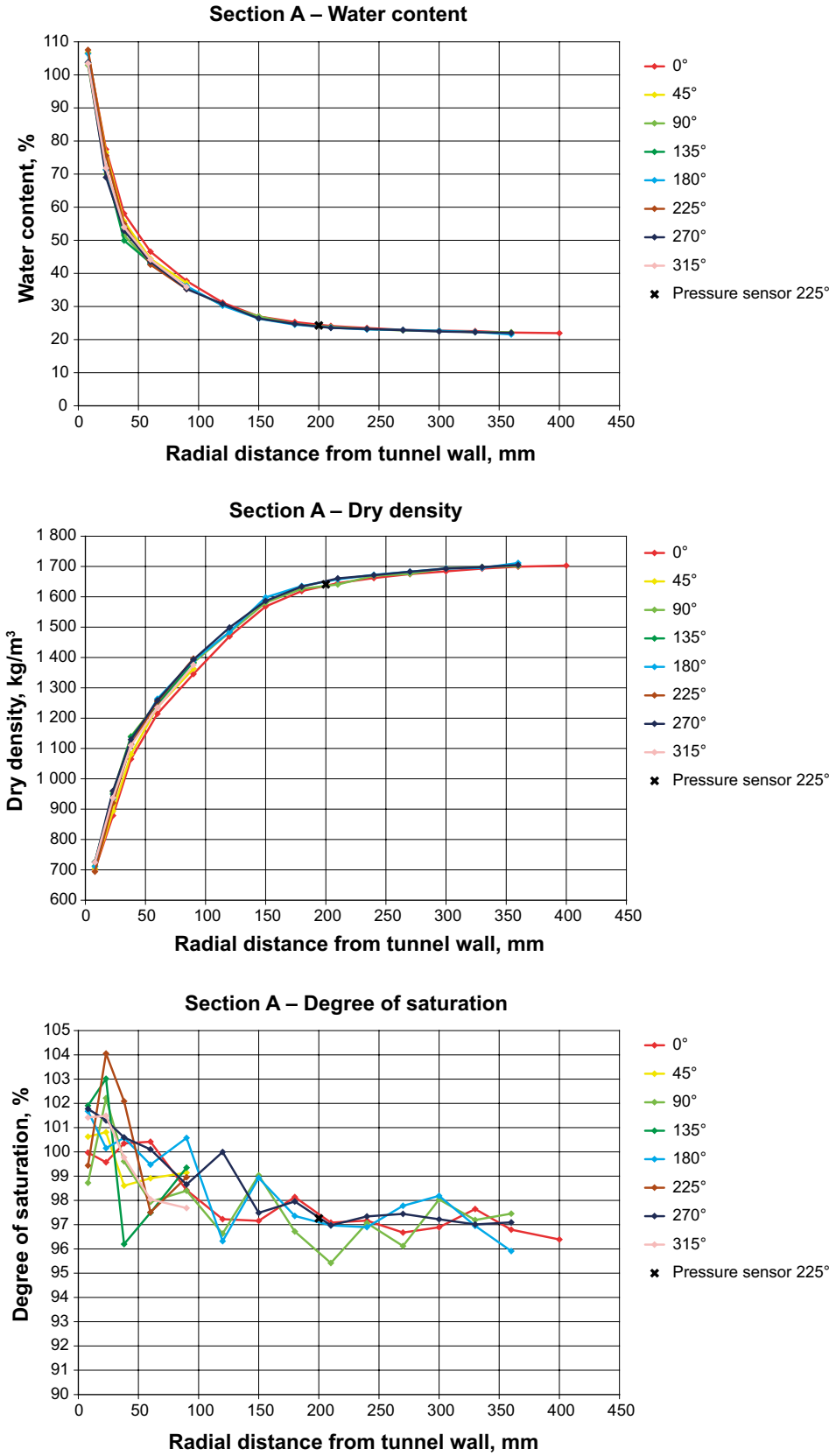

Figure C-3. *BB III. Section A data.*

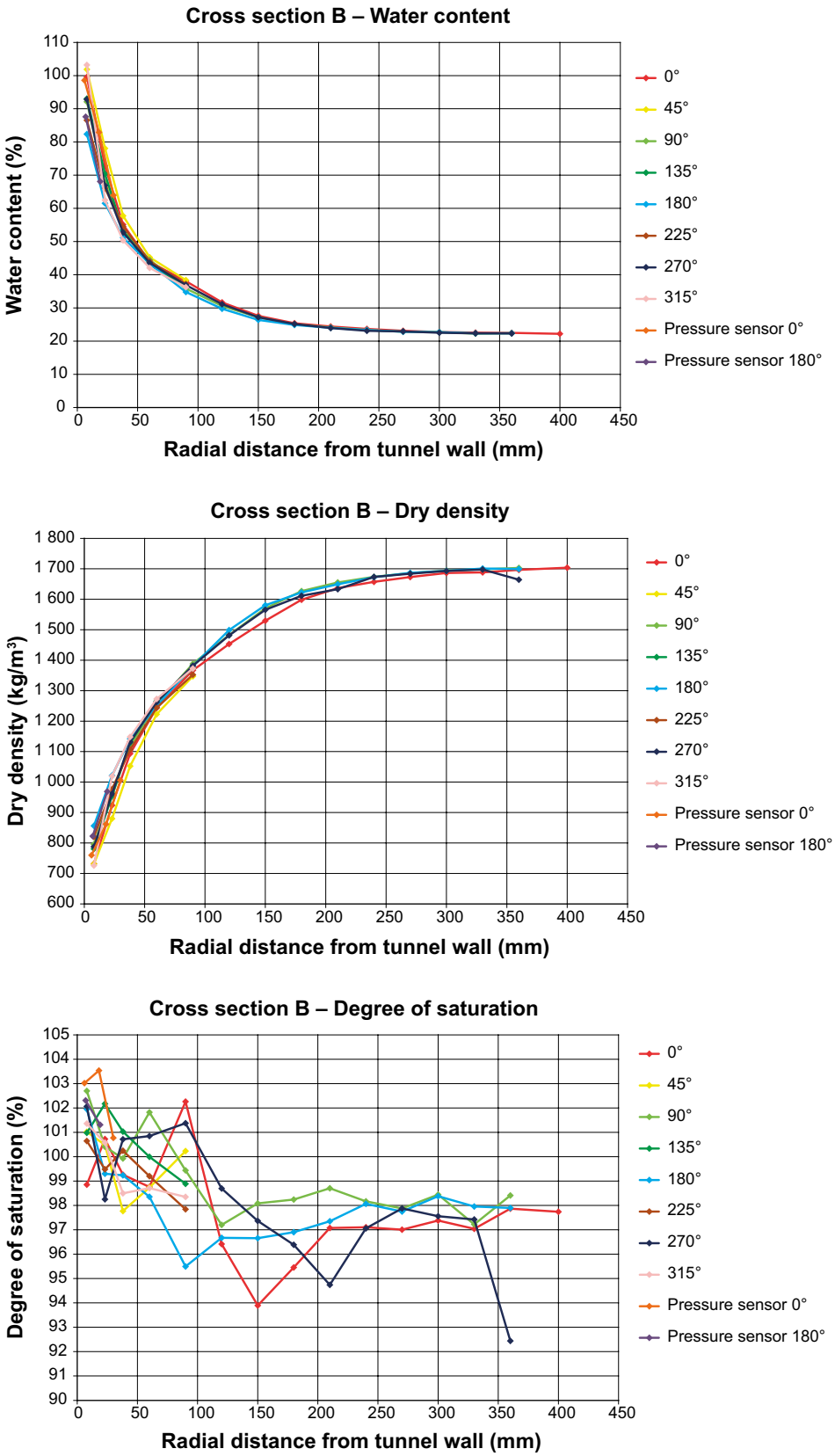

Figure C-4. *BB III. Section B data.*

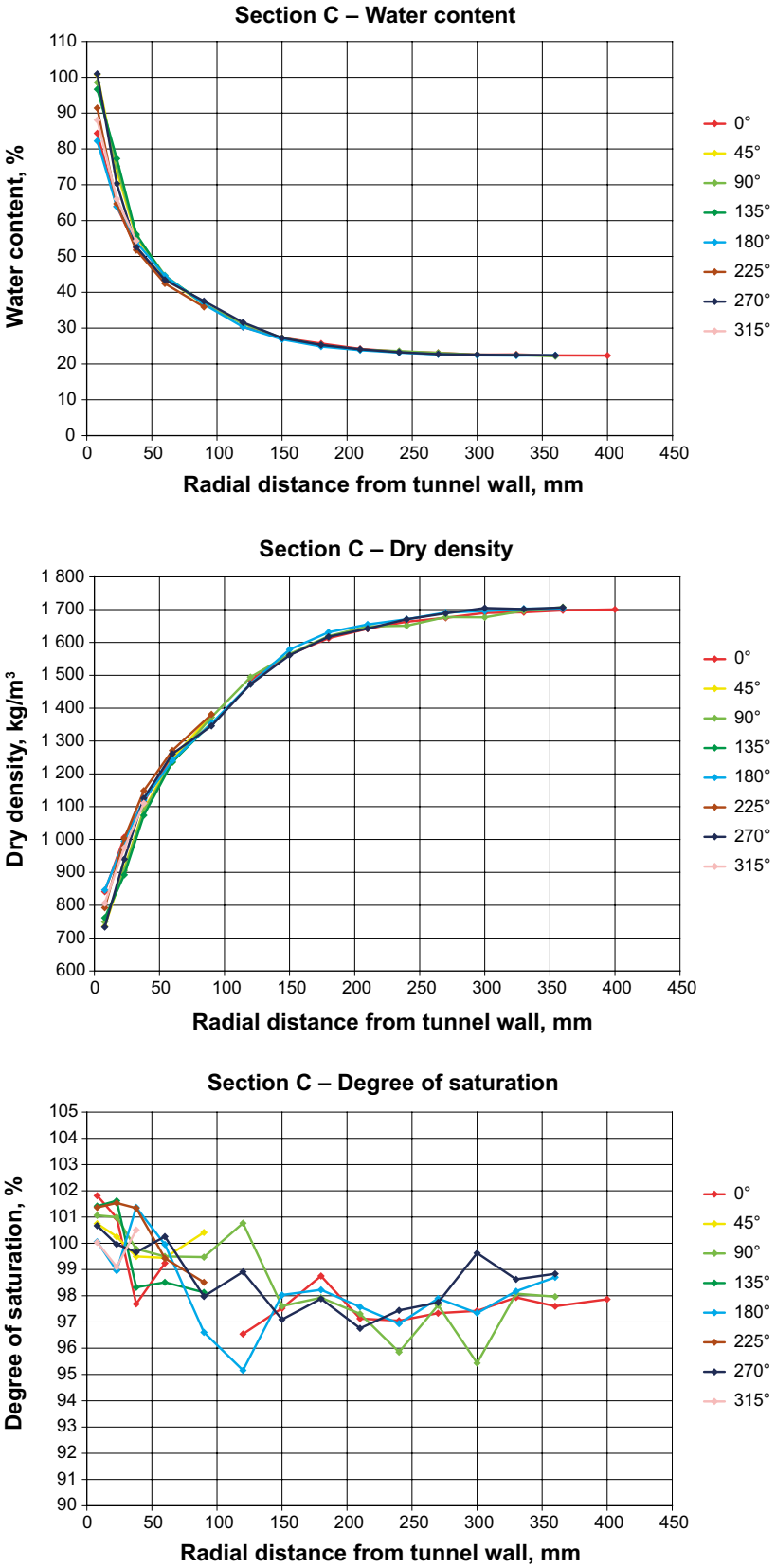

Figure C-5. *BB III. Section C data.*

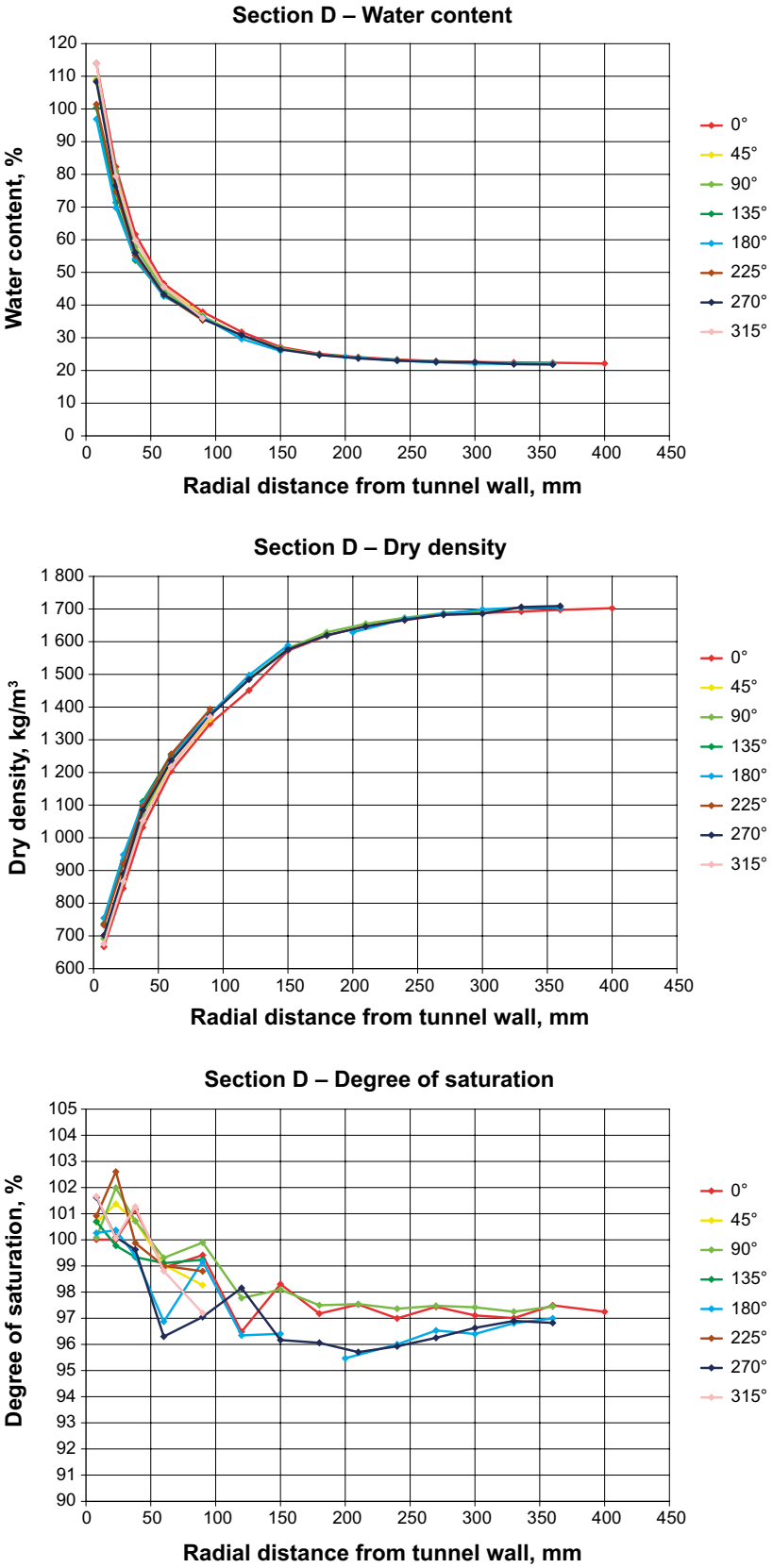

Figure C-6. *BB III. Section D data.*

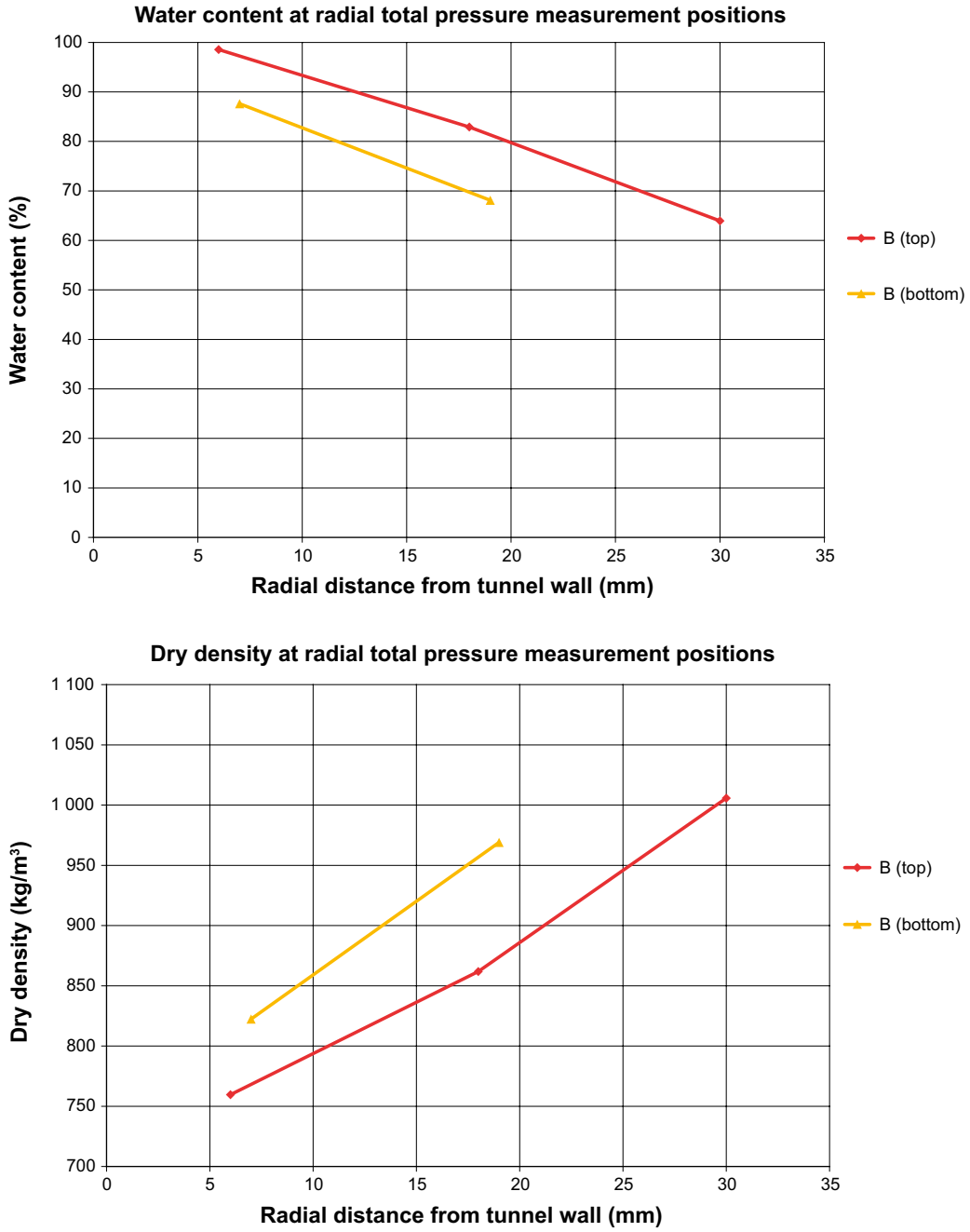

Figure C-7. *BB III. Radial total pressure measurement position data.*

Appendix D

Additional BB IV information

D1 BB IV: Sensor information

Table D-1 shows a compilation of all the sensors used in the test. The load cells used for radial total pressure (C1, C2) had a capacity of 445 and 2 225 N, respectively and the ones used for axial total pressure (A1, A2) had a capacity of 4 450 N. The pressure was transferred to the load cells by pistons with a diameter of 20 mm, corresponding to a maximum swelling pressure of 1 400 and 7 000 kPa for the two radial sensors and 14 000 kPa for the axial sensors. This was considered sufficient for the potential total pressure in both directions. The pore pressure sensors had a working range between 0–1 000 kPa. This was expected to cover the potential pore pressure with wide margin.

Table D-1. Compilation of instruments used in the BB IV test.

Sensor type	Position	Number	Supplier	Model	Remark	Signal
Load cell	C1	1	Honeywell	53BR	Radial: 0–445 N (0–1 400 kPa)	V
Load cell	C2	1	Honeywell	53CR	Radial: 0–2 225 N (0–7 000 kPa)	V
Load cell	A1, A2	2	Honeywell	53CV	Axial: 0–4 450 N (0–14 000 kPa)	V
Pore pressure	Water inlet/outlet	2	Druck Amtele	PTX610	0–1 000 kPa	mA
Temperature	Test cell	1	UK	PT100	Test cell	mA
Temperature and RH	Room climate	1	Vaisala	HMP230	Room climate	mA

D2 BB IV: Early pressure evolution

Figure D-1 shows the total pressure and pore pressure evolution during the first hours of the test. Before the test starts, a radial total pressure of between 1 and 7 kPa was registered due to a certain pre-stress of the load cells.

After closing the inlet and de-airing valves the pore pressure increased immediately. The corresponding pressure increase could also be seen on one of the radial pressure sensors (positioned at the top) while no pressure response was registered at the sensor positioned at the bottom.

Some comments regarding the early pressure evolution follows below:

- The artificial water filling took 1 hour and 7 minutes. After about 30 minutes it was discovered that the lower water inlet was clogged. The valves into the test cell were closed during cleaning and this is the reason for the pore pressure peak at this time (0.5 hours).
- When the artificial filling was finished (approx. 1.2 hours), the inlets to the filter were connected to a vessel containing saline water. This explains the second pore pressure peak (1.2 hours). The height of the water head was approx. 2 meters (distance from water level in vessel to the bottom of BB test cell). The registered pore pressure at top and bottom are assessed to be very logical.
- Water seems to have reached one of the axial sensors early during the water filling (A1). The pressure at this position increased rather fast.
- The radial pressure at sensor C2 was very low for approx. 7.2 hours but at this time the pressure took a jump to 13–14 kPa. The reason for this is probably that the piston, transferring the pressure to the load cell, had some resting friction. It should, however, be noted that all pressures were still very low.

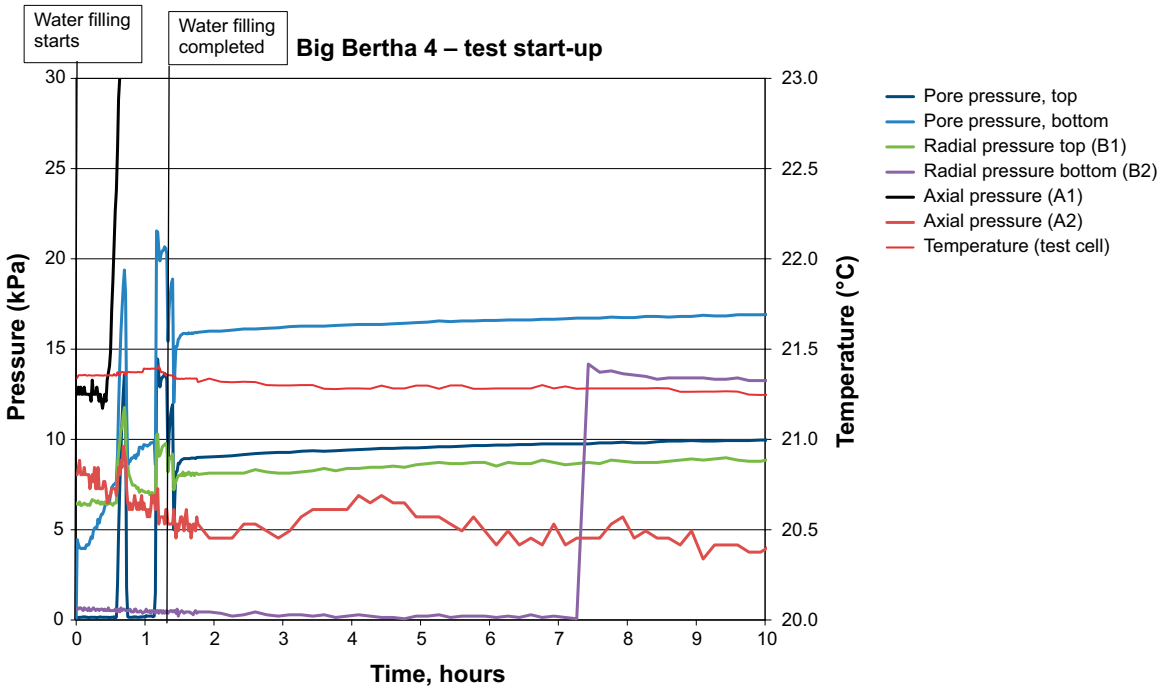

Figure D-1. *BB IV. Pore pressure, radial/axial total pressure and temperature plotted versus time during the first hours of the test.*

D3 BB IV: Room climate

The registered relative humidity of the room, temperature of the room and temperature of the test cell are shown in Figure D-2. The test was started in the beginning of September 2014 and was terminated in the beginning of March 2015 after 180 days.

The part of the laboratory used for this test has no climate control. The room temperature has, however, been rather constant during the first hundred days, mainly between 22 and 24 °C but has after that increased slightly. The temperature increase depends probably on the fact that two ovens, placed in the same room as the test cell, were started. The temperature of the test cell has, however, been rather constant during the test time, mainly between 21 and 23 °C.

The test cell is a closed system and therefore the variations in the relative humidity of the room are not expected to have any influence on the test results. The temperature variations have had a small influence on the pressure measurements due to heat induced expansion of the bentonite and water inside the test cell. This is further addressed in Section 8.3 where the total pressure data is discussed.

D4 BB IV: SC position

The SC-rock gap width was first determined at the test assembly and then also during the test dismantling. Table D-2 shows the results from the measurements. There are some small differences observed in the SC-rock gap width before and after the test. It is probable that the swelling pressure from the bentonite blocks has moved the SC somewhat in relation to the test cell and it may also have reshaped the, not perfectly round, SC shell. Thereby, the SC-rock gap width might have been changed. The small distances measured for cross-section A, in directions 180°, 225° and 270°, probably depends on that the foot at this position was pushed through the plastic filter (2 mm thick) installed on the enclosure wall.

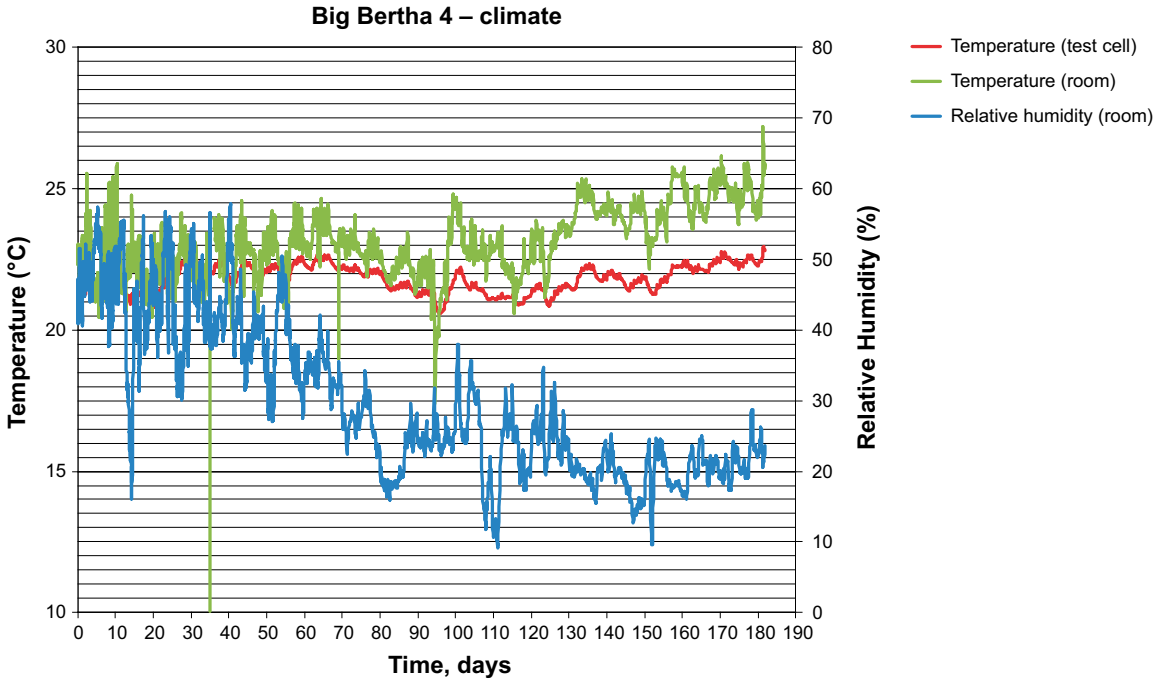

Figure D-2. *BB IV. Registered relative humidity and temperature of the room and temperature of the test cell plotted versus time.*

Table D-2. The SC-rock gap width was determined at test assembly and at test dismantling. There are some small differences observed in the SC-rock gap width before and after the test. In the table "drift wall" = "inner surface of the test cell".

Cross section	Direction [°]	Distance drift wall-SC [mm]	
		Before	After
A	0	45.6	49.9
A	45	45.5	49.7
A	90	44.3	45.4
A	135	44.2	43.6
A	180	44.4	42.1
A	225	45.5	40.9
A	270	46.4	41.0
A	315	47.1	46.5
D	0	46.1	46.4
D	45	45.5	48.5
D	90	44.7	46.1
D	135	44.4	43.8
D	180	44.2	40.4
D	225	45.0	43.0
D	270	46.1	42.0
D	315	46.5	45.2

The measurements made on the SC before test assembly are provided in Table D-3 and an explanation for the directions used is shown in Figure D-3.

Table D-3. Determination of SC diameter before test start. The directions are shown in Figure D-3.

Cross section	Direction [°]	Diameter [mm]
A	0–180	710.2
A	45–225	710.7
A	90–270	707.5
A	135–315	710.0
C	0–180	707.0
C	45–225	711.1
C	90–270	710.2
C	135–315	711.0

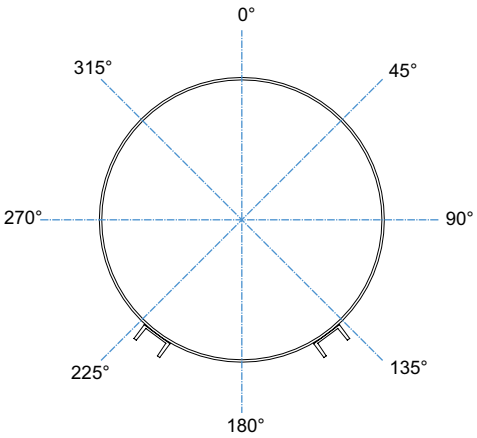

Figure D-3. *BB IV. Figure showing the SC and the directions used for the measurements of the diameter.*

D5 BB IV: Analysis data

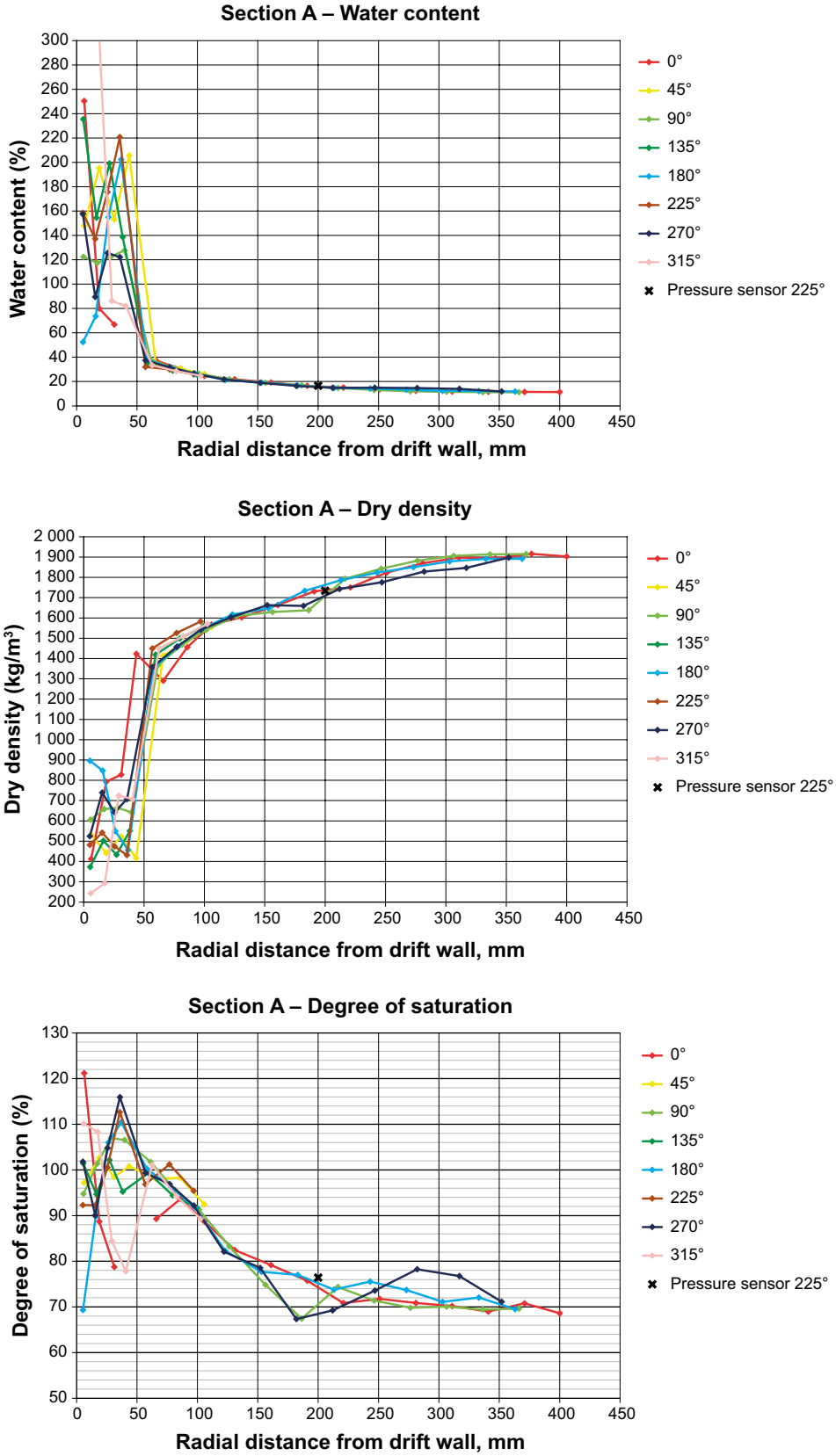

Figure D-4. *BB IV. Radial profiles showing the water content distribution (upper), the dry density distribution (middle) and the degree of saturation (lower) in cross section A.*

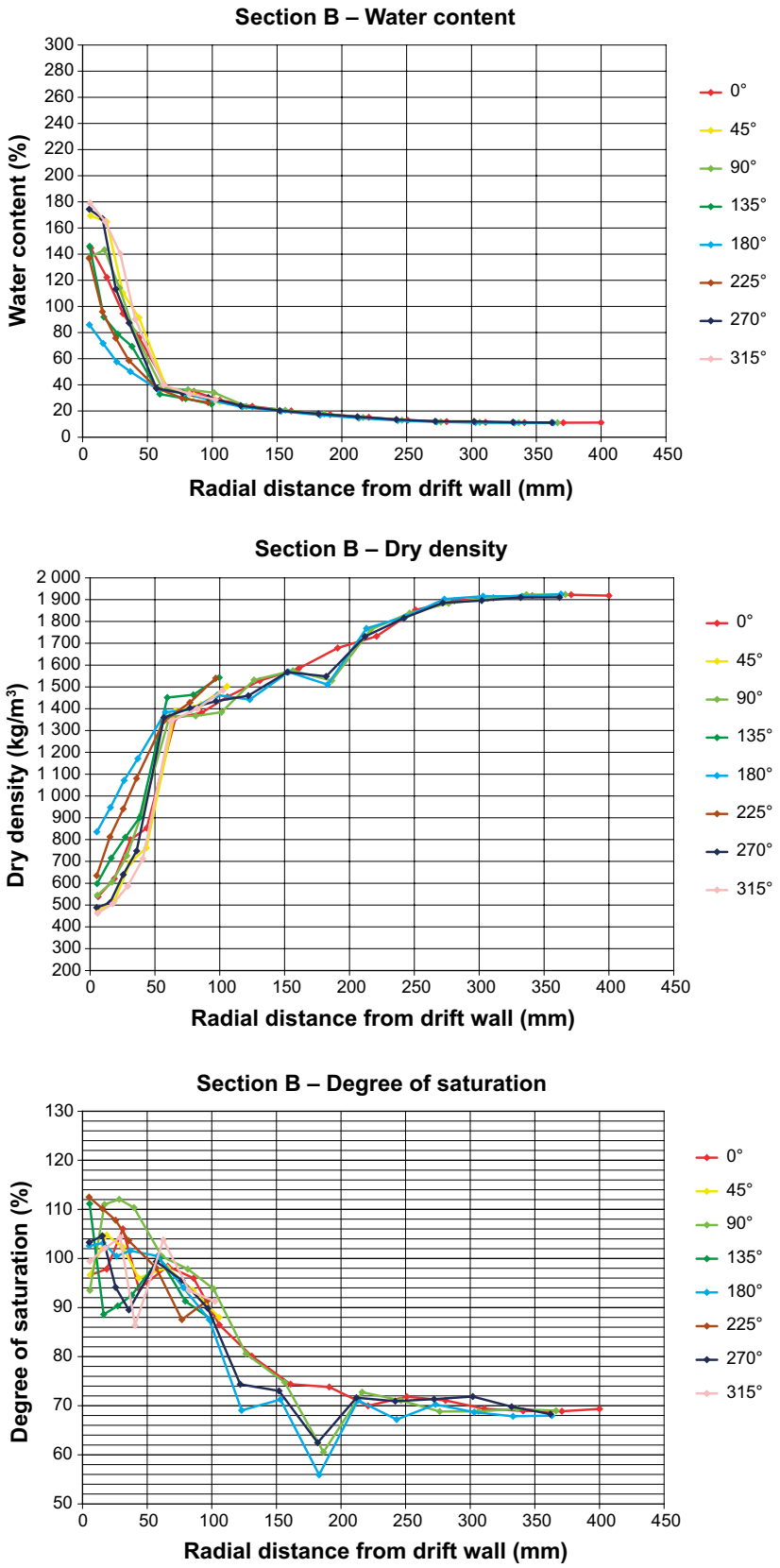

Figure D-5. *BB IV. Radial profiles showing the water content distribution (upper), the dry density distribution (middle) and the degree of saturation (lower) in cross section B.*

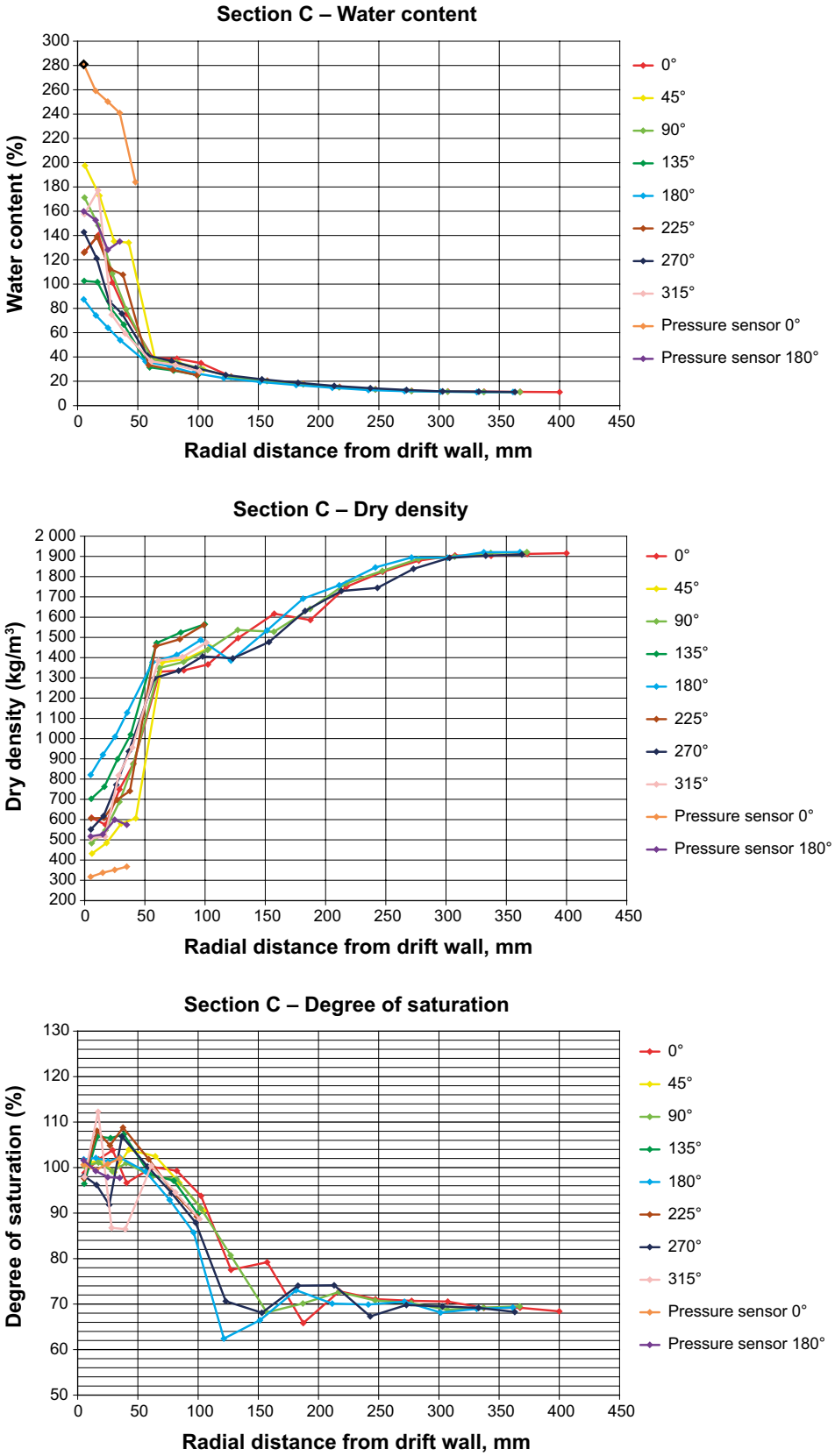

Figure D-6. *BB IV. Radial profiles showing the water content distribution (upper), the dry density distribution (middle) and the degree of saturation (lower) in cross section C.*

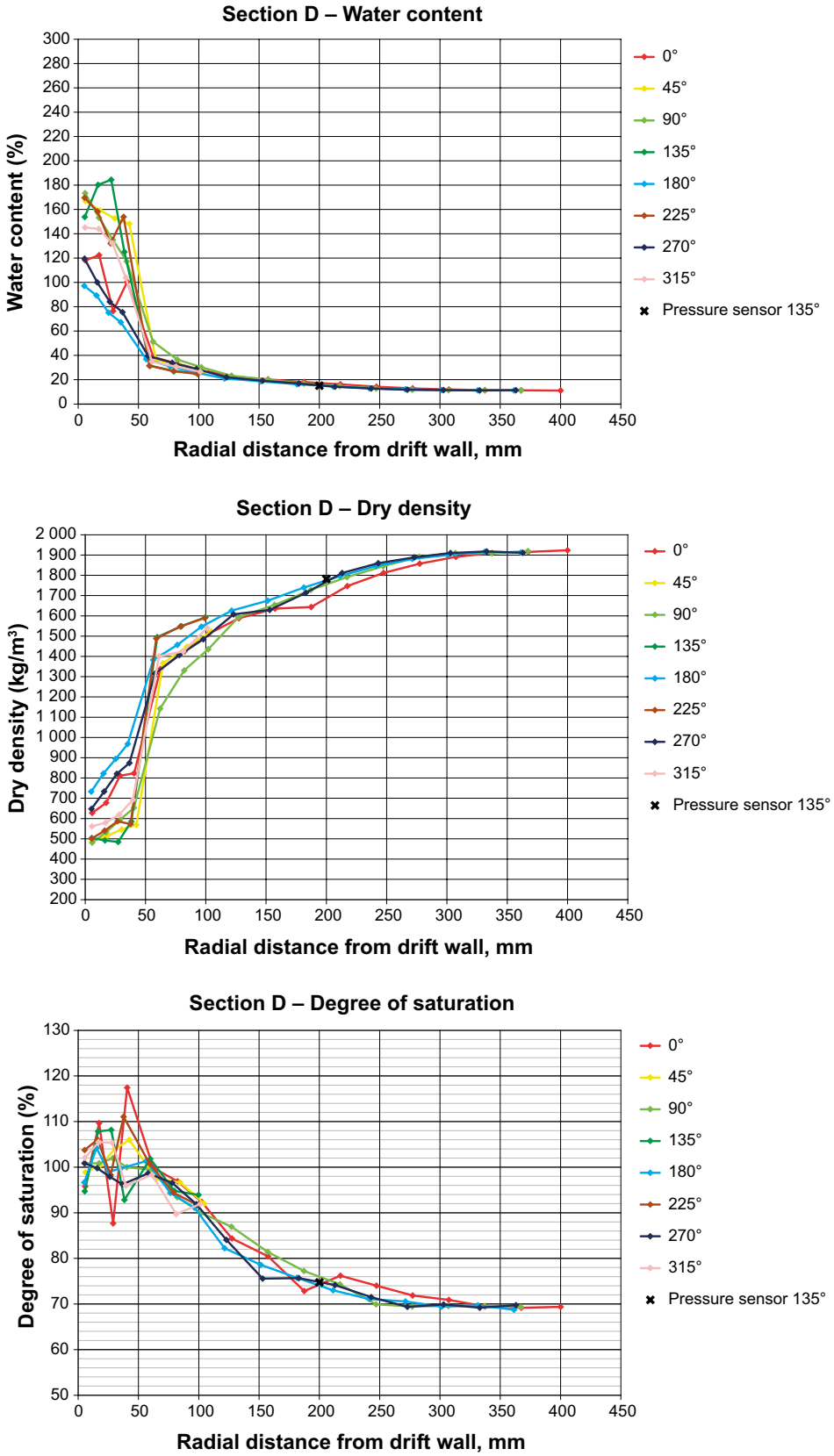

Figure D-7. *BB IV. Radial profiles showing the water content distribution (upper), the dry density distribution (middle) and the degree of saturation (lower) in cross section D.*

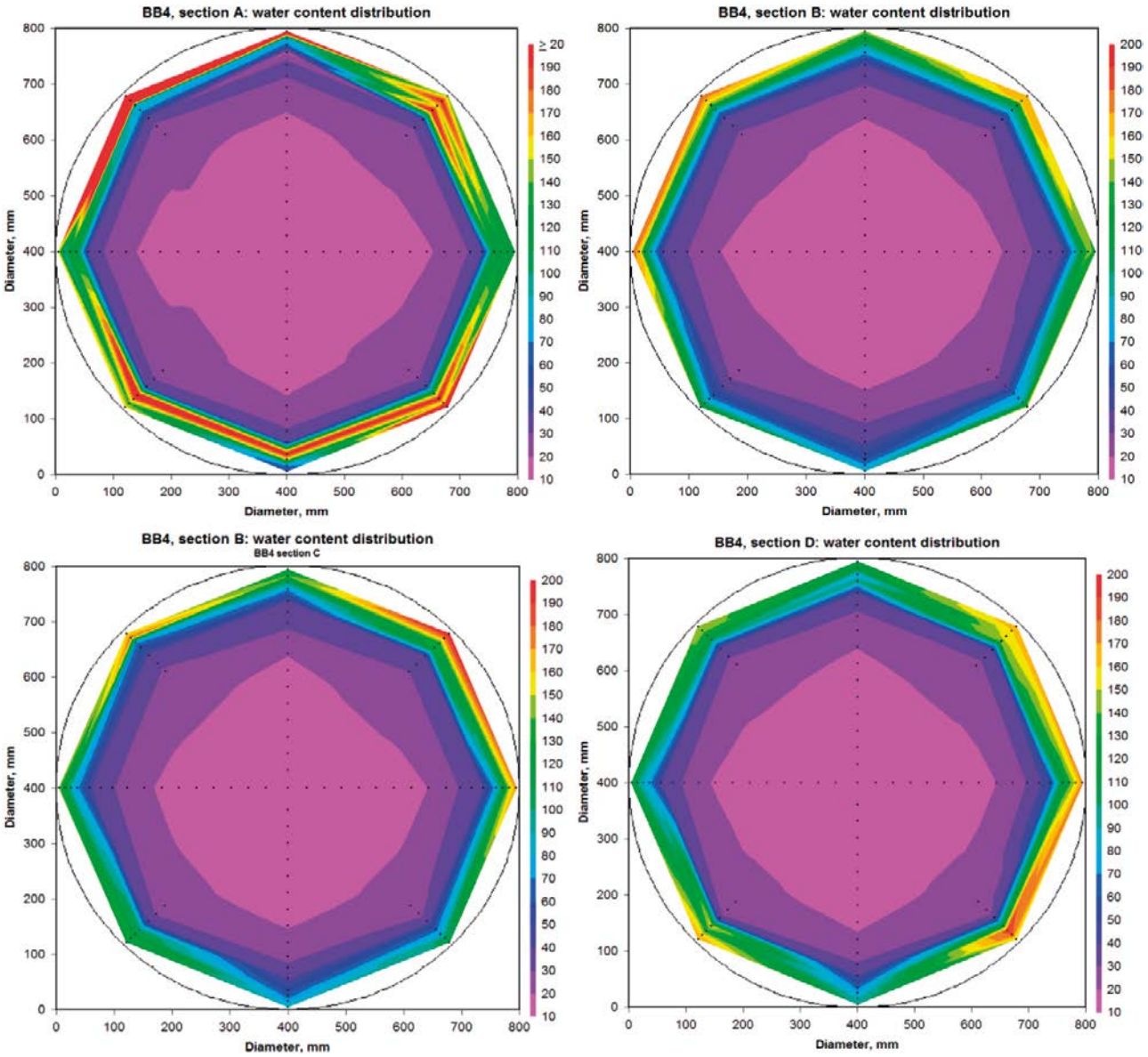

Figure D-8. *BB IV. Contour plots showing the water content distribution in the four cross sections investigated.*

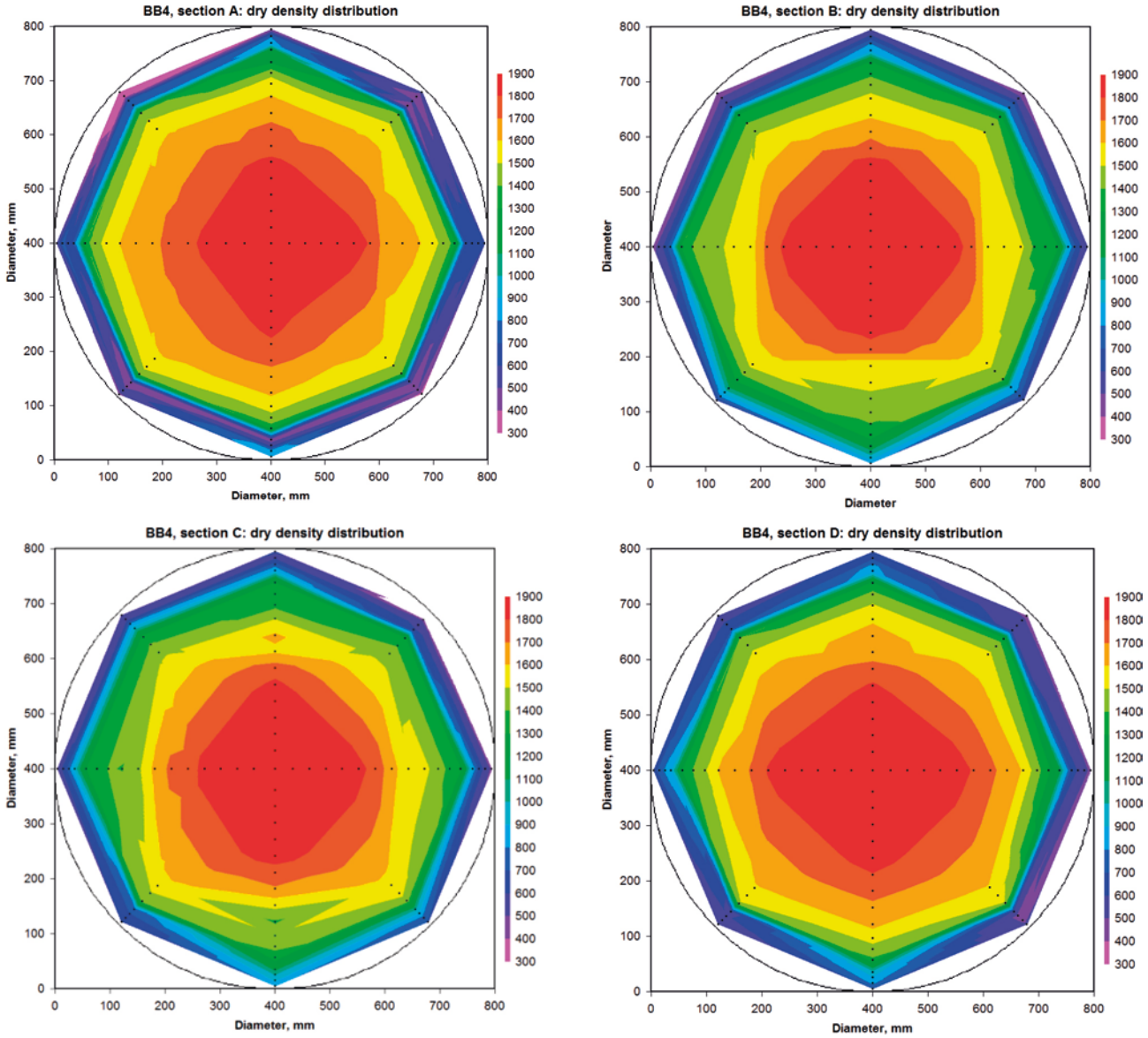

Figure D-9. *BB IV. Contour plots showing the dry density distribution in the four cross sections investigated.*

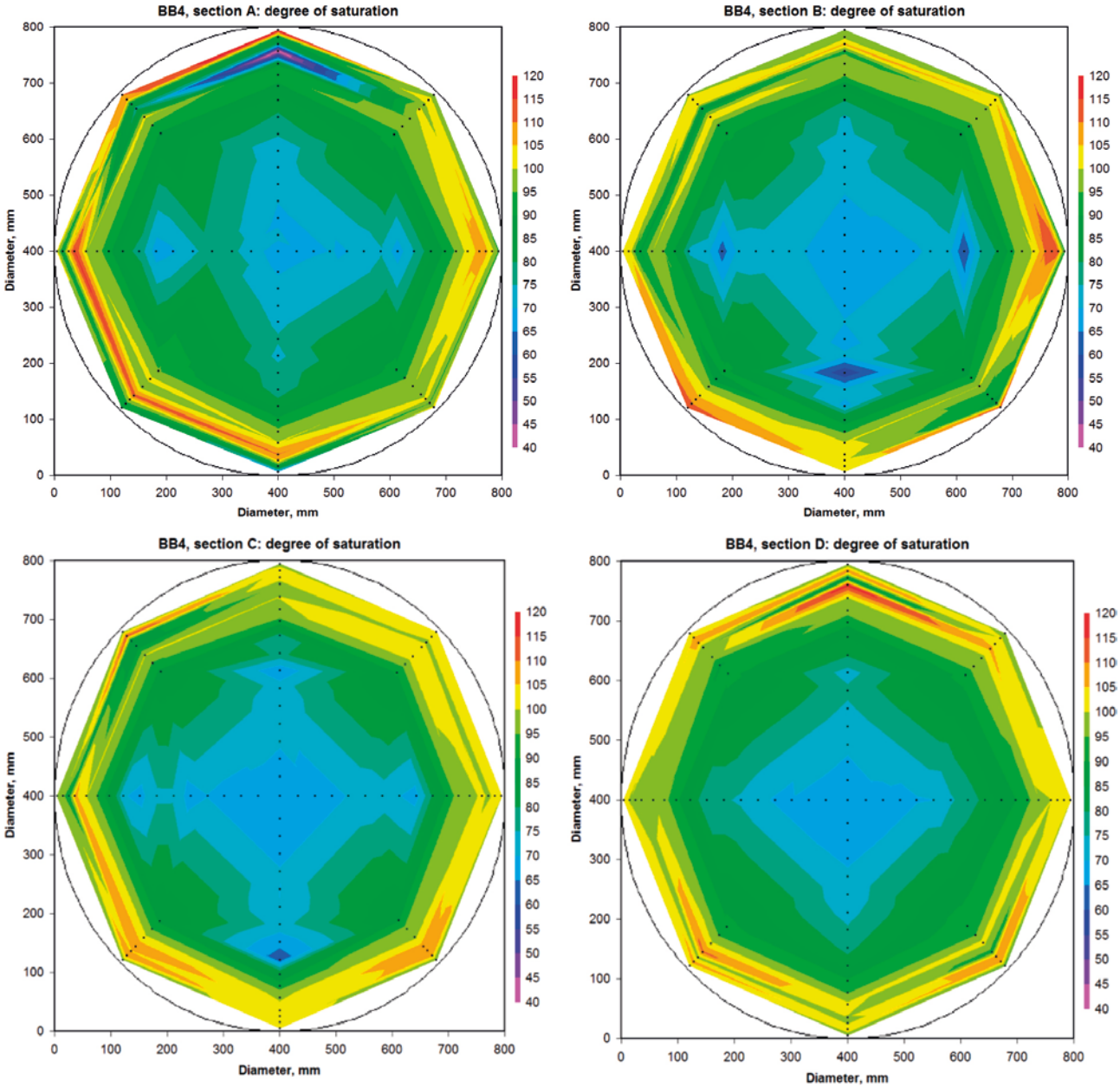

Figure D-10. *BB IV. Contour plots showing the degree of saturation distribution in the four cross sections investigated.*

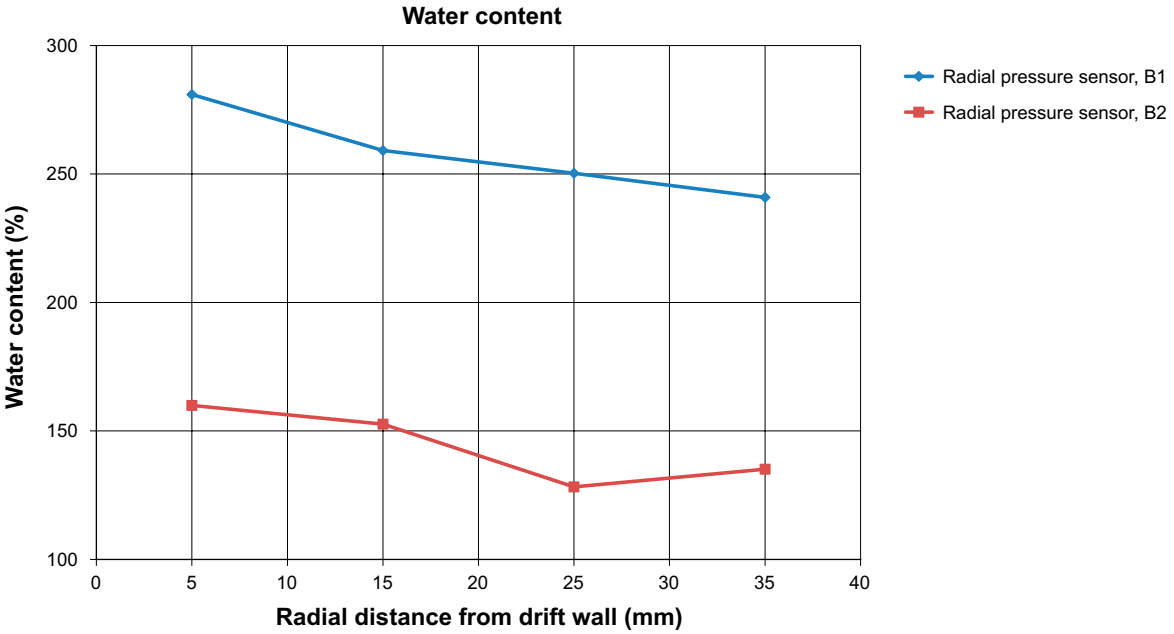

Figure D-11. *BB IV. Water content in the samples taken just inside the radial total pressure measurement positions.*

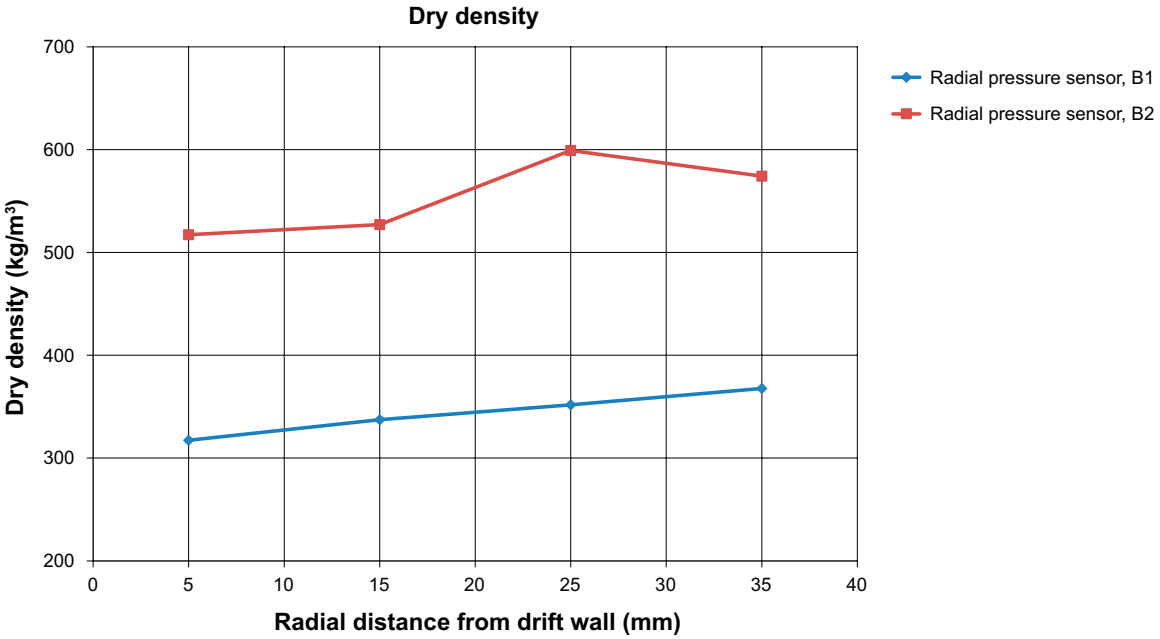

Figure D-12. *BB IV. Dry density in the samples taken just inside the radial total pressure measurement positions.*

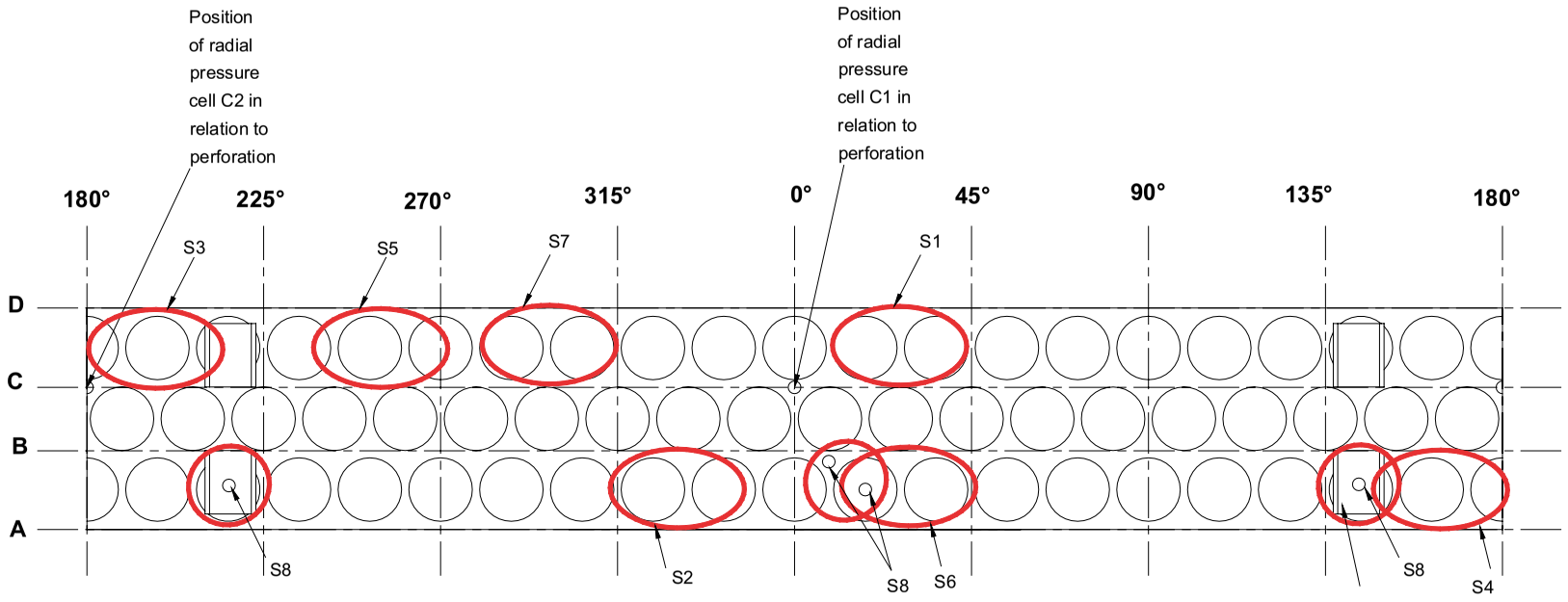

Figure D-13. *BB IV. Schematic showing the unfolded SC. The red rings shows were specimens have been cut out from the SC-rock gap. In addition the positions of feet and the positions of the radial pressure sensors in relation to the perforation are also marked.*

Table D-4. BB IV. Data from the analysis of samples taken just inside the radial and axial total pressure measurement positions. Swelling pressures at test dismantling are added to the table.

Description	Cross section	Direction [°]	Radial distance from cell [mm]	Water content [%]	Dry density [kg/m^3]	Degree of saturation [%]	Total pressure [kPa]
Radial, C1	C	0	5	280.9	317	101	410
Radial, C1	C	0	15	259.1	337	99	
Radial, C1	C	0	25	250.3	352	101	
Radial, C1	C	0	35	240.9	368	102	
Radial, C2	C	180	5	159.9	517	102	378
Radial, C2	C	180	15	152.6	527	99	
Radial, C2	C	180	25	128.2	599	98	
Radial, C2	C	180	35	135.1	574	98	
Axial, A2	A	225	200	16.6	1734	76	0
Axial, A1	D	135	200	15.1	1782	75	2380

D5.1 BB IV: Results – SC-rock gap: Specimen S1

This specimen was taken from the area between cross-section C and D, in direction between 0° and 45° (see photo provided in Figure 4-28). Four samples were cut out above the perforated holes and one in between the perforated holes, Figure D-14. Each sample was divided at three levels at different distances from the drift wall (inner test cell wall). In total 15 samples were analyzed regarding water content and density.

The results from the tests are shown in Figure D-15. All samples were assessed to be water saturated. The variation in density and water content between the different positions and between the three levels is significant. The samples taken above the perforated hole had a dry density between 600 and 1 050 kg/m^3, with the lowest densities close to the enclosure wall. The dry density between the perforated holes is significantly lower, between 450 and 850 kg/m^3.

D5.2 BB IV: Results – SC-rock gap: Specimen S2

This specimen was taken from the area between cross-section A and B, in direction between 315° and 0° (see photo provided in Figure 4-20). Four samples were cut out above the perforated holes and three in between the perforated holes, Figure D-16. Each sample was divided at three levels at different distances from the drift wall (inner test cell wall). In total 21 samples were analyzed regarding water content and density.

The results from the tests are shown in Figure D-17. All samples are assessed to be water saturated. The variation in density and water content between the different positions and between the three levels is, however, strong. The samples taken above the perforated hole have a dry density between 800 and 1 130 kg/m^3, with the lowest densities close to the test cell wall. The dry density between the perforated holes is lower, between 420 and 950 kg/m^3. It is also obvious that the four samples taken above the perforation have a very similar radial density profile while the variation in density is much higher depending on level for three samples taken from the area between the perforated holes.

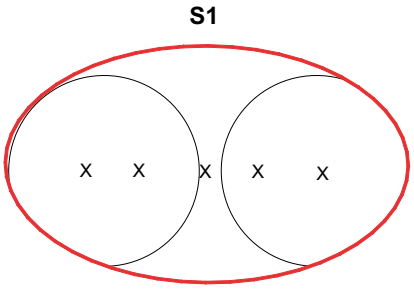

Figure D-14. *BB IV. Schematic drawing showing the approximate positions of the samples taken from specimen S1, see also overview provided in Figure 4-41.*

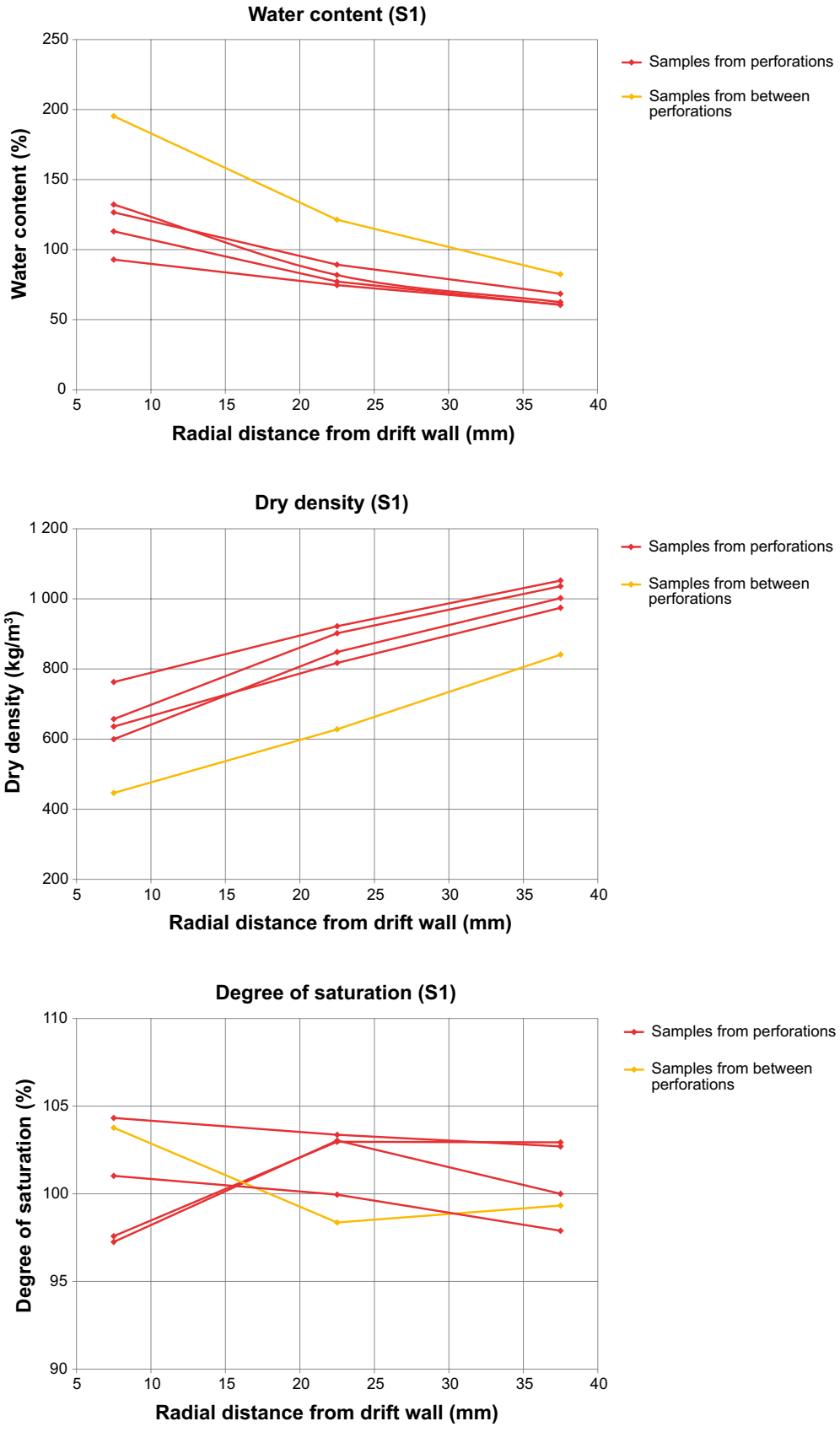

Figure D-15. *BB IV. Upper: Water content distribution plotted versus the distance from the inner test cell wall (drift wall). Middle: Dry density plotted versus the distance from the inner test cell wall (drift wall). Lower: Degree of saturation plotted versus the distance from the inner test cell wall (drift wall).*

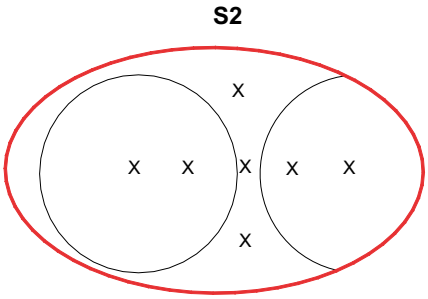

Figure D-16. *BB IV. Schematic drawing showing the approximate positions of the samples taken from specimen S2, see also overview provided in Figure 4-41.*

D5.3 BB IV: Results – SC-rock gap: Specimen S3

This specimen was taken from the area between cross-sections C and D, in direction between 180° and 225° (see photo provided in Figure 4-29). Samples were cut at every cm along the length of the specimen at three levels at different distances from the drift wall (inner test cell wall), Figure D-18. In total 48 samples were analyzed regarding water content (one sample was unfortunately dropped before weighing after the drying).

The results from the tests are shown in Figure D-19. The variation in water content between the different positions and between the three levels is strong. The samples taken above the perforated hole has a water content of 55–60 % close to the SC shell (Level C), between 65–75 % at Level B (in the middle of the SC-rock gap) and between 80–110 % at Level A (close to the test cell wall). The water content outside the perforated hole is higher (lower density). One sample was taken from the clay just at the position of the entrance to the foot; see Figure D-18. The water content at this position was 140 %.

D5.4 BB IV: Results – SC-rock gap: Specimen S4

This specimen was taken from the area between cross-sections A and B, in direction between 150° and 180°. Three samples were cut out above the perforated holes and two in between the perforated holes, Figure D-20. Each sample was divided at three levels, positioned at different distances from the drift wall (inner test cell wall). In total 15 samples were analyzed regarding water content.

The results from the tests are shown in Figure D-21. The variation in water content is not as high as e.g. in S1 and S2. The three samples taken above the perforated hole have all very similar water content distribution. The water content determined for one of the samples taken from between the perforations is very similar to those taken above perforation which probably depends on that the sample has been positioned very close to the perforated hole. The other sample taken from between the perforated holes has generally higher water content at all three sampled distances from the drift wall.

D5.5 BB IV: Results – SC-rock gap: Specimen S5

This specimen was taken from the area between cross-sections C and D, in direction between 240° and 270°. Two samples were cut out above the perforated holes and two in between the perforated holes, Figure D-22. Each sample was divided at three levels, positioned at different distances from the drift wall (inner test cell wall). In total 12 samples were analyzed regarding water content and density.

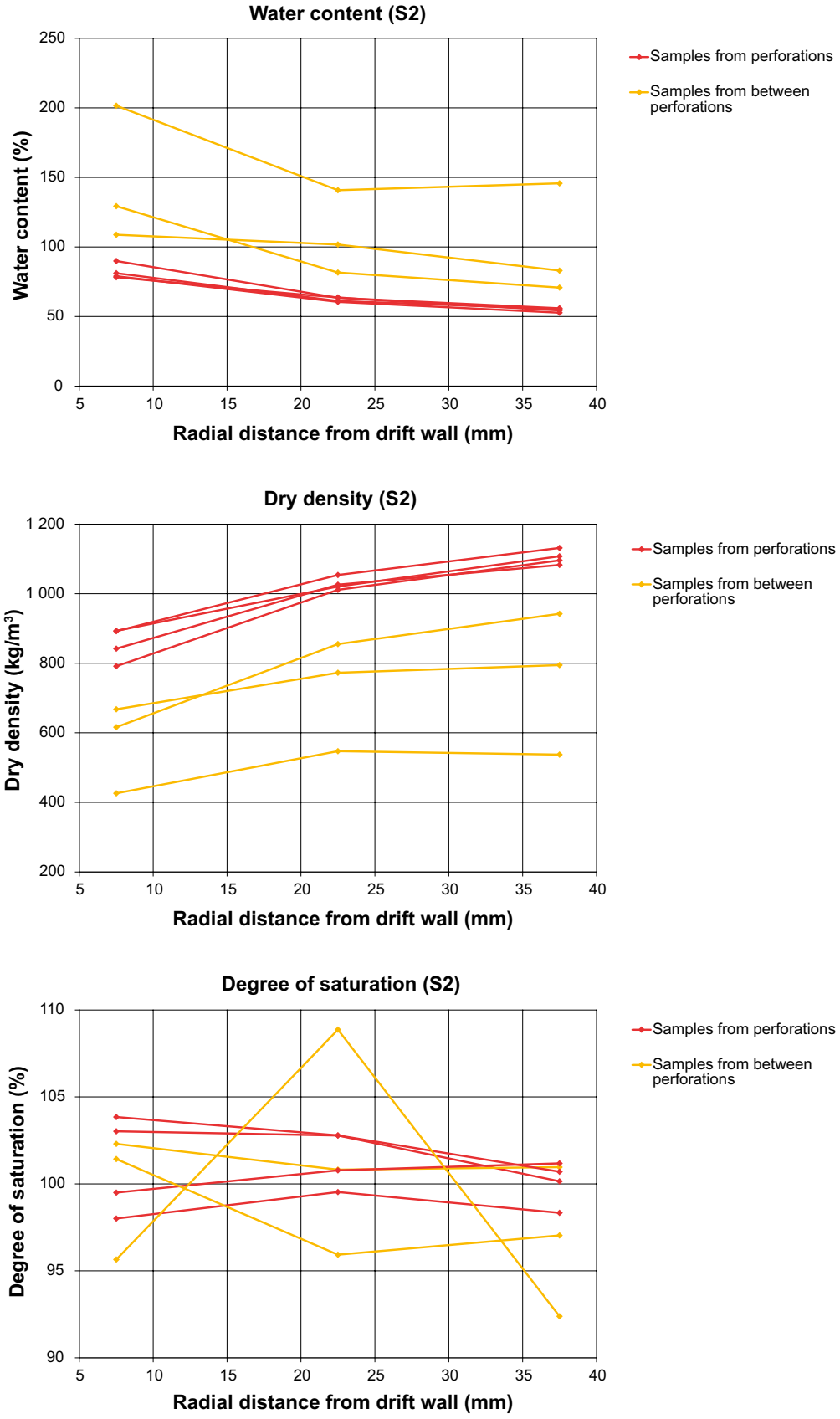

Figure D-17. *BB IV. Upper: Water content distribution plotted versus the distance from the inner test cell wall (drift wall). Middle: Dry density plotted versus the distance from the inner test cell wall (drift wall). Lower: Degree of saturation plotted versus the distance from the inner test cell wall (drift wall).*

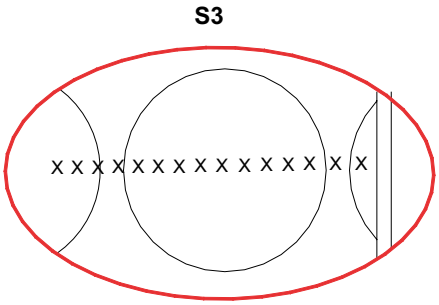

Figure D-18. *BB IV. Schematic drawing showing the approximate positions of the samples taken from specimen S3, see also overview provided in Figure 4-41.*

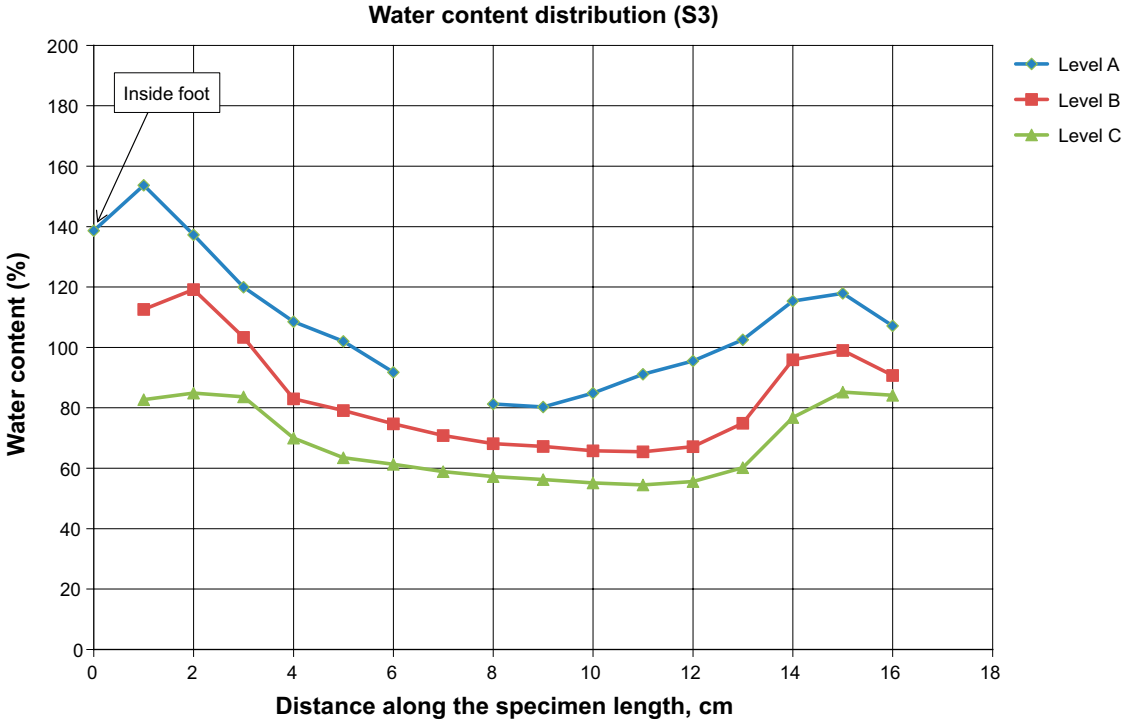

Figure D-19. *BB IV. Water content distribution plotted versus the distance along the specimen length.*

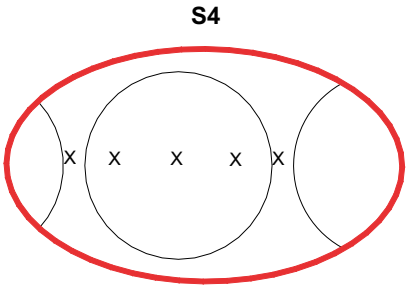

Figure D-20. *BB IV. Schematic drawing showing the approximate positions of the samples taken from specimen S4, see also overview provided in Figure 4-41.*

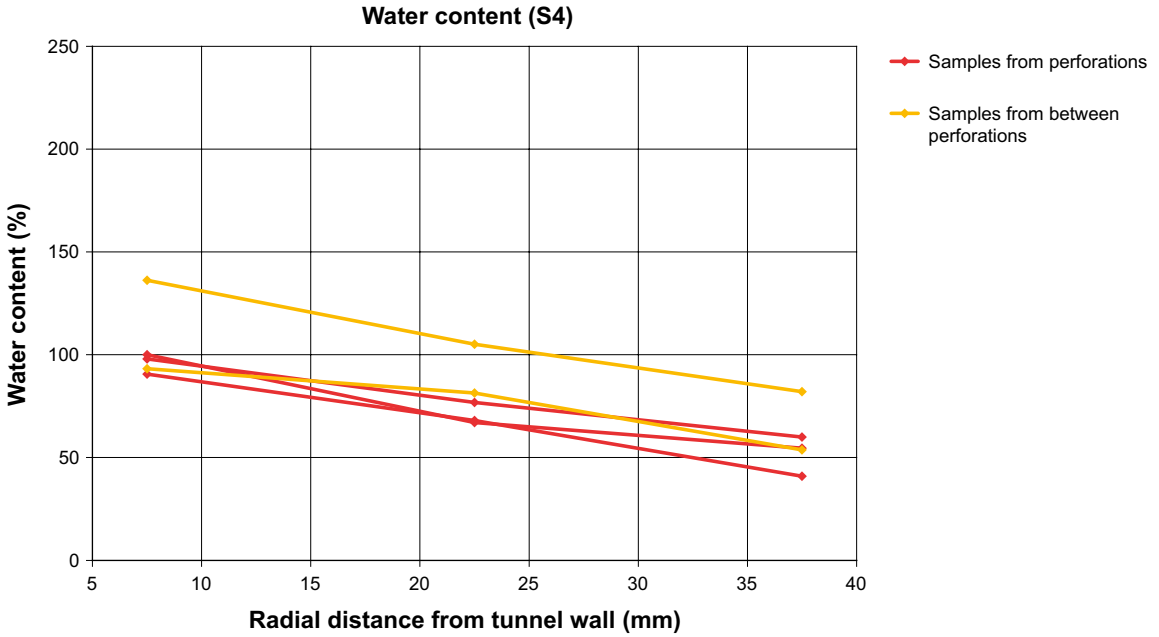

Figure D-21. *BB IV. Water content distribution plotted versus the distance along the specimen length.*

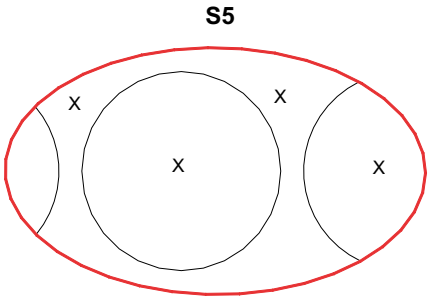

Figure D-22. *BB IV. Schematic drawing showing the approximate positions of the samples taken from specimen S5, see also overview provided in Figure 4-41.*

The results from the tests are shown in Figure D-23. All samples are assessed to be water saturated. The variation in water content between the different positions is rather similar to specimen S4. The samples taken above the perforated hole have a dry density between 750 and 1 030 kg/m^3, with the lowest densities close to the test cell wall. The dry density between the perforated holes is lower, between 580 and 700 kg/m^3. The two samples taken above the perforation have a very similar radial density profile while the variation in density is much lower for samples taken from the area between the perforated holes.

D5.6 BB IV: Results – SC-rock gap: Specimen S6

This specimen was taken from the area between cross-sections A and B, in direction between 0° and 45°. Samples were cut at every cm along the length of the specimen at three levels positioned at different distances from the drift wall (inner test cell wall), Figure D-24. In total 60 samples were analyzed regarding water content.

The results from the tests are shown in Figure D-25. The variation in water content between the different positions and between the three levels is strong. The samples taken above the perforated hole (approximately 2–12 cm distance of the specimen length) has a water content of 75–80 % close to the SC shell (Level C), between 95–120 % at Level B (in the middle of the SC-rock gap) and between 120–170 % at Level A (close to the test cell wall). The water content increases markedly, the closer to the edge of the perforated hole and the highest water contents are found in between two perforated holes e.g. at a distance of 1 and 13 cm along the specimen length where the water content is close to 200 % at the outermost parts (Level A).

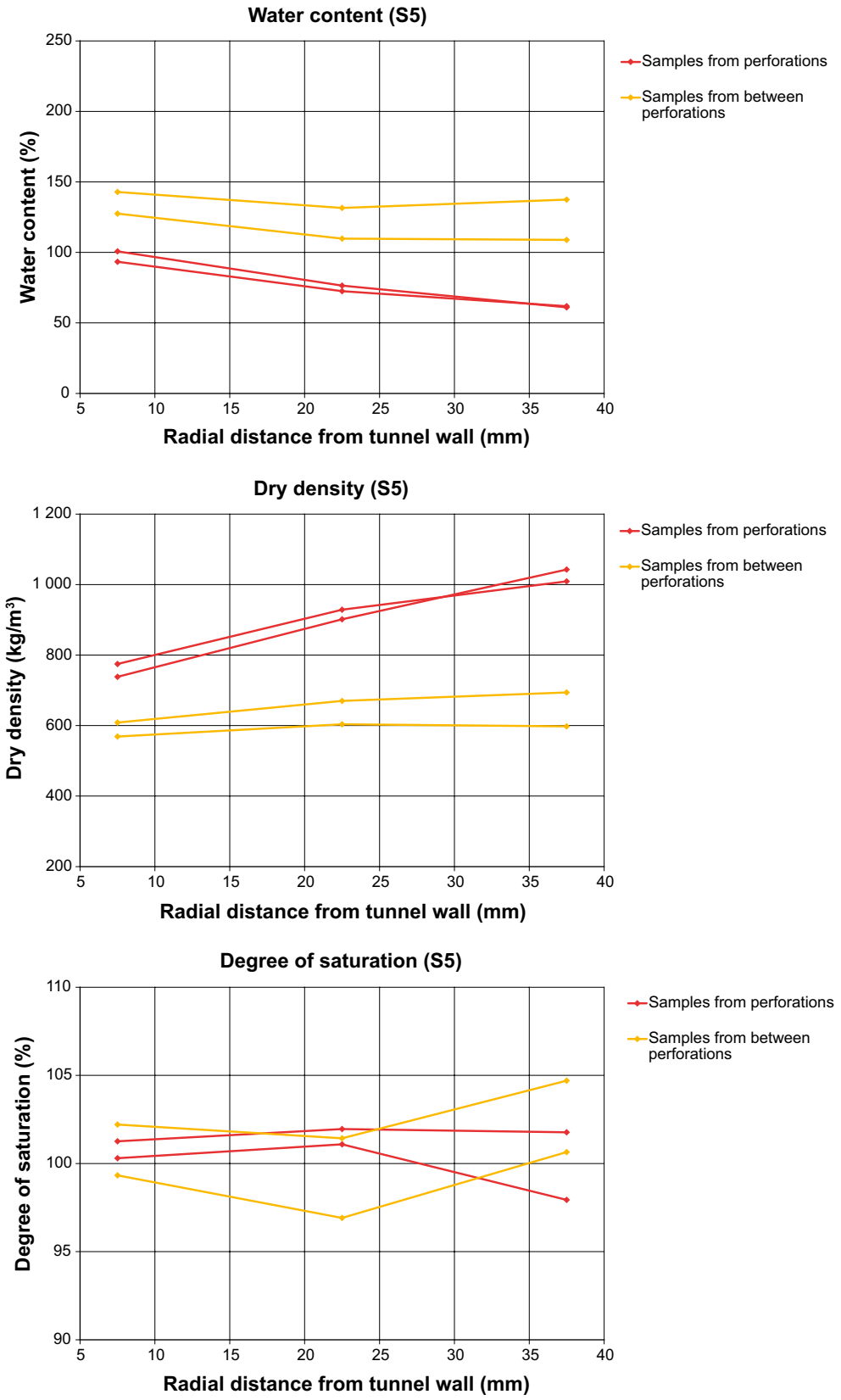

Figure D-23. *BB IV. Upper: Water content distribution plotted versus the distance from the inner test cell wall (drift wall). Middle: Dry density plotted versus the distance from the inner test cell wall (drift wall). Lower: Degree of saturation plotted versus the distance from the inner test cell wall (drift wall).*

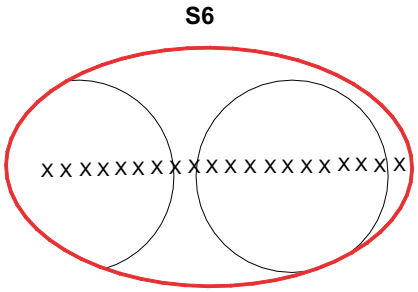

Figure D-24. BB IV. Schematic drawing showing the approximate positions of the samples taken from specimen S6, see also overview provided in Figure 4-41.

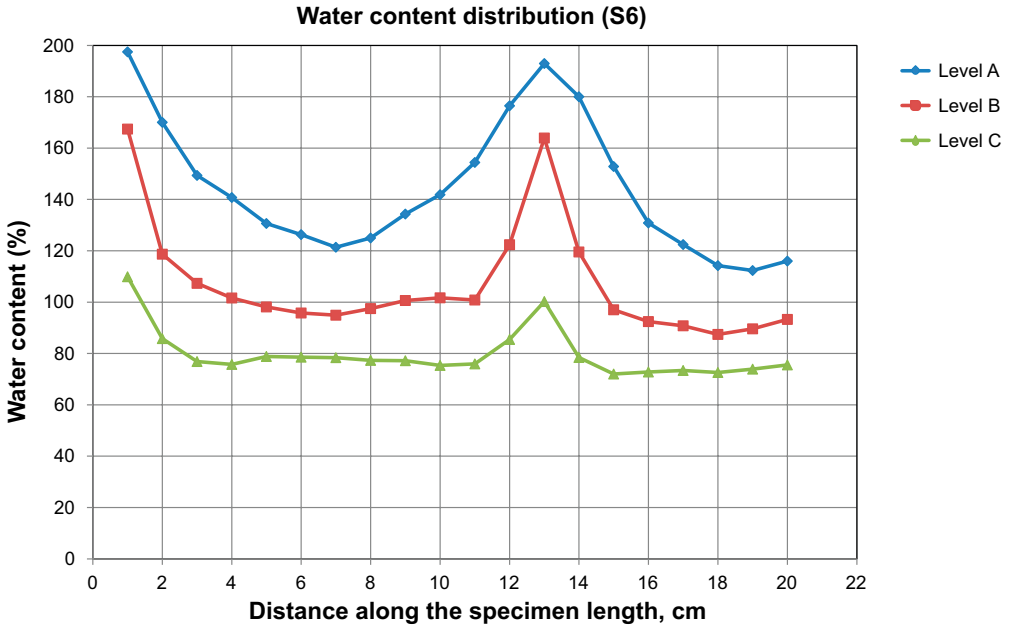

Figure D-25. BB IV. Water content distribution plotted versus the distance along the specimen length.

The rather dense sampling of specimens S3 and S6 illustrates well the heterogeneous bentonite in the SC-rock gap. There are obvious differences in water content (and density) both depending on the position in relation to the perforation and also depending on the radial distance from the test cell wall.

D5.7 BB IV: Results – SC-rock gap: Specimen S7

This specimen was taken from the area between cross-sections C and D, in direction between 290° and 315°. Four samples were cut out above the perforated holes and four in between the perforated holes, Figure D-26. Each sample was divided at three levels, positioned at different distances from the drift wall (inner test cell wall). In total 24 samples were analyzed regarding water content.

A photo showing the specimen is provided in Figure D-27. The photo shows the surface that has been in contact with the SC shell. The bentonite that had been in direct contact with the steel is evidently discolored.

The results from the tests are shown in Figure D-28. The results from the water content measurements on the samples taken above the perforated holes are all very similar (red lines in graph). The water content determined in between the perforated holes (yellow lines) is markedly higher but the relative difference between these samples is also small.

Figure D-26. *BB IV. Photo showing specimen S7. The central, discolored area, has been beneath the SC shell.*

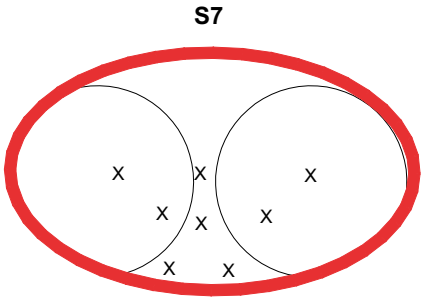

Figure D-27. *BB IV. Schematic drawing showing the approximate positions of the samples taken from specimen S7, see also overview provided in Figure 4-41.*

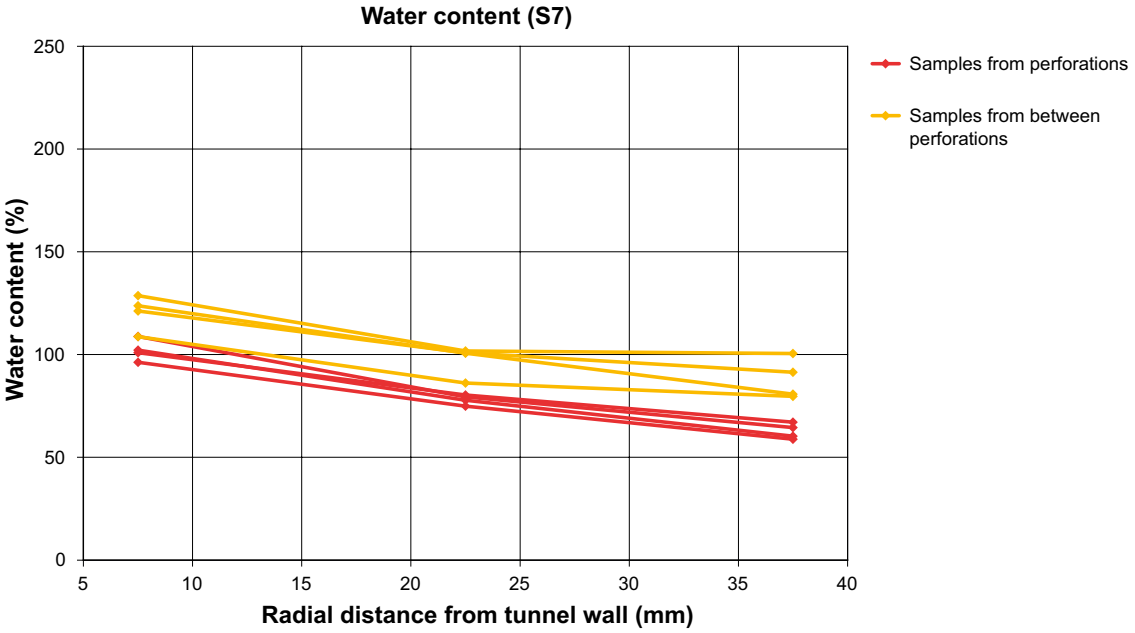

Figure D-28. *BB IV. Water content distribution plotted versus the distance along the specimen length.*

D5.8 BB IV: Results – SC-rock gap: Specimens S8

These specimens include four core-drilled samples drilled out from the area between cross-sections A and B. Two of the core-drilled samples were drilled out in direction between 10° and 25°, at the level for the inside of the SC shell; one sample was drilled out at the middle of a perforated hole and one at the midpoint between the perforations, see photo provided in Figure 4-23. The other two core-drilled samples were drilled out from the area inside the SC shell at the two feet positioned in section A-B. In addition samples were taken from the inside of the feet positioned in direction 216.5° i.e. inside the U-shape of the feet. In total 8 samples were analyzed regarding water content and density

The results from the tests are shown in Table D-5. From the results the following can be concluded:

1. The two samples drilled out from inside the SC shell and from the middle of a perforated hole respectively (sample 1 and 2) show that there is a very clear difference in density between these two positions. The bentonite inside the SC shell has not swelled as much as the bentonite in the middle of a perforated hole which has resulted in a clear difference in density.
2. The sampling of the bentonite inside the SC shell at the position of the feet (samples 3 and 4) shows that the feet have restricted the swelling of the bentonite locally at these positions.
3. The inside of the feet was completely filled with bentonite gel. The density was, however, rather low, between 300 and 400 kg/m^3.

Table D-5. BB IV. Table providing data from the analysis of bentonite samples taken just below the SC shell and inside the feet.

Sample	Description	Cross section	Direction [°]	Water content [%]	Dry density [kg/m^3]	Degree of saturation [%]
1	Between perforation	A, B	10	35.5	1384	98
2	In the middle of perforation	A, B	20	41.9	1280	99
3	Inside SC shell at foot position	A, B	143.5	31.8	1464	98
4	Inside SC shell at foot position	A, B	216.5	31.3	1488	100
5	Inside foot 1	C, D	216.5	221.8	396	102
6	Inside foot 2	C, D	216.5	241.8	368	103
7	Inside foot 3	C, D	216.5	207.5	413	101
8	Inside foot 4	A, B	216.5	301.2	295	99

Appendix E

Additional TZH information

E1 TZH: Sensor information

A compilation of the sensors used in the test is provided in Table E-1. The sensor numbers in the second column refers to the schematic drawing of the test layout provided in Figure 5-1.

Table E-1. TZH. Compilation of sensors used in the laboratory test. The sensor numbers in the second column refers to data provided in Figure 5-1.

Sensor type	Number	Supplier	Model	Remark	Signal
Load cell	1A, 1B, 2A, 2B	Honeywell	53CV	Radial: 0–4.4 kN (0–14 160 kPa)	V
Load cell	3A, 3B	Honeywell	53CR	Radial: 0–2.2 kN (0–7 080 kPa)	V
Load cell	Axial 1	Honeywell	53EP	Axial pressure, transition blocks: 0–222.4 kN (0–9 247 kPa)	V
Load cell	Axial 2	Honeywell	53DV	Axial pressure, pellet section: 0–44.5 kN (0–1 850 kPa)	V
Temperature and RH	1	Vaisala	HMP230	Room climate	mA

E2 TZH: Early pressure evolution

The pressure evolution during the first five days is provided in Figure E-1. As shown in the graph, a number of sensors reacted almost immediately (axial pressure against the end block and the three sensors in the pellet filling). The other sensors, measuring the radial pressure against the blocks, started to react after approximately 24 hours.

The data registration ended after 2 days depending on problems with the wireless data logger. The logger was, however, restarted and the data registration could then continue as planned after approximately 24 h.

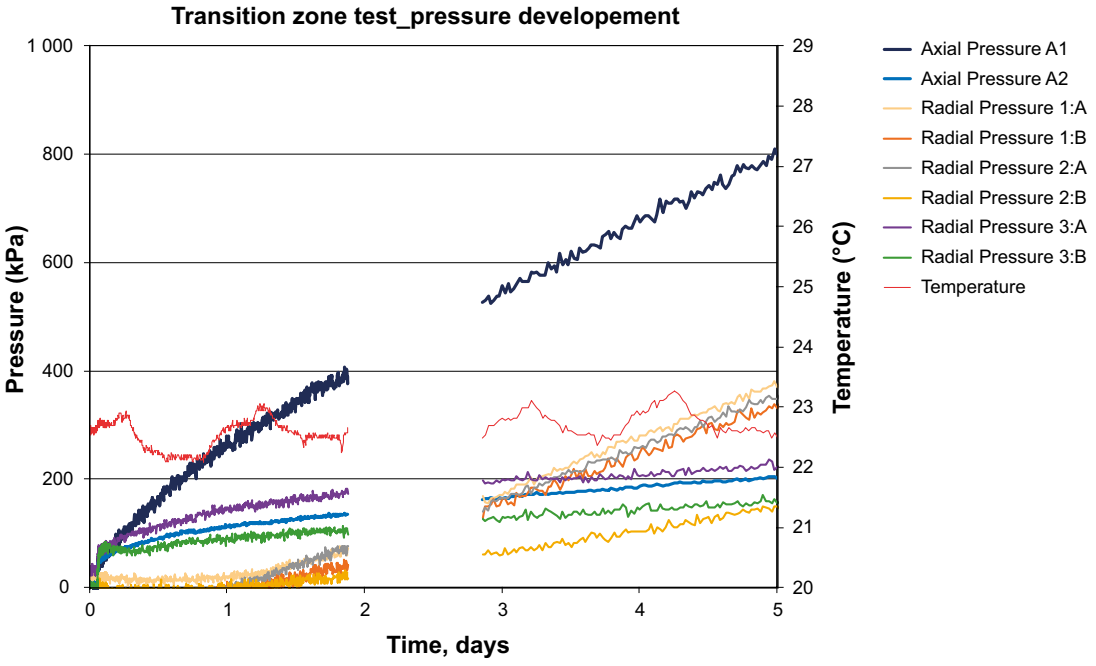

Figure E-1. *TZH. Axial and radial total pressure plotted versus time in the beginning of the test. The registered room temperature is also included.*

E3 TZH: Room climate

The measured temperature and relative humidity in the room are shown in Figure E-2. The test was performed in a part of the laboratory that had no climate control. The room temperature has, however, been rather constant during the test time, between 21 and 24 °C. The relative humidity has varied between 10 and almost 70 %. The test started December 1, i.e. during the winter, which is the explanation for the low RH during the first months. After approximately six months (beginning of June) the RH starts to increase and reaches the highest values during the summer.

The test cell is a closed system and the variation in relative humidity is not expected to have any influence on the test results. The effect of the temperature variations on the test results is, however, assessed to be very small, see e.g. investigations made by Birgersson et al. (2010). This is further addressed in Section 7.3 where the registered total pressure is discussed.

E4 TZH: Analysis data

The results from all sampling of the bentonite inside the test cell are provided in Figure E-3 to Figure E-10. Every figure shows the results from the sampling performed in one direction (A, B, C or D). Three graphs are provided, one showing the water content distribution, one showing the dry density distribution and one showing the degree of saturation.

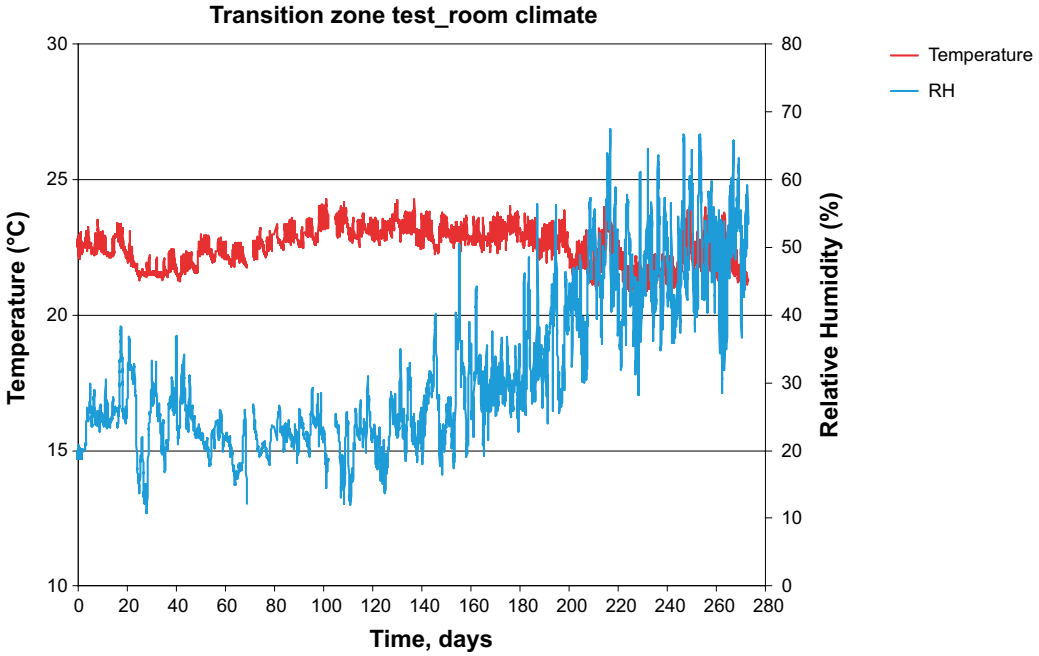

Figure E-2. *TZH. Graph showing the registered room temperature and relative humidity plotted versus time during the entire test duration.*

Table E-2. TZH. Comparison of block heights determined at the time for installation and after test termination. Note that it was not possible to detect all block interfaces during test termination.

Block no.	Block height at installation [mm]	Block height at termination [mm]	Change in height [mm]
1	50.7	52.0	1.4
2	50.8	51.7	0.9
3	50.0	51.5	1.5
4	50.6	51.5	0.9
5	50.5	51.2	0.7
6	50.5	51.6	1.2
7	50.8	51.8	1.0
8	50.3	51.7	1.4
9	50.1	51.5	1.4
10	43.0	44.4	1.3
11	50.3	51.0	0.8
12	50.2	51.0	0.9
13	50.4	na	na
14	50.1	na	na
15	50.6	na	na
16	50.2	na	na
17	51.0	na	na
18	26.1	na	na

The results are very similar in all four directions. In every cross section, samples taken from the same radius have almost the same water content and density. Regarding the samples taken from the distance block section (0–500 mm from the inner end), the water content and dry density are also very similar when comparing the samples taken in the block center (sample A1) with the samples taken at different radial distances from the center (A2, A3 and A4). The only samples that deviate are the ones taken at the periphery (A5). The water contents in these samples are somewhat higher and consequently the densities lower and there are also a larger variation in achieved results. The lower density here is logical since the homogenization is not complete when the blocks swell radially.

The graphs showing the water content and dry density distribution also show that all samples between 0 and about 500 mm from the inner end of the distance block section have almost the same water content and dry density while the samples taken after 500 mm have higher water content and lower density. This depends of course on the axial swelling of the blocks and subsequent compression of the pellet filled part.

All bentonite is fully saturated. The calculated degree of saturation varies somewhat, mainly between 99 to 102 % in the central parts and the explanation for this is probably due to the fact that the water content and density not are determined on exactly the same sample (which is impossible) but on samples that are very close to each other. There is, however, a tendency that the highest degrees of saturation, 101–102 %, are found on the pellet side i.e. in the former pellet filled section and in the blocks that had swelled and contributed to the compaction of the pellets. The reason for this is not clear.

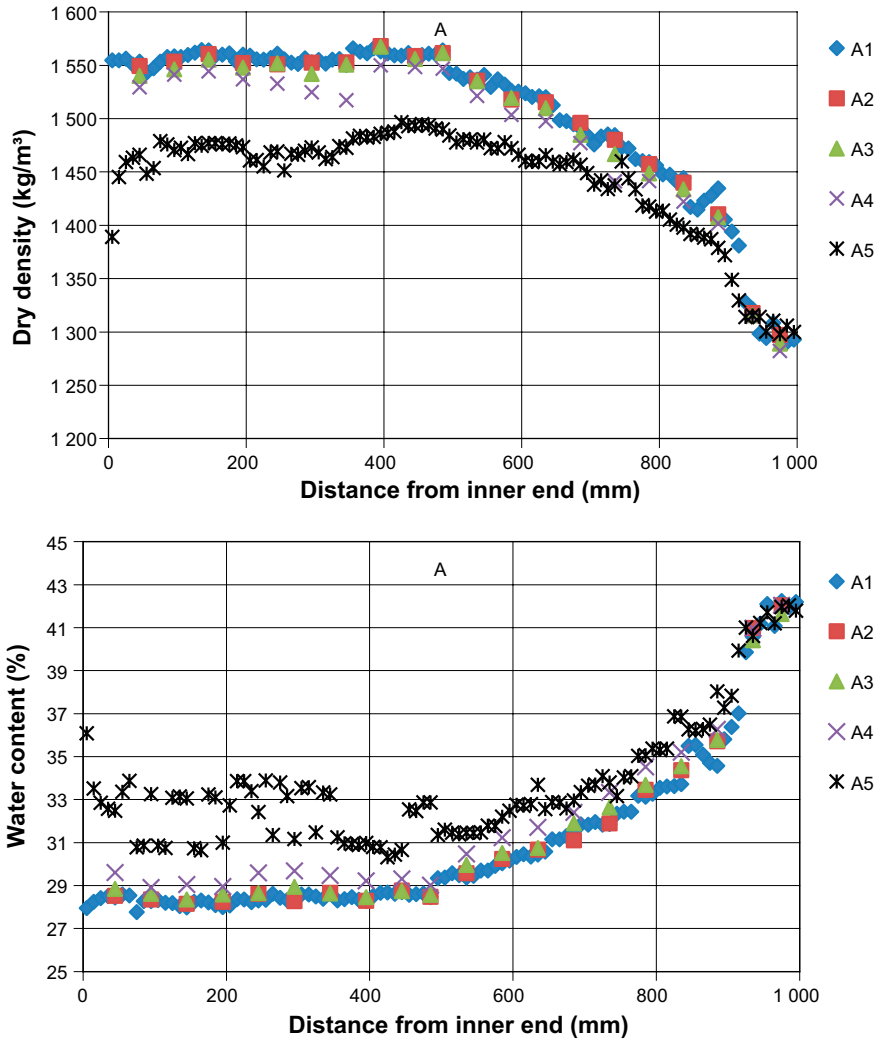

Figure E-3. *TZH. Results from sampling performed in direction A. Upper: Dry density plotted versus the distance from the inner end of the distance block section. Lower: Water content plotted versus the distance from the inner end of the distance block section.*

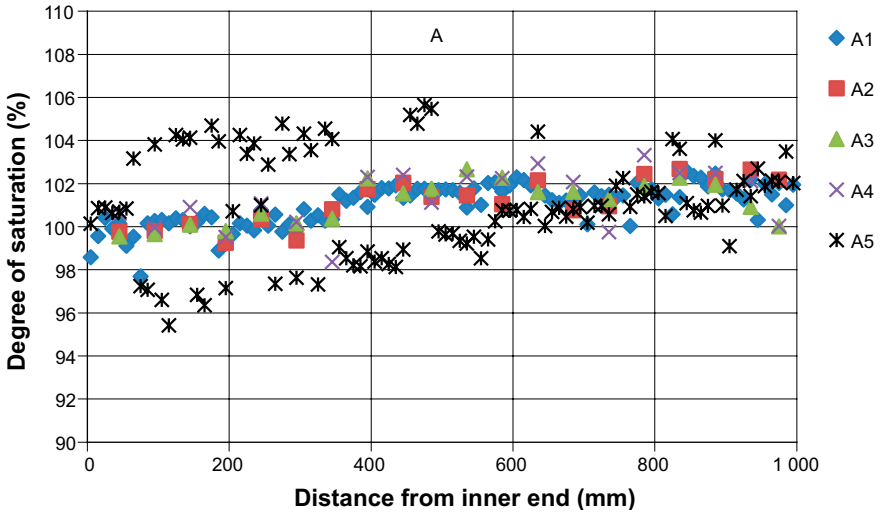

Figure E-4. *TZH. Results from sampling performed in direction A: Degree of saturation plotted versus the distance from the inner end of the distance block section.*

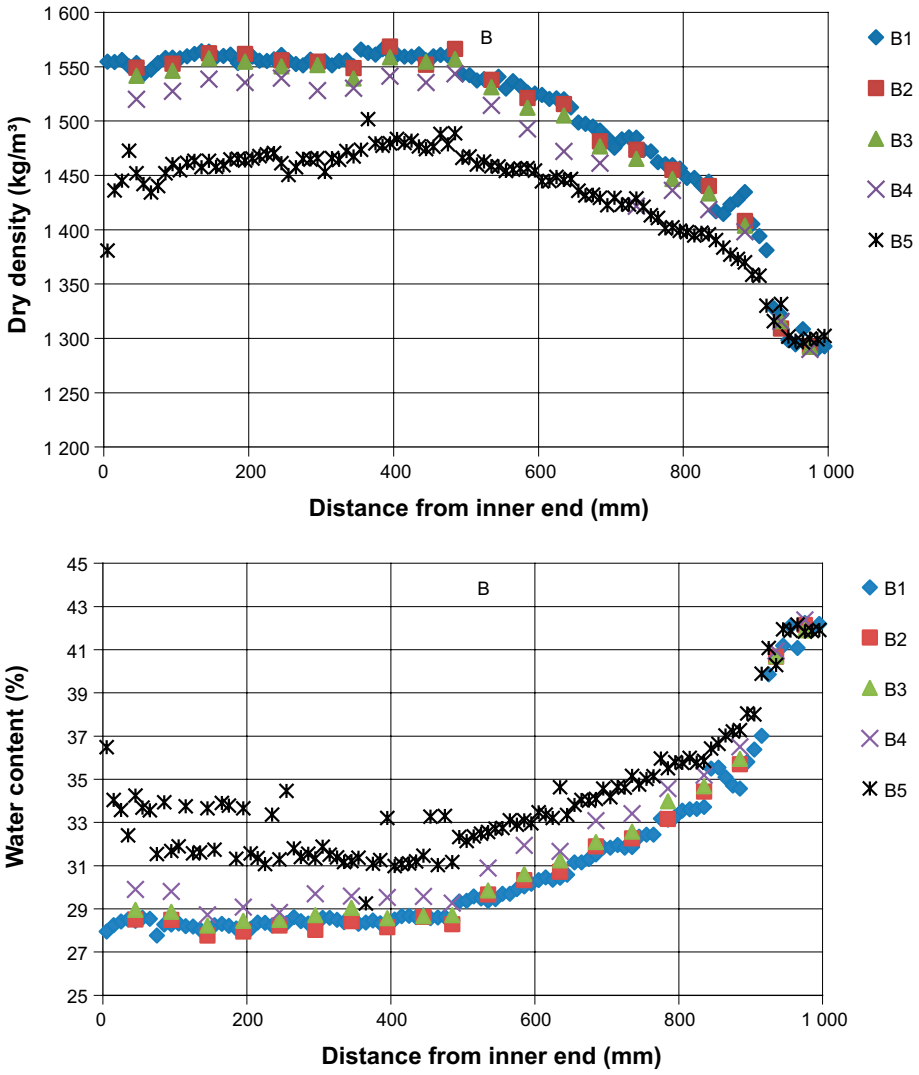

Figure E-5. *TZH. Results from sampling performed in direction B. Upper: Dry density plotted versus the distance from the inner end of the distance block section. Lower: Water content plotted versus the distance from the inner end of the distance block section.*

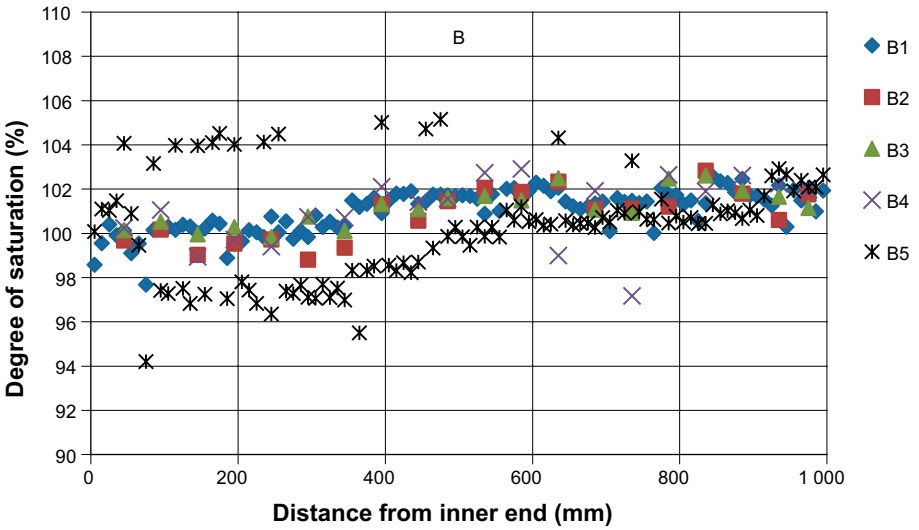

Figure E-6. *TZH. Results from sampling performed in direction B: Degree of saturation plotted versus the distance from the inner end of the distance block section.*

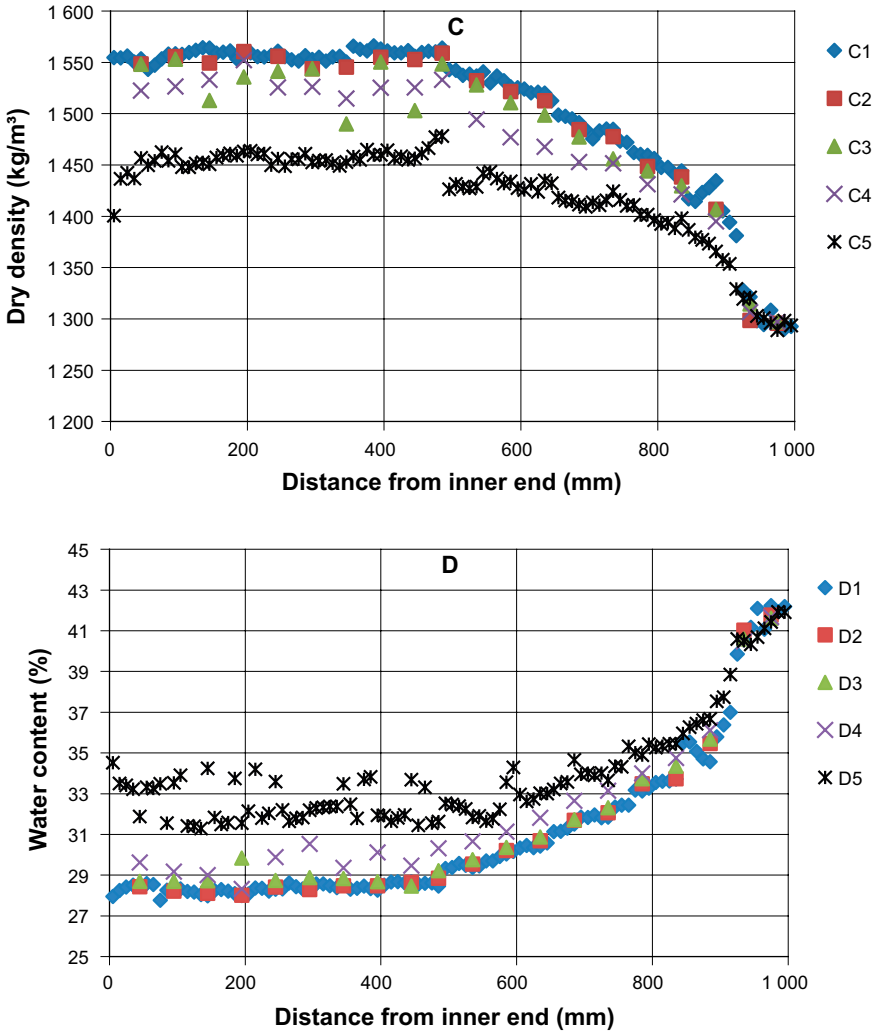

Figure E-7. *TZH. Results from sampling performed in direction C. Upper: Dry density plotted versus the distance from the inner end of the distance block section. Lower: Water content plotted versus the distance from the inner end of the distance block section.*

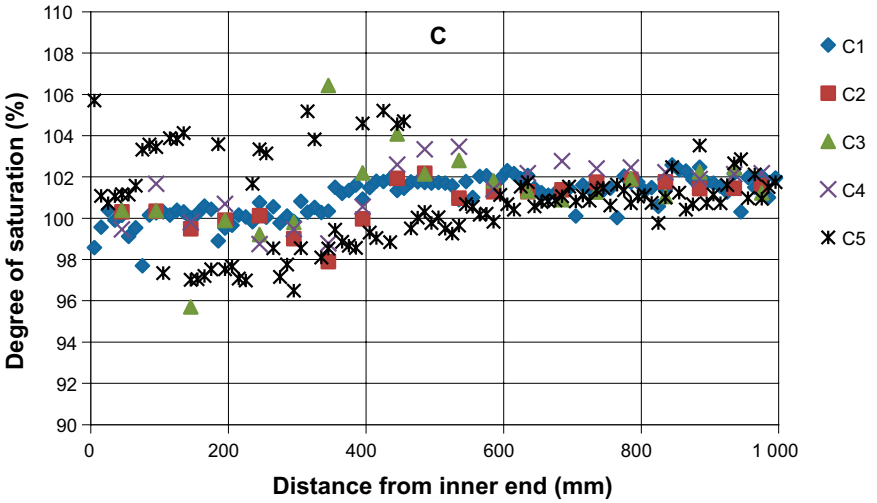

Figure E-8. *TZH. Results from sampling performed in direction C: Degree of saturation plotted versus the distance from the inner end of the distance block section.*

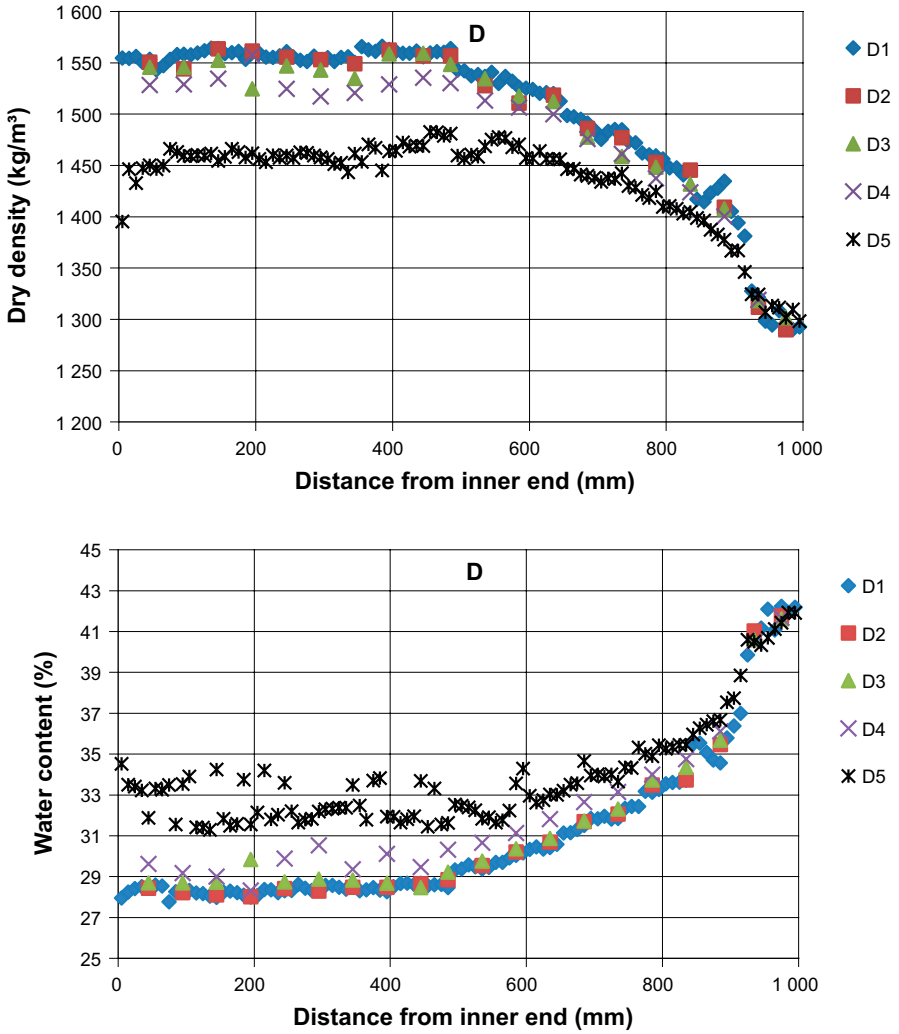

Figure E-9. *TZH. Results from sampling performed in direction D. Upper: Dry density plotted versus the distance from the inner end of the distance block section. Lower: Water content plotted versus the distance from the inner end of the distance block section.*

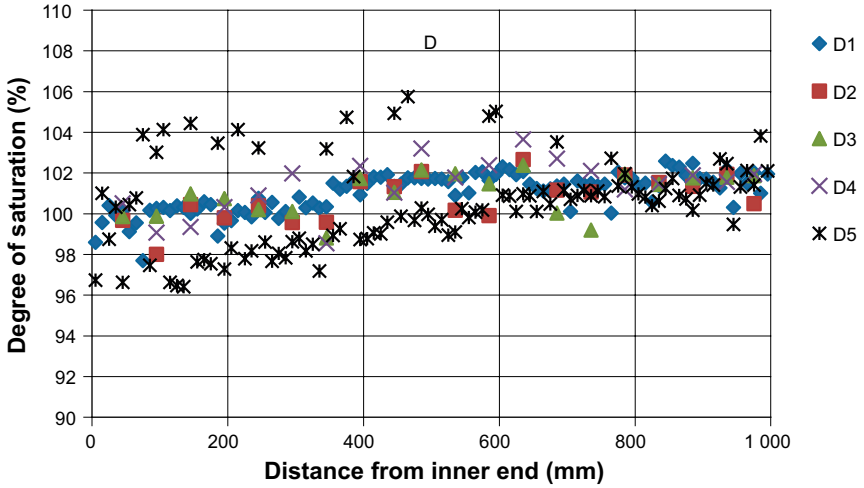

Figure E-10. *TZH. Results from sampling performed in direction D: Degree of saturation plotted versus the distance from the inner end of the distance block section.*

E5 TZH: Dimensioning of the transition zone in KBS-3H

E5.1 Prerequisites

The initial conditions and geometries of the system are described in Figure E-11. The bentonite properties have been simplified so that it has been assumed to be completely saturated and homogenized from start. The average density after radial swelling has been used for the transition blocks.

E5.2 Geometry

- Radius=0.925 m
- Distance from the filling block to the plug filled with pellets: 1.3 m

E5.3 Initial properties

The average dry density of the transition block section is calculated from the geometries and the initial dry density of the blocks:

Block diameter: D=1.765 m.

Drift diameter: D=1.85 m.

Dry density of the blocks: ρ_{db}=1 712 kg/m^3.

Average calculated dry density: $\rho_d = \rho_{db} \cdot 1.765^2/1.85^2$ = 1 558 kg/m^3.

The initial conditions are thus:

- Dry density of the pellet filling rdp=1 000 kg/m^3.
- Average dry density of the transition block section rdt=1 558 kg/m^3.
- Swelling pressure of the transition block section according to Equation E-1 ps=5.931 MPa.

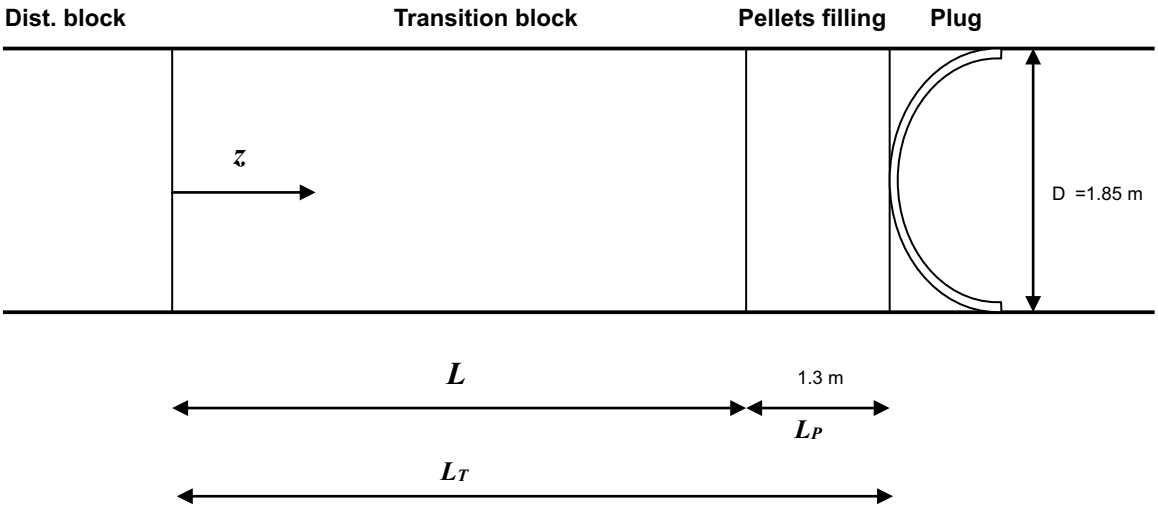

Figure E-11. *TZH. Basic geometry used for the calculation.*

The relation between swelling pressure and dry density can for MX-80 be described by Equations E-1 and E-2 (Börgesson et al. 1995).

$$p = p_r \left(\frac{e}{e_r} \right)^{\frac{1}{\beta}} \tag{E-1}$$

where

e = void ratio,

e_r = reference void ratio (=1.1),

p = swelling pressure (at e),

p_r = reference swelling pressure (at e_r) (=1 000 kPa),

β = −0.19.

$$\rho_d = \frac{\rho_s}{1+e} \tag{E-2}$$

where

ρ_s = dry density,

e = void ratio,

ρ_s = density of solids = 2 780 kg/m^3.

E5.4 Dimensioning calculations

The calculations are made in the following way: The large difference in density and resulting swelling pressure of the bentonite in the transition block zone and the bentonite in the pellet filling results in a swelling of the bentonite from the transition block zone and compression of the bentonite in the pellet filling. There will not be a complete homogenization due to the shear resistance (friction angle) between the bentonite and the rock. Instead there will be a swelling pressure (and thus density) gradient between the plug and the end of the transition zone. The length of the transition block zone will be dimensioned by the position where the density is unchanged.

The dry density distribution can be calculated from the swelling pressure distribution by combining Equations E-1 and E-2 with the following Equations E-3 and E-4 that describe the axial swelling pressure as a function of the axial distance from the unaffected bentonite at equilibrium after completed swelling in a cylindrical confinement (see e.g. Åkesson et al. 2010).

$$p = p_0 \cdot e^{-\frac{2z\tan\phi}{r}} \tag{E-3}$$

$$z = -\frac{r}{2\tan\phi} \ln\frac{p}{p_0} \tag{E-4}$$

where

z = axial distance from the unaffected bentonite,

r = radius,

p = swelling pressure at z,

p_0 = swelling pressure at z = 0,

ϕ = friction angle (=5°-30° depending on the swelling pressure and the roughness of the rock surface).

The swelling can be modelled according to Equations E-1 to E-3. Combining the expressions in Equations E-1 and E-3 for the swelling pressure yields Equation E-5.

$$p_r\left(\frac{e}{e_r}\right)^{\frac{1}{\beta}} = p_0 \cdot e^{-\frac{2z\tan\phi}{r}} \tag{E-5}$$

Applying Equation E-2 for the relation between void ratio and dry density and

e_r=1.1 = reference void ratio,

p_r =1 000 kPa = reference swelling pressure at e_r=1.1,

p_0= 5 931 kPa = swelling pressure at z = 0,

yield Equation E-6:

$$1000 \cdot \left(\frac{\left(\frac{\rho_s}{\rho_d}\right)-1}{1.1}\right)^{\frac{1}{\beta}} = 5931 \cdot e^{-\frac{2z\tan\phi}{r}} \tag{E-6}$$

$$\frac{\frac{\rho_s}{\rho_d}-1}{1.1} = \left(5.931 \cdot e^{-\frac{2z\tan\phi}{r}}\right)^{\beta} \tag{E-7}$$

$$\frac{\rho_s}{\rho_d} = 1.1 \cdot e^{-\frac{2z\tan\phi}{r}\beta} \cdot 5.931^{\beta} + 1 \tag{E-8}$$

Applying β = −0.19, r = 0.925 m and ρ_s = 2.78 t/m^3 yields

$$\frac{2.78}{\rho_d} = 0.784 \cdot e^{\frac{0.38 \cdot z \cdot \tan\phi}{0.925}} + 1 \tag{E-9}$$

$$\rho_d = \frac{2.78}{0.784 \cdot e^{0.41 \cdot z \cdot \tan\phi} + 1} \tag{E-10}$$

Equation E-10 thus yields the dry density distribution along the drift axis after force equilibrium. But in order to settle the required length of the transition zone L we need to use the fact that the mass of bentonite lost in the transition zone due to swelling is the same as the mass gained in the 1.3 m long pellet filling part due to the same swelling and subsequent compression of the pellet filling meaning that the total dry mass of bentonite between the plug and the unaffected distance block section is the same before and after swelling.

The dry mass dm_s over an axial length of dz of the drift can be formulated with Equation E-11.

$$\begin{aligned} dm_S &= \rho_d \cdot \pi r^2 dz = \frac{2.78}{0.784 \cdot e^{0.41 \cdot z \cdot \tan\phi} + 1} \cdot \pi r^2 dz \\ dm_S &= \frac{2.78\pi 0.925^2 dz}{0.784 \cdot e^{0.41 \cdot z \cdot \tan\phi} + 1} = \frac{7.47}{0.784 \cdot e^{0.41 \cdot z \cdot \tan\phi} + 1} dz \end{aligned} \tag{E-11}$$

$$dm_S = \frac{9.528}{e^{0.41 \cdot z \cdot \tan\phi} + 1.276} dz \tag{E-12}$$

In order to calculate the total mass M_{ST} we have to integrate the mass from z=0 to $z = L$+1.3 m = L_T, but at first we change Equation E-12 to Equation E-13:

$$dm_S = \frac{a}{e^{b \cdot z} + c} dz \tag{E-13}$$

where

a=9.528,

b=0.41·tanϕ,

c=1.276.

Integration according to Equation E-14 yields the total mass M_{ST} according to Equation E-15.

$$M_{ST} = \int_{z=0}^{z=L_T} dm_S = \int_{z=0}^{z=L_T} \frac{a}{e^{b \cdot z} + c} dz \tag{E-14}$$

$$M_{ST} = \frac{aL_T}{c} - \frac{a}{bc} \ln(c + e^{bL_T}) + \frac{a}{bc} \ln(c + 1) \tag{E-15}$$

We thus have a general expression of the distribution of the total dry mass over the length of the transition zone and the pellet filling after swelling.

The initial dry mass of bentonite in the transition zone (over the length L) is calculated according to Equation E-16

$$M_{S1} = \rho_d \pi r^2 L = 1.558 \cdot \pi \cdot 0.925^2 \cdot L = 4.190L \tag{E-16}$$

The initial mass of dry bentonite in the pellet filling (L_P) is according to Equation E-17

$$M_{S2} = \rho_d \pi r^2 L_P = 1.0 \cdot \pi \cdot 0.925^2 \cdot 1.3 = 3.494 \tag{E-17}$$

The total dry mass is thus

$M_{ST}=M_{S1}+M_{S2}$=4.190L+3.494=4.190(L_T−1.3)+3.494 (E-18)

By combining Equations E-15 and E-18 we can calculate L_T for different friction angles. By including the total length in Equation E-3 we can also calculate the swelling pressure on the plug. Table E-3 shows the results.

Table E-3. TZH. Results of the calculations.

Friction angle ϕ [°]	Total length of transition zone L_T [m]	Length of transition block L [m]	Swelling pressure on the plug [kPa]
5	7.61	6.31	1413
10	5.67	4.37	771
20	3.74	2.44	315
30	2.98	1.68	146

The required length of the transition zone and the resulting swelling pressure on the plug are thus very dependent on the friction angle. The friction angle for swelling pressures between 1 and 10 MPa is about ϕ=10° and it increases with decreasing swelling pressure. However, the friction angle between bentonite and a smooth plane surface of rock can be lower (about 50 % according to Börgesson et al. 1995), which perhaps would motivate to use ϕ=5°.

Figure E-12 shows the total length of the transition zone L_T as a function of the applied friction angle. Figure E-13 shows the swelling pressure on the plug as a function of the friction angle. Finally Figure E-14 shows the density distribution along the entire transition zone at different friction angles.

Figure E-15 shows a relation between swelling pressure (expressed as average effective stress) and the friction angle of MX-80 derived by Börgesson et al. (1995).

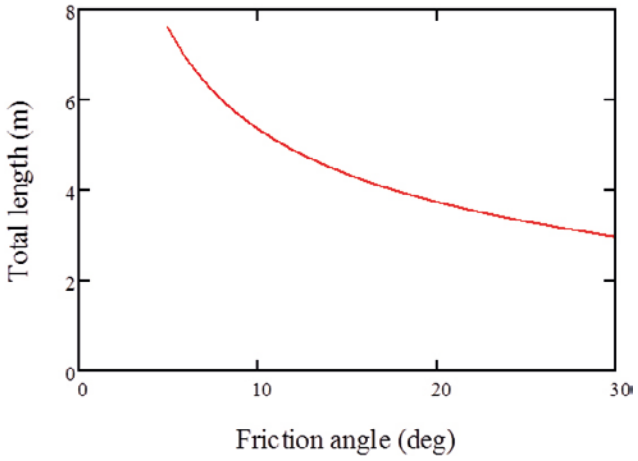

Figure E-12. *TZH. Total length of the transition zone L_T as a function of the applied friction angle.*

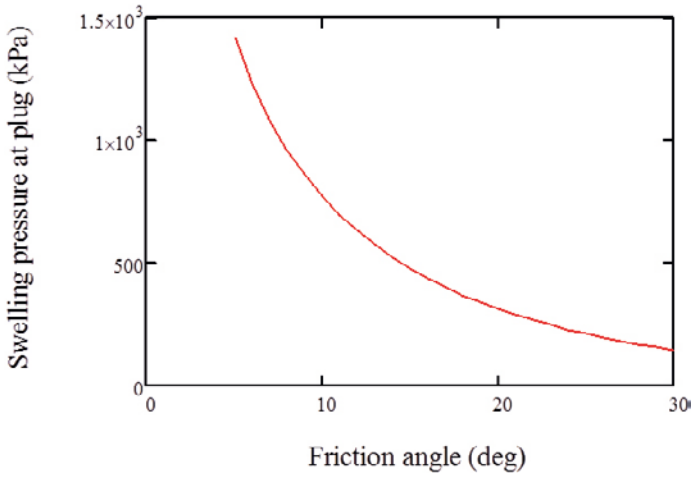

Figure E-13. *TZH. Swelling pressure on the plug as a function of the friction angle*

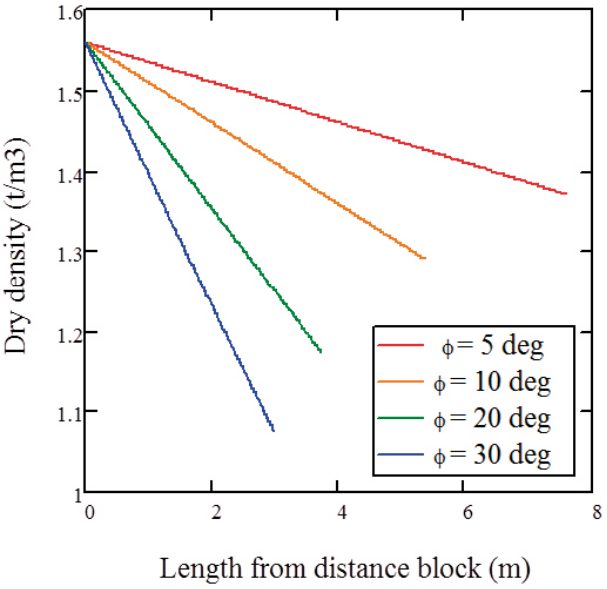

Figure E-14. *TZH. Density distribution along the entire transition zone at different friction angles.*

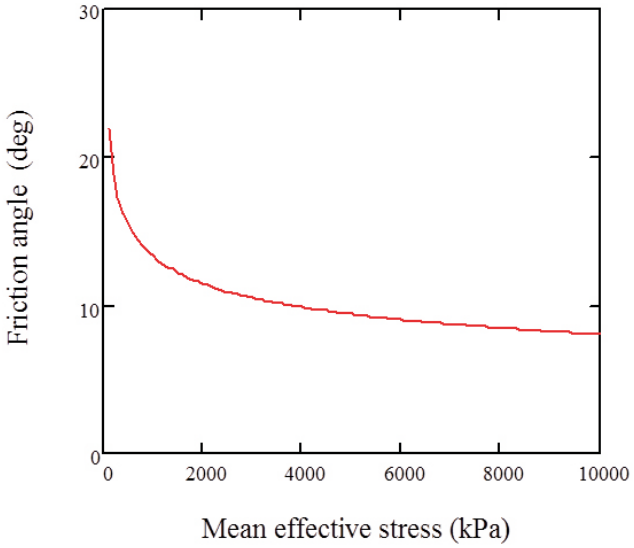

Figure E-15. *TZH. Relation between swelling pressure (expressed as average effective stress) and the friction angle of MX-80*

E5.5 Uncertainties

There are several simplifications and uncertainties related to these calculations. The following simplifications have been made:

1. The geometry of the plug is simplified and the extra pellet filled void caused by the valve form of the plug not included. This means that the results are slightly pessimistic (a little too high stresses on the plug).
2. No account has been taken to the initial slot between the bentonite blocks and the rock surface and the resulting radial density distribution.
3. No account has been taken to the water saturation phase, which in combination with the slot at the rock surface may affect the stress path during swelling.
4. The analytical calculation includes several simplified assumptions:
   a. No consideration of the hysteresis effects at loading and unloading has been taken.
   b. Potential radial stress gradients caused by the axis-symmetric swelling has not been taken into account.
   c. Potential differences between radial and axial stresses at uniaxial swelling and compression have not been taken into account.

It is difficult to estimate the importance of these simplifications. However, similar analytical calculation techniques have been used in different situations for KBS-3V and comparisons with FEM-calculations have shown reasonable agreement (Åkesson et al. 2010).

Another uncertainty is of course the friction angle between the bentonite and the rock and if future investigations or development of the drilling technique show that the rock surface is smooth this has to be taken into account.

Since there is a distance block section between the super container and the transition zone according to the present design, this is judged to yield enough safety margins for the uncertainties caused by the simplified calculation method. If, however, the distance block section is removed it is advisable to do more careful FEM-calculations of this case.

E6 TZH: Dimensioning of the KBS-3H transition zone scale tests

The diameter of the scale test will be 171 mm, which in comparison with the actual drift diameter 1 850 mm yields the scale 0.093 (1:10.8). The required length of the transition block zone and the expected swelling pressure on the plug etc. at different assumed friction angles have been estimated in a PM (Dimensioning of the transition zone in KBS-3H). Since those calculations refer only to stresses and strains after equilibrium and since the evolution in time is not included the results can be directly scaled down to the dimensions of the scale tests. This is also seen in Equation E-5 where the swelling pressure is a function of the ratio z/r where z is the distance from the unaltered part and r is the radius of the drift.

So if the pellet filling is $0.093 \times 1\,300$ mm = 121 mm the resulting length of the transition zone will be according to Table E-4 (derived from Table E-3). The tube in the scale test must at least be as long as L_T in order to keep the initial swelling pressure at the "distance block side".

Table E-4. TZH. Required length of the transition blocks and the required total length of the equipment.

Friction angle ϕ [°]	Total length L_T [mm]	Length of transition block L [mm]	Swelling pressure on the plug [kPa]
5	708	587	1413
10	527	406	771
20	348	227	315
30	277	156	146

The swelling pressure on the plug will of course be the same since the relation z/r is the same. The resulting relations are shown in Figure E-16 to Figure E-19.

The actual friction angle can be considered an average of the friction angles in the actual stress range. The friction angle in the stress range 500–4 000 kPa is according to Figure 4 10–15 degrees. These friction angles correspond to the peak strength. Since the residual strength is about half the peak strength it is obvious that we have to dimension the test according to the friction angle 5 degrees in order to be sure that we can keep the original density at the "distance block side", which means that the test tube needs to be at least 0.7 m long.

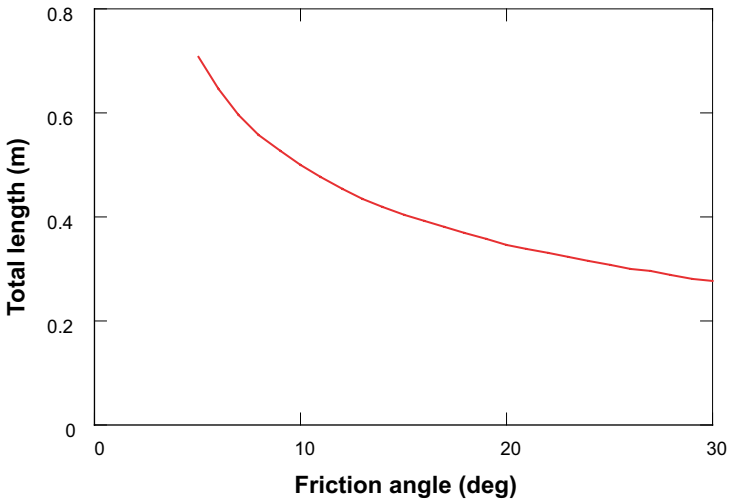

Figure E-16. *TZH. Total length of the transition zone L_T as a function of the applied friction angle.*

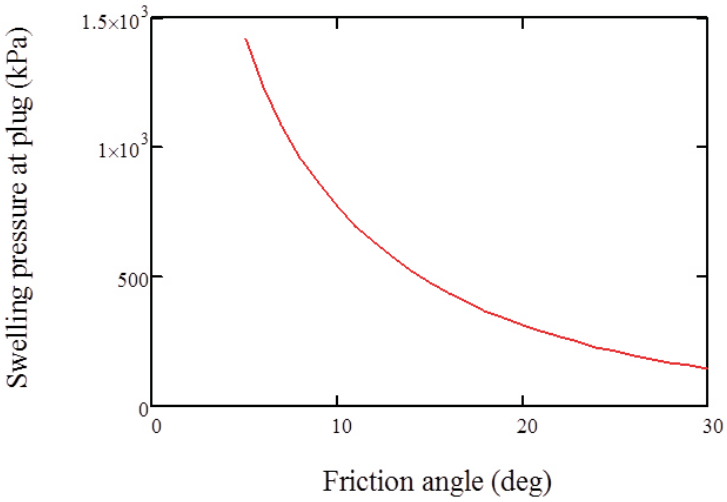

Figure E-17. *TZH. Swelling pressure on the plug as a function of the friction angle.*

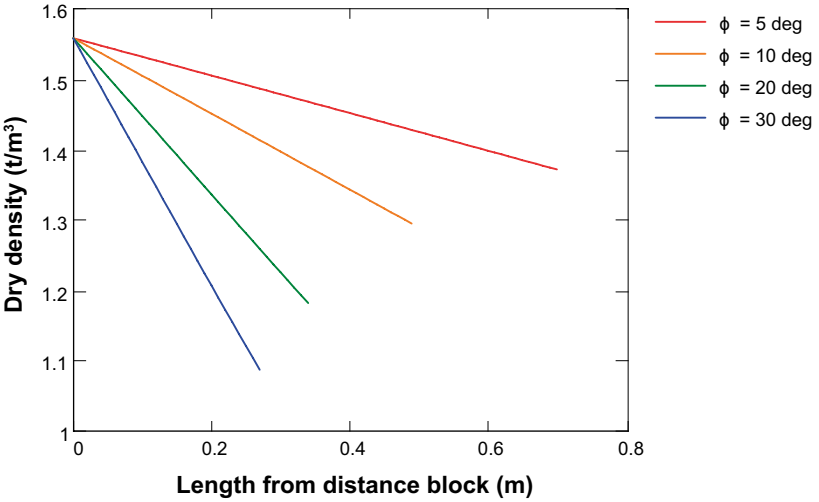

Figure E-18. *TZH. Density distribution along the entire transition zone at different friction angles.*

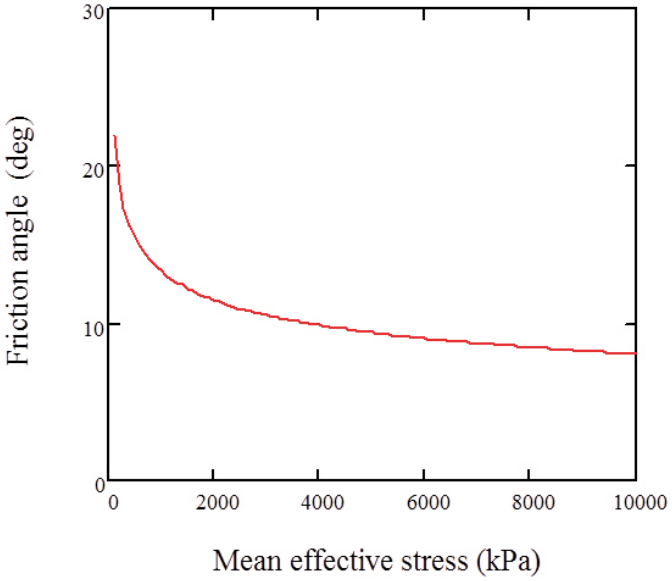

Figure E-19. *TZH. Relation between swelling pressure (expressed as average effective stress) and the friction angle of MX-80.*

Arkitektkopia AB, Bromma, 2017

SKB is responsible for managing spent nuclear fuel and radioactive waste produced by the Swedish nuclear power plants such that man and the environment are protected in the near and distant future.

skb.se